OPTIMAL DESIGN OF VARIABLE STIFFNESS COMPOSITE STRUCTURES USING LAMINATION PARAMETERS

Samuel Tsunduka IJsselmuiden

Stellingen

behorende bij het proefschrift

Optimal Design of Variable Stiffness Composite Structures Using Lamination Parameters

Samuel Tsunduka IJsselmuiden
3 Oktober 2011

1. Het ontwerpen van composieten laminaten door middel van lamination parameters is relatief ongecompliceerd. Daarentegen, jezelf en anderen overtuigen dat het bekomen ontwerp logisch is, is minder eenvoudig.

2. De tijd die besteed wordt aan het out-of-the-box denken kan vaker beter besteed worden aan het definiëren van de correcte box waarin gedacht kan worden.

3. Het maximaliseren van de laminaatstijfheid wordt vaak als alternatief gebruikt voor het maximaliseren van de laminaatsterkte. Doorgaans is enkel het tegengestelde waar.

4. Het is enigszins ironisch dat koolstofversterkte kunststoffen omarmd worden door de transportsector met het oog op het verminderen van het brandstofgebruik.

5. De tijd is aangebroken om naast productieproblemen ook ontwerpproblemen op te lossen met behulp van automated fiber placement technologie.

6. De sleutel tot het correct maken van beslissingen is niet kennis. Het is begrip. We hebben een overvloed aan het eerstgenoemde en een wanhopig gebrek aan het laatstgenoemde.

   "Waar is de wijsheid die we in kennis zijn verloren?
   Waar is de kennis die we in informatie zijn verloren?" – T.S. Eliot

7. Het ontwikkelen van nauwkeurige en betrouwbare virtuele testmethoden is noodzakelijk indien variabele-stijfheidsconstructies hun intrede willen maken in de luchtvaartindustrie.

8. Wetten die niet gehandhaafd kunnen worden, moeten in de eerste plaats niet gemaakt worden.

9. Eetstokjes zijn een effectieve manier om gewicht te verminderen.

10. "Spreek tegen een man in een taal die hij begrijpt, dat gaat naar zijn hoofd. Spreek tegen een man in zijn eigen taal, dat gaat naar zijn hart"
    – Nelson Mandela

Deze stellingen worden opponeerbaar en verdedigbaar geacht en zijn als zodanig goedgekeurd door de promotor, Prof. dr. Zafer Gürdal

Propositions

accompanying the thesis

Optimal Design of Variable Stiffness Composite Structures Using Lamination Parameters

Samuel Tsunduka IJsselmuiden
3 October 2011

1. Use of lamination parameters for composite laminate design is relatively straightforward. Convincing yourself and others that the obtained design actually makes sense is less trivial.

2. The time taken to think out-of-the-box is often far better spent on defining the right box to think in.

3. Maximizing laminate stiffness is often seen as a suitable surrogate for maximizing laminate strength. However, generally only the opposite is true.

4. It is somewhat ironic that carbon fiber composites are being embraced by the transport sector to reduce fuel consumption.

5. The time is ripe for automated fiber placement technology to be used to solve design problems instead of only manufacturing problems.

6. The key to good decision making is not knowledge. It is understanding. We are drowning in the former and desperately lacking the latter.
   "Where is the wisdom we have lost in knowledge?
   Where is the knowledge we have lost in information?" – T.S. Eliot

7. The development of accurate and reliable virtual testing methods is essential if variable stiffness composite structures are to be adopted by the aerospace industry.

8. Laws that cannot be enforced should not be made in the first place.

9. Chopsticks are an effective means of reducing weight.

10. "If you speak to a man in a language he understands, that goes to his head. If you speak to a man in his language, that goes to his heart."
    – Nelson Mandela

These propositions are considered opposable and defendable and as such have been approved by the supervisor, Prof. dr. Zafer Gürdal

Optimal Design of Variable Stiffness Composite Structures Using Lamination Parameters

Optimal Design of Variable Stiffness Composite Structures Using Lamination Parameters

PROEFSCHRIFT

ter verkrijging van de graad van doctor
aan de Technische Universiteit Delft,
op gezag van de Rector Magnificus Prof. ir. K.C.A.M. Luyben,
voorzitter van het College voor Promoties,
in het openbaar te verdedigen
op maandag 3 oktober 2011 om 12.30 uur
door

Samuel Tsunduka IJSSELMUIDEN

ingenieur luchtvaart en ruimtevaart
geboren te Soutpansberg, Zuid Afrika.

Dit proefschrift is goedgekeurd door de promotor:

Prof. dr. Z. Gürdal

Samenstelling promotiecommissie:

Rector Magnificus	voorzitter
Prof. dr. Z. Gürdal	Technische Universiteit Delft, promotor
Dr. M.M. Abdalla	Technische Universiteit Delft, copromotor
Prof. dr. R. Curran	Technische Universiteit Delft
Prof. dr. R.T. Haftka	University of Florida, Verenigde Staten van Amerika
Prof. dr. A.S. Herrmann	Universität Bremen, Duitsland
Prof. dr. N. Olhoff	Aalborg Universitet, Denemarken
Prof. dr. V.V. Toropov	University of Leeds, Verenigd Koninkrijk
Prof. dr. D.J. Rixen	Technische Universiteit Delft, reservelid

This research work was supported by Delft University of Technology and the AUTOW project, part of the European Union Sixth Framework Program.

AUTOW Project Partners:

ISBN: 978-94-6113-032-7

Printed by Wöhrmann Print Service, Zutphen, The Netherlands
Typeset by the author with the LaTeX Documentation System

师傅领进门，修行在个人

Teachers open the door,
You must walk through it yourself.

Dedicated to you who taught me ...

Summary

Fiber reinforced composite materials have gained widespread acceptance for a multitude of applications in the aerospace, automotive, maritime and wind-energy industries. Automated fiber placement technologies have developed rapidly over the past two decades, driven primarily by a need to reduce manufacturing costs and improve product consistency and quality.

The introduction of new technologies often stimulates novel means of exploiting them, such as using the built-in fiber steering capabilities to manufactured composite laminates with continuously varying fiber orientation angles, yielding a so called variable stiffness laminate. These laminates allow the full potential of composite materials to be harnessed by enlarging the design space to create substantially more efficient structural designs, which has been demonstrated both theoretically and experimentally in the recent past. Despite the apparent potential, the design tools currently available to engineers do not exploit the steering capabilities of automated fiber placement machines to obtain more efficient structural solutions.

The design of composite structures is by no means a trivial task. Composite structures are inherently difficult to optimize due to a combination of discrete and continuous design variables as well as generally non-convex design problems with multiple solutions. Variable stiffness laminates are even more complex to design, as the optimization problem is no longer limited to a single or several laminate designs, but consists essentially of obtaining an optimal layup at every point in the structure. Ensuring fiber continuity and laminate manufacturability complicates the design problem even further. The large number of design variables and constraints associated with variable stiffness design problems make them unusually challenging problems to solve.

The substantial increase in structural efficiency possible when using variable stiffness laminates and the lack of available design tools motivated the development of computationally tractable design optimization routine for variable stiffness composite structures. The complexity of the design problem necessitated the development of a multi-step approach, shown schematically in the figure below. Separating structural performance related design drivers and manufacturing related design drivers allows the most suitable optimization algorithms to be used where necessary. In a first step, the optimal laminate stiffness distribution is obtained for the considered structural performance metric and constraints. Using lamination parameters to parameterize the structural stiffness allows the optimization problem to be solved efficiently, as will be discussed later. Design drivers such as maximum in-plane stiffness, strength, natural frequency and buckling can be included at this stage of the optimization. The

obtained optimum solution provides the designer with a conceptual stiffness distribution best satisfying the desired structural performance requirements. In a second step, the fiber angle distribution, essentially representing point-wise laminate stacking sequence, required to match the obtained optimum stiffness distribution is determined. Manufacturing constraints, such as minimum curvature, thickness buildup, or permeability, can be incorporated at this stage. In a final step, the obtained fiber angle distributions are converted to continuous fiber paths for manufacturing.

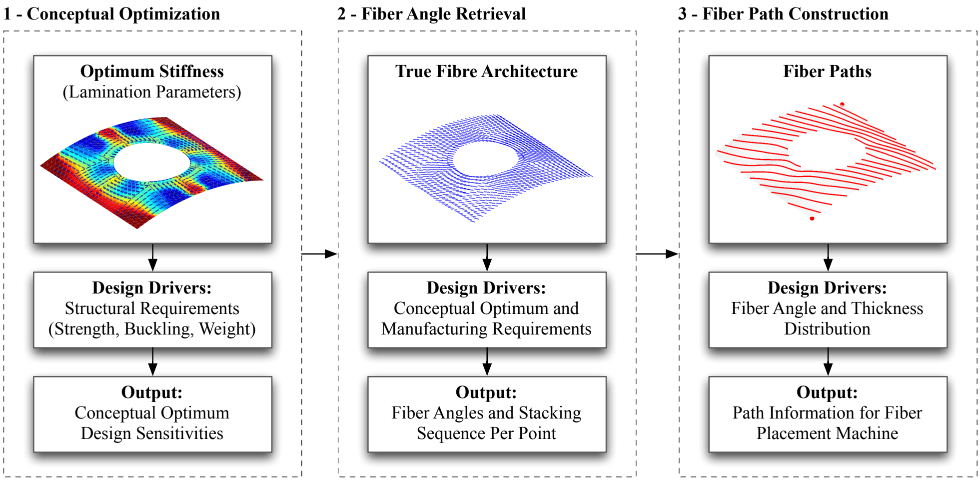

Figure 1: *Schematic overview of the developed multi-step optimization approach*

The responses of variable stiffness composite structures, required at the various steps of the design process, are typically evaluated using a finite element method by assigning different stiffness properties to each element in the model. In structural optimization, approximations of the structural response are often developed to minimize the number of computationally expensive finite element analyses needed during the design process. In order to develop a computationally tractable design framework it was essential to develop an effective approach to approximate the response of variable stiffness structures. The development of a generic conservative convex separable approximation specifically for composite structures and its implementation within a design framework using lamination parameters is presented in this thesis.

The developed convex conservative separable approximation, following Svanberg (2002), has two parts, the first part is to ensure that the function value and the gradient of the approximation meet those of the original function, while the second term is used to control the overall approximation conservativeness and convexity by appropriately scaling this term after each successive design iteration. The approximation is expressed directly in terms of the laminate stiffness matrices, known from classical lamination theory, and is therefore independent of the chosen laminate parameterization scheme. A function approximation is generated by expanding the function linearly and/or reciprocally with respect to the laminate stiffness matrices, similar to the traditionally used conservative approximation. Instead of using derivative information to determine which terms are expanded linearly and which terms are expanded reciprocally, physical insight into the response being approximated is used to guarantee convexity by expanding the non-convex terms linearly. Using lamination parameters to parametrize the laminate stiffness matrices allows the convex nature of the approximation to be retained. Additionally, lamination parameters allow the laminate stiffness matrices to be expressed using a minimum number of continuous design variables, allowing efficient gradient based optimization algorithms to be used.

An efficient design optimization framework, based on the aforementioned conservative convex separable approximations, is developed and enables the solution of variable stiffness design optimization problems with several thousand design variables. The optimizer consists of three loops, one, a convergence control loop, two, a global optimization loop, and three, a local optimization loop, where the latter two loops correspond to the optimization problems that result when using the dual method. The convergence control loop is used to dynamically control the degree of conservativeness of the considered approximations and to decide if the optimal solution of the approximate subproblem is accepted for the following iteration. The global optimization loop consists of solving for the Lagrange multipliers associated with the constraints. The local loop is used to solve the local separable approximations iteratively in terms of lamination parameters to obtain the optimum stiffness distribution. The separable nature of the response approximations allows the local optimization problems to be solved in parallel, further reducing computation time on multi-processor computer systems. Typically, less than thirty finite element analyses are required to converge to the optimal solution of a problem with several thousand design variables and several hundred constraints, while roughly 80-90% of the performance gains are typically achieved within the first 3-5 design iterations.

One of the limitations, and perhaps objections to using lamination parameters for composite design, has been the difficulty of incorporating strength constraints into the optimization process. In order to facilitate the acceptance of the approach, a method of including the Tsai-Wu strength criteria in the most general setting is developed. Analytical expressions for conservative failure envelopes in terms of two strain invariants are derived that are no longer an explicit function of the laminate stacking sequence. The derived envelope is shown to accurately represent the factor of safety for practical laminates under in-plane loading, however, for bending dominated problems it may be too conservative. A failure index is subsequently defined and used to formulate an optimization problem to design laminates for maximum strength under combined axial and shear loads. The designs are subsequently compared to the equivalent maximum stiffness designs. Strength-optimal and stiffness-optimal designs for various materials and load conditions are obtained and are found to be similar for a large range of problems. However, differences were also found, particularly for compression-shear loaded panels. Laminate strength is found to be significantly more sensitive to the final laminate design than laminate stiffness, which implies that design for maximum strength will result in near-optimal laminate stiffness, however, the opposite is not necessarily true.

Approximations for several specific design optimization problems related to buckling are developed. Initial work is focused on developing convex separable approximations of the buckling load of plates. It is shown, using the eigenvalue problem used to solve for linear buckling, that a homogenous convex approximation for the inverse buckling load factor is obtained when expanding the geometric stiffness matrix lin-

early in terms of the laminate in-plane stiffness while expanding the material stiffness matrix reciprocally in terms of laminate bending stiffness. A convex approximation to maximize laminate stiffness is also developed. A trade-off study between maximum laminate stiffness and maximum laminate buckling load of a plate under uniaxial compression is conducted. Numerical results demonstrate that significant improvements in structural performance are possible and that a variable stiffness laminate with overall stiffness equivalent to a quasi-isotropic laminate can be designed to have twice the buckling load. In-plane load redistribution is found to be the primary mechanism resulting in improved buckling load and post-buckling analysis demonstrated that variable stiffness laminate designs have similar or superior post-buckling stiffness when compared to the equivalent constant stiffness solutions. A simplified method of including thermals stresses during the buckling design optimization process is also developed, since the pre-buckling stress state significantly influences a panels buckling behavior. For the plate buckling problem under consideration, residual thermal stresses are shown to beneficially influence the compressive load carrying capacity of a plate if the temperature difference between curing temperature and operating temperature are not excessive. The range of operating temperatures over which a panel exhibits good buckling behavior increases significantly when including thermal effects in the design process. Later, the approximation of the inverse buckling load factor is extended to include laminate thickness as a design variable, which requires additional linearization of the terms linear in the laminate stiffness matrices. Compared to the optimal variable stiffness design with constant thickness further improvements in the buckling load, 30-100% depending on the minimum bound thickness, are obtained.

When thickness variation is included in the variable stiffness design routine for maximum laminate buckling load, both load redistribution and increased laminate bending stiffness are found to play a role in the improved structural performance. Using the insight gained from studying variable stiffness plates, a convex approximation of the inverse buckling load for general structures is derived. Convexity of the approximation is guaranteed by expanding the terms associated with the geometric stiffness matrix linearly with respect to the laminate stiffness matrices and expanding the terms associated with the material stiffness matrix reciprocally. An example problem, a curved panel subject to a uniform pressure load, is presented to demonstrated the applicability of the derived approximation.

Two practical design applications are studied with several industrial partners to demonstrate the effectiveness of the developed design approach. A first problem considers the design of a simplified window belt section for maximum tensile strength. Numerical results highlight that variable stiffness laminates, including manufacturing constraints, can be found that have a 50% higher failure load compared to the best constant stiffness design. A second design problem focuses on the design of an aircraft wing rib to meet a range of imposed design requirements with buckling as a primary design driver. Other than demonstrating the benefit of using stiffness variation for more practical structures, the analysis for this design problem is conducted entirely using an external commercial finite element solver. Also for this more practical design problem the optimizer was found to perform satisfactorily.

Samenvatting

Vezelversterkte kunststoffen, ook wel composieten genoemd, worden tegenwoordig op grote schaal gebruikt voor verscheidene toepassingen in de luchtvaart-, ruimtevaart-, automobiel-, maritieme-, en windenergie-industrie. De focus op het reduceren van hun productiekosten en het garanderen van een hoge productkwaliteit heeft ertoe geleid dat geautomatiseerde productietechnologieën voor composieten, zoals automated fiber placement (AFP), de afgelopen twee decennia een snelle ontwikkeling hebben ondergaan.

Nieuwe technologieën kunnen vaak op innovatieve manieren benut worden. Een voorbeeld hiervan zijn de automated fiber placement machines die door hun mogelijkheid om de vezeloriëntatie nauwkeurig te controleren, vezels gestuurd op een mal kunnen plaatsen. Het is dus mogelijk om de vezeloriëntatie, en bijgevolg de stijfheid, continue te laten variëren in een constructie. Een laminaat waarin de vezeloriëntatie continue veranderd wordt, wordt tevens een variabele-stijfheidslaminaat (VS) of variable stiffness laminate genoemd. Door de laminaatstijfheid continue te laten variëren is het mogelijk om optimaal gebruik te maken van de materiaaleigenschappen en daardoor grote verbeteringen in structurele efficiëntie te behalen. Deze mogelijke verbeteringen zijn in het verleden zowel theoretisch als experimenteel aangetoond. Ondanks dit potentieel zijn er tot op heden nog geen ontwerptools beschikbaar waardoor ingenieurs gemakkelijk gebruik kunnen maken van de verbreding in ontwerpmogelijkheden die automated fiber placement machines bieden.

Het ontwerpen van constructies die vervaardigd worden uit vezelversterkte kunststoffen is geen onomwonden proces. De complexiteit omtrent het optimaliseren van deze constructies wordt enerzijds veroorzaakt doordat de ontwerpvariabelen zowel een discreet als continu karakter kunnen hebben en anderzijds doordat de ontwerpproblemen vaak niet-convex zijn. Het ontwerpen van laminaten waarbij de stijfheid in het laminaat kan variëren van locatie tot locatie brengt nog een grotere uitdaging met zich mee omdat in dit geval de optimalisatieopdracht niet beperkt wordt tot een enkel of meerdere laminaatontwerpen, maar in wezen een optimale laminaatsamenstelling bewerkstelligd moet worden voor elk punt in de constructie. Dit moet tevens gebeuren zonder dat de continuïteit van de vezelpaden en de produceerbaarheid van de laminaten in het gedrang worden gebracht.

Ondanks de bijkomende complexiteit die variabele-stijfheidslaminaten veroorzaken, zijn deze laminaten uiterst interessant omdat ze een substantiële toename in structurele efficieñtie met zich kunnen meebrengen. Deze potentiële efficiëntieverbetering en het feit dat tot op heden geen toepasbare ontwerptools beschikbaar zijn, heeft de

ontwikkeling van een efficiënte optimalisatieroutine voor het ontwerp van variabele-stijfheidslaminaten gedreven. De complexiteit van het ontwerpprobleem, zoals hierboven reeds besproken is, heeft geleid tot het ontwikkelen van een stapsgewijze optimalisatieroutine. Dit wordt tevens toegelicht in Figuur 1. Allereerst wordt er een onderscheid gemaakt tussen ontwerpcriteria die van belang zijn voor de structurele prestaties van het laminaat en diegene die van belang zijn voor zijn produceerbaarheid zodat de meest toepasselijke optimalisatiealgoritmes gebruikt kunnen worden in elke situatie. In een eerste stap wordt er getracht de laminaatstijfheidsverdeling te bekomen die de optimale structurele prestatie weergeeft. Met het oog op het efficiënt oplossen van de optimalisatie-probleem wordt er gekozen voor lamination parameters om de stijfheidsverdeling te parameteriseren, zoals later nader toegelicht zal worden. Prestatieparameters die van belang zijn voor het ontwerp, zoals de stijfheid, sterkte, natuurlijke frequentie en knik, kunnen in de eerste stap van de optimalisatieroutine worden opgenomen. Wanneer alle gewenste structurele prestatieparameters in acht worden genomen, kan de optimale conceptuele stijfheidsverdeling voor het ontwerpprobleem gevonden worden. In de tweede stap wordt de vezelhoekverdeling bepaald die deze optimale stijfheidsverdeling kan garanderen. In deze fase kunnen evenzeer productiecriteria beschouwd worden, zoals de minimale kromming van het vezelpad, de toename in laminaatdikte of de permeabiliteit. Het doel van de laatste stap is om de bekomen vezelhoekverdelingen om te zetten in continue vezelpaden die gebruikt kunnen worden voor productie.

Vaak wordt er gebruik gemaakt van een eindige-elementenmethode om de respons van de variabele-stijfheid composieten constructies, die vereist zijn bij de verschillende fases in het ontwerpproces, te evalueren. Hiervoor worden in het eindige-elementenmodel verschillende stijfheidseigenschappen toegekend aan elke element. Met het oog op het minimaliseren van het aantal eindige-elementenberekeningen dat uitgevoerd moet worden tijdens het ontwerpproces, wordt er dikwijls beroep gedaan op benaderingen van de structurele respons. Om een ontwerpkader te creëren waarin rekening wordt gehouden met de vereiste rekenkracht, was het van essentieel belang dat er een effectieve procedure werd ontwikkeld om de respons van de variabele-stijfheidsconstructies te benaderen. In deze thesis wordt er nader ingegaan op een generieke conservatief convex scheidbare benadering (Conservative convex separable approximation, verkort tot CCSA) die speciaal ontwikkeld werd voor het optimaliseren van composieten constructies en hoe dit binnen het ontwerpkader gebruikt wordt.

Deze benadering, die gebaseerd is op Svanberg (2002), is opgebouwd uit 2 termen. De eerste term garandeert dat de functiewaarde en de gradiënt van de benadering overeenkomen met deze van de originele functie. De tweede term controleert de algemene conservativiteit en convexiteit van de benadering door deze term naar behoren te schalen na elke opeenvolgende ontwerpiteratie. De benadering zelf wordt uitgedrukt in termen van de laminaatstijfheidsmatrices, bekend van de klassieke laminatentheorie (CLT), en is daarom volledig onafhankelijk van het gekozen laminaat parameterseringsschema. Een benadering van de functie wordt bewerkstelligd door de functie lineair en/of invers met betrekking tot de laminaatstijfheidsmatrices te ontwikkelen. In plaats van gebruik te maken van de functieafgeleide om te bepalen welke termen lineair en welke termen invers worden ontwikkeld, wordt beroep gedaan op het fysische inzicht in de respons dat wordt benaderd. Convexiteit kan vervolgens worden gegarandeerd door de niet-convexe termen lineair te ontwikkelen. Door lamination parameters te gebruiken om de laminaatstijfheidsmatrices te parameteriseren kan het convexe karakter van de benadering worden behouden. Bovendien bieden lamination parameters de mogelijkheid om de laminaatstijfheidsmatrices uit te drukken met behulp van een minimaal aantal continue ontwerpvariabelen. Dit leidt ertoe dat efficiënte gradiënt-gebaseerde optimalisatiealgoritmen gebruikt kunnen worden om het ontwerpprobleem op te lossen.

Een efficieñt ontwerp-optimalisatiekader dat gebaseerd is op de eerder genoemde conservatief convex scheidbare benaderingen, is ontwikkeld en maakt het mogelijk om variabele-stijfheidsontwerp optimalisatieproblemen op te lossen met enkele duizenden ontwerpvariabelen. De optimalisatieroutine bestaat uit drie lussen: één, een convergentie controlelus; twee, een globale optimalisatielus; en drie, een lokale optimalisatielus, waarbij de laatste twee lussen overeenkomen met de optimalisatieproblemen die bekomen worden wanneer de dual-method (Fleury and Schmit Jr., 1980) wordt gebruikt. De convergentie controlelus wordt gebruikt om de conservativiteitsgraad van de beschouwde benaderingen dynamisch te controleren en om te beslissen of de optimale oplossing van het benaderde sub-probleem aanvaardbaar is voor de volgende iteratie. De globale optimalisatielus zoekt een oplossing voor de Lagrange-multiplicatoren die betrekking hebben op de randvoorwaarden. De lokale optimalisatielus zoekt iteratief naar een oplossing voor de lokaal scheidbare benaderingen, met behulp van lamination parameters, zodat de optimale stijfheidsverdeling bekomen kan worden. Het scheidbare karakter van de responsbenaderingen stelt de lokale optimalisatieproblemen in staat om parallel opgelost te worden. Dit vermindert tevens de rekentijd op multi-processor computersystemen. Normaalgezien worden minder dan dertig eindige-elementenanalyses vereist om naar een optimale oplossing te convergeren, terwijl ongeveer 80-90% van de prestatietoenames in het algemeen bekomen worden tijdens de eerste 3-5 ontwerp iteraties.

Een van de beperkingen, en misschien bezwaren tegen het gebruik van lamination parameters voor het ontwerp van composieten, is de moeilijkheid om randvoorwaarden omtrent sterkte in het optimalisatieproces op te nemen. Om de methode aanvaardbaar te maken is een methode ontwikkeld waarbij het Tsai-Wu sterktecriterium in de meest algemene vorm in acht wordt genomen. Analytische uitdrukkingen voor een conservatief sterktecriterium zijn ontwikkeld in termen van twee rekinvarianten en is daarom niet langer een expliciete functie van de vezeloriëntatie. Het bekomen sterktecriterium geeft nauwkeurig de veiligheidsfactor weer voor praktische laminaten die worden onderheven aan belasting in het vlak. Daarentegen, voor problemen die vooral uit het vlak zijn belast kan dit sterktecriterium te conservatief zijn. Een sterkteverhouding wordt gedefinieerd en wordt vervolgens gebruikt om een optimalisatieprobleem te formuleren om laminaten die belast worden door een combinatie van axiale en afschuifkrachten voor maximale sterkte te ontwerpen. De ontwerpen worden vervolgens vergeleken met de equivalente maximale stijheidsontwerpen. De optimale-sterkte en optimale-stijfheidsontwerpen voor verscheidene materialen en krachtcondities worden bekomen en blijken gelijk te zijn voor een breed scala aan problemen. Verschillen worden echter ook opgemerkt, in het bijzonder voor druk-afschuiving belaste panelen. De laminaatsterkte blijkt opmerkelijk gevoeliger te zijn aan het uiteindelijke laminaatontwerp dan aan de laminaatstijfheid. Dit betekent dat het ontwerp voor maximale sterkte resulteert in een bijna optimale laminaatstijfheid, terwijl het tegengestelde niet altijd geldt.

Benaderingen voor verschillende specifieke ontwerp-optimalisatieproblemen die gerelateerd zijn aan knik zijn ontwikkeld. Tijdens het initiële onderzoek is vooral aandacht besteed aan het ontwikkelen van convex scheidbare benaderingen voor de knikbelasting van platen. Het is aangetoond, op basis van het eigenwaardeprobleem dat gebruikt wordt om de lineaire kniklast te bepalen, dat een homogeen convexe benadering voor de inverse kniksbelastingsfactor bekomen kan worden wanneer de geometrische stijfheidsmatrix lineair ontwikkeld wordt in termen van de laminaatrekstijfheid, terwijl de materiaalstijfheidsmatrix invers ontwikkeld wordt in termen van laminaatbuigstijfheid. Een convexe benadering om de laminaatstijfheid te maximaliseren is eveneens ontwikkeld. Een studie is uitgevoerd waarbij de afweging gemaakt wordt tussen maximale laminaatstijfheid en maximale laminaatknikbelasting van een plaat onder uniaxiale druk. Numerieke resultaten tonen aan dat opmerkelijke verbeteringen in structurele prestatie mogelijk zijn en dat een variabele-stijfheidslaminaat met een algemene stijfheid die equivalent is aan die van een quasi-isotropische laminaat ontworpen kan worden zodat deze twee keer de drukkracht kan weerstaan. Het is aangetoond dat de verbeterde weerstand tegen drukbelasting vooral veroorzaakt word door een herverdelen van de belasting in het vlak. Een post-knikbelastingsanalyse heeft laten zien dat ontwerpen van variabele-stijfheidslaminaten een gelijkaardige of superieure postknikstijfheid hebben in vergelijking met equivalente constante-stijfheidslaminaten.

Gezien de pre-knikspanning het knikgedrag van een paneel opmerkelijk beïnvloed is er eveneens een vereenvoudigd model ontwikkeld waarbij thermische spanningen in het knik-ontwerpoptimalisatieproces meegerekend kunnen worden. De thermische spanningen blijken een gunstig effect te hebben op de kniklast van een plaat wanneer het temperatuurverschil tussen de uithardingstemperatuur en de operationele temperatuur niet overdreven groot is. Het bereik van operationele temperaturen waarbij een paneel een goed knikgedrag vertoont, wordt opmerkelijk groter wanneer de thermische effecten opgenomen worden in het ontwerpproces. Naderhand is de benadering van de inverse kniksbelastingsfactor uitgebreid zodat de laminaatdikte als een ontwerpvariabele meegerekend kan worden. Hierdoor kunnen verdere verbeteringen van 30-100% in knikbelasting bekomen worden, afhankelijk van de minimale dikte, in vergelijking met het optimale variabele-stijfheidsontwerp met een constante dikte. Het kan opgemerkt worden dat zowel belastingsherverdeling als een vergrootte laminaatbuigstijfheid een rol spelen in het verbeteren van de structurele prestatie wanneer diktevariatie meegenomen wordt in de variabele-stijfheidontwerproutine voor maximale laminaatknikbelasting. Door gebruik te maken van het inzicht dat verworven is tijdens het bestuderen van variabele-stijfheidsplaten kan een convexe benadering voor de inverse kniksbelastingfactor voor algemene schaalconstructies afgeleid worden. De convexiteit van de benadering kan gegarandeerd worden door de termen die betrekking hebben tot de geometrische stijfheidsmatrix lineair te ontwikkelen in termen van de laminaatstijfheidsmatrices en door de termen die betrekking hebben tot de materiaalstijfheidsmatrix invers te ontwikkelen. Aan de hand van een voorbeeldprobleem wordt de toepasbaarheid van de afgeleide benadering aangetoond.

Twee praktische ontwerpapplicaties zijn nader bestudeerd in samenwerking met verschillende industriële partners om de effectiviteit van het ontwikkelde ontwerpoptimalisatiekader en de geassocieërde benaderingen aan te tonen. Een eerste probleem gaat dieper in op het ontwerp van een vereenvoudigde raamsectie voor maximale trekkracht. Numerieke resultaten duiden aan dat variabele stijfheidslaminaten, productiebeperkingen in rekening nemend, gevonden kunnen worden die een 50% hogere breeklast hebben in vergelijking tot het beste constante-stijfheidontwerp. Een tweede ontwerpprobleem focust zich op het ontwerp van een vliegtuigvleugelrib dat aan een scala van opgelegde ontwerpcriteria moet voldoen, met knik als het belangrijkste ontwerpcriterium. Naast het aantonen van het voordeel dat het gebruik van stijfheidvariatie voor meer algemene constructies met zich meebrengt, wordt de hele analyse voor het ontwerpprobleem uitgevoerd op basis van een externe commerciële eindige-elementenoplosser. Het optimalisatiekader blijkt tevens voor dit meer praktische ontwerpprobleem voldoende te functioneren.

Preface

While this preface is likely to represent the beginning of your journey through these pages, it signals that the end of mine is approaching. While this preface includes no scientific content, it will probably be read with the most interest. While this preface is the shortest section in this thesis, its words carry the most meaning. It is strange, the least words are spent on what is undoubtedly the most significant part of my journey; the personal relationships and friendships that have been created and strengthened over the past four years. It is this for which I am most grateful!

So many of you have supported and encouraged me along this journey, which started long before the first words of this thesis were written. Thank you for giving me the space and time to explore, for letting me make mistakes, for always being ready to help me find the right direction. Thank you for taking the time to listen to me, for asking the right questions and for making me challenged my own assumptions. Thank you for the many meaningful discussions and for those discussions that helped me take my mind off things. Thank you for the reassurance and for always being ready to help so that I could focus on what was important. Thank for listening with interest and pretending to understand what I was talking about. Thank you for making this an incredible journey!

U Y F H F W P U I N Q E A F C R T E S M D B K A L S O M A K A Y J Z S Y T F M W
S P A R G A G N F K A Z R V Z A O T I E I M E I R U T B B K F G V H A Z U U I X
U K A N P X U S H U Y I S M G C R T M A U R X N Q N E E T J U L I E N F V U S H
A N U A I S R X H Z T R T K I E O E D N W G A D O E I F P A I L A C R A E Q H T
K Y N K F V S A Z T E P Z S H D P I E C Z N A N V I A B M H F O T S I R K R A H
B G F I B T L W P N W H G N I G O R L K X U T E D H T A C T A N N A M R R E H T
E O L Z K J O R T O J I V I Y R V A P D T V R D L A M Y M T I N N K B E D E Q E
N K N N B G T R W X C L K P R Y H M H O P A A V K L U E K Y H F I W A I X O S B
A J O N P T A Z B A I I E B Z H J C I H W T N C S M O E I R E O J E F L A V X S
R N L Z E P O M Y T P P L E I N A D N O S F Z V G M A C O A H I O D A U G D P E
R S W G W M H R J T H P F E A E B I E I V Q O G I X L A U L W L M C T J N I F I
U X B O G G A G N I P E L H L X W Q R L A U R A F R I Z P T H W Q S S R E Y Q L
C I T G B Y R M R L T G M S T C P H M H H Z A X A G N V X W G O J T O E S H Y J
O U P S B T M B A A L A L D F U C L J Y K G A V O T E Y J K Z B F T M H P W O E
A D B Z M U H X F N D K L T Y O A D Q D A P A P N O B S B D Y H D F L U X F T N

Thank you all so very much!
Samuel

Contents

List of Symbols

Abbreviations:

AFP	Automated fiber placement
CCSA	Conservative convex separable approximation
CLT	Classical lamination theory
CS	Constant stiffness laminate
CSD	Constant stiffness design
CTE	Coefficient of thermal expansion
DAV	Dassault Aviation
DMO	Discrete material optimization
IAI	Israel Aerospace Industries
IFB	Institut für Flugzeugbau, University of Stuttgart
KKT	Karush-Kuhn-Tucker conditions
LP	Lamination parameters
LV	Linear variation
LVD	Linear variation design
NLR	Dutch National Aerospace Laboratories
QI	Quasi-isotropic laminate
RTM	Resin transfer molding
VS	Variable stiffness laminate
VSD	Variable stiffness design

Greek Symbols:

α	A term used to scale the relative contribution of two different responses in an multi-response objective function
$\alpha_{1,2}$	Coefficients of thermal expansion along the primary material directions
α_i	A term containing function derivatives for terms dependent explicitly on laminate thickness
ϵ	In-plane strain
ϵ_c	Principle compressive failure strain

ϵ_t	Principle tensile failure strain
η	Scaling term used in the proximal point algorithm, see page 59
γ	In-plane shear strain
γ	Scaling term used to update the damping term, ρ, between successive design iterations, see page 63
κ	Curvatures related to out-of-plane bending and twisting
κ	Fiber path curvature, rate of change of fiber angles, see page 35
λ	Buckling load multiplier
λ_s	Factor of safety for strength, see page 76
μ	Lagrange multiplier
ν	Poisson's ratio
ϕ	Used to denote the rotation of the axis of variation with respect to the principle material axis when defining fiber paths using linear variation, see page 18
ρ	Term used to scale the convex term of an approximation, see page 60
σ	In-plane normal stress
τ	In-plane shear stress
θ	Fiber angle orientation
θ_k	Ply orientation angle of the k^{th} layer

Roman Symbols:

a	Plate length
A_{ij}	Components of the in-plane stiffness matrix, see page 42
b	Plate width
B_{ij}	Components of the bending-extension coupling stiffness matrix, see page 42
d	Characteristic length when defining fiber paths using linear variation
D_{ij}	Components of the bending stiffness matrix, see page 42
E_1	Longitudinal modulus
E_2	Transverse modulus
f, f_j	Arbitrary (j^{th}) function
f_D	Denotes the convex term appended to obtain a conservative convex separable approximation
F_{ij}	Coefficients of the Tsai-Wu failure criterion, see page 72
f_P	Denotes the function approximation used to obtain conservative a convex separable approximation
f_S	Denotes the total conservative convex separable approximation
G_{12}	Shear modulus
G_{ij}	Coefficients of the Tsai-Wu failure criterion in terms of strain, see page 73
h	Total laminate thickness
$I_{1,2}$	Volumetric strain invariants (1) and maximum shear strain (2), see page 74
K_{po}	Postbuckling stiffness
K_{pr}	Prebuckling stiffness
M	Moment resultant
M	Denotes total number of functions or modes considered
N	Stress resultant

N	Denotes total number of design variables considered
Q_{ij}	Components of the reduced lamina stiffness matrix, see page 40
R	Radius
r_b	Inverse buckling load factor, $1/\lambda$
r_c	Scalar representing structural compliance
r_s	Failure index, see page 77
S	Shear failure stress
$T_{0,1}$	Used to denote the initial (0) and final (1) fiber orientation angle when defining fiber paths using linear variation, see page 18
$T_{d,o,c}$	Design, operating or curing temperature
t_k	Thickness of the k^{th} ply
tr	Matrix trace
U_i	Material invariant properties, see page 40
u_i	Material invariants defined in terms of Tsai-Wu strain coefficients, G_{ij}
$V_{\mathbf{A}}$	In-plane lamination parameters, see page 42
$V_{\mathbf{B}}$	Coupling lamination parameters, see page 42
$V_{\mathbf{D}}$	Out-of-plane lamination parameters, see page 42
W	Width
w	Weight
w_i	Local weighing factor of the i^{th} design region, see page 60
$X_{c,t}$	Longitudinal compressive and tensile failure stress
x_i	Arbitrary (i^{th}) design variable
$Y_{c,t}$	Transverse compressive and tensile failure stress

Vectors and Matrices:

$\boldsymbol{\Gamma}_i$	Material invariant matrices to define laminate stiffness matrices, see page 42
$\boldsymbol{\Lambda}_i$	Material invariant matrices to define thermal stress resultants, see page 43
$\boldsymbol{\mu}$	Vector of Lagrange multipliers
$\boldsymbol{\Phi}$	Matrix of function derivatives with respect to the inverse of the laminate stiffness matrices associated with a given design region
$\boldsymbol{\Psi}$	Matrix of function derivatives with respect to laminate stiffness matrices associated with a given design region
$\boldsymbol{\Omega}$	Vector of function derivatives with respect to the thermal stress resultants associated with a given design region, see page 195
$\mathbf{a}$	Eigenvector
$\overline{\mathbf{B}}$	Strain displacement matrix
$\mathbf{e}$	Vector of average in-plane strains
$\mathbf{f}$	Load vector
$\mathbf{g}$	Gradient vector
$\mathbf{H}$	Hessian matrix
$\mathbf{I}$	Identity matrix
$\mathbf{K}_b$	Global bending stiffness matrix, only used when considering plates
$\mathbf{K}_g$	Global geometric stiffness matrix, only contains out-of-plane degrees of freedom when considering plates

$\mathbf{K}_m$	Global material stiffness matrix, only contains in-plane degrees of freedom when considering plates
$\mathbf{n}$	Vector of in-plane stress resultants
$\mathbf{u}$	Vector of displacements and rotations
$\mathbf{V}$	Vector of design variables including lamination parameters and eventually laminate thickness
$\mathbf{x}$	Vector of arbitrary design variables

Other:

$\bar{\ }$	Terms within the approximation that are dependent explicitly on thickness
$\breve{\ }$	Denotes sensitivity matrices that include the contribution of the convex damping term
$\check{\ }$	Terms within the approximation that are expanded reciprocally
$\hat{\ }$	Terms that have been normalized by, or represent a reference value
$\hat{\ }$	Terms within the approximation that are expanded linearly
$\mathcal{A}$	Area of a given region
$\mathcal{C}$	Arbitrary constant term
$\mathcal{C}_i$	Scalar convex term
$\mathcal{L}$	Lagrangian function
$\mathcal{V}$	Volume of the structure
$\tilde{\ }$	Denotes an approximate function

Subscript:

$_0$	Denotes the point about which an approximation is generated
$_e$	Denotes terms associated with the e^{th} element in a finite element model
$_i$	Counter for design variables or to denote elements of matrices or tensors
$_j$	Counter for functions or to denote elements of matrices or tensors
$_s$	Denotes a symmetric laminate

Superscripts:

*	Used to denote optimum design of a current iteration
^{b}	Denotes terms in the approximation associated with laminate bending stiffness terms
^{L}	Lower bound on design variables
^{m}	Denotes terms in the approximation associated with laminate membrane stiffness terms
Th	Denotes terms associated with thermal loads
^{T}	Vector or matrix transpose
^{U}	Upper bound on design variables

Glossary of Terms

automated fiber placement an automated manufacturing technology that combines individual tow control found in filament winding machines with compaction and cut-restart capabilities found in tape laying machines.

buckling load the load at which a structure loses its elastic stability. Theoretically this is caused by a bifurcation in the solution to the static equilibrium equations.

buckling mode (shape) the deformed equilibrium state of a structure associated with a given buckling load.

classical lamination theory is at the basis of laminate stiffness formulation and allows the in-plane stress resultants and moment resultants to be related to the in-plane strains and laminate curvatures via the so called ABD matrices. Classical lamination theory is essentially an extenuation of classical plate theory to composite laminates, see page 39.

compliance used to refer to the overall structural compliance and essentially represents the inverse of the structural stiffness. The more compliant a structure, the less resistant it is to deformation due to applied loads or moments.

compliance matrix the inverse of the stiffness matrix, and allows in-plane laminate strains and out-of-plane laminate curvatures to be related to the stress resultants and moment resultants, see classical lamination theory.

composite material (or composites for short) are engineered materials made from two or more constituent materials with significantly different physical or chemical properties which remain separate and distinct on a macroscopic level within the finished structure.

conceptual optimum used to refer to the optimal stiffness distribution obtained for a given design problem when using continuous design variables. This optimum does not consider constraints that must be accounted for when manufacturing variable stiffness laminates, hence represents a theoretical optimum.

course (or band) a collection of adjacent tows make up a course or band.

curing the process of changing the physical properties of a matrix material from a liquid to a solid by chemical reaction, by the action of heat and catalysts, alone or in combination, with or without pressure.

curvature constraint a constraint placed on the maximum fiber path curvature to ensure that no local tow buckling or wrinkling occurs during manufacturing. See also minimum turning radius.

curvilinear fiber paths a term often used to refer to variable stiffness laminates, highlighting that the fiber paths are no longer straight.

damping used to refer to an additional term appended to a response approximation used to control the convergence of successive optimization iterations by altering the convexity and conservativeness of the approximation , see page 58.

deposition rate refers to the rate at which fibers are placed on the mold, usually expressed in terms of kilogram per hour.

design region a term used to identify a region with which the considered design variables are associated. When designing variable stiffness laminates, design variables are often associated with the elements or nodes of the underlying finite element model.

direct stiffness modeling when the laminate stiffness matrices in each element or design region are defined directly or via a continuous parametrization, such as lamination parameters.

fiber bridging when tows detach from the mold surface after placement due to excessive convex curvature of the mold.

fiber angle deviation the difference between the designed fiber orientation angle and the actual fiber orientation on the manufactured component.

fiber angle distribution used to refer generically to the spatially varying fiber angle orientation of a given ply or laminate within a variable stiffness composite structure.

fiber areal weight weight of fiber per unit area of tape or fabric.

fiber path denotes the trajectory followed by a given fiber over the surface of a composite part. When using automated fiber placement the fiber path is generally used to denote the trajectory of (the center line of) an entire band or course and not an individual fiber.

gap a void or space between adjacent tows or courses within a ply which may occur during manufacturing.

lamina see ply.

laminate two or more lamina stacked together to form a single material.

lamination parameters are a set of twelve continuous parameters, based on classical lamination theory, which fully describe the stiffness properties of a laminate, see page 41.

linear variation term used to define a class of variable stiffness laminates which consist of a linear variation of the fiber orientation angle between two predefined points along a given direction, see page 18.

minimum cut length minimum length of a tow that can be placed by a fiber placement machine, which is governed primarily by the internal tow-control mechanisms of the machine. Machine software is typically programmed to ignore any tows that are too short.

minimum turning radius the minimum fiber path radius that can be placed by a fiber placement machine to avoid local buckling or wrinkling of tows, see also curvature constraint.

optimization (or mathematical programming) refers to a process in which the best element or solution is selected from some set of available alternatives. Several methods have been developed to solve optimization problems, the most suitable method is highly dependent on the nature of the problem being solved.

overlap partial collocation of adjacent tows or courses within a ply which may occur during manufacturing, resulting in local thickness buildup.

parallel path a path replication strategy in which successive courses within a single play are placed adjacent to each other without any gaps of overlaps occurring at the course boundaries, see page 11.

Pareto front refers to the set of optimal solutions found for a multi-objective optimization problem. Pareto optimal solutions represent solutions for which no improvement in a single objective function can be made without a deterioration in one or more of the remaining objective functions.

ply a single layer of fiber reinforced material within a laminate manufactured by placing several repeated courses using a selected course replication strategy.

reciprocal interpolation used to convert the stiffness matrices defined at the nodes of a finite element model to the stiffness matrices of the associated element. Instead of interpolating the stiffness matrices directly, they are computed by interpolated the corresponding compliance matrices, see page 46.

shifted path a path replication strategy in which successive courses are generated by translating and/or rotating a reference path such that the fiber orientation angle remains the same along a predefined direction, see page 11.

staggering a process in which subsequently placed plies are offset with respect to each other to avoid the collocation of overlaps and or gaps within the laminate, see page 12.

stiffness distribution used to refer generically to the spatially varying stiffness within a variable stiffness composite structure.

stiffness used to refer to the overall structural stiffness, in other words how well a given structure is able to resist deformation due to an applied force or moment.

stiffness matrix is used to relate the stress resultants and moment resultants to the in-plane strains and out-of-plane curvatures of a laminate, see also classical lamination theory.

stress resultant represents the integration of the stresses through-the-thickness of a laminate, see page 41.

tow a bundle of fibers with specific width and fiber areal weight used in automated fiber placement machines. Tows are often manufactured by splitting pre-impregnated tape.

tow drop a term used to refer to the process in which individual tows are terminated during the placement of a course or band with a fiber placement machine.

variable angle tow laminate an alternate term used to refer to variable stiffness laminates.

variable stiffness laminate a laminate within which the fiber orientation angle, and therefore the stiffness properties, vary continuously with spacial location.

CHAPTER 1
Introduction

"Nothing is less productive than to make more efficient what should not be done at all."

Peter Drucker

Structures, and the materials which compose them, are at the core of human wellbeing and development, from providing a safe living environment to transporting us to the moon! In the aerospace industry in particular, where structural reliability, weight and cost are crucial, the search for improved structural solutions is unrelenting. Composite materials are one of the means which the aerospace industry is continuing to explore to meet ever increasing structural demands. Over the past several decades, composite materials have been successfully applied in aerospace for both secondary and primary structural applications. With the first flight of the Boeing 787 becoming a reality and the Airbus A350-XWB on its way, there is no doubt that composites in the aircraft industry have gone mainstream.

The ever increasing commercial interest in composites has driven developments in material systems, manufacturing processes and structural design. For composite structures, more so than for metallic structures, the interdependence of these three fields is of crucial importance. To exploit the benefits of composite material systems fully, appropriate and economically sustainable manufacturing technologies and design methods must be explored. Automated fiber placement (AFP) is one of the manufacturing technologies which has been developed over the past three decades to meet industrial demands, as will be elaborated on in section 1.2. The introduction of new technologies often stimulates novel means of exploiting it. The built-in fiber steering capabilities of AFP machines allows composite laminates to be manufactured with continuously varying fiber orientation angles, yielding a variable stiffness laminate. These laminates allow the full potential of composite materials to be harnessed by enlarging the design space to create substantially more efficient structural designs.

The aim of this chapter is to place the goal of this thesis, to develop an efficient variable stiffness laminate design framework, into context. A short introduction of composite materials is presented in 1.1 followed by a discussion on automated fiber placement machines and its advantages and limitations in section 1.2.1. Variable stiffness laminates are introduced in more detail and the available design approaches are reviewed in section 1.3. Finally the objectives of this thesis will be highlighted, followed by a short description of the thesis layout, in section 1.4.

1.1 A Short Introduction to Composites

A composite material, as the name suggests, is a material system which consists of two or more phases on a macroscopic scale. The constituents will generally have significantly different physical or chemical properties and are combined to create a material with properties superior to those of its constituents. Composite materials typically consist of a discontinuous, stiffer and stronger fibrous phase, called the reinforcement, and a continuous, less stiff phase which is called the matrix. Due to the different chemical compositions of the the separate phases an inter-phase may exist between the reinforcement and the matrix. The properties of a composite material therefore depend on the physical and chemical properties of its constituents, their geometry and distribution. The different phases in a typical composite material are shown schematically in Figure 1.1.

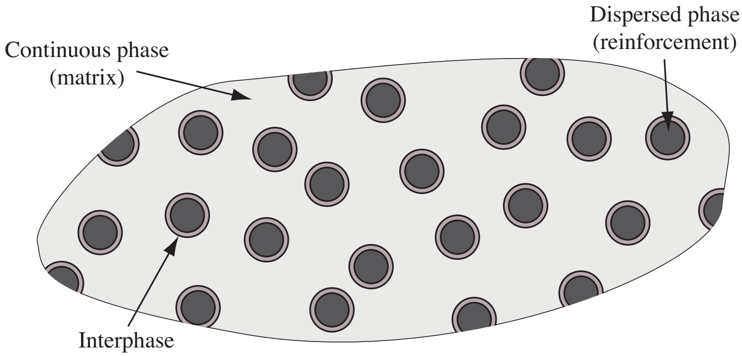

Figure 1.1: *Phases of a composite material*

Fibrous material can be introduced in several different forms, ranging from random chopped strands to woven fabrics to unidirectional tapes or tows. Unidirectional materials with long continuous fibers are predominantly used in aerospace applications. The matrix material, or resin, fixes the fibrous material in the desired geometry after curing. Matrix materials can generally be classified into one of two categories; those which cure irreversibly, known as thermoset resins, and those which soften when heated and set once cooled in a reversible process, known as thermoplastic resins.

Fibers are typically arranged in a sequence of layers, each of which is called a lamina, to form a laminate, as shown in Figure 1.2. The order in which laminae are stacked is referred to as the laminate stacking sequence. Stiffness and strength properties of a single fiber reinforced layer may differ significantly in two mutually perpendicular directions, referred to as principle material directions or principle material axis. In contrast to homogenous metallic materials which exhibit directionally independent elastic properties (isotropic), unidirectional lamina are called orthotropic and exhibit directionally dependent elastic properties in the plane of the layer (anisotropic). Stiffness properties in the fiber direction (E_1), are usually an order of magnitude larger than in the transverse direction (E_2). Strength properties of unidirectional lamina depend both on fiber orientation and on load direction. Lamina strength is typically characterized in terms of five quantities; longitudinal tensile strength (X_t), longitudinal compressive strength (X_c), transverse tensile strength (Y_t) transfers compressive strength (Y_c), and shear strength (S). Stiffness and strength values for several common composite materials are provided in Appendix A.

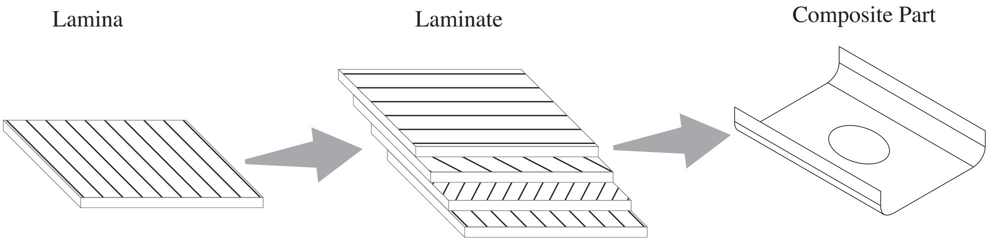

Figure 1.2: *Multiple laminae are stacked to form a laminate, which in turn is integrated into a composite part*

Manufacturing plays an important role in the realization of composite structures. A variety of fabrication methods are available to produce composite parts and typically consist of three steps,

1. Placing fibrous material
2. Impregnating fibers with resin
3. Curing

In a first step fibers are placed with the desired fiber orientation at the appropriate location within the mold. This can be achieved manually, known as hand-layup, or via automated technologies such as filament winding, automated tape laying or automated fiber placement. In a second step the fibers are impregnated with a selected resin. Nowadays manual resin application is uncommon and infusion or injection methods are used, such as resin transfer molding (RTM) and injection molding. In a final step the matrix material is allowed to harden, known as curing. For aerospace applications curing is typically conducted in an autoclave at elevated temperature and pressure to improve the final material properties.

In order to shorten manufacturing times and lower costs, industry continuously aims to reduce the number of manufacturing steps and increase processing speeds. For example, the impregnation step can be eliminated by pre-impregnating fibers before placing them. Similarly in-situ curing techniques are being developed to do away with expensive autoclave curing cycles. The latest generation of thermoplastic composite materials allow all three steps to be combined into one, hence facilitating mass production of composite parts.

Mechanical properties of high performance composite materials are governed primarily by the final placement and orientation of fibers. Traditional manufacturing processes, both open and closed mold, are dependent on skilled labour to precisely place the fibrous material. This is both expensive and prone to errors in fiber alignment and stacking. Hence the composite industry has dedicated a significant amount of research to developing automated manufacturing technologies, such as pick-and-place, tape laying and fiber placement machines. New manufacturing technologies may subsequently lead to novel structural concepts, as will be shown for automated fiber placement.

1.2 Fiber Placement Technology and its Applications

The use of composite materials in commercial aircraft has risen considerably over the past two decades, as can be seen from Figure 1.3. More than 50% of the structural weight of the Boeing 787 and the Airbus A350 consists of composite material. According to recent market research by Lucintel, the value of composite use in the global aerospace market is estimated to reach a total of $5.1 billion towards the end of the decade. With such large amounts of composite material being used, the aerospace industry has invested heavily in developing technologies to reduce costs and improve efficiency. Automated fiber placement technology aims to meet these goals by,

- increasing automation / reducing manual labour
- increasing production volume
- improving product quality and reproducibility
- reducing the number of rejected parts
- reducing material waste, by only placing the required material

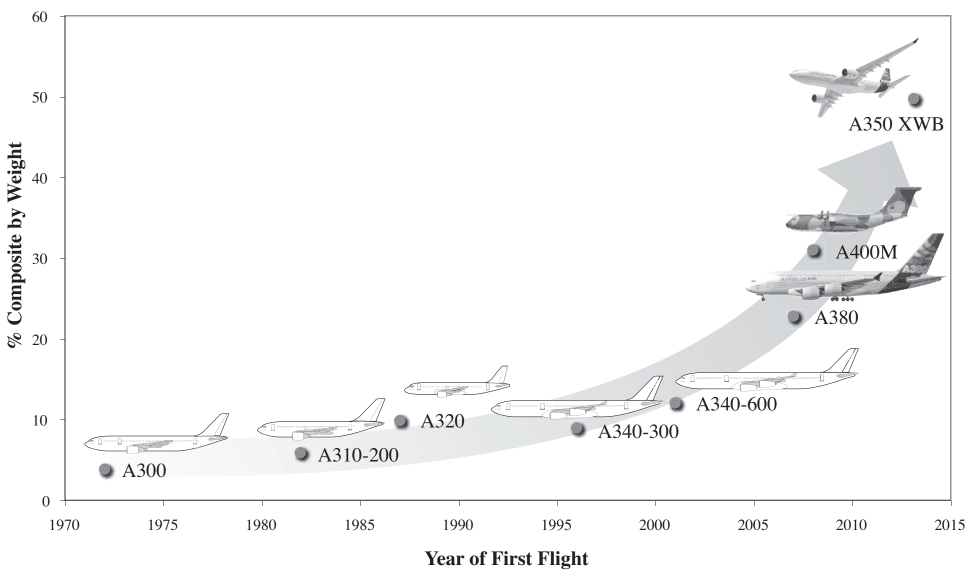

Figure 1.3: *Trends in the use of composite materials in Airbus aircraft, similar trends are seen for the equivalent range of Boeing aircraft*

1.2.1 Overview of Fiber Placement Technology

The development of Automated Fiber Placement (AFP) machines started in the late 1980s; AFP is a unique composite manufacturing technology which combines individual tow control found in filament winding machines with compaction and cut-restart capabilities of automated tape laying. Modern fiber placement systems consist of seven axes, a 6-axis robotic arm or gantry assembly and a rotational axis of the mandrel, an example can be seen in Figure 1.4. Current AFP machines allow up to 32 individually controlled tows, collectively known as a course or band, to be placed on an arbitrary surface. Tows can be added or dropped at any point along the path of the machine head, to increase or decrease the total course width as required. Tows typically vary in width from an eighth of an inch (3.2 mm) to an inch (25.4 mm). AFP machines can be adapted to accommodate the wide range of fibrous materials in use in the aerospace industry, such as carbon, aramid and glass. The majority of AFP machines currently in service process thermoset pre-impregnated materials. Thermo-plastic fiber placement and dry-fiber placement systems are showing great promise for future applications.

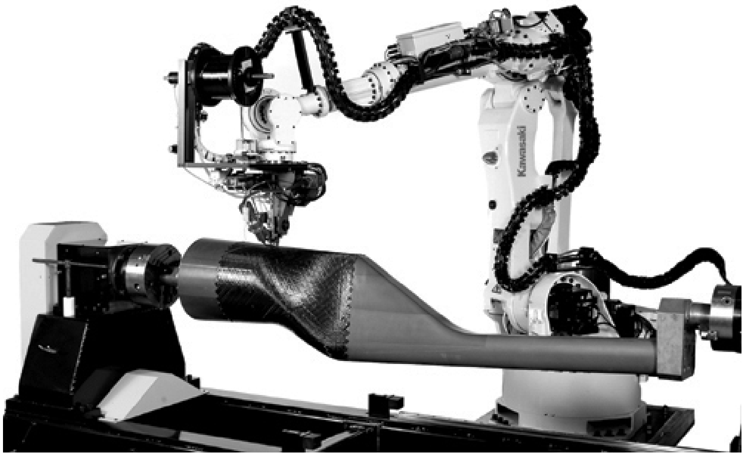

Figure 1.4: *Example of an advanced fiber placement machine (Automated Dynamics)*

Tows are placed on a mandrel surface via a tow placement head, shown schematically in Figure 1.5. The tows are typically guided from a climatically controlled creel chamber, where pre-impregnated material is stored on bobbins, to the mold surface via a network of individual tow guidance rollers and tensioning mechanisms. Current fiber placement machines use passive tow-feeding, where friction between tow, compaction roller and tool surface provides the required force. Tows can be cut and restarted individually via a cutting mechanism and restart rollers. A heating unit is placed prior to material deposition to activate material tackiness which improves adhesion to the mandrel surface and finally a compaction roller places the fibers securely on the mold's surface.

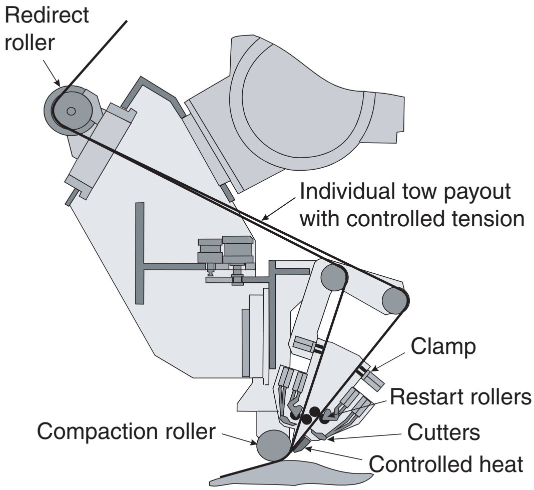

Figure 1.5: *Schematization of a fiber deposition head used for automated fiber placement (Reproduced from Evans Evans (2001))*

1.2.2 Manufacturing Characteristics and Limitations

As with any manufacturing technology, there are always process specific aspects which should be taken into account when designing. Several issues may arise with automated fiber placement related either to part geometry, the required fiber path or to machine specifications. These issues and the parameters influencing them are summarized in Table 1.1 and are treated in more detail in this section.

Table 1.1: *Overview of manufacturing issues related to automated fiber placement and the parameters which influence them*

Issue	**Influenced by:**					
	Tow Width	Course Width	Fiber Path	Material	Machine	Geometry
Jagged Boundary	✓	✓	✓			
Min. Cut Length				✓	✓	
Collision					✓	✓
Fiber Bridging			✓	✓	✓	✓
Min. Turning Radius	✓			✓		
Gaps or Overlaps	✓	✓	✓			✓
Fiber Angle Deviation		✓	✓			✓
Deposition Rate	✓	✓	✓	✓	✓	✓

Part, Ply or Course Boundaries

In order to place a course its initial and end point must be defined. In fiber placement software this is generally achieved using boundaries, which can be natural such as part edges or user defined such as ply boundaries. A boundary may also be defined between intersecting courses. Most modern fiber placement machines allow tows to be terminated individually. Since tows can only be cut normal to their placement direction, jagged or saw-tooth edges will occur at boundaries which are not normal or parallel to the placement direction, as can be seen in Figure 1.6. The jagged edge will result in either small gaps, overlaps or a combination of the two. The gap or overlap size is controlled by a coverage parameter. If tows are not permitted to overlap a boundary, Figure 1.6(a), it is referred to as 0% coverage; 50% coverage, Figure 1.6(b), is used when half of the tow overlaps the boundary and 100% coverage refers to the case where no gaps are present at the boundary, as shown in Figure 1.6(c).

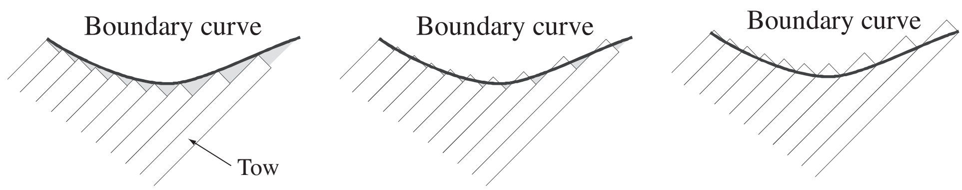

(a) 0% Coverage (b) 50% Coverage (c) 100% Coverage

Figure 1.6: *Jagged edge formed at a boundary for different coverage parameter values (Reproduced from Tatting and Gürdal (2003))*

The boundary quality is influenced by tow width if individual tow cutting is available or by band width if all tows must be cut simultaneously. The angle between the boundary and the placement direction also influences the size of the gaps and overlaps. If tows approach the boundary perpendicularly no gaps or overlaps are formed, however, if the tows are almost parallel to the boundary, large, slender, triangular gaps or overlaps will be present.

Minimum Cut Length

When placing a tow it is fed by pinching rollers from the cutting mechanism to the compaction roller at the mold surface, as can be seen from Figure 1.5. It is therefore not feasible to place a tow in a controlled manner that is shorter than the distance between the cutting mechanism and the compaction roller. A constraint on a minimum cut length is imposed to ensure that each tow can be correctly placed. The constraint is often implemented directly in the fiber placement machine management software, which simply does not allow the machine to place tows shorter than this predefined length. A designer should keep this in mind as it may lead to unwanted voids in the laminate or at ply boundaries, as can be seen in Figure 1.7. The unwanted voids can be accounted for by increasing the length of tows which are too short, however, this may lead to undesired overlaps.

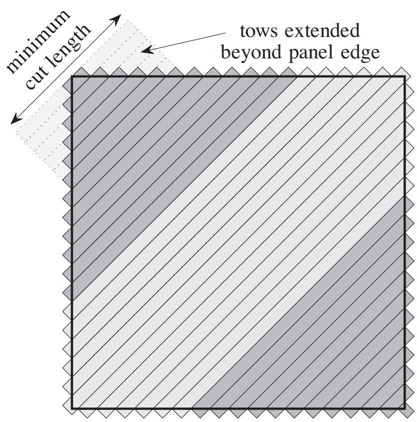

(a) Tows must be extended to exceed the minimum cut length if they are to be placed

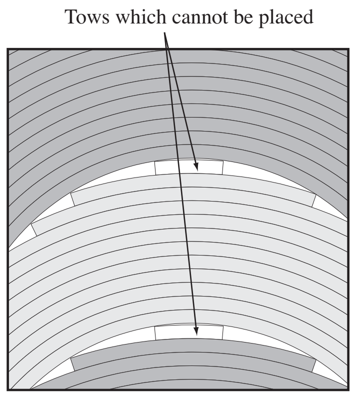

(b) Internal tows are not placed if they violate the minimum cut length constraint

Figure 1.7: *Possible issues which may arise due to the minimum cut length constraint (Reproduced from Blom (2010))*

Machine-Mold Collision

In automated manufacturing processes a machine's working envelope dictates possible part dimensions. The machine envelope is typically defined in terms of maximum travel along, and maximum rotation about the x, y and z axes. In order to manufacture large parts a track is often incorporated such that a robot arm or gantry translate over a larger distance along a single axis. Modern fiber placement software allow production runs to be simulated in advance to ensure that all fiber paths are manufacturable without running into machine limitations. Collision avoidance sensors may also be included on the machine head directly as a security measure. When placing fibers on parts with concave surfaces it is important to limit the minimum part radii such that the machine head does not impact the mold surface, as shown in Figure 1.8.

Fiber Bridging

Another aspect which must be considered when defining the minimum allowable concave part radius is a phenomenon called fiber bridging, shown schematically in Figure 1.8. Tows are always subject to tensile forces in the feeding mechanism and may therefore separate from the mold surface when placing on concave sections. Fiber bridging and therefore the minimum concave radius are influenced by material properties, fiber path and machine parameters. Materials with more tack are less likely to release from the mold after placement and hence can follow tighter curvatures. Machine parameters such as compaction pressure, placement speed, heating temperature and tow pretensioning forces may also influence the minimum allowable mold radius.

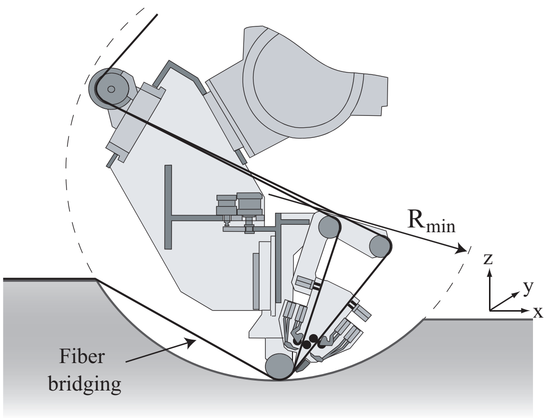

Figure 1.8: *Concave part geometry may lead to machine-mold collisions or fiber bridging*

Minimum Turning Radius

Fiber steering may be introduced either to follow geometric contours of a part or as a design feature to improve structural efficiency. In order to follow a steered path, individual tows are forced to deform in-plane. The inner radius of a steered tow is smaller than the outer radius, hence resulting in compressive forces along inner edge and tensile forces along the outer edge. If the compressive forces exceed a specific threshold, local fiber buckling will occur. The resulting out-of-plane undulations are undesirable since they adversely affect laminate properties. A minimum turning radius, or maximum allowable curvature, can therefore be defined such that no fiber buckling occurs. The curvature constraint can be applied at tow or course level. The minimum turning radius is influenced by tow width, material stiffness and tackiness and by machine parameters such as compaction pressure and placement speed.

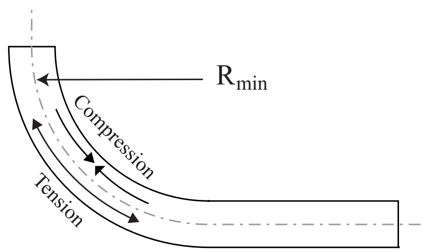

Figure 1.9: *A minimum turning radius should be defined to mitigate local fiber buckling along the tow inner radius due to excessive compressive forces*

Gaps and Overlaps

In order to manufacture a ply that covers the entire mandrel surface, several adjacent courses must be placed. For parts which are not simply multiples of the course width, it is important to consider the course repetition pattern as it influences the final laminate configuration significantly. Gaps, overlaps or fiber angle deviations may occur depending on how adjacent courses are placed. To illustrate this consider the conical structure, represented by the developed two dimensional surface, shown in Figure 1.10. It has to be fully covered by a 0° ply, which is defined by projecting the axis of revolution onto the cone's surface. The geometric nature of the example requires more material to be placed on the right side of the cone than on the the left side.

Two course replications strategies are typically used, which are known as the parallel path method and shifted path method. Parallel paths are created by placing each course adjacent to the previously placed course, without allowing any gaps or overlaps to occur at the course boundaries, as shown in Figure 1.10(a). The parallel path method is by far the most common path replication strategy and is used by default by most automated fiber placement machines. The consequence of this placement strategy is that each path, other than the original path, may be misaligned with respect to the true 0° direction on the mandrel surface. The degree of misalignment increases as more parallel paths are placed. A possible remedy is to split the ply into several segments within which the courses remain parallel, as shown in Figure 1.10(b). A consequence of segmenting the ply is that gaps and/or overlaps will occur at the segment boundaries.

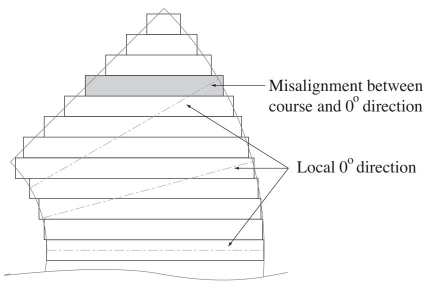

(a) Parallel path

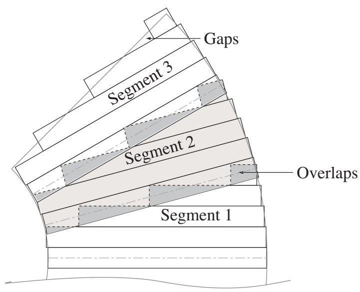

(b) Parallel path with segments

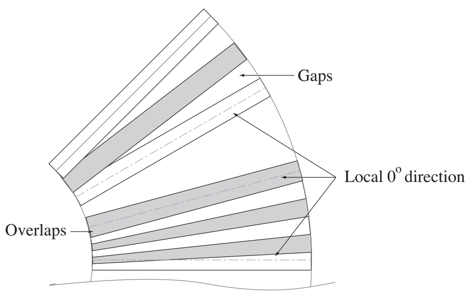

(c) Shifted path

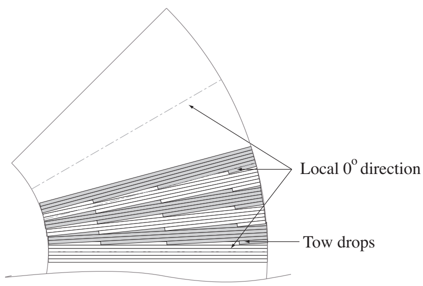

(d) Shifted path with tow drops

Figure 1.10: *Illustrative example of different path replication strategies to create a laminate from multiple courses on the surface of a cone. The local* 0° *direction is defined by projecting the axis of revolution onto the surface.*

The shifted path method consists of translating and/or rotating a reference path such that the fiber angle orientation remains the same along a predefined direction. In Figure 1.10(c) path shifting is illustrated for two cases; in the lower half paths are shifted such that no gaps occur, resulting in significant course overlaps at the cone's apex. In the upper part of the cone, paths are shifted such that no overlaps occur, resulting in large gaps at the cone's base. The shift distance can also be selected to be in between the aforementioned limits, resulting in a combination of gaps and overlaps. If the machine allows individual tows to be cut and restarted, they can be added or dropped along the path to avoid gaps and overlaps, as shown in Figure 1.10(d). Individual tows can also be dropped for the segmented parallel path method, reducing gap or overlap sizes.

When fiber steering is introduced, similar phenomena appear for the different path repetition strategies, as can bee seen in Figure 1.11. If a steered path is defined by its center line, subsequent parallel paths will require the fiber path to change in order to remain adjacent to the previous path. The designer should keep this in mind as it may result in fiber angles that do not match the intended fiber angles corresponding to the designed fiber path. Parallel paths also require a change in fiber path curvature, which may subsequently trigger the constraint on minimum turning radius. Gaps or overlaps will occur when paths are defined by shifting the original path along a fixed axis, as can be seen in Figure 1.11(b). Overlaps can be avoided by dropping tows along the fiber path, as shown in Figure 1.11(c).

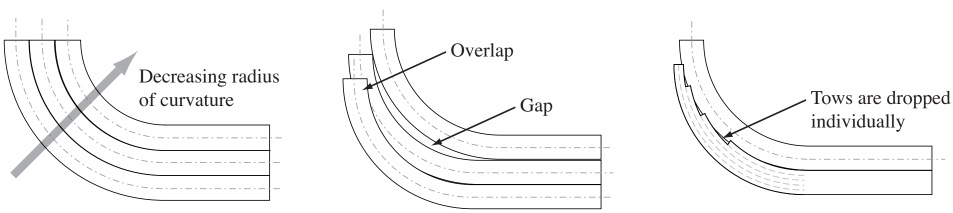

(a) Parallel path (b) Shifted path (c) Shifted path with tow drops

Figure 1.11: *Schematic overview of three different path steering strategies*

No matter which path repetition method is used, small gaps and overlaps will undoubtedly occur. To retain structural integrity it is important that the designer ensure these small defects are not concentrated in a single region of the structure. Gürdal et al. (2005) introduced the concept of ply shifting or staggering as a means of avoiding the collocation of imperfections within a laminate. The same method, illustrated in Figure 1.12, can be used to reduce the amount of thickness buildup that occurs for laminates manufactured using the shifted path method while allowing tow overlaps.

Fiber angle deviations

Each course placed within a ply consists of several adjacent tows which are parallel to one another. Therefore, similar to the aforementioned parallel path strategy, fiber angle deviations may occur between each tow in the band when paths are steered, as

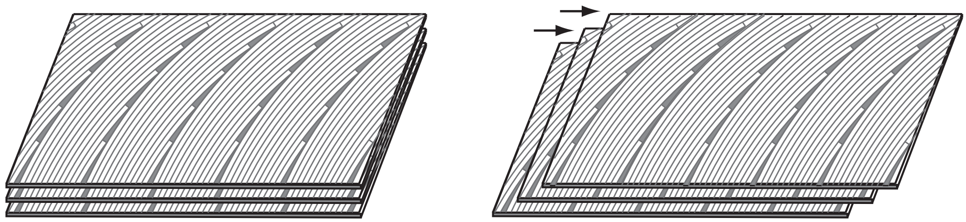

(a) Steered plies without staggering

(b) Steered plies with staggering

Figure 1.12: *Local imperfections can be evenly distributed throughout the laminate by staggering plies (Reproduced from Lopes (2009))*

illustrated in Figure 1.13. When the desired fiber angle at the center of the course, θ_c, is defined along a specific axis, x, the fiber angles at other locations along the same axis in the course are not necessarily the same. The designer should therefore keep in mind that defining fiber angles based on the fiber angle at the course centerline may lead to discrepancies between the model and the manufactured part. The largest deviations occur at the course boundaries, hence this effect is more pronounced for wider courses. The fiber path and part geometry also influence the amount of the fiber angle deviation that occurs. For example, straight paths on a flat surface will not result in any fiber angle deviation. In the case of the aforementioned conical structure, small deviations with respect to the local 0° direction will occur within each course even if the course centerline is aligned correctly.

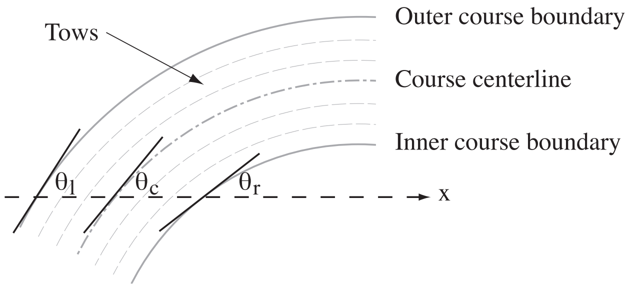

Figure 1.13: *When steering fiber angles at the course boundary may deviate from that defined at the center ($\theta_l > \theta_c > \theta_r$)*

Another source of fiber angle deviation may arise directly from choices made to simplify manufacturing. It is common to manufacture the 90° ply in a single, continuous winding path for structures of revolution, such as cylindrical and conical shells, however, this implies that the fiber path should be rotated slightly, usually a few degrees depending on the structural radius and course width, with respect to the true 90° direction.

Deposition Rates

A crucial aspect of manufacturing fiber placed parts is the rate at which they can be produced. Deposition rate is the most common performance metric for fiber placement, in other words, how much material can be placed in a fixed amount of time [kg/hr]. It is therefore no surprise that AFP machine manufactures are continuously improving the speeds at which their machines can operate and increasing the number of tows which can be placed simultaneously. Other than machine specifications, almost every aspect relating to fiber placement influences the deposition rate. For example, placing wider tows allows more material to be placed per pass, however, as a consequence steering performance will diminish and will result in a process resembling automated tape laying. Another ramification of using wider tows is that gaps and overlaps in the structure will become larger and may therefore significantly impact laminate properties. Material properties such as tackiness and required activation energy also influence process speeds. Similarly, the chosen stacking sequence, desired amount of steering and part geometry will affect the achievable deposition rates.

1.2.3 Fields of Application

Fiber placement technology has improved drastically over the past three decades and is being used by an increasing number of aerospace manufacturers (Evans, 2001). Boeing Helicopters was the first company to apply fiber placement in a production environment in the early 1990's. Boeing and Hercules were funded to develop a process to fiber place the aft fuselage section for the Bell/Boeing V22 Osprey. Initially the aft fuselage section was built up of nine individual panels built using hand layup, with redesigning for fiber placement a single monolithic structure could be manufactured allowing the required amount of fasteners to be reduced by 34%. The trim and assembly labour was reduced by 53% and the amount of material scrap produced was reduced by 90%. Fiber placement was later applied for the production of fuselage skins of the F/A-18 Super Hornet, allowing Northrop Grumman to reduce labour costs by 38% with respect to hand layup.

Fiber placement is also being used in commercial applications. Raytheon Aircraft, uses AFP to manufacture fuselage sections for its Premier I and Hawker Horizon business jets. The sandwich structure used for the fuselage is manufactured from a honeycomb core and graphite facesheets. The design allows for a fuselage shell without frames or stringers, eliminating the need for riveting and resulting in more useable space for passengers or cargo. The improved design has allowed Raytheon to realize weight savings, material savings, a reduced part count, a reduced tool count, reduced shop flow time and increased part quality.

Now, well into the 21st century, fiber placement had become mature enough to be applied on a large scale in the commercial aviation environment. The Boeing 787 Dreamliner was the first commercial airliner to be manufactured primarily from composite materials. Several manufactures are working together with Boeing to fabricate wing and fuselage sections at multiple locations around the world. The cured parts are subsequently transported to the Boeing Everette plant for final assembly. For example, Alenia Aeronautica manufactures section 44 and 46 in their new composite facility in Grottagie. Each section is in the region of 10m long, has a diameter of approximately 6m and contains roughly 2000kg of carbon fiber. The sections are manufactured using the latest generation fiber placement machines made by Ingersoll Machine Tools. Similarly for the next generation wide-body aircraft from Airbus Industries, the A350 – XWB, large portions of the fuselage barrel and wings are and will be manufactured using fiber placement technology.

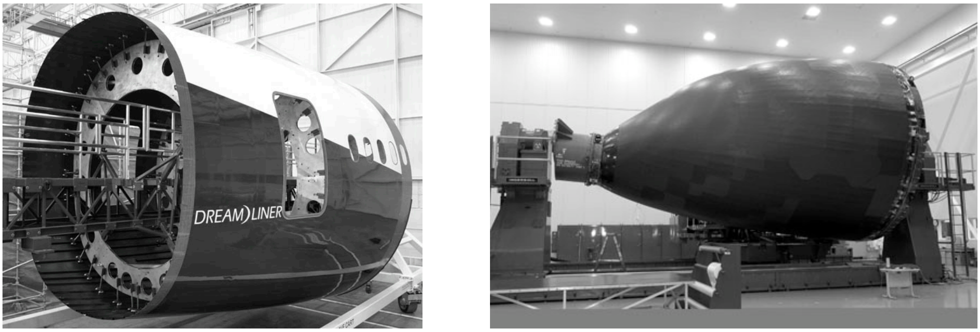

(a) Fuselage section (b) Nose cone

Figure 1.14: *Automated fiber placement is used to manufacture large sections of the Boeing 787 Dreamliner (Source Boeing Media)*

Fiber placement technology has made it possible to produce large yet intricate structures while helping to reduce labour costs, the amount of scrap material produced, and it has increased product quality. However, AFP remains an expensive technology and therefore is only applied when it can be economically justified. Aircraft often have service lives in excess of 60 000 flight hours and millions of nautical miles. Large operating cost savings can be achieved by reducing structural weight and increasing maintenance intervals. The aerospace sector, where relatively large, expensive parts are produced in small series, has been an ideal industry to introduce and apply fiber placement technology, however, as machine costs start to decrease and production rates increase fiber placement technology becomes attractive for other end users, such as the automotive, maritime and wind-energy industries, which will or are starting to integrate fiber placement into their production environment.

1.3 Variable Stiffness Laminates and their Design

Laminates traditionally consist of several plies, stacked in a predefined order, with uniform fiber angle orientation throughout each ply. The stiffness properties of these laminates are therefore independent of spatial location and these laminates are therefore referred to as constant stiffness laminates. Variable stiffness laminates are laminates within which stiffness properties *are* a function of spatial location, in other words stiffness properties change from point to point. This stiffness variation may be discrete, by defining several different patches within a laminate, or continuous, by varying the fiber angle orientation continuously within a ply's domain. Schematic examples of both discrete and continuous variable stiffness laminates are shown in Figure 1.15.

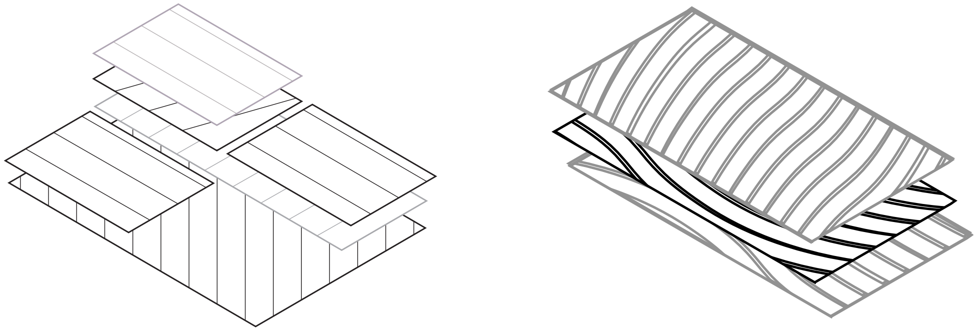

(a) Multi-patch laminate

(b) Continuous fiber angle variation

Figure 1.15: *Schematic representation of two variable stiffness laminates. The first is achieved by defining several different constant stiffness patches within a single laminate and the second consisting of one or more plies with continuously varying fiber angle orientation*

Continuous stiffness variation is essentially a generalization of discrete stiffness variation, which still stems from the more traditional method of defining laminates using a fixed stacking sequence. The built-in fiber steering capability of automated fiber placement machines makes it possible to steer tows in practically any direction on the mandrel surface. This provides a unique opportunity to harness the anisotropic properties of composite materials by steering fibers such that the desired stiffness is achieved at the desired location within a laminate. Therefore, in the context of this thesis, the term variable stiffness laminates refers to the most general form of stiffness variation, namely laminates within which the fiber angle in a ply is allowed to vary continuously with spacial location. In the literature these laminates may also be referred to as laminates with curvilinear fiber paths or variable angle tow laminates.

The primary focus of the research conducted for this thesis was to develop an efficient design framework for variable stiffness laminates, such that the advantages offered by automated fiber placement and composite materials are fully exploited. It is therefore important that the reader clearly understands what variable stiffness laminates are, how they are modeled, analyzed and ultimately designed. In this section the aforementioned topics will be clarified in the form of a succinct review of the literature. The aim is to provide a broad overview of methods currently available to model, analyze and design variable stiffness laminates. For a more in-depth evaluation of parameterization schemes and the optimization algorithms used for variable stiffness design the interested reader is referred to an extensive review provided by Ghiasi et al. (2010). Literature relating specifically to the topic of each subsequent thesis chapter is referred to and discussed where applicable.

1.3.1 Modeling Variable Stiffness Laminates

In order to study variable stiffness laminates and structures, a systematic approach to defining stiffness variation within a laminate needs to be defined. Several approaches have been developed in the past, which can be roughly classified into three categories:

one, discrete stiffness representation, where the fiber orientation angles and stacking sequence for each individual design region are defined independently. Two, direct stiffness modeling, where the terms in the stiffness matrices describing the laminate stiffness properties for a given design region are defined directly as variables or indirectly via a set of intermediate variables. Three, the efforts made to ensure continuity of the fiber path definition using a functional representation of the fiber paths and varying a predefined set of parameters to change the path trajectory.

Discrete Stiffness Representation

Discrete fiber angle representation is the most commonly used method for defining stiffness variation within a structure. It is essentially an intuitive extension of a multi-patch laminate, as shown in Figure 1.15(a), to a level where a laminate is defined locally at *each* point in the structure. Practically this results in a fiber angle and stacking sequence being defined at specific points within a discretized structure, as shown in Figure 1.16. The variable stiffness laminate discretization is typically based on the underlying discretization required for structural analysis, such as when using the finite element method.

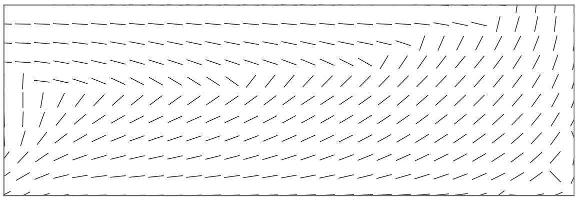

Figure 1.16: *Example of discrete fiber angle distribution (Source Setoodeh et al. (2006b))*

Hyer and Charette (1991) were among the first to study variable stiffness laminates and the influence of stiffness tailoring on the buckling load of a panel with a hole. They present a finite element model of a quarter plate, which is discretized into 18 elements. Subsequently, a single fiber angle orientation is used as a design variable within an element. Hence each element consists of a unique laminate of the form $(\pm 45/\theta_6)_s$, where θ is considered to be a local design variable and constant within that element. Even with only a single design variable per element, the tailored design shows significant improvements with respect to a baseline for both buckling and strength. A similar method is presented in Katz et al. (1989), in which the fiber angle orientations for a panel with a hole are designed for maximum compressive strength.

In order to expand the design space, the next logical step is to define a design variable for the orientation of each ply within a local laminate, as has been done in Hammer (1999). Associating design variables with the fiber orientation angles defined for each element has the advantage of providing the largest possible design space for a given mesh density. The drawback of this approach is that fiber continuity is difficult to impose and ensuring convergence for discrete stacking sequences remains challenging.

Stegmann and Lund (2005) introduced a method termed, discrete material optimization (DMO), in which the stiffness properties of each finite element are defined by selecting the most suitable stiffness properties from a predefined set of materials. The method stems from topology optimization where the objective is to determine if a specific element should or should not contain material. At element level, the constitutive matrix is setup as a weight sum of candidate material constitutive matrices, however, for meaningful results, the weights of all but one material must be forced to zero, as is commonly done in topology optimization. The same method has been extended to multi-layer structures. A drawback of this method is the need for defining candidate materials and, as with the previous method, ensuring fiber angle continuity between adjacent elements is difficult.

Direct Stiffness Modeling

Instead of using local stacking sequence information to indirectly model local laminate stiffness properties, it is also possible to consider the terms in the stiffness matrices used for analysis directly. In terms of classical lamination theory, see subsection 2.3.1, this implies that the entries of the ABD matrices are considered as design variables. The advantage of this approach is that the number of design variables are independent of the number of plies in the laminate. The design variable set is restricted to the 18 entries of the symmetric ABD matrix. Difficulties with this method can arise since the design variables are not free to be chosen arbitrarily. This may be remedied by defining the stiffness matrix entries via intermediate variables.

Lamination parameters, first introduced by Tsai and Pagano (1968), are the most commonly used direct stiffness parameterization. Lamination parameters uniquely define a laminates stiffness properties and allow an arbitrary stiffness distribution to be modeled with the minimum number of design variables regardless of the number of discrete layers. In the most general case a total of 12 lamination parameters together with total laminate thickness are required to define the ABD matrix fully. Lamination parameters allow the local stiffness properties to be defined using a finite set of convex, continuous design variables, and are therefore well suited to optimization using efficient gradient based algorithms. Post-processing is required to determine the actual fiber angle distribution from the lamination parameter distribution.

The polar-method, originally presented by Verchery (1979), is a minimal invariant representation of in-plane elasticity. Laminate stiffness properties can be expressed based on 18 parameters in the most general case. Vannucci (2006) has shown that several laminate design problems can be expressed based on physical interpretation of the polar invariants and can be conveniently solved from a mathematical perspective. Even though laminate stiffness can be expressed in terms of continuous design variables, the design space has been shown to be non-convex. As is the case with lamination parameters, the stiffness properties must be converted to a laminate stacking sequence in a post-processing step.

Functional Fiber Path Representation

Olmedo and Gürdal (1993) were the first to introduce a fiber path parameterization scheme to study buckling of variable stiffness plates. They define the fiber angles as varying linearly along either the x or y axis and the authors demonstrate buckling load improvements of up to 80% with respect to the best straight fiber designs. Later, Tatting and Gürdal (2002) generalize the path definition formulation to vary linearly along an arbitrarily defined axis, x', such that the fiber angle, $\theta(x')$ is defined as,

$$\theta(x') = \phi + (T_1 - T_0)\frac{|x'|}{d} + T_0 \tag{1.1}$$

where T_0 and T_1 are the fiber angles at the beginning and the end of the characteristic length d. The orientation of x' with respect to the global x-axis is defined by the angle ϕ. The terms in equation (1.1) are represented graphically in Figure 1.17. Olmedo and Gürdal (1993) also introduce a compact notation such that plies with linear variation can be denoted as $\phi < T_0, T_1 >$.

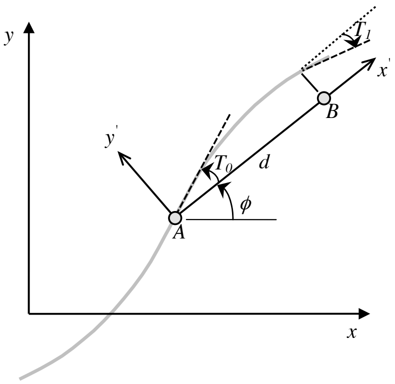

Figure 1.17: *Schematic representation of a fiber path defined using linear variation, which can be compactly denoted as $\phi < T_0, T_1 >$ and where d represents a predefined length over which the variation occurs (Reproduced from Gürdal et al. (2008))*

Blom et al. (2008) extend the formulation of linear variation to include multiple segments such that the fiber angle becomes a function of predefined angles at fixed stages, as $< T_0, T_1, \ldots T_n >$. An example of multi-segment linear variation on a conical surface is presented in Figure 1.18. Including multiple segments provides additional design freedom when more intricate stiffness variation needs to be achieved. In further work, Blom et al. (2009c) report on the manufacturing and testing of a variable stiffness shell designed for bending using piece-wise linear variation of the fiber orientation angle along the circumferential coordinate. The advantage of linear variation is that only a few design variables are necessary to define stiffness variation and fiber continuity is guaranteed, however, the design space is always limited to the set of design variables used for the parameterization.

Blom et al. (2009a) also investigate the use of geodesic, constant angle and constant curvature paths to prescribe fiber angle variation over conical shells as shown in Figure 1.19. Geodesic paths have no in-plane curvature and are well known from filament winding. A constant angle path is defined such that the fiber angle orientation along the entire path remains the same. Similarly, constant curvature ensures that the fiber path curvature is uniform along the path. In all three of the aforementioned definitions the fiber path is fully described by a single angle and the part geometry, hence significantly limiting the design freedom. Since the critical curvature for each of the path definitions is readily available, curvature constraints can be applied without

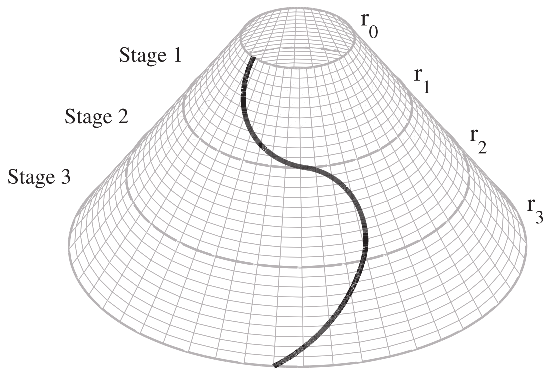

(a) Cone with three stage linear variation

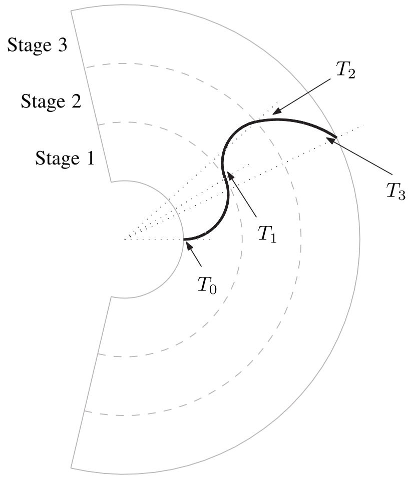

(b) Cone developed to a 2D surface

Figure 1.18: *Example of multi-stage linear fiber angle variation on a developable surface, with* $T_0 = 0°, T_1 = 80°, T_2 = -30°, T_3 = -60°$ *(Reproduced from Blom et al. (2008))*

difficulty. Other methods of using functions to define fiber angle variation along a single axis have been proposed. Parnas et al. (2003) present a method which uses cubic polynomials to define fiber paths, whereas Honda et al. (2008) define fiber paths as continuous parabolic functions. These methods all have the advantage of ensuring fiber path continuity, however, the scope of the number of design variables, and therefore the scope of the solution, is often limiting.

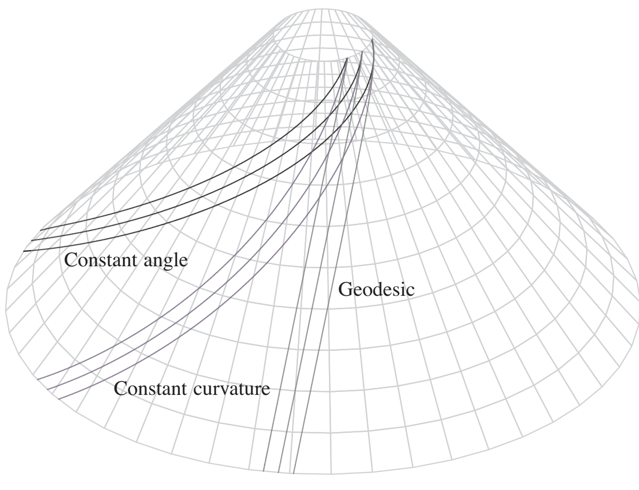

Figure 1.19: *Example of a geodesic, constant angle and constant curvature path on a cone (Reproduced from Blom et al. (2009a))*

In order to increase the number of design variables and hence expand the available design space, fiber paths can be expressed in terms of more complex functions such as Lobatto polynomials, as has been done by Alhajahmad et al. (2008). In the formulation presented by Alhajahmad et al. (2008), the definition of non-linear fiber angle variation along both spatial surface coordinates is possible. The fiber angle orientation at normalized coordinate locations (ξ, η) is defined as,

$$\theta(\xi, \eta) = \sum_{i=0}^{m-1} \sum_{j=0}^{n-1} T_{ij} L_i(\xi) L_j(\eta) \tag{1.2}$$

where m and n are the the number of basis functions, L_i and L_j are the Lobatto polynomials and T_{ij} are the unknown coefficients used as design variables. The number of design variable can therefore be increased by increasing the number of included basis functions m and n. An example of fiber paths defined using Lobatto polynomials is presented in Figure 1.20.

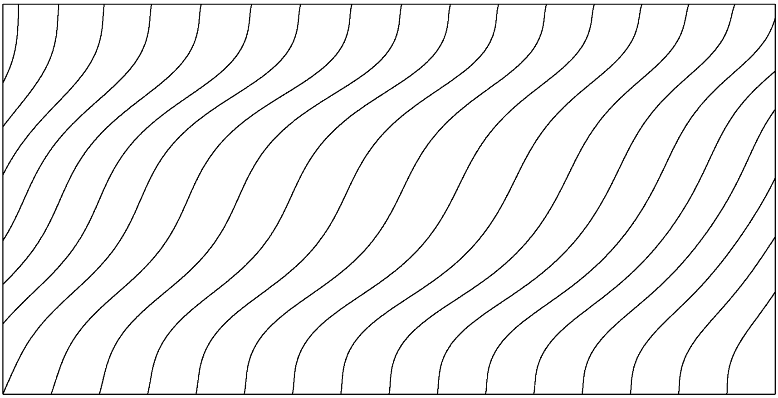

Figure 1.20: *Example of fiber paths defined using Lobatto polynomials on a rectangular domain (Reproduced from Alhajahmad et al. (2008))*

Klees et al. (2009) use hierarchical shape functions, based on Lobatto polynomials, to express fiber angle distributions over the plate. Similarly to the formulation presented by Alhajahmad et al. (2008), the number of design variables can be increased by increasing the polynomial order. An additional advantage of the formulation presented by Klees et al. (2009) is that curvature estimates, which are required to apply manufacturing constraints, can be efficiently computed.

Nagendra et al. (1995) use non-uniform rational b-splines, also known as NURBS, to generate a set of manufacturable basis paths. The global fiber paths are subsequently defined as a linear combination of the pre-defined basis paths. These scaler multiples are therefore used as design variables. NURBS are well suited to defining paths on complex surfaces and are often used directly by fiber placement machines to define path trajectories, however, determining a suitable set of basis paths which are used for design is no trivial task and therefore limits the applicability of this approach.

Schueler et al. (2004) present two methods of approximating the location of fiber placed tows on a NURBS surface based on a pre-defined initial curve. The methods focus on how to propagate arbitrarily defined paths to cover the entire part surface. The first method consists of approximating offset curves on a free form surface using the geometric constraints of the fiber placement process. The second method is used to approximate a curve on a free form surface that can be used to generate a laminate family ply. Both methods require the definition of an initial path, and since this approach models every tow, it allows the designer to consider the actual manufactured laminate instead of a functional representation thereof.

Defining paths using streamlines based on functional requirements is another possibility. Tosh and Kelly (2000) present two methods for defining fiber trajectories in a laminate. The first makes use of principle stress vectors, which always result in two patters: tensile principal stress trajectories and compressive principal stress trajectories. Depending on the loading, one of these two patterns will be dominant and therefore the suggestion is made to add more plies following the dominant pattern. An example of tensile principle stress trajectories for a pin-loaded hole is presented in Figure 1.21. The second method makes use of load paths, which are essentially the streamlines for a given load level. In other words they are defined as the regions in which the load in a selected direction remains constant from the point of application in a structure through to the point of reaction out of the structure. Both methods assume that the intrinsic information available from stresses or load levels is sufficient to define a fiber path, however, this may not necessarily be the case. Additionally it is difficult to ensure manufacturability of the defined paths.

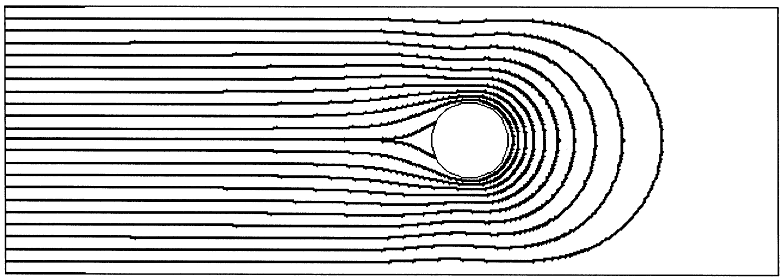

Figure 1.21: *Example of tensile principle stress trajectories for a pin-loaded hole(Reproduced from Tosh and Kelly (2000))*

1.3.2 Analyzing Variable Stiffness Laminates

Once the structural stiffness distribution has been defined, the desired response information must be computed, which is typically done using analytical, semi-analytical or numerical methods. Analytical methods typically require numerous simplifying assumptions to be made before being able to solve the governing equations. Hence their use in modeling variable stiffness responses is limited, however, several semi-analytical methods have been used in the past.

Semi Analytical or Specialized Codes

The Ritz method, which is a direct method for finding approximate solution to boundary value problems, has been applied extensively in the past to compute vibration and buckling modes. However, to compute buckling modes of variable stiffness laminates, the complex pre-buckling plane stress state must first be modeled. Martin and Leissa (1989) are among the first to develop a procedure based on the Ritz method to determine both stresses and displacements for sheets with arbitrary fiber spacing. Gürdal and Olmedo (1993) present closed form solutions for the in-plane structural response of variable stiffness laminates for three distinct boundary conditions. Later, Olmedo and Gürdal (1993) use the in-plane closed form solutions in combination with the Ritz method to compute the critical buckling load of a variable stiffness panels.

Kassapoglou (2008) presents a Rayleigh-Ritz solution to compute buckling loads of panels with an arbitrary number of patches. The energy of a panel is formulated in terms of the out-of-plane displacements. Minimizing the energy with respect to the unknown coefficients in the expression for displacement results in an eigenvalue problem the solution of which yields the buckling load.

Several specialized computational routines have been developed over the last three decades to design minimum weight stiffened panels. These codes include PASCO (Stroud and Anderson, 1981) and VICONOPT (Williams et al., 1991), that both make use of the finite-strip based analysis code VIPASA. The code PANDA2 developed by Bushnell (1987), also makes use of the finite strip method to analyze and design composite panels. The aforementioned codes are computationally efficient, however, are not well suited to variable stiffness design since the stiffness is generally considered constant over a single strip. A modification has been applied by researchers at the University of Bath to VICONOPT to study panels with linear stiffness variation.

Semi-analytical and specialized design codes are numerically efficient which makes them well suited when a large number of structural analyses are required, however, due to their specialized nature, the type of problems which can be studied is limited.

Finite Element Methods

The finite element method is a numerical technique for finding approximate solutions to partial differential equations. The method originates from the need to solve complex elasticity and structural analysis problems in the aerospace and civil engineering industries. Modern day finite element analysis remains the method of choice for solving complex structural analysis problems over a broad range of industries. Numerous commercial codes are available and applicable to a wide variety of structural, and non-structural, analysis problems. In this approach, a problem is discretized and modeled using a suitable set of elements that are interconnected at points called nodes. Each element contains information about its physical property, such as thickness, density, modulus, coefficient of thermal expansion etc. The response is subsequently computed by solving a system of equations resulting from the assembly of the individual element properties. Since individual properties can be defined per element, this approach is well suited to studying variable stiffness structures. Hyer and Charette (1991) are the first to use the finite element method to design variable stiffness structures. Due to its general applicability, this approach is used extensively for variable stiffness design. Finite difference discretization has also been implemented to solve several structural problems, see for example Grenestedt (1991) and Khani et al. (2009). For both methods the number of design variables available to describe an arbitrary stiffness distribution is limited by the number of elements used to discretize the system.

Cellular Automata

Setoodeh (2005) and Abdalla (2004), have implemented a cellular automata based analysis method to model and design variable stiffness structures. Instead of solving for the structural response using the complete system of equations, as is done for finite element analysis, cellular automata solves for the structural response using field variables, such as displacement, using local update rules. The field variables are updated using predefined update rules in an iterative scheme until a converged solution is found. This approach is inherently parallel, and allows extensive use of this computing paradigm to improve computation efficiency.

1.3.3 Designing Variable Stiffness Laminates

Once a design is defined and its structural response can be evaluated, the parameters defining the design must be selected such that predefined design criteria are met. This is achieved by defining an objective function, which is used to evaluate the optimality of the design and the constraints that guarantee design feasibility. An automated process, called design optimization, is subsequently used to obtain the optimal set of design parameters.

Design optimization of composite structures is a complex task, partly due to the mixed integer and continuous design variables required to describe them and partly due to the complexity of the design space. Several different optimization strategies are available and can roughly be classified into one of two categories: one, direct search methods and two, gradient based methods. Hybrid methods have also been developed in an effort to capitalize on the advantages of a specific algorithm while mitigating its disadvantages by iteratively switching with another algorithm not suffering from the same disadvantages.

Direct Search Methods

The complex nature of composite design often makes it difficult to evaluate meaningful gradient information. Direct search methods do not required derivative information and can therefore provide a useful outcome. Direct search methods can be subdivided into *deterministic* and *stochastic* methods. Enumeration, a rudimentary direct search method, consists simply of computing the design response for each possible design variable value and then selecting the set resulting in the optimal response. This approach results in an excessive number of function evaluations, which is not feasible for practical design applications. Pattern search methods, such as Hooke and Jeeves or Nelder-Mead, reduce the number of function evaluations required to find an optimum by intelligently selecting iteration points based on previous design points. The aforementioned methods typically cannot be used to guarantee that the global optimum has been found. To mitigate this issue, algorithms have been developed to combine global and local search tactics. By intelligently sampling and subdividing the search domain, regions that are more likely to contain the global optimum are targeted thereby reducing the number of unnecessary function evaluations. The DIRECT algorithm by Jones et al. (1993) is an example of a globally optimum deterministic search method. Due to the relatively large number of function evaluations required, deterministic methods are generally not efficient at solving problems with large number of design variables, which is typically the case with composite structures.

Stochastic methods have been used extensively for composite design due to their relative robustness, ability to handle discrete variables and global search nature. Genetic algorithms are by far the most popular stochastic method used for conventional composite design (Gürdal et al., 2010). Tatting and Gürdal (2002) use a purpose built genetic algorithm to design variable stiffness panels based on linear variation by obtaining the parameter set defining optimal fiber paths. Alhajahmad (2010) uses simulated annealing to design variable stiffness panels based on Lobatto polynomials. The primary disadvantage of stochastic methods is the large number of function evaluations that are required. These can easily run into several hundred thousand depending on the number of design variables, and therefore, are often only suitable if stiffness variation can be described using a small set of design variables.

Gradient Based Methods

Gradient-based methods make use of derivatives with respect to all design variables of the objective function and constraints to determine a descent direction. The number of design variables and constraints therefore significantly influence computation time. Even though additional computational effort is required to compute derivatives, this is usually outweighed by significantly faster convergence rates. Gradient based optimizers can be subdivided into two groups, those based on optimality criteria and those based on mathematical programming.

Optimality criteria require the derivation of a suitable criteria based on the Karush-Kuhn-Tucker (KKT) conditions (Karush, 1939; Kuhn and Tucker, 1951). Subsequently, an iterative procedure is typically developed to obtain the optimum design. Pedersen (1989) derive a criteria for minimum and maximum elastic strain energy density to design the the optimal material orientation of an orthotropic material. Later Pedersen (1991) design the thickness and orientation of a uniformly loaded cantilever, by aligning the material axis with the principle strains while thickness was optimized using strain energy. Setoodeh et al. (2005) have shown that the optimality criteria for minimum compliance variable stiffness design reduce to the minimization of the complementary strain energy at every point in the domain.

Mathematical programming methods, often referred to as optimization, have been studied extensively and have been successfully implement for a large range of structural optimization problems. Numerous algorithms exist ranging from first order steepest-decent methods to more complex methods using Hessian information to improve convergence rates. Setoodeh et al. (2006b) use a combination of sequential quadratic programming and method of feasible directions to design variable stiffness panels for maximum stiffness.

Gradient-based optimization methods are typically well suited to studying large structural optimization problems due to the relatively low number of function evaluations required, however, they can only guarantee convergence to local optima and therefore the obtained solution will depend on the nature of the design space and the initialization point.

1.4 Objectives and Layout of this Thesis

Automated fiber placement machines make it possible to manufacture an entirely new class of tailored composite structures, allowing the full potential of composite materials to be exploited. As has been shown in numerous theoretical and experimental studies in the past and discussed briefly in earlier sections, tailoring local stiffness properties allows for significant design improvements. Despite this, the design tools currently available to engineers do not exploit the steering capabilities of automated fiber placement machines.

Design optimization of steered fiber paths to meet specific design requirements is difficult and computationally expensive. The design and computational challenges relate both to the cost of evaluating the function values and the non-convex nature of the design problem. For example, to evaluate manufacturing constraints, detailed course-level and tow-level information is required, which is typically expensive to evaluate. Additionally, the generally non-convex nature of the variable stiffness laminate design problem complicates the search for a global optimum.

The primary goal of the presented research was to develop a computationally tractable optimization approach to design variable stiffness structures and address its implementation for several design problems. An overview of the developed optimization framework is presented in chapter 2. A short background of variable stiffness laminate design is provided and the proposed multi-step design approach is outline. The optimization framework consisted essentially of three steps, one, the optimal conceptual stiffness distribution was designed to meet the imposed structural requirements, two, the local fiber angle distribution was retrieved such that manufacturing requirements were met while attempting to retain the performance improvements realized in the first step, and three, the fiber angle distribution was converted to continuous fiber paths which can be used for manufacturing purposes.

The research presented in this thesis focused primarily on the development of a conservative convex structural approximation methodology, presented in chapter 3, which was subsequently used to approximate several structural response types. The approximation was formulated directly in terms of the laminate stiffness matrices and is therefore independent of the chosen laminate parameterization scheme, however, when parametrizing laminate stiffness in terms of lamination parameters, the convex properties of the approximation are retained. One of the limitations, and perhaps objections to using lamination parameters for composite design, has been the difficulty of incorporating strength constraints into the optimization process. In order to facilitate the acceptance of the approach, a method of including strength is presented in chapter 4.

In the past buckling, a multi-modal structural response, has proven to be a challenging variable stiffness design problem to solve (Setoodeh et al., 2009). Hence, a large portion of the research carried out and presented in this thesis was dedicated to implementing buckling approximations within the proposed conceptual design framework. Buckling of variable stiffness plates is studied in chapter 5. Past experimental results demonstrated that curing induced residual thermal stresses present in variable stiffness structures could significantly influence their buckling response. Therefore, a simplified method of including thermal loads into the buckling optimization routine was developed and is presented chapter 6. Modern fiber placement machines are also equipped with on-the-fly cut and restart capabilities, making it possible to vary laminate thickness quasi-continuously over the structure. In order to investigate the effects this may have on buckling performance, the optimization approach was extended to include thickness as a design variable, which is reported in chapter 7. Finally, based on insight gained from previously developed buckling approximations, an approximation of the buckling load of a general shell structure was derived and is presented in chapter 8.

Several realistic design problems were studied together with industrial partners to demonstrate the capabilities of the developed optimization approach. The first design problem, see chapter 9, considered the design of a business jet window-belt section for maximum strength. In a second design study, presented in chapter 10, the wing-rib of a similar business jet was designed to meet an imposed set of design requirements.

General conclusions and recommendations regarding the present work are presented chapter 11. The conducted research work is only a beginning, therefore some thoughts on future challenges that should be tackled are also discussed. However, returning to the quote with which this chapter opened,

> "*Nothing is less productive than to make more efficient what should not be done at all.*"

the goal of the research done for this thesis was then:

to demonstrate that developing an efficiently design tool for variable stiffness composite structures is both productive and worthwhile.

CHAPTER 2

Design Optimization Framework

"I have had my results for a long time: but I do not yet know how I am to arrive at them."

Carl Friedrich Gauss

The design of composite structures is by no means a trivial task. Composite structures are inherently difficult to optimize due to a combination of discrete and continuous design variables as well as generally non-convex design problems with multiple solutions. Variable stiffness laminates are even more complex to design, as the optimization problem is no longer limited to a single or several laminate designs, but consists essentially of obtaining an optimal layup at every point in the structure. Ensuring fiber continuity and laminate manufacturability complicates the design problem even further.

An overview of the developed variable stiffness design framework is presented in this chapter. To develop an efficient design optimization strategy it is important to consider the nature of the responses, constraints and design variables which are to be used. Carefully considering how a design problem is parameterized can significantly simplify the optimization problem to be solved. Parameters influencing variable stiffness composite structures and aspects that may drive their design are discussed in section 2.1. A description of the multi-step optimization framework developed to optimize variable stiffness composite structures is presented in section 2.2. A cornerstone of the developed design framework is the use of lamination parameters to model a laminate's spatially varying stiffness properties. Lamination parameters and how they relate to a laminate's stiffness properties is presented section 2.3. The advantages and limitations of the developed design framework are discussed in section 2.4.

2.1 Identifying and Selecting Design Drivers

Fiber placed composite structures consist of several million individually placed tows, each a few millimeters wide, to build up laminates with possibly several hundred plies with part sizes in the order of several meters or more. The design of such structures can essentially be approached from two directions: *bottom-up*, where each individual tow or course path is defined, which yields the laminate and part stiffness to best meet design requirements or *top-down*, where part stiffness is designed to best meet design requirements and fiber paths are subsequently determined to yield the required laminate stiffness.

Choosing the right level of abstraction has significant consequences for the complexity of the design problem to be solved and implicitly defines the scope of possible solutions. Additionally, design and manufacturing constraints can only be imposed if sufficient detail is available. The different levels of abstraction are shown schematically in Figure 2.1, along with examples of manufacturing and design constraints that can be imposed at that specific level.

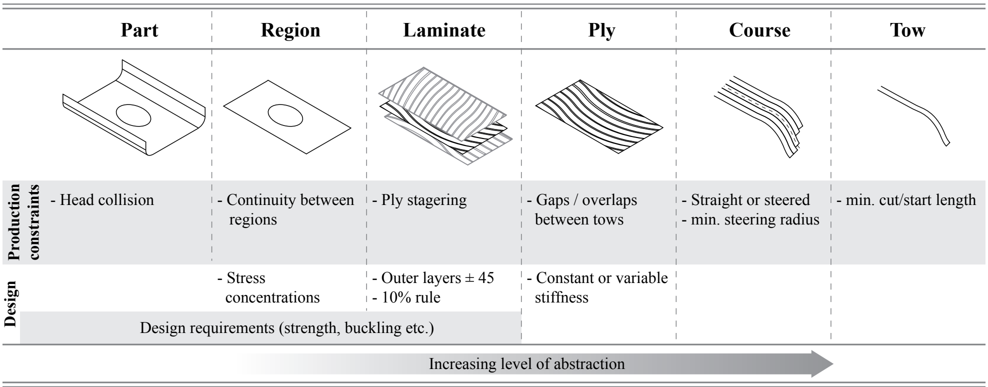

Figure 2.1: *The considered level of abstraction determines what information is available to the designer*

At *Part* level, production constraints, such as avoiding head-collision, or restrictions on minimum and maximum part curvature, to avoid fiber bridging, can be imposed. Part geometry is typically fixed before starting laminate design, therefore, it is reasonable to assume that these constraints will have been taken into account by the design engineer. Structural response requirements such as maximum displacement, minimum buckling load etcetera can also be defined at part level. At *Region* level, the designer may want to ensure ply or laminate continuity between different regions. Ply staggering, a technique to avoid path overlaps or gaps from consistently occurring at the same location, can be applied at *Laminate* level to avoid excessive thickness buildup or resin filled regions. Ply composition constraints such as the 10% rule, which enforces a minimum number of plies along several predefined directions, may also be imposed at *Laminate* level. At *Ply* level, details about course-replication are available, and therefore it must be determined if gaps or overlaps, or a combination of the two, occur between adjacent courses. The designer at this point can choose between using straight or steered fiber paths. At *Course* level, the constraints on minimum steering radius can be imposed and finally at *Tow* level minimum cut-restart limits can be defined. The required level of abstraction is therefore partially imposed by the information needed to evaluate the considered design drivers.

The design drivers listed in Figure 2.1 pertain primarily to structural performance metrics, manufacturing criteria and typically applied design rules. It may also be necessary to consider other design requirements, such as design for minimum cost, as will be discussed further below. To facilitate further discussion it is important to clarify the scope of a considered design problem.

A structural component is often part of a larger design and manufacturing system in which design choices are made on multiple levels, for example, design for manufacturing may include ensuring manufacturability using an already selected manufacturing technology and entail selecting the most suitable manufacturing method. Selecting the most suitable manufacturing method is often a complex trade-off between methods available, global costs or even company strategy, and goes beyond the scope of the current discussion. The design drivers discussed in the following sections are focused primarily on factors directly influenced when designing variable stiffness composite structures using fiber placement technology and on determining the level of abstraction required to evaluate the design driver.

2.1.1 Design for Structural Performance

A structural performance metric, such as the buckling load or the structural weight, is unsurprisingly most commonly used as a design driver for structural optimization. The reason is twofold; one, it is relatively straightforward to define and interpret performance metrics in terms of meaningful design variables and hence the approach tends to yield tangible results for structural engineers. Two, in aerospace, structural weight is often associated with direct operating costs (Curran et al., 2004), hence it is generally assumed that designing for optimal structural performance will result in structures with lower weights and costs. Additionally the growing scarcities of raw materials and fossil fuels support this premiss.

Considering variable stiffness laminates, it is interesting to note that typical design requirements such as stiffness, buckling load or strength can be defined on part-level, laminate-level or ply-level, as can be seen in Figure 2.1. A structural response can usually be computed based on an equivalent stiffness material model, such as Classical Lamination Theory (CLT). Therefore, in terms of structural design and optimization, it is neither necessary nor realistic to model each tow, as an equivalent stiffness distribution is usually sufficient. This observation is at the basis of the developed design approach described in section 2.2.

2.1.2 Design for Manufacturability

Earlier variable stiffness design studies, such as those presented in Haftka and Starnes (1988) and Hyer and Charette (1991), focused primarily on demonstrating how stiffness tailoring could result in significant structural improvements. However, the discrete nature of the obtained solutions were not suitable for continuous manufacturing processes. Ensuring fiber path continuity, necessary for manufacturing, was achieved primarily by using continuous functions to parameterize fiber paths as discussed in section 1.3.1. Tatting and Gürdal (2002) have developed expressions to determine the maximum radius of curvature for steered paths defined using linear variation. Overlapping, which occurs due to steering, was also taken into account. Similarly, Blom (2010) uses continuous fiber path parameterization together with detailed information about path overlaps and tow cut and restart locations to design variable stiffness cylindrical shells. Several other manufacturing related criteria such as machine-mold collisions or laminate permeability may also be considered as design criteria to be incorporated into the design process.

Detailed information about the laminate construction is necessary to impose manufacturing constraints such as minimum steering radius or cut and restart locations. Evaluating these design drivers thus often requires high fidelity models. The computational costs coupled with such models becomes restrictive in an optimization routine, and therefore, it is often not feasible to include such detail at design level. The development of accurate fiber path approximations, which capture sufficient course and towpath details, will enable a more general implementation of manufacturing related design drivers.

2.1.3 Design for Cost

Cost is an important design driver in almost any context, however it is typically difficult to incorporate into a design optimization scheme due to the intricate nature of cost functions, which are influence by material, manufacturing and operating costs. Material costs and direct operating costs are often minimized implicitly through structural weight minimization as outlined by Curran et al. (2004). Therefore, the discussion below is primarily focused on manufacturing related costs. The majority of cost models available in the literature are often based on manual manufacturing processes. Kassapoglou (1997) includes an elaborate cost function related to several aspects influencing a manufacture process based on hand layup while optimizing stiffened composite panels. Manne and Tsai (1998) present a method for predicting the manufacturing cost of multi-patch laminates based on laminate complexity, which is related to the number of ply drop-offs within the structure.

The drive to automate manufacturing processes, such as by using automated fiber placement, is commonly due to cost considerations such as reducing labour costs, minimizing amounts of wasted material and number of scraped parts due to production errors. As with manual manufacturing methods, manufacturing costs in automated process are often strongly dependent on manufacturing time. Hence production costs can be lowered by increasing machine deposition rates using intelligent path planning and by reducing overall laminate complexity, be it by minimizing the number of cut and restart actions within a ply or by reducing the amount of steering. Imposing design requirements related specifically to manufacturing costs therefore requires detailed information about the laminate stacking sequence and fiber paths. As is the case for manufacturing related design drivers, it is often not feasible to include such detail at design level. It is interesting to note that the similarity between manufacturing and cost related design drivers may enable costs to be included implicitly in an optimization routine when considering manufacturing design drivers.

2.2 A Multi-Step Optimization Framework

The primary aim of the conducted research presented in this thesis was to develop an optimization framework for variable stiffness structures that was sufficiently general to be applicable to a large range of design problems but remained computationally tractable. Hence suitable modeling, analysis and optimization methods had to be selected and combined to form a robust framework capable of handling a general set of design drivers for variable stiffness composite shell structures.

Variable stiffness design can be approached from two directions, either *bottom-up* or *top-down*, as discussed in section 2.1. The former requires detailed tow and course information to be parametrized and is therefore inherently more focused on manufacturing related criteria, as can been seen from Figure 2.1. The latter tends to neglect detailed tow-level information and is therefore inherently more focused on global structural performance. However, if a general approach is to be developed, both structural performance and manufacturing considerations must be accounted for. Ideally, more complex design drivers such as designing for cost, should also be incorporable into the design framework.

In order to develop a design framework it is necessary to be able to *model* the stiffness variation, *analyze* the structural response associated with the stiffness variation and *optimize* the design to meet the imposed requirements. A discussion on the different methods available to model, analyze and design variable stiffness composite laminates was presented in section 1.3. The different methods and their advantages and disadvantages are recapitulated in Table 2.1 to facilitate further discussion.

Selecting appropriate modeling and optimization methods is not a trivial task, as they are often interdependent, therefore, we started by selecting a suitable analysis method. Using specialized or semi-analytical methods is typically computationally efficient, however, this comes at the expense of being restricted to a fixed set of problems that can be solved. Cellular automata has been shown to be an effective analysis and design method (Abdalla, 2004; Setoodeh, 2005). The method is highly parallel, due to the inherent local problem formulation, which may be used to improve computational efficiency substantially. As an analysis tool, however, it is still at the research level and its inherent local nature complicates solving global structural responses. A number of finite element methods have been developed over the past half century that are applicable to a large range of structural analysis problems. They have proven to be robust analysis tools and are the method of choice for industrial applications when modeling complex structural components. To mitigate the disadvantages associated with commercial codes, an elementary in-house finite element code was programmed to facilitate research, details can be found in appendix B. Depending on model complexity, it can take anywhere from seconds to days to compute a single response using finite element methods. Considering the number of design variables required to define variable stiffness structures, it is essential that the number of individual finite element analyses required to obtain an optimum solution be reduced to a minimum.

In order to manufacture a composite part with automated fiber placement technology, each individual course path and tow drop must be considered. This level of detail is also required to impose constraints such as minimum curvature, cut-restart locations and tow gaps and overlaps. Parametrizing fiber paths directly restricts the available design space and typically results in non-convex problem formulations, necessitating the use of algorithms that are able to find a global optimum. Such algorithms often require large number of function evaluations, resulting in problems that cannot be solved in a feasible timespan. Direct stiffness modeling, be it fiber angles directly or via intermediate parameters, allows for the most general description of stiffness variation and hence captures the full design space. Making use of lamination parameters, which are introduced in section 2.3, removes difficulties associated with

Table 2.1: *Summary of modeling, analysis and design methods with their respective advantages and disadvantages. A more elaborate discussion can be found in section 1.3.*

Modeling Method	**Advantages**	**Disadvantages**
Discrete Representation (Fiber angle or stacking sequence per design region)	+ Largest possible design space	- Non-convex, computationally expensive - Mixed continuous & discrete design variables - Large number of design variables - Difficult to guarantee continuity
Direct Stiffness Modeling (e.g. Lamination Parameters)	+ Largest possible design space + Convex, continuous design variables + Fixed number of design variables per region	- Post-processing required for fiber paths
Fiber Path Parameterization (Functional Representation)	+ Limited # of design variables + Continuous paths + Curvature constraints can be applied directly	- Design space limited by parameterization - Non-convex, computationally expensive - Primarily used for developable surfaces
Analysis Method		
Semi Analytical / Specialized	+ Computationally efficient + Promotes fundamental problem understanding	- Limited range of applicability
Finite Element Methods	+ Applicable to a large range of problems + Commercial grade tools available + Computationally efficient + Robust and well proven	- Limited output provided by software - Limited flexibility of commercial codes
Cellular Automata	+ Highly parallel, computationally efficient + Topology included readily	- Still at research level - Difficult to model global responses
Optimization Method		
Direct Search Methods	+ No gradient information required + Well suited to non-convex problems	- Require huge number of iterations - Convergence not guaranteed
Gradient Based Methods	+ Require few iterations	- Requires gradient information - Global optimum not guaranteed

discrete design variables and provides a convex design space, both desirable features when optimizing with efficient gradient based algorithms. The primary disadvantage of using such variables is a lack of ply, course and tow-level information required to evaluate manufacturing related design drivers.

The complexity of the variable stiffness structural design problem necessitated a multi-step approach, which exploits the advantages of several of the aforementioned design methods while attempting to mitigate their primary drawbacks. The developed framework was based on a multi-step approach presented by IJsselmuiden et al. (2009) to design fully blended multi-panel structures. In an initial step the authors use approximations in terms of laminate stiffness properties, parametrized using lamination parameters, and efficient gradient based optimization algorithms to determine optimal laminate stiffnesses. In a second step individual laminate stacking sequences are obtained while ensuring ply continuity between panels using so called guide-based blending (Adams et al., 2004). An inexpensive local approximation of the bucking load, based on the initially found optimum laminate stiffnesses, is used as an objective function for a genetic algorithm to obtain the stacking sequence. Intermediate updates of the local approximation are conducted to improve solution accuracy.

The multi-step framework by IJsselmuiden et al. (2009) has three important features, one, structural performance is optimized using efficient gradient based algorithms to solve successive approximations. These approximations are parametrized using lamination parameters that are continuous design variables and have a convex design space. This allows the largest possible design space to be captured while simultaneously limiting the number of required finite element analyses to obtain the optimum solution. Two, instead of using a more common least-squared distance approach to convert lamination parameters to retrieve a laminate stack, see for example Autio (2000), the same physically meaningful approximation of the structural response developed in the initial step is used. Hence, the obtained laminate stacks match structural performance targets more accurately. The advantage of using more accurate methods of converting lamination parameters into a laminate stack has also been noted in previous research, for example by Herencia et al. (2008). Three, manufacturing related constraints, i.e. ply continuity between panels, are only incorporated in the second step, once detailed ply information is available.

Separating structural performance related design drivers and manufacturing related design drivers allows the most suitable optimization algorithms to be used where necessary. A multi-step design optimization framework was therefore developed for variable stiffness structures, outlined in Figure 2.2. In a first step, the laminate stiffness distribution optimizing the considered structural performance is obtained. Design drivers such as in-plane stiffness, strength, natural frequency and buckling can be included at this stage of the optimization. The obtained optimum solution provides the designer with a conceptual stiffness distribution best satisfying the desired structural performance requirements. In a second step, the fiber angle distribution, essentially representing point-wise laminate stacking sequence, required to match the obtained optimum stiffness distribution is determined. Manufacturing constraints, such as minimum curvature, thickness buildup, or permeability, can be incorporated at this stage. In a final step, the fiber angle distributions are converted to continuous fiber paths which can be used for manufacturing. Each of the three aforementioned steps are discussed in more detail in sections 2.2.1, 2.2.2 and 2.2.3 respectively.

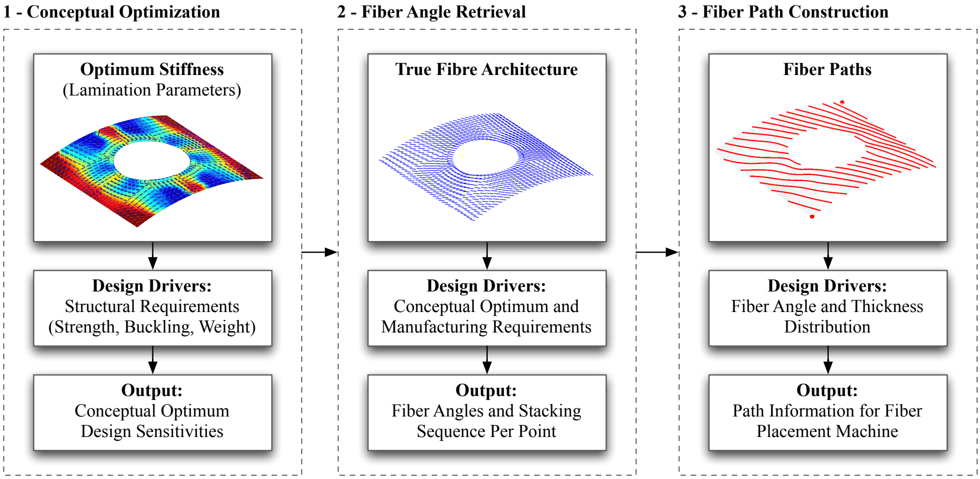

Figure 2.2: *Schematic overview of the developed multi-step optimization approach*

2.2.1 Conceptual Stiffness Optimization

The first step of the variable stiffness optimization framework requires the stiffness distribution to be determined by optimizing predefined structural performance metrics. A successive approximation scheme of performance related design drivers was implemented to obtain a tractable optimization problem, by minimizing the number of finite element analysis required to converge to an optimum. The primary focus of the work presented in this thesis is the development of conservative convex separable approximations, presented generically in chapter 3, for several structural response types. The developed approximations are derived as a function of the laminate stiffness matrices directly, and are therefore not dependent on the chosen laminate stiffness parametrization scheme.

In order to optimize the structural performance a suitable parameterization of the structural stiffness properties must be selected. Lamination parameters were selected to model laminate stiffness properties for the conceptual optimization step and are described in detail in section 2.3. Lamination parameters allow the stiffness properties of an arbitrary laminate to be expressed in terms of twelve continuous design variables, irrespective of the number of plies present in the laminate. If the laminate is balanced and symmetric, which is often desired from a design perspective, the number of parameters required to define the laminate stiffness properties reduces to four. The lamination parameter design space is also convex and it has been shown that several laminate design problems are convex when posed in terms of lamination parameters (Hammer et al., 1997). Laminate design problems posed in terms of lamination parameters are therefore well suited to being solved using efficient gradient-based optimization algorithms allowing, together with the developed structural approximations, the optimum stiffness distribution to be obtained with a minimum number of finite element computations.

The conceptual stiffness distribution gives the designer insight into the mechanisms resulting in improved performance and provides a benchmark of the best performance for a given design problem. The majority of the work presented in this thesis is related to the approximation development and the use of lamination parameters to obtain a conceptual optimum stiffness distribution. The relevant topics will be discussed in more detail in subsequent chapters. The approximations developed in this thesis are also well suited to solving the inverse problem as will be discussed in the next section.

2.2.2 Fiber Angle Retrieval

Once an optimal laminate stiffness distribution has been obtained, in this case in terms of lamination parameters, a stacking sequence retaining the performance gains of the optimal conceptual stiffness distribution must be found. Several methods have been developed in the past to obtain a laminate stacking sequence from lamination parameters. Heuristic algorithms, see for example Autio (2000), have been used most successfully to solve this complex non-convex inverse problem. At this stage it is important to include constraints that guarantee manufacturable solutions are found. As discussed in subsection 1.2.2, several manufacturing details related specifically to fiber placement must be considered, such as the minimum steering radius to avoid tow wrinkling, location of gaps and overlaps due to fiber path steering and minimum tow length. Previously developed fiber angle retrieval methods have been limited to primarily straight fiber laminates or multi-panel laminates and do not consider fiber path curvature or continuity. Therefore, when extending this methodology to variable stiffness laminates, without the appropriate constraints, the obtained fiber angle distributions are often not continuous and hence not manufacturable, see for example Setoodeh et al. (2006b) and Honda and Narita (2008). To construct a feasible variable stiffness laminate the obtained fiber angle distribution must account for manufacturing limitations, such as minimum steering radius. Constraints on the fiber path radius is included either as an average curvature constraint per ply or as a local point-wise curvature constraint, as discussed in the two following subsections.

Average Curvature Constraints

Fiber path curvature can be interpreted as a measure of the rate of change in fiber angle. The curvature, κ, can therefore be expressed as the norm of the divergence of the fiber angle, θ:

$$\kappa = \|\nabla\theta\| \tag{2.1}$$

Analogous to the finite element method, linear shape functions can be used to construct a pseudo-stiffness matrix, representing a measure for the change in fiber angle orientation, as presented by Pilaka (2010). The author formulated the approximate fiber path curvature of an element, κ_e, as:

$$\kappa_e^2 = \frac{1}{2}\boldsymbol{\theta}_e^T \cdot \mathbf{K}_e \cdot \boldsymbol{\theta}_e \tag{2.2}$$

where $\boldsymbol{\theta}_e$ is a vector of fiber angles at the element nodes and $\mathbf{K}_e$ is a curvature operator expressing the change in fiber angle orientation. Constraining fiber path curvature at every point within a laminate would result in a large number of local constraints. To avoid issues arising when solving an optimization problem with an excessive number of constraints, an average curvature constraint was formulated per ply as:

$$\frac{1}{2}\boldsymbol{\theta}^T \cdot \mathbf{K} \cdot \boldsymbol{\theta} \leq \kappa_{max} \tag{2.3}$$

where $\boldsymbol{\theta}$ and $\mathbf{K}$ are now the vector of fiber angles and curvature operator assembled for an entire ply.

Quadratic approximations of the average curvature constraints and the structural response were subsequently formulated by Pilaka (2010), and were based on the conservative convex separable approximation at the conceptual optimum found in the first step. A gradient based optimizer is subsequently used to solve the quadratic problem, which is highly non-convex due to the parametrization in terms of fiber orientation angles. Gradient based optimization routines can only guarantee convergence to a local optimum, therefore, a suitable initial design point must be obtained to ensure solutions are found which capture the performance gains of the conceptual optimization step. Due to the non-convex nature of the inverse problem this is best achieved using heuristic search algorithms. A multi-objective asexual genetic algorithm using hierarchical shape functions to parameterize fiber paths is presented in Klees et al. (2009). The objective functions include both the conservative convex separable approximation of the structural performance and the maximum average curvature of all the plies present in the laminate. The Pareto front that is obtained provides the designer with a trade-off between structural performance and the amount of fiber steering present in the design. Points along the Pareto front can subsequently be used to initiate the gradient based optimization process described above.

Local Curvature Constraints

The aforementioned design method makes use of a global average curvature constraint per ply which results in smooth fiber angle distributions being obtained, however, to guarantee laminate manufacturability curvature constraints should be satisfied at every point within the laminate. A fiber angle retrieval scheme making use of point-wise curvature constraints based on the curvature definition presented in equation (2.2) has been developed by van Campen (2011). In an initialization step, a genetic algorithm is used to obtain the fiber angle distribution best matching the optimum conceptual laminate stiffness distribution. Curvature constraints are neglected at this stage and the stacking sequence at each design point within the laminate is obtained based either on least-squared fit with the optimum lamination parameter distribution or using the conservative convex separable approximation at the conceptual optimum. The optimum fiber angle distributions including manufacturing constraints are subsequently obtained using a cellular automata framework coupled with a gradient based optimizer. The curvature is approximated locally based on the fiber angle distributions of neighboring elements. The constraints are included in the overall objective function evaluated at each point within the cellular automata framework via a local penalty term. The inherent local nature of the cellular automata framework mitigates the issues which arise when using a large number of constraints in a global optimization problem, as is done by Pilaka (2010). An additional advantage of using local penalization of the objective function is that including other point-wise constraints such as local through-the-thickness permeability or local thickness buildup is relatively straightforward.

Accuracy of Response Approximations

The aforementioned fiber angle retrieval methods make use of the developed conservative convex separable approximations to include the structural response as either an objective function or as a constraint. These approximations are based on gradient information of the various responses obtained at the conceptual optimum found in the first step of the multi-step design framework. As with most approximations, the accuracy with which a function value is predicted deteriorates away from the vicinity of the approximation point. Studying several practical example problems has shown that the laminate stiffness distribution of manufacturable design may indeed differ significantly with respect to the initially found conceptual optimum laminate stiffness distribution. Hence, the accuracy of the approximations used to predict the structural response may become inadequate. Two solutions may be considered to improve the accuracy of the structural approximations.

One, the derivatives used to generate the approximations can be updated during the fiber angle retrieval step, similar to the method proposed by IJsselmuiden et al. (2009) when solving a multi-panel blending problem. Once an initial manufacturable design is found, the sensitivities required to approximate the structural responses are updated and the fiber angle retrieval algorithm is rerun. The update process is repeated until a converged solution is found. This approach has been demonstrated successfully by van Campen (2011) and allows manufacturable fiber angle distributions to be obtained that have a superior structural performance to those solutions found using traditional least-square fit algorithms in lamination parameter space.

Two, an approximation of the considered response can be developed which is accurate over a larger portion of the design space. Response surface methods are frequently used to generate global response approximations, however, as the number of design variables increases the computational cost of generating a response surface becomes restrictive. Irisarri et al. (2011) present an innovative multi-point approximation method based on an improved Shepard's method (Shepard, 1968). First the conservative convex separable approximation used for the conceptual stiffness optimization is constructed at multiple points in the design space. These approximations are subsequently combined using a distance measure in stiffness space based on Shepard's method to obtain a global approximation. The number of points used to generate the global approximation are updated iteratively based on sensitivity data computed at the optimum found after any given iteration. The global approximation, when parameterized in terms of fiber angles, is no longer convex and is therefore solved using a genetic algorithm. The method is shown to be efficient for both straight fiber laminate and multi-patch laminate design and is currently being extended to variable stiffness laminates.

2.2.3 Fiber Path Construction

In the final step of the multi-step optimization framework, the fiber angle distributions obtained in the previous step must be converted to continuous fiber paths that can be used as input for most fiber placement software. Fiber angle distributions can be used to generate continuous fiber paths using a streamline methodology, as introduced by Blom et al. (2009b) for planar structures. The approach has been extended to arbitrary surfaces by Nagy et al. (2009).

Streamlines, analogous to those used to visualize aerodynamic flows, can be used to represent the centerline of a course and are defined by all the points in a domain that have the same constant function value:

$$\psi(\xi, \eta) = \mathcal{C} \tag{2.4}$$

where ψ is the stream function and ξ, η represent the parametric surface coordinates and the constant represents the ply thickness. As is shown by Nagy et al. (2009), given a fiber angle distribution, $\theta(\xi, \eta)$, the stream function can be obtained by solving the following partial differential equation:

$$\nabla\psi \cdot \mathbf{p} = 0 \tag{2.5}$$

where $\mathbf{p}$ represents a unit vector on the parts surface corresponding to the local fiber angle orientation. The solution is fully defined by the conditions imposed at the inflow boundary, as is the case for aerodynamic flows.

The streamlines represent the path of the course centerline, therefore, unless streamlines are parallel, successively placed courses with a fixed finite width will inevitably result in thickness variation within the ply. The amount of overlap depends on the distance between adjacent streamlines, the closer the streamlines are together the more thickness buildup occurs. Given a target fiber angle distribution the choice of inflow boundary conditions therefore influences the final thickness distribution, as can be seen schematically from the example presented in Figure 2.3. For the example shown in Figure 2.3(a), uniform thickness was assumed at the inflow boundary, i.e. all courses are adjacent to one another, however, in this case the resulting fiber paths, aiming to match the required fiber angle distribution, do not cover the entire ply surface. In the second example, Figure 2.3(b), the inflow boundary conditions were optimized to ensure total ply coverage while minimizing the number of overlaps within the ply. Several methods to optimize the inflow boundary conditions are presented by both Blom et al. (2009b) and Nagy et al. (2009), each of which are aimed at minimizing the collocation of overlaps and gaps or minimizing the number of overlaps or a combination of the two.

2.3 Laminate Stiffness Modeling using Lamination Parameters

In order to model and design composite structures, the relationship between material properties, ply orientations, stacking sequence and the structural response must be defined and understood. The constitutive equations, which relate laminate stress resultants and laminate strains, are derived in the following subsection. The relation between laminate stiffness properties and lamination parameters, which are used as design variables for laminate optimization, are presented in subsections 2.3.2 and 2.3.3, followed by the definition of their feasible regions in subsection 2.3.4. A brief discussion on the physical interpretation of lamination parameters is provided in subsection 2.3.5. Finally, the formulation used to model variable stiffness laminates is presented in subsection 2.3.6.

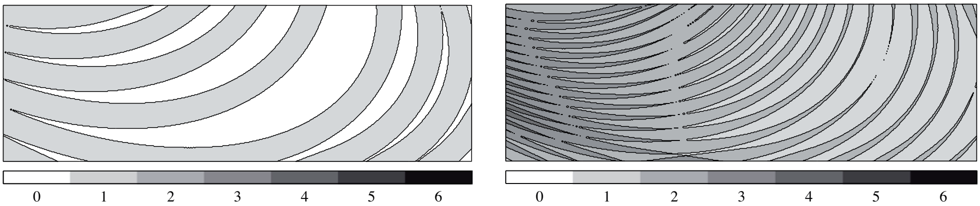

(a) Uniform inflow boundary conditions

(b) Boundary conditions optimized for minimum maximum thickness

Figure 2.3: *Example of thickness variation that occurs within a steered fiber ply with constant course width due to different inflow boundary conditions(Source Blom et al. (2009b))*

2.3.1 Mechanics of Composite Laminates

Classical Lamination Theory (CLT) forms the basis of laminate stiffness formulation, and assumes that N orthotropic and/or isotropic layers are perfectly bonded by an infinitely thin, non-shear-deformable bond-line. Bending of the laminate follows the classical Kirchhoff-Love pure bending assumptions; that a straight line perpendicular to the mid-plane before deformation remains straight and perpendicular to the same plane. The length of that line also remains unchanged. Hence, through-the-thickness deformations in the laminate are zero, and the strains in the out-of-plane direction z are neglected. The layer(s) are also thin compared to the in-plane dimensions of the layer(s), and the stress components in the z direction are assumed to be negligible so that an approximate state of plane stress prevails.

The stresses in a single lamina loaded along its principle axes can be related to lamina strains via the following constitutive relation for orthotropic materials:

$$\left\{ \begin{array}{c} \sigma_1 \\ \sigma_1 \\ \tau_{12} \end{array} \right\} = \left[\begin{array}{ccc} Q_{11} & Q_{12} & 0 \\ Q_{12} & Q_{22} & 0 \\ 0 & 0 & Q_{66} \end{array} \right] \left\{ \begin{array}{c} \varepsilon_1 \\ \varepsilon_1 \\ \gamma_{12} \end{array} \right\} \tag{2.6}$$

where the Q_{ij}'s are the reduced laminate stiffness components, defined in terms of the material's longitudinal modulus (E_1), transverse modulus (E_2), shear modulus (G_{12}) and poisson ratio (ν_{12}) as:

$$Q_{11} = \frac{E_1}{1 - \nu_{12}\nu_{21}}, \quad Q_{12} = \frac{\nu_{12} E_1}{1 - \nu_{12}\nu_{21}}, \quad Q_{22} = \frac{E_2}{1 - \nu_{12}\nu_{21}}, \quad Q_{66} = G_{12} \tag{2.7}$$

A laminate is subsequently constructed by stacking multiple plies with a given thickness, t_k, and orientation angle with respect to the laminate axis, θ_k, as can be seen in Figure 2.4.

Using the set of CLT assumptions, in-plane stresses of the kth layer positioned at a through-the-thickness location $z_{k-1} < z < z_k$ are given by:

$$\left\{ \begin{array}{c} \sigma_x \\ \sigma_y \\ \tau_{xy} \end{array} \right\}_k = \left[\begin{array}{ccc} \overline{Q}_{11} & \overline{Q}_{12} & \overline{Q}_{16} \\ \overline{Q}_{12} & \overline{Q}_{22} & \overline{Q}_{26} \\ \overline{Q}_{16} & \overline{Q}_{26} & \overline{Q}_{66} \end{array} \right]_k \left\{ \begin{array}{c} \varepsilon_x^\circ + z\kappa_x \\ \varepsilon_y^\circ + z\kappa_y \\ \gamma_{xy}^\circ + z\kappa_{xy} \end{array} \right\} \tag{2.8}$$

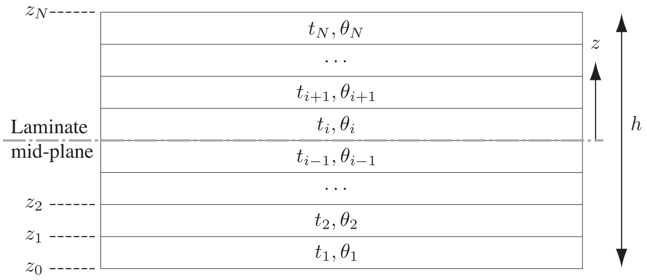

Figure 2.4: *Schematic view of a composite laminate consisting of N laminae with orientation θ_k, thickness t_k and located at distance z_k from the mid-plane*

where $\overline{Q}_{ij}$'s are the lamina stiffness components in the laminate coordinate system of the k^{th} layer and are given by:

$$\begin{aligned}
\overline{Q}_{11} &= U_1 + U_2 \cos 2\theta_k + U_3 \cos 4\theta_k \\
\overline{Q}_{12} &= U_4 - U_3 \cos 4\theta_k \\
\overline{Q}_{22} &= U_1 - U_2 \cos 2\theta_k + U_3 \cos 4\theta_k \\
\overline{Q}_{66} &= U_5 - U_3 \cos 4\theta_k \\
\overline{Q}_{16} &= (U_2 \sin 2\theta_k + 2U_3 \sin 4\theta_k)/2 \\
\overline{Q}_{26} &= (U_2 \sin 2\theta_k - 2U_3 \sin 4\theta_k)/2
\end{aligned} \tag{2.9}$$

where the U_i's are completely described by the material properties of the k^{th} layer, are invariant with respect to the orientation angle of that particular layer and are defined as:

$$\begin{aligned}
U_1 &= (3Q_{11} + 3Q_{22} + 2Q_{12} + 4Q_{66})/8 \\
U_2 &= (Q_{11} - Q_{22})/2 \\
U_3 &= (Q_{11} + Q_{22} - 2Q_{12} - 4Q_{66})/8 \\
U_4 &= (Q_{11} + Q_{22} + 6Q_{12} - 4Q_{66})/8 \\
U_5 &= (Q_{11} + Q_{22} - 2Q_{12} + 4Q_{66})/8
\end{aligned} \tag{2.10}$$

From equation (2.8) it is clear that the through-the-thickness distributions of in-plane stresses are either constant, when laminate curvatures κ_i are zero, or linear in each layer. However, even if all the layers are made of the same basic material, because of discontinuity of the orientation angle from one layer to another, stresses jump at the layer boundaries, as can be seen in Figure 2.5. Hence it is difficult to write stress-strain relations for the entire laminate. That is, even though there exists a spatial distribution of strains (ϵ_i^0 and κ_i) resulting from deformation of the laminate as a whole, there is no stress like quantity corresponding to these strains. A remedy to this situation is to define a set of stress like quantities that are obtained by integrating the layer stresses throughout the laminate thickness, h, as shown in the first part of equation (2.11). The N's in the equation are often referred to as the stress resultants. Similarly, using through-the-thickness integration of the moments of the stresses, we can define the moment resultants, M's.

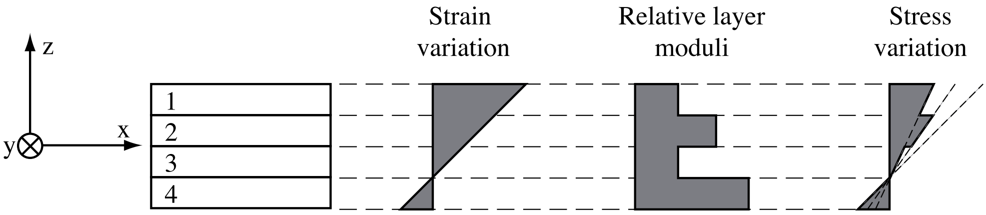

Figure 2.5: *Illustration of linear strain variation and discontinuous stress variation in a laminate (Reproduced from Daniel and Ishai (1994))*

$$\begin{array}{lll} N_x = \int_{-\frac{h}{2}}^{\frac{h}{2}} \sigma_x dz & N_y = \int_{-\frac{h}{2}}^{\frac{h}{2}} \sigma_y dz & N_{xy} = \int_{-\frac{h}{2}}^{\frac{h}{2}} \tau_{xy} dz \\ M_x = \int_{-\frac{h}{2}}^{\frac{h}{2}} \sigma_x z dz & M_y = \int_{-\frac{h}{2}}^{\frac{h}{2}} \sigma_y z dz & M_{xy} = \int_{-\frac{h}{2}}^{\frac{h}{2}} \tau_{xy} z dz \end{array} \tag{2.11}$$

Substituting layer stresses from equation (2.8) into the above definitions, one obtains the constitutive relations for the laminate, given by:

$$\begin{Bmatrix} N_x \\ N_y \\ N_{xy} \end{Bmatrix} = \begin{bmatrix} A_{11} & A_{12} & A_{16} \\ A_{12} & A_{22} & A_{26} \\ A_{16} & A_{26} & A_{66} \end{bmatrix} \begin{Bmatrix} \varepsilon_x^0 \\ \varepsilon_y^0 \\ \gamma_{xy}^0 \end{Bmatrix} + \begin{bmatrix} B_{11} & B_{12} & B_{16} \\ B_{12} & B_{22} & B_{26} \\ B_{16} & B_{26} & B_{66} \end{bmatrix} \begin{Bmatrix} \kappa_x \\ \kappa_y \\ \kappa_{xy} \end{Bmatrix} \tag{2.12}$$

$$\begin{Bmatrix} M_x \\ M_y \\ M_{xy} \end{Bmatrix} = \begin{bmatrix} B_{11} & B_{12} & B_{16} \\ B_{12} & B_{22} & B_{26} \\ B_{16} & B_{26} & B_{66} \end{bmatrix} \begin{Bmatrix} \varepsilon_x^0 \\ \varepsilon_y^0 \\ \gamma_{xy}^0 \end{Bmatrix} + \begin{bmatrix} D_{11} & D_{12} & D_{16} \\ D_{12} & D_{22} & D_{26} \\ D_{16} & D_{26} & D_{66} \end{bmatrix} \begin{Bmatrix} \kappa_x \\ \kappa_y \\ \kappa_{xy} \end{Bmatrix} \tag{2.13}$$

where:

$$\begin{array}{lcl} A_{ij} & = & \sum_{k=1}^{N} (Q_{ij})_k (z_k - z_{k-1}) \\ B_{ij} & = & \frac{1}{2} \sum_{k=1}^{N} (Q_{ij})_k \left(z_k^2 - z_{k-1}^2\right) \\ D_{ij} & = & \frac{1}{3} \sum_{k=1}^{N} (Q_{ij})_k \left(z_k^3 - z_{k-1}^3\right) \end{array} \tag{2.14}$$

The **A** and **D** matrices are the extensional and flexural, i.e. bending, stiffness matrices, respectively. The **A** matrix relates the in-plane stress resultants to the mid-plane strains, and the **D** matrix relates the moment resultants to the curvatures. The **B** matrix relates the in-plane stress resultants to the curvatures and the moment resultants to the mid-plain strains and is called the bending-extension coupling matrix.

This coupling can be very useful for certain structural applications, however, the coupling is typically considered to be undesirable, and the **B** matrix can be avoided by a symmetric placement of the layers with respect to the mid-plane of the laminate. Besides using symmetry, there are other ways to avoid coupling, as demonstrated in Caprino and Visconti (1982).

2.3.2 Lamination Parameters

The constitutive relations presented in the previous section include the design variables in the $\overline{Q}_{ij}$ terms, which include the layer orientation angles via equation (2.9), and thicknesses of layers as difference of layer boundary locations, $z_k - z_{k-1}$. In many engineering problems elements of the **A**,**B**, and **D** matrices appear directly in either the objective function(s) or in the constraints. Hence, what is typically designed is the individual elements of these matrices. A more convenient form of representing these matrices is based on the use of lamination parameters (LP) introduced by Tsai and Hahn (1980), which are defined as non-dimensional through-the-thickness integration of the layer orientation angles as:

$$\begin{aligned}
(V_{1\mathbf{A}}, V_{2\mathbf{A}}, V_{3\mathbf{A}}, V_{4\mathbf{A}}) &= \int_{-\frac{1}{2}}^{\frac{1}{2}} (\cos 2\theta, \sin 2\theta, \cos 4\theta, \sin 4\theta)\, d\overline{z} \\
(V_{1\mathbf{B}}, V_{2\mathbf{B}}, V_{3\mathbf{B}}, V_{4\mathbf{B}}) &= 4\int_{-\frac{1}{2}}^{\frac{1}{2}} \overline{z}\,(\cos 2\theta, \sin 2\theta, \cos 4\theta, \sin 4\theta)\, d\overline{z} \\
(V_{1\mathbf{D}}, V_{2\mathbf{D}}, V_{3\mathbf{D}}, V_{4\mathbf{D}}) &= 12\int_{-\frac{1}{2}}^{\frac{1}{2}} \overline{z}^2\,(\cos 2\theta, \sin 2\theta, \cos 4\theta, \sin 4\theta)\, d\overline{z}
\end{aligned} \tag{2.15}$$

where $V_{\mathbf{A}}$, $V_{\mathbf{B}}$ and $V_{\mathbf{D}}$ are referred to as the in-plane, coupling and bending lamination parameters respectively and $\overline{z}$ is the normalized through the thickness dimension.

It should be noted that in laminates the layer orientation angles typically do not vary continuously but are piece-wise linear, i.e. constant in each layer. Hence, the integral in equations (2.15) can be replaced by summations. Regardless of how the lamination parameters are computed, they allow laminate stiffness matrices to be expressed simply as linear functions of the material invariants as:

$$\begin{aligned}
\mathbf{A} &= h\,(\mathbf{\Gamma}_0 + \mathbf{\Gamma}_1 V_{1\mathbf{A}} + \mathbf{\Gamma}_2 V_{2\mathbf{A}} + \mathbf{\Gamma}_3 V_{3\mathbf{A}} + \mathbf{\Gamma}_4 V_{4\mathbf{A}}) \\
\mathbf{B} &= \frac{h^2}{4}\,(\mathbf{\Gamma}_1 V_{1\mathbf{B}} + \mathbf{\Gamma}_2 V_{2\mathbf{B}} + \mathbf{\Gamma}_3 V_{3\mathbf{B}} + \mathbf{\Gamma}_4 V_{4\mathbf{B}}) \\
\mathbf{D} &= \frac{h^3}{12}\,(\mathbf{\Gamma}_0 + \mathbf{\Gamma}_1 V_{1\mathbf{D}} + \mathbf{\Gamma}_2 V_{2\mathbf{D}} + \mathbf{\Gamma}_3 V_{3\mathbf{D}} + \mathbf{\Gamma}_4 V_{4\mathbf{D}})
\end{aligned} \tag{2.16}$$

where the $\mathbf{\Gamma}_i$'s are fully defined by the material invariants (2.10) as:

$$\mathbf{\Gamma}_0 = \begin{bmatrix} U_1 & U_4 & 0 \\ U_4 & U_1 & 0 \\ 0 & 0 & U_5 \end{bmatrix}, \mathbf{\Gamma}_1 = \begin{bmatrix} U_2 & 0 & 0 \\ 0 & -U_2 & 0 \\ 0 & 0 & 0 \end{bmatrix} \mathbf{\Gamma}_2 = \begin{bmatrix} 0 & 0 & U_2/2 \\ 0 & 0 & U_2/2 \\ U_2/2 & U_2/2 & 0 \end{bmatrix},$$

$$\mathbf{\Gamma}_3 = \begin{bmatrix} U_3 & -U_3 & 0 \\ -U_3 & U_3 & 0 \\ 0 & 0 & -U_3 \end{bmatrix}, \mathbf{\Gamma}_4 = \begin{bmatrix} 0 & 0 & U_3 \\ 0 & 0 & -U_3 \\ U_3 & -U_3 & 0 \end{bmatrix} \tag{2.17}$$

Since typically the laminate response can be fully described using only the stiffness matrices, lamination parameters may be used as design variables instead of ply orientation angles and stacking sequence. The representation shown above then leads to linear dependence of the **ABD** matrices on these variables that may be beneficial for design optimization.

2.3.3 Modeling Thermal Stresses with Lamination Parameters

Lamina thermal properties exhibit similar directional behavior as lamina stiffness properties, hence classical lamination theory can also be applied to incorporate thermal effects. Thermal stress and strains may result from either residual stresses present due to curing or to external thermal loading. Assuming that the thermal load variation is constant through the thickness of the laminate, constitutive relations, similar to equation (2.12) and (2.13), relating stress and moment resultants to the mid-plane thermal strains and curvatures can be derived (Gürdal et al., 1999) and expressed as:

$$\begin{aligned} \mathbf{N} + \mathbf{N}^{Th} &= \mathbf{A}\boldsymbol{\epsilon}^{\mathbf{0}} + \mathbf{B}\boldsymbol{\kappa} \\ \mathbf{M} + \mathbf{M}^{Th} &= \mathbf{B}\boldsymbol{\epsilon}^{\mathbf{0}} + \mathbf{D}\boldsymbol{\kappa} \end{aligned} \tag{2.18}$$

where $\mathbf{N}^{th}$ and $\mathbf{M}^{Th}$ are the thermal load and moment vectors defined as:

$$\mathbf{N}^{Th} = \int_{-\frac{h}{2}}^{\frac{h}{2}} \bar{\mathbf{Q}} \cdot \boldsymbol{\epsilon}^{Th} dz \quad \text{and} \quad \mathbf{M}^{Th} = \int_{-\frac{h}{2}}^{\frac{h}{2}} \bar{\mathbf{Q}} \cdot \boldsymbol{\epsilon}^{Th} z dz \tag{2.19}$$

where $\bar{\mathbf{Q}}$ is the transformed reduced stiffness matrix of the k^{th} layer, as defined in equation (2.9). The thermal strains, $\boldsymbol{\epsilon}^{Th}$, are induced by an applied temperature difference, ΔT, and are a function of the lamina longitudinal and transverse coefficients of thermal expansion (CTE), α_1 and α_2 respectively. Factoring out the terms dependent on ply orientation, it can be shown that the thermal load vector and moment can also be expressed in terms of lamination parameters as:

$$\begin{aligned} \mathbf{N}^{Th} &= h(\boldsymbol{\Lambda}_{\mathbf{0}} + V_{1\mathbf{A}}\boldsymbol{\Lambda}_{\mathbf{1}} + V_{2\mathbf{A}}\boldsymbol{\Lambda}_{\mathbf{2}})\Delta T \\ \mathbf{M}^{Th} &= \frac{h^2}{4}(V_{1\mathbf{B}}\boldsymbol{\Lambda}_{\mathbf{1}} + V_{2\mathbf{B}}\boldsymbol{\Lambda}_{\mathbf{2}})\Delta T \end{aligned} \tag{2.20}$$

where $V_{i\mathbf{A}}$ and $V_{i\mathbf{B}}$ are the normalized in-plane and coupling lamination parameters respectively, h is the laminate thickness and $\boldsymbol{\Lambda}_i$ are vectors defined as:

$$\begin{aligned} \boldsymbol{\Lambda}_0 &= (\alpha_1 Q_{11} + (\alpha_1 + \alpha_2)Q_{12} + \alpha_2 Q_{22}) \cdot \{1\ 1\ 0\}^T \\ \boldsymbol{\Lambda}_1 &= (\alpha_1 Q_{11} + (\alpha_1 - \alpha_2)Q_{12} - \alpha_2 Q_{22}) \cdot \{1\ -1\ 0\}^T \\ \boldsymbol{\Lambda}_2 &= (\alpha_1 Q_{11} + (\alpha_1 - \alpha_2)Q_{12} - \alpha_2 Q_{22}) \cdot \{0\ 0\ 1\}^T \end{aligned} \tag{2.21}$$

where α_1 and α_2 are the coefficients of thermal expansion along the primary material directions, and Q_{ij} are the reduced lamina stiffness components, as defined in equation (2.7), and are only dependent on material properties.

2.3.4 Feasible Region of Lamination Parameters

It has been shown that the laminate stiffness matrices can be expressed as a linear function of lamination parameters. However, lamination parameters cannot be selected arbitrarily since the trigonometric functions used in equation (2.15) are related. Therefore, it is necessary to prescribe a range of lamination parameters values, know as a feasible region, which result in physically meaningful laminate stiffness matrices. The feasible domain for the in-plane lamination parameters is defined as (Hammer et al., 1997):

$$\begin{gathered} 2V_{1\mathbf{A}}^2(1 - V_{3\mathbf{A}}) + 2V_{2\mathbf{A}}^2(1 + V_{2\mathbf{A}}) + V_{3\mathbf{A}}^2 + V_{4\mathbf{A}}^2 - 4V_{1\mathbf{A}}V_{2\mathbf{A}}V_{4\mathbf{A}} \le 1 \\ V_{1\mathbf{A}}^2 + V_{2\mathbf{A}}^2 \le 1 \\ -1 \le V_{i\mathbf{A}} \le 1 \ (i = 1, \ldots, 4) \end{gathered} \tag{2.22}$$

Grenestedt (1991) proved that the feasible region for an arbitrary set of lamination parameters is convex, hence equation (2.22) prescribes a closed, convex surface in $\mathbb{R}^4$. Considering the special case of balanced symmetric laminates, where $V_{2\mathbf{A}} = V_{4\mathbf{A}} = 0$, as will be discussed in subsection 2.3.5, the feasible region simplifies to:

$$\begin{gathered} V_{3\mathbf{A}} \geq 2V_{1\mathbf{A}}^2 - 1 \\ -1 \leq V_{i\mathbf{A}} \leq 1 \ (i = 1, 3) \end{gathered} \tag{2.23}$$

An identical set of expressions can be obtained for the out-of-plane lamination parameters, $V_{i\mathbf{D}}$. The feasible region prescribed by equation (2.22) is applicable when solving design problems that are dependent on either in-plane or out-of-plane lamination parameters.

Practical design problems often require both extensional and flexural laminate properties to be designed simultaneously, thus requiring a combined feasible region of in-plane and out-of-plane lamination parameters to be defined. Currently no analytical expression for the combined feasible domain is known. Diaconu and Sekine (2002) present an approximation scheme based on a variational approach to obtain the feasible domain for any set of lamination parameters implicitly. Bloomfield et al. (2009) present a method for deriving analytical expressions approximating the combined feasible region by predefining a set of ply angles. Setoodeh et al. (2006a) present a method for approximating the feasible region for an arbitrary set of lamination parameters. Using the convex nature of the feasible region, the authors develop a numerical approach based on successive convex hull approximations allowing an approximate feasible region to be expressed as a set of linear constraints (hyperplanes). These linear constraints are readily included as constraints into any standard structural optimization problem. The linear approximations presented by Setoodeh et al. (2006a) were used to define the feasible region in the majority of the work presented in this thesis.

2.3.5 Physical Interpretation of Lamination Parameters

Laminae are typically an order of magnitude stiffer in the fiber direction than in the transverse direction. Composite engineers can therefore often intuitively interpret laminate behavior based on fiber angles and stacking sequence. The use of lamination parameters provides a more abstract method for defining laminate stiffness, however, their meaning can be interpreted physically to some extent.

Consider the in-plane stiffness matrix, $\mathbf{A}$, which is defined in equation (2.16) as a linear combination of material dependent matrices, $\mathbf{\Gamma}_i$, defined in equation (2.17), multiplied the laminate thickness, h. It is therefore necessary to understand the individual contribution of each $\mathbf{\Gamma}_i$ in order to understand the influence of lamination parameters on laminate stiffness. These matrices are repeated below for convenience:

$$\mathbf{\Gamma}_0 = \begin{bmatrix} U_1 & U_4 & 0 \\ U_4 & U_1 & 0 \\ 0 & 0 & U_5 \end{bmatrix}, \mathbf{\Gamma}_1 = \begin{bmatrix} U_2 & 0 & 0 \\ 0 & -U_2 & 0 \\ 0 & 0 & 0 \end{bmatrix} \mathbf{\Gamma}_2 = \begin{bmatrix} 0 & 0 & U_2/2 \\ 0 & 0 & U_2/2 \\ U_2/2 & U_2/2 & 0 \end{bmatrix},$$

$$\mathbf{\Gamma}_3 = \begin{bmatrix} U_3 & -U_3 & 0 \\ -U_3 & U_3 & 0 \\ 0 & 0 & -U_3 \end{bmatrix}, \mathbf{\Gamma}_4 = \begin{bmatrix} 0 & 0 & U_3 \\ 0 & 0 & -U_3 \\ U_3 & -U_3 & 0 \end{bmatrix}$$

The first matrix, $\mathbf{\Gamma}_0$, is identical to the in-plane stiffness matrix of a quasi-isotropic laminate divided by its thickness. Therefore, if all in-plane lamination parameters are zero, $V_{i\mathbf{A}} = 0$, only $\mathbf{\Gamma}_0$ contributes to the laminate in-plane stiffness, see equation (2.16), and hence the in-plane stiffness matrix corresponds to that of a quasi-isotropic laminate. Lamination parameters can therefore be thought of as terms that alter the stiffness matrix of a quasi-isotropic laminate in order to introduce orthotropy.

The second matrix, $\mathbf{\Gamma}_1$, alters components A_{11} and A_{22} in the stiffness matrix, and hence influences the direction of axial stiffness. In other words, as $V_{1\mathbf{A}} \to 1$, A_{11} increases and A_{22} decreases, meaning that more fibers are aligned with the laminate material axis, corresponding roughly to a laminate with a larger percentage of $0°$ plies. Similarly, as $V_{1\mathbf{A}} \to -1$, A_{11} decreases and A_{22} increases, corresponding to a laminate with a larger percentage of $90°$ plies.

The third and fifth matrix, $\mathbf{\Gamma}_2$ and $\mathbf{\Gamma}_4$, alter components A_{16} and A_{26} in the stiffness matrix, and hence influence the amount of extension-shear coupling present in the laminate. If $V_{2\mathbf{A}} = V_{4\mathbf{A}} = 0$ the laminate is balanced and no extension-shear coupling occurs.

The influence of $\mathbf{\Gamma}_3$ on the in-plane stiffness matrix is slightly more intricate, as it influences A_{11}, A_{12}, A_{22} and A_{66}. As $V_{3\mathbf{A}} \to 1$, both the value of A_{11} and A_{22} will increase while simultaneously decreasing A_{12} and A_{66}. This implies an increase in both axial and transverse stiffness while decreasing the shear stiffness with respect to the quasi-isotropic laminate defined by $\mathbf{\Gamma}_0$. Physically this can be interpreted as increasing the percentage of $0°$ and $90°$ plies while reducing the percentage of $45°$ plies. Conversely, as $V_{3\mathbf{A}} \to -1$, both A_{12} and A_{66} increase while A_{11} and A_{22} decrease.

Further physical insight may be gained by investigating the lamination parameters' feasible region for a balanced symmetric laminate, where $V_{2\mathbf{A}} = V_{4\mathbf{A}} = V_{i\mathbf{A}} = 0$. The feasible region, known as the Miki's diagram (Miki, 1982), is presented in Figure 2.6, and corresponds to the region prescribed by equation (2.23). Point A, corresponding to $V_{1\mathbf{A}} = V_{3\mathbf{A}} = 0$, represents a quasi-isotropic laminate. Point B, where $V_{1\mathbf{A}} = V_{3\mathbf{A}} = 1$, corresponds to a laminate consisting of only $0°$ plies, similarly, point F is a laminate consisting of only $90°$ plies. Tracing along the parabolic boundary from point A, through points B, C, D and E to point F represent cross-ply laminates ranging from 0°_s through $\pm 30^\circ_s$, $\pm 45^\circ_s$, $\pm 60^\circ_s$ to 90°_s.

All points on the boundary of the lamination parameters' feasible region can therefore be directly converted to an equivalent laminate of only one orientation angle. A straight line through any lamination parameter combination, $(V_{1\mathbf{A}}, V_{3\mathbf{A}})$, will intersect the feasible region boundary at two points. The distance between these intersection points and $(V_{1\mathbf{A}}, V_{3\mathbf{A}})$ can be used to compute the ratio of plies corresponding to the intersection points required to obtain matching laminate stiffness. Consider point G for example, which lies mid-way between point A and point F, and hence can be translated into a laminate with equal amounts of 0°_s and 90°_s plies. Similarly point A, lies twice as far point B as from point E and hence can be converted to a laminate with twice as many $60°$ plies as $0°$ plies, i.e. $[\pm 60, 0]_s$. The same point (A) is also midway

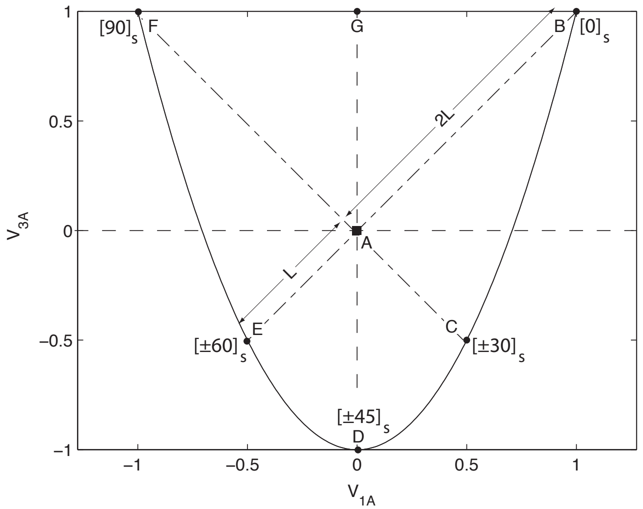

Figure 2.6: *Miki's diagram, representing the feasible region of the in-plane lamination parameters for balanced laminates, given by equation* (2.23)

between point D and point G, and it can therefore also be thought of as a laminate with an equivalent contribution of ±45° and [0, 90], in other words $[0, \pm 45, 90]_s$, the standard quasi-isotropic laminate layup. Theoretically, an infinite number of alternative laminates can be constructed for this combination of lamination parameters, all yielding an identical in-plane stiffness matrix.

It should also be noted that no two combinations of lamination parameters can be used to represent the same stiffness matrix, which is not the case when defining laminates in terms of fiber angles. The one-to-one relationship between lamination parameters and stiffness matrix is one of the advantages of designing in terms of lamination parameters since the structural response is often a function of the stiffness matrix and not of the laminate.

The lamination parameter diagram for the out-of-plane lamination parameters, $V_{1\mathbf{D}}$ and $V_{3\mathbf{D}}$), is identical to that presented in Figure 2.6. Therefore, the bending stiffness properties of a balanced symmetric laminate can be related to the out-of-plane lamination parameters in a similar logical manner. For example, laminates that are described by lamination parameters near point B will have high bending stiffness along the material axis and low bending stiffness in the transverse direction. The opposite is true for laminates described by points close to point F, while laminates described by points close to point D will have resistance against a twisting moment.

2.3.6 Modeling Variable Stiffness Laminates

Several methods are available to prescribe spatial laminate stiffness variation, as discussed in section 1.3.1. Intuitively, design variables have generally been associated directly with elements when using finite element analysis to model structural response. This approach provides the largest set of design variables for a fixed mesh density, When independent design variables are assigned per element, there is no guarantee that the obtained stiffness distribution is going to be continuous. This issue is well-known and is particularly prevalent in topology optimization where it results in checkerboard patterns.

Therefore, an important aspect of designing variable stiffness structures is to ensure continuous spatial stiffness variation. To ensure smoothness of the solution, design variables can be associated with the nodes rather than elements, however, stiffness properties per element are required to construct the element stiffness matrices necessary for analysis. One possibility is to use a finite element formulation that allows for the variation of stiffness properties of the element. For example, Huang and Haftka (2005) use bilinear interpolation to determine the orientation at the center of a quadrilateral element based on the fiber angles defined at the four nodes. A simpler approach is to compute an average stiffness value for each element based on its nodal stiffness, and therefore, considerably simplifying the construction of element stiffness matrices as well as the calculation of sensitivities with respect to nodal variables.

Instead of computing element stiffness properties as a weighed average of nodal stiffness properties, the element compliance is computed as the average of the nodal compliance. This approach, called reciprocal interpolation, is introduced by Abdalla et al. (2007) and is effective for producing smooth lamination parameter distributions. The average element compliance is therefor given by:

$$\bar{\mathbf{A}}_e^{-1} = \sum_{i \in \mathcal{I}_e} w_{e,i} \mathbf{A}_i^{-1} \tag{2.24}$$

where i denotes the node numbers and $\mathcal{I}_e$ is the set of nodes connected to element e. The sum is weighed by integration weighing coefficients w_e such that for a smooth function, f:

$$\int\limits_{\Omega_e} f d\Omega \approx \int\limits_{\Omega_e} d\Omega \sum_{i \in \mathcal{I}_e} w_{e,i}\, f_i \tag{2.25}$$

The element stiffness matrix can subsequently be defined by inverting the element compliance defined by equation (2.24). Similar expressions are used for interpolating the inverse of the bending stiffness matrix. It also important to note that the definition of stiffness properties at nodes necessitates the use of consistent material coordinate axis definitions for all elements.

2.4 Advantages and Limitations of the Design Approach

As a summary, the design approach presented in this chapter was motivated by the insight outlined in section 2.2, where it was highlighted that an equivalent laminate stiffness formulation is typically sufficient to model most structural response types, whereas tow level information is often necessary to impose detailed manufacturing constraints. A multi-step design optimization framework for variable stiffness structures was outlined. In the first step the conceptual stiffness distribution maximizing the structural performance is obtained. In a second step, feasible fiber angle distributions are obtained to match the optimum conceptual stiffness distribution. In a final step, the fiber angle distribution is converted into a continuous set of fiber paths that can be used to manufacture the variable stiffness laminates using automated fiber placement machines.

The developed multi-step framework has several advantages, which relate primarily to the efficiency with which certain design objectives and constraints can be considered. Using a continuous laminate stiffness formulation with conservative convex separable approximations in an initial step allows efficient gradient based optimizers to be used to obtain the stiffness distribution to maximize structural performance. As will be demonstrated in subsequent chapters, fewer than thirty finite element analysis runs are typically necessary to obtain the optimum laminate stiffness distribution for problems with thousands of design variables. The separable nature of the developed structural approximations allows each design point to be solved in parallel, reducing the time required to obtain the optimum solution when multiple processors are available. The inherently discrete and detailed nature of the information required to evaluate design requirements associated with laminate stacking sequence and manufacturing, necessitates the use of heuristic algorithms. Solving the optimization problems directly for large structures with several design variables would quickly become restrictive. Knowledge of the optimum conceptual stiffness distribution allows the same structural response approximations to be used by the heuristic search algorithms, and hence improves the overall design framework efficiency. The multi-step nature of the developed design framework also facilitates the integration of additional design drivers, not developed here, at the appropriate level during the design. For example, layup rates can be maximized for the given design by including path planning algorithms when generating the fiber paths in the third step.

The disadvantages of the developed framework relate primarily to the difficulty surrounding the derivation of physically meaningful structural response approximation, especially when integrating the design approach into a commercial finite element analysis environment. The developed conservative convex separable approximations are presented in detail next in chapter 3, where the requirements imposed on the approximations are highlighted. The challenges of integrating the design framework with a commercial finite element code are demonstrated using a practical example in chapter 10.

One of the limitations of using lamination parameters for composite design has been the difficulty of incorporating strength constraints into the optimization process. A formulation for predicting laminate strength in lamination parameter space, based on Tsai-Wu, is presented chapter 4 and is subsequently used to maximize the failure strength of an example problem in chapter 9.

The developed design approach is inherently focused on structural performance, as the initial design step accounts mainly for structural performance metrics. Therefore, for problems which are driven primarily by manufacturing requirements, the design framework may become inefficient due to the possibility of an excessive number of design updates being required in the second and third step. Finally, the current design framework assumes that the part geometry has already been defined, however, including shape and/or topology optimization in the design process may yield significant improvements in structural performance in addition to the improvements obtained based on stiffness optimization alone.

CHAPTER 3

Optimization Methodology for Variable Stiffness Structures

"*Anyone who has never made a mistake has never tried anything new*"

Albert Einstein

An overview of the developed variable stiffness design optimization framework was presented in chapter 2, in which both the first and second optimization steps make use of structural response approximations. The derivation of suitable structural response approximations was therefore key to obtaining a tractable optimization problem. A generic form of the developed structural approximation method and its inclusion in an iterative design optimization framework is presented in this chapter.

An introduction to approximation methods based on a generic optimization problem is presented in section 3.1. An approximation scheme was derived specifically for composite laminate optimization problems, based on the globally convergent conservative convex approximation method (CCSA) of Svanberg (2002), and is presented in section 3.2. Two methods to ensure conservativeness and strict convexity of the derived approximation were implemented and these are discussed in section 3.3. In order to optimize the laminate stiffness distribution, corresponding to the first step of the developed design framework presented in chapter 2, the approximations were implemented within an iterative optimization loop, and the successive approximation scheme that was used is described in section 3.4, which differs slightly with respect to the CCSA method.

3.1 Introduction

A generic optimization problem is presented in subsection 3.1.1 to provide the context within which the structural approximation methods can be discussed. A brief introduction to structural approximation methods and several examples of approximations developed in the past are presented subsection 3.1.2.

3.1.1 Overview of the Design Problem

In structural optimization the design problem, given in equation (3.1), typically consists of minimizing a selected objective function, $f_0(\mathbf{x})$, subject to a given set of constraints, $f_j(\mathbf{x})$:

$$\begin{aligned} \min f_0(\mathbf{x}) & \\ f_j(\mathbf{x}) \leqslant 0 \quad & j = 1 \ldots m \\ x_i^L \leqslant x_i \leqslant x_i^U \quad & i = 1 \ldots n \end{aligned} \tag{3.1}$$

where $f_0(\mathbf{x})$ and $f_j(\mathbf{x})$ generally represent $m+1$ structural responses, such as structural stiffness, strength, buckling or total weight. The design variables, x_i or collectively $\mathbf{x}$, may be terms describing structural geometry, thicknesses or fiber angle orientations in composite laminates and are bound by x_i^L and x_i^U. It may also be desirable to consider non-structural related functions such as production time, manufacturability or cost, as discussed in section 2.1. In these cases, the design variables may no longer relate only to the structure, but also include parameters to define available materials or production methods.

A review of how ever-increasing computational power is used to solve structural optimization problems is presented in Venkataraman and Haftka (2004). The authors identified three areas for which computational resources have been used; namely modeling, analysis and optimization. The ease, or difficulty, with which problem (3.1) can be solved and the range of algorithms that can be used to solve it, therefore depend primarily on analysis complexity, model complexity and optimization complexity.

Clearly, the more complicated it is to evaluate each response present during optimization, the more computationally expensive, and possibly more complex, the design problem becomes. Minimum weight design of a wing, with fully coupled structural and aerodynamic models, is significantly more complex than considering the same problem with a static tip load. Similarly, analyzing non-linear post-buckling response of a structure is more complex than determining the linear bifurcation point. Increased analysis complexity does not automatically result in a more complex optimization problem, however, a change in the nature of the considered response may.

Model complexity is related to model fidelity and usually only effects required computation time and the accuracy of the obtained response, while the optimization problem remains essentially unchanged. For example, by generating a simplified model of the wing, the computational burden is reduced while the problem complexity remains the same. However, for variable stiffness laminates, design variables may be associated with individual elements of a finite element model, hence increasing model fidelity will result in a more complex optimization problem due to an increased number of design variables.

Optimization complexity is influenced by the number of considered responses, number of design variables and their nature. Increasing the number of either the responses or the design variables, inevitably increases design problem complexity and often effects the type of solution algorithms that can best be employed. The type of design variables and how they relate to the structural responses also greatly influences optimization problem complexity. Discrete design variables, such as the number of plies in a laminate or number of stiffeners on a panel, are notoriously difficult to handle using standard gradient based optimization techniques. Design variables which are interdependent also tend to render an optimization problem more complex. The nature of the response, in other words, how response and design variables relate, in particular a linear versus nonlinear relationship, also significantly influences the optimization problem complexity.

The computational cost associated with evaluating structural responses and sensitivities with respect to all design variables for every iteration usually precludes the direct solution of the optimization problem given in equation (3.1). Structural responses are typically implicit functions of design variables and hence must be evaluated numerically using finite element analysis, leading to excessive runtime to solve even modest problems. The restrictive computational burden imposed by the original problem can be alleviated by replacing it with an approximation, which is readily evaluated, as is discussed briefly below.

3.1.2 Structural Approximation Methods

Two types of approximations can be differentiated; one, *problem approximations*, in which a simpler equivalent problem is sought to replace the original problem, and two, *function approximations*, in which the structural responses required to evaluate the design problem are approximated explicitly in terms of design variables. Problem and function approximations can be created such that they are valid either only *locally* or *globally.*

Local problem approximations typically involve reducing the number of design variables or response functions to be used during optimization. Global problem approximations typically involve model simplifications by either using a coarser mesh or by replacing the original model with a simplified model. Hence neither local nor global problem approximations are attractive when developing a generic variable stiffness laminate design framework.

Global function approximations, such as response surface methods, are generally valid for the entire design space or a large portion of it. Multiple function evaluations are often necessary to obtain function approximations which are globally valid, and hence the computational expense can become restrictive when considering a large number of design variables. Therefore, local function approximation methods are considered here, and the original problem, equation (3.1), is replaced by a problem based on explicit approximations of the objective function, $\tilde{f}_0$, and constraints, $\tilde{f}_j$, such that:

$$\begin{aligned} &\min \tilde{f}_0(\mathbf{x}) \\ &\tilde{f}_j(\mathbf{x}) \leqslant 0 \qquad j = 1 \dots m \\ &x_i^L \leqslant x_i \leqslant x_i^U \quad i = 1 \dots n \end{aligned} \tag{3.2}$$

Solving problem (3.2) yields the optimum solution for the approximate problem. The obtained optimum is typically used to update the original design problem, which is subsequently used to generate a new approximate problem, continuing iteratively until a converged solution is found. Methods in which an approximate problem is solved iteratively are known as successive approximation methods, and are popular in structural optimization as they increase computational efficiency by reducing the number of structural analyses required to find an optimum.

Local function approximations are usually based on a Taylor series expansion of the original function, f, about a local design point, $\mathbf{x_0}$. Approximations are typically restricted to first order expansions due to the high computational cost associated with evaluating higher order derivatives. A linear approximation is the simplest, and is a first order Taylor series expansion of a function directly in terms of the design variables, x_i, as:

$$f_L = f(\mathbf{x}_0) + \sum_{i=1}^{n} \left(\left. \frac{\partial f}{\partial x_i} \right|_0 (x_i - x_{0i}) \right) \tag{3.3}$$

Linear approximations tend to be inaccurate, even near the approximation point, as they generally do not capture the underlying nature of the physical response well. Hence more suitable approximations have been developed, often based on intermediate variables, which ensure more linear behavior of the approximation. The reciprocal approximation, where a function is expanded in terms of the reciprocal of the design variable, $\frac{1}{x_i}$, is popular for structural applications and is given by:

$$f_I = f(\mathbf{x}_0) + \sum_{i=1}^{n} \left(\left. \frac{\partial f}{\partial x_i^{-1}} \right|_0 (x_i^{-1} - x_{0i}^{-1}) \right) \tag{3.4}$$

The reciprocal approximation's popularity stems primarily from earlier structural optimization of truss structures, where the cross-sectional areas of the truss elements were considered as design variables. For statically determinate structures, stresses and displacements are linear functions of the reciprocal of these design variables, however, the reciprocal approximation has also proven to be well suited when solving statically indeterminate problems.

The conservative approximation, introduced by Starnes and Haftka (1979), is a hybrid approximation based on both the linear and reciprocal approximations and is given by:

$$f_C = f(\mathbf{x}_0) + \sum_{i=1}^{n} \delta_i \left(\left. \frac{\partial f}{\partial x_i} \right|_0 (x_i - x_{0i}) \right) + (1 - \delta_i) \left(\left. \frac{\partial f}{\partial x_i^{-1}} \right|_0 (x_i^{-1} - x_{0i}^{-1}) \right) \tag{3.5}$$

where the first term in the summation stems from the linear approximation and the second term from the reciprocal approximation. Conservativeness is guaranteed by selecting the most conservative of the two contributing terms in equation (3.5) through parameter δ_i, defined as:

$$\delta_i = \begin{cases} 1 & \text{for } \frac{\partial f}{\partial x_i} x_{0i} \geqslant 0 \\ 0 & \text{otherwise} \end{cases} \tag{3.6}$$

It should be noted that the conservative approximation does not guarantee absolute conservativeness, i.e. it does not guarantee that the approximation is more conservative than the actual function value. It is only guaranteed to be more conservative than either the linear or reciprocal approximation.

All of the above approximations have the advantage of being separable, in addition the reciprocal approximation is also strictly convex. Approximating objective functions and constraints using the conservative approximation therefore results in a convex optimization problem, which is guaranteed to have a unique optimum and can be solved readily with dual methods. Several other separable, conservative, convex approximations have been developed in the past. A detailed review of different approximation methods available for structural optimization is presented in Barthelemy and Haftka (1993). An approximation scheme was developed specifically for the design of laminated composite structures and is presented in the following section.

3.2 Conservative Convex Separable Approximations

A large number of design variables are typically required to describe the stiffness properties of variable stiffness composite structures. In the optimization framework presented in chapter 2, the number of design variables is, in the most general case, proportional to the number of elements or nodes used to discretize the structure. Optimization problems containing several hundred thousand design variables are therefore not unrealistic and the adoption of an efficient optimization framework is therefore essential.

Conservative convex separable approximation methods (CCSA), introduced by Svanberg (2002), are well suited to solving inequality-constrained non-linear programming problems with a large number of design variables. Their efficiency is primarily due to the separability of the approximations. Separability also allows each problem to be solved in parallel, allowing the optimization algorithm to take advantage of the multicore processors prevalent in computers today. The conservative and convex nature of the approximations ensure that a single feasible solution is found for each subproblem of a successive approximation scheme. Additionally, Svanberg (2002) has proved that approximations falling into the class of conservative convex separable approximations are globally convergent, guaranteeing that an optimal solution will be found. The aforementioned advantages motivated the development of a generic approach to approximating an arbitrary response of a variable stiffness laminate and casting it into an optimization framework similar to that presented by Svanberg (2002). Therefore, a new approximation was derived with the following form:

$$f_S(\mathbf{x}) = f_P(\mathbf{x}) + \rho f_D(\mathbf{x}) \tag{3.7}$$

where the first term on the right hand side, f_P, is an approximation that ensures that both the function value and the gradient of the approximation match those of the original function. The second term, f_D, is an additional convexifying term that is scaled by a constant factor, ρ. This term is used to ensure the conservativeness and convexity of the approximation as a whole. The first term, f_P, is derived in this section while the second term and the corresponding scaling factor are treated in section 3.3.

For an approximation to be applicable within the framework given by Svanberg (2002) it must meet several requirements, which can be summarized as;

1. both f_P and f_D must be continuous, have continuous first and second order derivatives with respect to the design variables, $\mathbf{x}$, and must be separable
2. function value and gradients of the original function, f, must equal those of the approximating function, f_P, at the approximation point
3. the Hessian matrix of f_P must be positive semidefinite
4. the Hessian matrix of f_S must be positive definite

3.2.1 Approximations in Terms of Laminate Stiffness

The goal was to derive a generic expression of a separable, convex approximation that could be readily solved using commercially available optimization algorithms. The approximation is essentially a modified form of the conservative approximation, equation (3.5), of a structural response as discussed in subsection 3.1.2. Instead of imposing conservativeness via condition (3.6), which is related directly to the design variables, a physical interpretation of the structural response is used to discern between terms contributing to the linear and reciprocal terms. The approximation of a response function, f, about a local design point, $\mathbf{x_0}$, is expressed generically as:

$$f_P = f(\mathbf{x}_0) + \sum_{i=1}^{n} \left(\left.\frac{\partial \hat{f}}{\partial x_i}\right|_0 (x_i - x_{0i}) + \left.\frac{\partial \check{f}}{\partial x_i^{-1}}\right|_0 (x_i^{-1} - x_{0i}^{-1}) \right) \tag{3.8}$$

where $\hat{f}$ and $\check{f}$ are the parts of the response which are expanded *linearly* and *reciprocally* in terms of the design variables, respectively. The contribution of $\hat{f}$ and $\check{f}$ to the approximation depends on the physical nature of the considered response. The requirements imposed on the different terms are presented and discussed in section 3.2.2. A discussion of the direct application of the approximation formulation is left to chapters 5 to 8, in which the individual response approximations are discussed.

Classical lamination theory allows any given structural response to be characterized directly in terms of the laminate stiffness matrices, as presented in section 2.3. The design variables, x_i, in equation (3.8) can therefore be thought of as representing the n different stiffness terms used for the design. It is therefore convenient to rewrite equation (3.8) in the following form:

$$f_P = \sum_{i=1}^{N} \left(\left.\mathbf{\Psi}_i^m\right|_0 : \mathbf{A}_i + \left.\mathbf{\Psi}_i^b\right|_0 : \mathbf{D}_i + \left.\mathbf{\Phi}_i^m\right|_0 : \mathbf{A}_i^{-1} + \left.\mathbf{\Phi}_i^b\right|_0 : \mathbf{D}_i^{-1} \right) + \mathcal{C}_0 \tag{3.9}$$

where $i = 1 \ldots N$ are the N regions within the structure for which the stiffness is designed, $\mathbf{A}_i$ and $\mathbf{D}_i$ are the in-plane and flexural stiffness matrices of region i respectively, $\mathbf{A}_i^{-1}$ and $\mathbf{D}_i^{-1}$ are the inverse in-plane and flexural stiffness matrices of region i and:

$$\mathbf{\Psi}_i^m = \frac{\partial \hat{f}}{\partial \mathbf{A}_i}, \quad \mathbf{\Psi}_i^b = \frac{\partial \hat{f}}{\partial \mathbf{D}_i}, \quad \mathbf{\Phi}_i^m = \frac{\partial \check{f}}{\partial \mathbf{A}_i^{-1}}, \quad \mathbf{\Phi}_i^b = \frac{\partial \check{f}}{\partial \mathbf{D}_i^{-1}} \tag{3.10}$$

are the derivatives of the considered response with respect to the in-plane, or membrane, and flexural, or bending, stiffness matrices[1], denoted by superscripts m and b respectively, or their inverses, evaluated at the approximation point. The : operator represents a matrix inner product, which is the generalization of the dot-product to the matrix space, and hence essentially represents the sum of stiffness terms corresponding to region i. All remaining constant terms are considered collectively in $\mathcal{C}_0$.

[1]Note: the notation used deviates from mathematical convention, the objective is to highlight that part of the function is considered in terms of the stiffness matrices associated with a given design region while the remainder of the function is considered in terms of the inverse stiffness matrices or compliance matrices.

The approximation presented in equation (3.9) is expressed in terms of laminate stiffness matrices, **A** and **D**, instead of directly in terms of design variables. Doing so preserves the generality of the approximation since laminate stiffness matrices can be defined either directly, through intermediate variables such as lamination parameters, or by defining individual ply orientation angles and stacking sequences, as is done traditionally. Note that the approximation is therefore suitable at each step within the multi-step optimization framework presented in subsection 2.2, however, convexity in terms of design variables can only be guaranteed under certain conditions.

3.2.2 Approximation Requirements

The function approximation, f_P, must satisfy several requirements to be incorporated into a CCSA framework, as listed on page 53. It is easily verified that equation (3.9) is separable, continuous and twice differentiable with respect to an arbitrary stiffness related design variable, x. In this sense the approximation does not differ significantly with respect to the traditional conservative approximation by Starnes and Haftka (1979) given in equation (3.5).

It is important to investigate the conditions which result in convexity of the approximation, which is achieved by ensuring that the Hessian matrix is positive semidefinite. As was mentioned previously, the reason to expand a response both linearly and reciprocally, is to enforce approximation convexity. If all terms are expanded reciprocally, convexity of the approximation cannot be guaranteed, however, if non-convex terms are expanded linearly these terms do not affect overall approximation convexity. This is best understood by looking at the first and second variation of the approximate function, f_P, given in equation (3.9). The first and second variation with respect to the in-plane stiffness of the i^{th} design point are given by:

$$\delta f = \mathbf{\Psi}_i^m : \delta \mathbf{A}_i - \mathbf{\Phi}_i^m : \mathbf{A}_i^{-1} \cdot \delta \mathbf{A}_i \cdot \mathbf{A}_i^{-1} \tag{3.11}$$

$$\frac{\delta^2 f}{2} = \mathrm{tr}\left[\left(\mathbf{A}_\mathrm{i}^{-\frac{1}{2}} \cdot \delta \mathbf{A}_\mathrm{i} \cdot \mathbf{A}_\mathrm{i}^{-\frac{1}{2}}\right) \cdot \left(\mathbf{A}_\mathrm{i}^{-\frac{1}{2}} \cdot \mathbf{\Phi}_\mathrm{i}^\mathrm{m} \cdot \mathbf{A}_\mathrm{i}^{-\frac{1}{2}}\right) \cdot \left(\mathbf{A}_\mathrm{i}^{-\frac{1}{2}} \cdot \delta \mathbf{A}_\mathrm{i} \cdot \mathbf{A}_\mathrm{i}^{-\frac{1}{2}}\right)\right] \tag{3.12}$$

where tr represents the matrix trace.

To ensure approximation convexity the second derivative must be greater than or equal to zero, in other words the function must have non-negative curvature. On inspection of equation (3.12), and noting that the in-plane stiffness matrix is positive definite by definition, it can can be seen that non-negativity is guaranteed if $\mathbf{\Phi}^m$ is positive semidefinite. A similar expression can be derived for the second variation of the approximation function with respect to the flexural stiffness to show that $\mathbf{\Phi}^b$ must also be positive semidefinite to ensure approximation convexity.

Convexity of the developed approximation is dependent on the derivatives of the response with respect to the compliance matrices and can be guaranteed if these are positive semidefinite. This may be achieved by mathematically separating $\mathbf{\Phi}^m$ and $\mathbf{\Phi}^b$ into a positive semidefinite and negative definite part and subsequently expanding the negative definite part linearly. Alternatively, the derivatives of an approximated response with respect to stiffness can be based on physical insight gained from studying the nature of the considered response equations. In the research reported in this thesis the second approach, based on physical insight, was used to develop approximations for several different structural responses, as shown in chapters 5 to 8.

3.2.3 Lamination Parameters as Design Variables

An approximation meeting the requirements in section 3.2.2 and of the form given in equation (3.9) is separable and convex in terms of the elements of the laminate stiffness matrices, **A**, **D** and their reciprocals. It is not practical to design in terms of the individual elements of the laminate stiffness matrices, $A_{11}, A_{12}, \ldots$, primarily because the matrix elements are interdependent and cannot be selected arbitrarily. Parametrizing the approximation in terms of ply orientation angles results in a non-convex approximation, see for example Setoodeh et al. (2009). This problem is mitigated when parametrizing the approximation in terms of lamination parameters, since the stiffness matrices are linear functions of the lamination parameters, as can be seen from equation (2.16) on page 42. The approximation therefore retains all the required properties when using lamination parameters as design variables.

An additional advantage of the linear dependence of the extensional and flexural stiffness matrices on lamination parameters, is that the first and second order derivatives of the approximation with respect to the design variables are readily available. For example, the derivative of the approximate function of region i with respect to the first in-plane lamination parameter, $V_{i1\mathbf{A}}$ is given by:

$$\frac{\partial f_P}{\partial V_{i1\mathbf{A}}} = \mathbf{\Psi}_i^m : \mathbf{\Gamma}_1 - \mathbf{\Phi}_i^m : (\mathbf{A}_i^{-1} \cdot \mathbf{\Gamma}_1 \cdot \mathbf{A}_i^{-1}) \tag{3.13}$$

where $\mathbf{\Gamma}_1$ is a constant matrix fully defined by the material invariants as shown in equation (2.17). The derivatives with respect to the remaining lamination parameters can be computed similarly.

3.2.4 Laminate Thickness as a Design Variable

The on-the-fly cut and restart capabilities of modern fiber placement machines allows laminate thickness to be varied quasi-continuously over a structure. Alternatively, thickness variation may arise within a laminate due to the gaps and overlaps that occur due fiber steering, as highlighted in section 1.2.2. It was therefore also interesting to investigate how laminate thickness at each design point, h_i, can be included into the optimization process. A laminate's in-plane and bending stiffness are characterized by lamination parameters and laminate thickness, as can be seen from equation (2.16), see page 42. Since the approximation formulation presented in equation (3.9) is not given in terms of design variables directly, but in terms of stiffness matrices, thickness can be readily included as a design variable.

In order to include thickness generically as a design variable two modifications of the approximation were made; one, the approximation formulation, equation (3.9), was generalized to include terms dependent only on laminate thickness, and two, to retain the properties of the approximation the terms that were linear in stiffness had to be made linear in terms of the design variables. Additionally, to obtained meaningful results it was important that the total weight of the structure was bounded.

Approximation Generalization for Thickness

In the separable convex approximation, presented in section 3.2, the assumption is made that a structural response, f, can be approximated by expanding the response in terms of material stiffness matrices. This assumption remains valid if the response does not include terms that depend explicitly on laminate thickness, however, this is not always the case. For example, laminate weight is only a function of laminate thickness and therefore cannot be approximated using equation (3.9). The approximation can be extended to include an additional term, linear in laminate thickness, such that:

$$f_P = \sum_{i=1}^{N} \left(\boldsymbol{\Psi}_i^m \big|_0 : \hat{\mathbf{A}}_i + \boldsymbol{\Psi}_i^b \big|_0 : \hat{\mathbf{D}}_i + \boldsymbol{\Phi}_i^m \big|_0 : \mathbf{A}_i^{-1} + \boldsymbol{\Phi}_i^b \big|_0 : \mathbf{D}_i^{-1} + \alpha_i \big|_0 h_i \right) + \mathcal{C}_0 \quad (3.14)$$

where $\hat{\mathbf{A}}$ and $\hat{\mathbf{D}}$ are the material dependent terms of the in-plane and bending stiffness matrices, respectively, as explained in the following subsection, and α_i is the derivative with respect to local laminate thickness, h_i, of the terms, $\bar{f}$, which depend *explicitly* on thickness and is given by:

$$\alpha_i = \frac{\partial \bar{f}}{\partial h_i} \quad (3.15)$$

Linearization of Stiffness Terms

The convexity of the approximation presented in section 3.2 was guaranteed by expanding part of the response linearly in terms of laminate stiffness. Since laminate stiffness is a linear functions of lamination parameters, the approximation was also linear in terms of the design variables. However, when thickness is included as a design variable this is no longer the case. The terms linear in laminate stiffness can readily be linearized in terms of design variables. Consider for example the in-plane stiffness given by:

$$\mathbf{A}(\mathbf{V}, h) = \hat{\mathbf{A}}(\mathbf{V}) h \quad (3.16)$$

where $\hat{\mathbf{A}}$ is the material dependent part of the stiffness matrix and is only a function of lamination parameters and h is the laminate thickness. The first term in approximation (3.9) can therefore be linearized as:

$$\boldsymbol{\Psi}_i^m \big|_0 : \mathbf{A}_i \approx \boldsymbol{\Psi}_i^m \big|_0 : \left(\hat{\mathbf{A}}_{0i} h_i + \hat{\mathbf{A}}_i h_{0i} \right) + \mathcal{C} \quad (3.17)$$

where $\hat{\mathbf{A}}_{0i}$ and h_{0i} are the material dependent stiffness terms and thickness term at the approximation point, $\hat{\mathbf{A}}_i$ and h_i are the design variables related to the material dependent stiffness terms and thickness term for the i^{th} design point and $\mathcal{C}$ contains the remaining constant terms. The bending stiffness matrix can be linearized in an similar manner.

Bounding Structural Weight

Including thickness as a design variable typically results in an unbound optimization problem. Therefore, it is necessary to constrain the maximum structural weight or volume if meaningful results are to be obtained. Bounding the total structural volume is identical to bounding its weight if material density is uniform and this is achieved by including the following constraint in the optimization problem:

$$\mathcal{V} - \mathcal{V}_0 \leqslant 0 \tag{3.18}$$

where $\mathcal{V}_0$ is the upper bound on the total volume, $\mathcal{V}$, which can be expressed as:

$$\mathcal{V} = \sum_{i=1}^{N} \mathcal{A}_i h_i \tag{3.19}$$

where $\mathcal{A}_i$ is the area of the i^{th} region. The total volume can be treated as a structural response and can be cast into the approximation form presented in equation (3.14), and will only contribute to the linear thickness term $\alpha_i h_i$.

3.3 Ensuring Approximation Conservativeness and Convexity

A convex separable approximation scheme for arbitrary structural responses was developed and presented in section 3.2. Expressing a structural response in the form of the developed approximation scheme yields a convex approximation, however, this approximation may lack strict convexity or conservativeness. Convergence problems may be encountered when solving an optimization problem based on approximations lacking strict convexity while the presence of multi-modal responses, such as buckling, may further compound convergence difficulties.

Two different methods were adopted to ensure approximation conservativeness and strict convexity. Initially the proximal point algorithm was used to ensure convexity in terms of design variables directly, as presented in subsection 3.3.1. In later work a more general approach was developed by adding curvature to the convex separable approximations based on laminate stiffness properties, presented in section 3.2, as highlighted in subsection 3.3.2. An adaptive damping scheme, which dynamically scales the conservative convex term, was also developed to ensure monotonous convergence, this is presented in subsection 3.3.3.

3.3.1 Conservativeness and Convexity in Lamination Parameter Space

In early stages of this research work, the proximal point algorithm, following Rockafellar (1976), was implemented. Using the proximal point algorithm is an effective method to ensure design convergence using an iterative solution scheme while retaining approximation separability. A strictly convex approximation is obtained by appending a strictly convex function in terms of the design variables, such that:

$$f_S = f_P(\mathbf{x}) + \frac{\eta}{2}\|\mathbf{x} - \mathbf{x}_0\|^2 \tag{3.20}$$

where $\eta > 0$ and is a scaling factor that can be freely defined while $\mathbf{x}_0$ represents the design state at the approximation point. Note that the additional term does not affect either function value nor gradients at the approximation point and its contribution tends to zero as the solution converges. The proximal term is also twice continuously differentiable and has positive curvature, therefore it meets all the requirements imposed by Svanberg (2002) on the conservative convex term.

The response approximation presented in equation (3.9) is separable per design region, i, hence the proximal term can be included such that:

$$f_S = \sum_{i=1}^{N} \left(\mathbf{\Psi}_i^m : \mathbf{A}_i + \mathbf{\Psi}_i^b : \mathbf{D}_i + \mathbf{\Phi}_i^m : \mathbf{A}_i^{-1} + \mathbf{\Phi}_i^b : \mathbf{D}_i^{-1} + \frac{\eta}{2} \cdot \mathcal{C}_i \right) + \mathcal{C}_0 \tag{3.21}$$

were the scalar convex term, $\mathcal{C}_i$, is defined as:

$$\mathcal{C}_i = (\mathbf{V}_i - \mathbf{V}_{0i})^T \cdot (\mathbf{V}_i - \mathbf{V}_{0i}) \tag{3.22}$$

where $\mathbf{V}_i$ is the vector of design variables, which are the lamination parameters and eventually thickness, associated with the i^{th} design region, and $\mathbf{V}_{0i}$ is the vector of design variables at the approximation point.

Note that the value chosen for η is constant and essentially represents a move limit for the design variables, hence it influences the speed of convergence. Smaller values of η result in quicker convergence, however, as η tends to zero the local approximation may no longer be strictly convex.

The choice of η can be made somewhat less arbitrary by considering the approximate gradient of a function, $f(\mathbf{x})$, that is optimized:

$$\nabla f = \nabla f_0 + \eta \cdot \|x_i - x_{0i}\| + (\mathbf{H} + \eta \mathbf{I})\Delta \mathbf{x} = 0 \tag{3.23}$$

where x_i are the design variables, $\mathbf{H}$ is the Hessian matrix and $\mathbf{I}$ is the identity matrix. The Hessian matrix becomes negligible for large values of η and the gradient at the initial point, $\mathbf{x} = \mathbf{x}_0$, is therefore found to be:

$$\nabla f = \nabla f_0 + \eta \cdot \mathbf{I} \Delta \mathbf{x} \tag{3.24}$$

Therefore, if the change in design variables is limited to a maximum predefined value, η can be expressed as the maximum gradient over all elements at the initial point divided by the chosen move limit $\|\Delta \mathbf{x}\|$:

$$\eta \cdot \|\Delta \mathbf{x}\| = \min_i \nabla f_i(\mathbf{x}_0) \tag{3.25}$$

The design variables for equation (3.21) are lamination parameters, i.e. $\mathbf{x} \in [-1, 1]$, and hence a reasonable value for the move limit, $\|\Delta \mathbf{x}\|$, of 0.2 to 0.4 can be assumed.

In all the design studies presented in this thesis and conducted using the proximal point algorithm in lamination parameter space, a single value of η was computed for all the responses and it remained constant during the entire optimization process. In a more general setting it is not efficient to assume that the amount of conservativeness and convexity appended to each response remains the same during the optimization process. In later studies a more general and adaptable approach was developed, as discussed in the next subsection.

3.3.2 Conservativeness and Convexity in Stiffness Space

The proximal point algorithm discussed in the previous subsection was used successfully to solve several different design optimization problems, however, a more general formulation, expressed in terms of laminate stiffness instead of lamination parameters, would be more desirable. The aim was to derive a convexifying term, f_D, in the same form as the response approximation, f_P given in equation (3.9). Additionally the scaling of conservativeness and convexity, ρ, was allowed to vary dynamically during the optimization process as discussed below in subsection 3.3.3. The general form of the conservative convex separable approximation was given by:

$$f_S(\mathbf{x}) = f_P(\mathbf{x}) + \rho f_D(\mathbf{x}) \tag{3.7}$$

using the response approximation, f_P, derived in section 3.2 and given in equation (3.9). A convex term in stiffness space was subsequently defined as:

$$f_D = \sum_{i=1}^{N} w_i \left(\mathbf{A}_{0i}^{-1} : \mathbf{A}_i + \mathbf{D}_{0i}^{-1} : \mathbf{D}_i + \mathbf{A}_{0i} : \mathbf{A}_i^{-1} + \mathbf{D}_{0i} : \mathbf{D}_i^{-1} - 4\,\mathbf{I} : \mathbf{I} \right) \tag{3.26}$$

where each term in the summation is locally scaled through a positive weighing factor w_i, and $\mathbf{A}_{0i}$ and $\mathbf{A}_{0i}^{-1}$ represent the extensional stiffness and compliance matrices at the approximation point, $\mathbf{x}_0$, respectively. Similarly, $\mathbf{D}_{0i}$ and $\mathbf{D}_{0i}^{-1}$ respectively represent the flexural stiffness and compliance matrices at the approximation point. The last term ensures that the function value of the convex term is zero at the approximation point, where $\mathbf{I}$ is the identity matrix of size 3.

The local weighing factor, w_i, ensures that each separable term within a response approximation can be scaled proportionally. In this case scaling was chosen to be proportional to individual design region areas, $\mathcal{A}_i$, such that:

$$w_i = \frac{\mathcal{A}_i}{\sum_{i=1}^{N} \mathcal{A}_i} \tag{3.27}$$

It is easily verified that f_D meets all the requirements imposed by Svanberg (2002) on the conservative convex term for the CCSA framework. The function, f_D, is continuous and twice differentiable and does not affect function value nor gradient at the approximation point. The Hessian is positive definite as both the stiffness and compliance matrices are per definition positive definite.

Note that the convexifying term follows the form of the original approximation, equation (3.9), hence it is readily integrated into the optimization routine by modifying the original local response sensitivities such that:

$$\breve{\boldsymbol{\Psi}}_i^m \Big|_0 = \boldsymbol{\Psi}_i^m \Big|_0 + \rho w_i \mathbf{A}_{0i}^{-1} \tag{3.28}$$

where $\boldsymbol{\Psi}_i^m$ is the sensitivity matrix of the original response with respect to the in-plane stiffness matrix elements of the i^{th} design region as described in equation (3.10). The remaining sensitivity matrices can be modified similarly.

The only remaining difficulty is to determine a suitable value for the damping factor, ρ, which is discussed below.

3.3.3 Adaptive Damping Scheme

The damping parameter, ρ, ensures the convexity and conservativeness of the developed separable convex approximation. If large damping values are chosen the function approximations will be over conservative, which will lead to an excessive number of iterations being required to converge to the optimum solution. Using smaller damping values will increase the effective design freedom, however, if they are too small an excessive number of designs will be rejected, and this will also result in an excessive number of iterations. Therefore, the efficiency of the optimizer is greatly influenced by how the damping parameters are initialized and evolve.

A meaningful approach for obtaining initial damping values, and a discussion of a method that can be used to adapt the damping values during an iterative optimization process are presented in this section. The discussion is based on the iterative design optimization formulation presented in section 3.4, hence readers unfamiliar with this topic are recommended to first read section 3.4.

Damping Initialization

An expression for an initial damping factor was derived as an average damping value for all considered structural responses. The approach used is similar to that presented in section 3.3.1, however, in this case a damping term is computed that results in a reasonable move limit in stiffness and compliance space. Consider the Lagrangian of a constrained optimization problem, which is given by:

$$\mathcal{L} = \sum_{j=0}^{m} \mu_j f_{Sj} = \sum_{j=0}^{m} \mu_j \left(f_{Pj} + \rho_j f_{Dj} \right) \tag{3.29}$$

where f_{Sj} is the conservative approximation of the response, f_{Pj}, augmented by a scaled convex term, f_{Dj}, as given in equation (3.7), and μ_j is the Lagrange multiplier or dual variable associated with the j^{th} response of m responses. Since the Lagrange multipliers are not known a priori an average damping term can be computed by assuming that all the Lagrange multipliers are identical and scaled to unity such that equation (3.29) becomes:

$$\mathcal{L} = \sum_{j=0}^{m} f_{Pj} + \rho_s f_D \tag{3.30}$$

where ρ_s is an average damping parameter scaling for all responses, which is related to the individual damping terms $(j+1)\rho_j = \rho_s$.

The objective is therefore to find a value of ρ_s that results in a reasonable move limit in stiffness space. In order to make the selection of the scaling factor less arbitrary, consider the change in design variables, $\Delta \mathbf{x}$, which results from a step change in the Newton Method:

$$\Delta \mathbf{x} = -\mathbf{H}^{-1}(\mathbf{x}_0) \nabla f(\mathbf{x}_0) \tag{3.31}$$

where $\mathbf{H}$ and ∇f are the Hessian matrix and gradient vector of the considered function and $\mathbf{x}_0$ is the initial set of design variables related to the laminate stiffness. The gradient is only a function of the function approximation, f_{Pj}, for the developed approximation, and if the damping term is assumed to be dominant the Hessian matrix reduces to the identity matrix, such that:

$$\Delta \mathbf{x} = -\rho_s \sum_{j=0}^{m} \nabla f_{Pj}(\mathbf{x}_0) \tag{3.32}$$

Solving for the distance between two subsequent design iterations in design variable space, $\|\Delta \mathbf{x}\|$, which is equivalent to $\|\Delta \mathbf{A}_i\|$ and $\|\Delta \mathbf{D}_i\|$ when considering the stiffness matrices as the design variables, it can be shown that the scaling factor, ρ_s, can be defined as:

$$\rho_s^2 = \sum_{j=0}^{m} \sum_{i=1}^{N} \frac{w_i}{2} \Big((\|\mathbf{\Psi}_{i,j}^m \mathbf{A}_i - \mathbf{\Phi}_{i,j}^m \mathbf{A}_i^{-1}\|)^2 + (\|\mathbf{\Psi}_{i,j}^b \mathbf{D}_i - \mathbf{\Phi}_{i,j}^b \mathbf{D}_i^{-1}\|)^2 \Big) \tag{3.33}$$

the above equation (3.33) does not guarantee non-zero values of the damping terms, therefore the triangular inequality, defined as:

$$\|\mathbf{A} - \mathbf{B}\| \leq \|\mathbf{A}\| + \|\mathbf{B}\| \tag{3.34}$$

was used to ensure non-zero values of the norm. The damping factor was therefore defined as:

$$\rho_s^2 = \sum_{j=0}^{m} \sum_{i=1}^{N} \frac{w_i}{2} \Big((\|\mathbf{\Psi}_{i,j}^m \mathbf{A}_i\| + \|\mathbf{\Phi}_{i,j}^m \mathbf{A}_i^{-1}\|)^2 + (\|\mathbf{\Psi}_{i,j}^b \mathbf{D}_i\| + \|\mathbf{\Phi}_{i,j}^b \mathbf{D}_i^{-1}\|)^2 \Big) \tag{3.35}$$

Defining a damping scaling based on equation (3.35) results in a damping term, f_D, which is of the same order of magnitude as the response term f_P in equation (3.7). This may initially result in unnecessarily large damping, hence this term is typically scaled to be equal to 1-10% of the value computed using equation (3.35).

Damping Strategy

An average damping factor is computed initially for all considered structural responses, however, it is beneficial to control the damping factor per response individually. This allows the amount of curvature added to already conservative approximations to be relaxed while increasing curvature for those which are not conservative, with the aim to improve convergence rates. The damping parameters are updated in every iteration, as explained in section 3.4. To ensure that conservativeness of a response is not retained unnecessarily, it is important to ensure that the damping parameter values can both increase and decrease after each iteration.

The damping factor of the j^{th} response for the following iteration, k^*, was updated using the following relationship:

$$\rho_j^{(k^*)} = \gamma^* \rho_j^{(k)} \tag{3.36}$$

where γ^* is a strictly positive number given by:

$$\gamma^* = \begin{cases} \gamma^-_{min} & \text{if} \quad \gamma \leqslant \gamma^-_{\min} \\ \gamma & \text{if} \quad \gamma^-_{\min} < \gamma < 1 \\ \gamma^+_{min} & \text{if} \quad 1 \leqslant \gamma \leqslant \gamma^+_{\min} \\ \gamma & \text{if} \quad \gamma^+_{\min} < \gamma < \gamma^+_{\max} \\ \gamma^+_{max} & \text{if} \quad \gamma \geqslant \gamma^+_{\max} \end{cases} \tag{3.37}$$

where γ^-_{min} is a lower bound on γ^*, hence limiting the amount of damping that can be removed per iteration if the response is conservative, while γ^+_{min} and γ^+_{max} are numbers larger than unity, defining respectively the minimum and maximum amount of damping to be added per iteration if the approximate response is not conservative. The term γ is defined as the following exponential function:

$$\gamma = \exp\left(\frac{f_j^{(k^*)} - f_{Pj}^{(k^*)}}{f_{Dj}^{(k^*)}}\right) \tag{3.38}$$

where in $f_j^{(k^*)}$, $f_{Pj}^{(k^*)}$ and $f_{Dj}^{(k^*)}$ are the actual function value, approximate function value and additional convex term respectively, at the optimum found for the k^{th} iteration. An exponential function was selected to scale the damping term between iterations as this allowed damping to be added rapidly if the approximation was not conservative while only allowing gradual removal if the approximation was conservative. The main argument for the selection of an exponential function therefore lies in the assumption that a feasible step, even if it is conservative, is more valuable than a rejected design point.

The selection of lower and upper bounds for γ^* is somewhat arbitrary. The following values were used for the range of problems considered in this thesis, these yielded good convergence results, and are provided as a guideline:

$$\gamma^-_{min} = 0.95, \qquad \gamma^+_{min} = 1.05, \qquad \gamma^+_{max} = 2.00 \tag{3.39}$$

It is also worth noting that since damping parameters are scaled individually for each approximate response, it is important to ensure that the appropriate damping factor is used for the corresponding approximate response. This is particularly relevant for problems where eigenvalues are sorted numerically and not based on their eigenmode, which characterize the structural response. Therefore, it is useful to employ mode-tracking algorithms, see Eldred et al. (1995), to ensure damping factors are correlated with their corresponding approximate response.

3.4 Overview of the Successive Approximation Scheme

The complexity surrounding the solution structural optimization problems typically requires an iterative solution strategy to be used. Several approximation methods have been implemented successfully for numerous structural optimization problems, see section 3.1. A generic optimization problem, given by (3.1), is solved by successively generating and solving an approximate subproblem, given by (3.2). The components required to generate a conservative convex separable approximation of an arbitrary response were developed and discussed in sections 3.2 and 3.3. Below an approximate separable subproblem is solved using dual methods as discussed in subsection 3.4.1 followed by a short discussion of including multi-modal responses, such as buckling, as an objective function in subsection 3.4.2. Finally, an overview of the iterative design optimization scheme, based on the CCSA framework by Svanberg (2002), is presented in subsection 3.4.3.

3.4.1 Solving the Approximate Subproblem

The approximate subproblem, given by equation (3.2), with objective function, $\tilde{f}_0$, m individual constraints, $\tilde{f}_j$, and n design variables, x_i, with lower and upper bounds, x_i^L and x_i^U, respectively is repeated below for convenience:

$$\begin{aligned} \min \tilde{f}_0(\mathbf{x}) & \\ \tilde{f}_j(\mathbf{x}) \leqslant 0 & \qquad j = 1 \dots m \\ x_i^L \leqslant x_i \leqslant x_i^U & \qquad i = 1 \dots n \end{aligned}$$

The function approximations, $\tilde{f}_j$ for $j = 1 \dots m$, now represent the conservative convex separable approximations developed previously, f_{Sj} given in equation (3.7). The subscript S associated with this approximation is omitted in the following discussion for clarity.

Dual Formulation

The constrained optimization problem given equation (3.2) is often referred to as the *primal problem*. When the approximating functions are separable and convex the primal problem can be solved efficiently using the dual method presented in Fleury and Schmit Jr. (1980). Using the Karush-Kuhn-Tucker conditions (Karush, 1939; Kuhn and Tucker, 1951) a function, $\mathcal{L}$, known as the Lagrangian, can be written as:

$$\mathcal{L}(\boldsymbol{\mu}, \mathbf{x}) = \sum_{j=0}^{m} \mu_j f_j(\mathbf{x}) \tag{3.40}$$

where μ_j is a non-negative scaler, known as a Lagrange multiplier, associated with the j^{th} response and $\mathbf{x}$ is a vector of all design variables. The Lagrange multiplier of the objective function, μ_0, is per definition equal to unity. The *dual problem* is subsequently given by:

$$\max_{\boldsymbol{\mu}} \mathcal{L}_C(\boldsymbol{\mu}) \qquad \text{s.t.} \qquad \mu_j \geq 0 \tag{3.41}$$

where $\mathcal{L}_C$ is known as Falk's dual or the complementary Lagrangian and is defined as the minimum of the Lagrangian, equation (3.40), over all design variables as:

$$\mathcal{L}_C = \min_{\mathbf{x}} \mathcal{L}(\mathbf{x}(\boldsymbol{\mu})) \tag{3.42}$$

where the Lagrange multipliers, $\boldsymbol{\mu}$, are fixed while solving for the optimal primal variables, $\mathbf{x}$. For convex problems, the optimal solution of the dual problem and primal problem are identical given that the Karush-Kuhn-Tucker conditions are met.

The dual formulation allows the search for optimal primal and dual variables to be separated. Additionally, the separability of the developed approximations allows the search for each optimal primal variable to be conducted independently, hence, the search for primal variables is called the *local* optimization problem. Since the dual variables affect the optimal solution of all primal variables being considered, the search for optimal dual variables is called the *global* optimization problem.

Local Optimization Problem

Recalling the approximation form given in equation (3.7), the conservative convex separable approximation of an arbitrary structural response, f_j, can be given by:

$$f_j = \sum_{i=1}^{N} \left(\breve{\boldsymbol{\Psi}}^m_{i,j} : \mathbf{A}_i + \breve{\boldsymbol{\Psi}}^b_{i,j} : \mathbf{D}_i + \breve{\boldsymbol{\Phi}}^m_{i,j} : \mathbf{A}_i^{-1} + \breve{\boldsymbol{\Phi}}^b_{i,j} : \mathbf{D}_i^{-1} + \breve{\alpha}_{i,j} h_i \right) + \mathcal{C}_0 \tag{3.43}$$

where $\breve{\boldsymbol{\Psi}}^m_{i,j}$ is the sensitivity matrix containing the derivatives of the j^{th} response with respect to the elements of in-plane stiffness matrix, $\mathbf{A}_i$, for the i^{th} design region including the convexifying terms as explained in equation (3.28). Similarly, $\breve{\boldsymbol{\Psi}}^b_{i,j}$ is the sensitivity matrix of the j^{th} response with respect to the elements of flexural stiffness matrix, $\mathbf{D}_i$, etcetera and $\breve{\alpha}_{i,j}$ are the derivatives of the terms dependent *explicitly* on laminate thickness, h_i.

The separability of equation (3.43) allows the search for optimal primal variables to be conducted as N independent local optimization problems as:

$$\min_{\mathbf{x}_i} \left(\breve{\boldsymbol{\Psi}}^m_{i} : \mathbf{A}_i + \breve{\boldsymbol{\Psi}}^b_{i} : \mathbf{D}_i + \breve{\boldsymbol{\Phi}}^m_{i} : \mathbf{A}_i^{-1} + \breve{\boldsymbol{\Phi}}^b_{i} : \mathbf{D}_i^{-1} + \breve{\alpha}_{i} h_i \right) \tag{3.44}$$

where $\mathbf{x}_i$ is the vector of design variables associated with the i^{th} design region. The local optimization problem (3.44) is only subject to the constraints imposed on the design variables. Since the dual variables, μ_j, are constant during the local optimization problem, the sensitivities can be summed over all responses. For example, the combined sensitivity matrix with respect to the in-plane stiffness matrix can be expressed as:

$$\breve{\boldsymbol{\Psi}}^m_{i} = \sum_{j=0}^{m} \mu_j \breve{\boldsymbol{\Psi}}^m_{i,j} \tag{3.45}$$

Lamination parameters were used as design variables to solve the local optimization problem given in (3.44). Thus, the problem is only constrained by the lamination parameters' feasible domain as explained in section 2.3.4. An additional advantage of expressing the design problem in terms of lamination parameters is that the first and second derivatives can be computed analytically, as shown in section 3.2.3. Therefore, the local optimization problem is readily solved using an efficient gradient based optimization method such as sequential quadratic programming (SQP).

Global Optimization Problem

The global optimization problem requires that the optimal set of dual variables is determined. This is achieved by solving the dual problem, equation (3.41), for which the gradients can be easily shown to be equal to the negative value of the respective Lagrange multiplier:

$$\frac{\partial \mathcal{L}_C}{\partial \mu_j} = -\mu_j \tag{3.46}$$

The global optimization can be efficiently solved using a standard Sequential Quadratic Programming (SQP) algorithm when few responses are present. However, in the implementation discussed here an interior-point method was used, which provided more consistent convergence rates when large number of constraint functions are present.

3.4.2 Solving Multi-Modal or Min-Max Problems

The majority of the optimization problems discussed in the remainder of this thesis are related to buckling, which is a multi-modal response. Considering only the critical mode in optimization problems based on a multi-modal responses will typically result in erratic solution convergence, as discussed by Seyranian et al. (1994) and Bruyneel et al. (2008). Multi-modal responses are characterized by the nature of the critical failure mechanism, which changes as the design changes. Buckling and vibrations are typical multi-modal structural responses, since the critical mode shape is a function of the structural design. For example, consider a structure for which mode one is a global buckling mode while mode two is a local buckling mode. While optimizing the design for mode one, mode two may become critical and this will require a completely different structural solution from that of mode one. If the optimizer is unable to identify the multi-modal nature of a response the design will iterate continuously between the different critical modes present in the structural response.

Multiple modes are readily integrated into the design scheme presented in section 3.4.1 using a method similar to the bound formulation presented by Olhoff (1989). Introducing an independent parameter, β, the optimization problem can be posed as:

$$\min \beta \quad \text{s.t.} \quad \beta \geq f_j \tag{3.47}$$

where f_j, for $j = 1, 2, \ldots M$, are the first M eigenvalues and the largest value f_j is critical. This may seem counter intuitive, since for both buckling and vibration problems the smallest eigenvalue is critical, however, it will be shown in chapter 5 that it is useful to consider the inverse eigenvalues instead of the eigenvalues directly.

Similar to section 3.4.1 Lagrangian can be formulated as:

$$\mathcal{L}(\boldsymbol{\mu}, \mathbf{x}) = \left(1 - \sum_{j=1}^{M} \mu_j\right)\beta + \sum_{j=1}^{M} \mu_j f_j(\mathbf{x}) \tag{3.48}$$

resulting in the following dual problem:

$$\max_{\boldsymbol{\mu}} \mathcal{L}_C(\boldsymbol{\mu}) \quad \text{s.t.} \quad \mu_j \geq 0 \tag{3.49}$$

where solving for the complimentary Lagrangian, $\mathcal{L}_C$, now results in two conditions:

$$\mathcal{L}_C = \min_{\mathbf{x}} \sum \mu_j f_j \quad \text{and} \quad \sum \mu_j = 1 \tag{3.50}$$

Note that the intermediate variable, β, is no longer present in the dual-formulation and that the form of the problem is essentially identical to that presented previously in section 3.4.1. The only difference is the additional constraint ensuring that all Lagrange multipliers associated with the multi-modal response sum to unity, which is readily included when solving the dual problem (3.41).

In multi-modal design problems it may be desirable to avoid modal interaction, which may result in unstable post-buckling behavior, by imposing mode spacing constraints. This can be achieved by including a spacing parameter, ξ_j, in the constraint of the bound formulation in equation (3.47), such that $\beta \geq f_j/\xi_j$ as was done by Setoodeh et al. (2009).

In this subsection the bound formulation has been shown to be an effective method for including multi-modal structural responses, such as buckling, in the design optimization problem. It is however equally suited to solving min-max problems, for example when minimizing the maximum failure index within a laminate.

3.4.3 Iteration Scheme

A generic conservative convex separable approximation in terms of laminate thickness and stiffness properties was derived in section 3.2. An additional term, to ensure conservativeness and strict convexity of the approximation, was appended to the function approximation and scaled dynamically via a constant factor ρ, as discussed in section 3.3. The dual method was subsequently implemented in section 3.4.1 and used to solve a generic constrained optimization problem by separating the optimization problem into a *local* and *global* problem.

All of the aforementioned components will now be assembled in this section and used to present a holistic overview of the laminate stiffness optimization process, which is shown schematically in Figure 3.1. After problem *initialization* (0), the optimization consists of a *convergence control loop* (1) containing a *global* (2) and *local* (3) optimization loop that corresponds to the optimization problems that result from the dual method. The *convergence control loop* is used to dynamically control the degree of conservativeness of the considered responses and to decide if the optimal solution of the approximate subproblem is accepted for the following iteration. The *global* optimization loop consists of solving for the Lagrange multipliers associated with the constraints. The *local* loop is used to solve the local separable approximations iteratively in terms of lamination parameters to obtain the optimum stiffness distribution.

A starting set of design variables, $\mathbf{x}_0$, is defined in the *initialization* step (0). Typically, all lamination parameters are set to zero, corresponding to a quasi-isotropic laminate, and a constant initial thickness distribution is assumed. The initial set of design variables is then used to compute the structural stiffness properties and a finite element analysis is run to compute the function values and sensitivities required to construct the approximate subproblem and to compute the initial damping scaling factors, ρ_j.

In the *convergence control loop* (1), the current damping factors are used to make the response approximations more conservative and convex by augmenting the sensitivity matrices to include damping information, as shown in equation (3.28). The modified sensitivities are subsequently passed to the optimization loops, which are

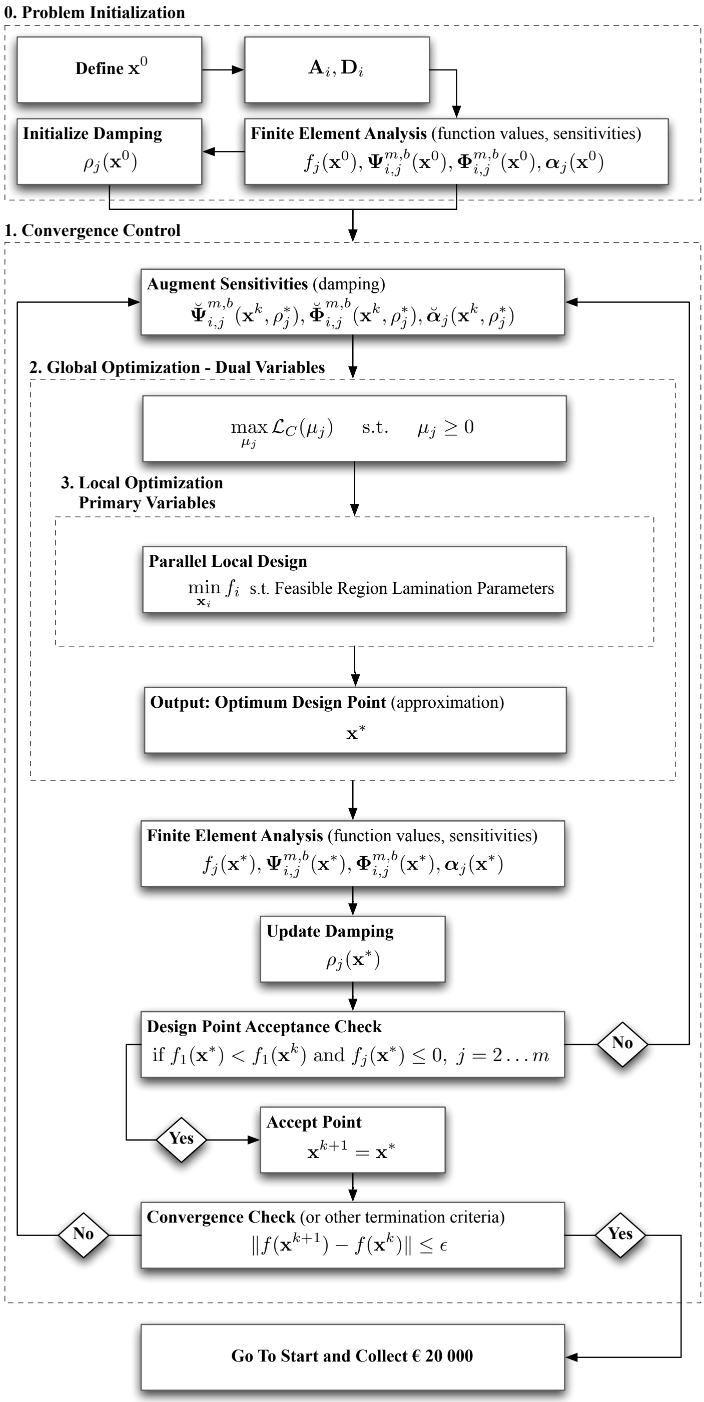

Figure 3.1: *Overview of optimization steps required to obtain the optimal conceptual stiffness distribution*

described in the next paragraph. The optimum design point, $\mathbf{x}^*$, obtained after the completion of the global and local optimization loops is then used to update the finite element model and compute the current response and sensitivity data, which is subsequently used to update the damping factors $\rho_j(\mathbf{x}^*)$. Note that the damping factor update occurs even if the current design point is not accepted. The current function values, $f_j(\mathbf{x}^*)$, are compared to those of the the previous accepted iteration and the constraints are checked for violation to ensure that a feasible descent step has been made. If this is not the case, new damping factors, $\rho_j(\mathbf{x}^*)$, are used to rerun the optimization from the previously accepted design point, $\mathbf{x}^k$. If the design point is accepted, $\mathbf{x}^{k+1} = \mathbf{x}^*$, the updated sensitivity information is then used to run the next optimization loop until the defined convergence or termination criteria is met.

The dual method is used to solve each of the successive approximate subproblems. It consists of two optimization loops, a *global* loop (2) that maximizes the complimentary Lagrangian in terms of the Lagrange multipliers, μ_j, and an *local* loop (3) that minimizes an approximate response in terms of the primary design variables, $\mathbf{x}$. In the current implementation an interior-point method is used to solve for the Lagrange multipliers while a sequential quadratic program is used to solve for the primary variables. In the inner loop the Lagrange multipliers remain constant and hence the optimization problem can be posed as n separate local optimization problems which can be solved in parallel. The objective function, f_i, for the i^{th} local problem is constructed using a linear combination of all the sensitivities associated with point i, as defined in equation (3.45), multiplied by the respective laminate stiffness terms.

Differences with Respect to CCSA

In the CCSA framework presented in Svanberg (2002), the author differentiates between *inner* and *outer* iterations. Each successful outer iteration results in a new design point, while inner iterations are used to determine appropriate damping factors, ρ_j, such that the approximation is conservative. A design is only accepted if all constraints are satisfied and conservative, and if the objective function decreases and is conservative. In the inner iterations, each of the damping factors is increased based on the difference between actual and approximate function value. If the approximation is not conservative, while the damping factors remain unchanged if the approximation is already conservative. In each outer iteration, the damping factors are reset to 10% of their final value from the inner iteration, hence allowing conservativeness to be removed.

The developed approach differs from that originally presented by Svanberg (2002) in several ways; one, the initial values of the damping parameters, ρ, are computed based on the initial approximate subproblem instead of assuming an initial value of unity. This was done with the aim of reducing the number of rejected designs, as is explained in section 3.3.3. Two, a design point is accepted if it results in an improved design even if the approximate function and constraint values are not conservative, following the feasible decent step approach presented by Groenwold et al. (2009), which still guarantees global convergence. Three, the damping parameters are updated in each iteration, irrespective of design update acceptance. These differences are primarily motivated by the premise that it is inefficient to reject information obtained from design points which result in an improved design, even if the the approximations are not conservative.

CHAPTER 4

Strength Evaluation in Lamination Parameter Space

"Strength does not come from physical capacity. It comes from an indomitable will"

Mohandas Gandhi

Lamination parameters are particularly suitable for solving laminate optimization problems efficiently, as was introduced in chapter 1 and highlighted in chapter 2. A limitation of using lamination parameters is the difficulty with which constraints on laminate strength can be incorporated into the design process. Strength constraints are often based on failure criteria, such as the Tsai-Wu criterion (Daniel and Ishai, 1994), which depend on material properties and explicitly on ply angles, precluding the use of lamination parameters. Therefore, strength constraints have only been incorporated with lamination parameters in optimization problems for the special case when ply angles are restricted to a pre-determined discrete set, as shown in Gürdal et al. (1999). Kogiso et al. (2003) also use the Tsai-Wu failure criterion for a fixed set of ply angles when maximizing laminate reliability using lamination parameters. Laminate failure is determined by relating ply strength to the maximum allowable strain for that ply via a strength ratio. Groenwold and Haftka (2006) have also investigated laminate optimization for strength, limiting the design to a single orientation angle.

An investigation of incorporating the Tsai-Wu failure criterion into lamination parameter design in its most general setting is presented in this chapter. The Tsai-Wu failure criterion is mapped onto strain space, a useful approach first demonstrated by Nakayasu and Maekawa (1997). When the failure criterion is written in terms of

This chapter is based on the paper, *Implementation of strength based failure criteria in the lamination parameter design space* by S.T. IJsselmuiden, M.M. Abdalla, and Z.Gürdal, which appeared in the AIAA Journal, 46(9):1826-1834, July 2008. Note: symbols may have been changed to maintain consistency throughout this thesis.

strain components in global coordinates, rather than material coordinates, the ply angle appears explicitly. Subsequently, a conservative failure envelope is constructed by finding a region in strain space that is safe regardless of the ply angle. In other words, the failure envelope is valid for any ply orientation angle. An analytical solution is obtained for this conservative failure envelope. It is shown in the following that two different envelope equations may apply depending on material stiffness properties and failure stresses. It is also shown that the envelope equation is a function of only two strain invariants.

Laminate optimization for maximum stiffness is relatively straightforward to implement and hence is often used as a substitute maximum strength design. Therefore, it is also interesting to compare the optimal solutions obtained when maximizing stiffness and maximizing strength for a given load. The objective of the strength-based optimization is to minimize a failure index, which is equivalent to maximizing the factor of safety, as proposed by Groenwold and Haftka (2006). The objective of the stiffness-based optimization is to minimize compliance. The optimization is carried out for several different materials, for a range of stiffness ratios (E_1/E_2), and for a combination of axial and shear loading. Results of these optimizations show that the correlation between stiffness and strength driven designs is generally favorable, but that the degree of correlation depends both on material properties and loading.

Analytical expressions for conservative failure envelopes, based on the Tsai-Wu failure criterion, are derived in section 4.1. The obtained envelopes are used to derive an expression for laminate strength in section 4.2. The optimization problems for both maximum stiffness and maximum strength are formulated in section 4.3, followed by several numerical design studies in section 4.4 and conclusions in section 4.5.

4.1 Developing a Failure Envelope

Ply orientation angles are typically unavailable when using lamination parameters to parameterize a laminate's stiffness. Therefore, conservative failure envelopes, which are valid for any ply orientation angle, were derived and are presented in this section. The goal was to determine a region in strain space that guaranteed no failure would occur within a laminate, irrespective of the ply orientation angles present. The Tsai-Wu failure criterion was used as the underlying failure criterion for the derivations presented below. However, other failure criteria, such as the maximum-strain criterion or Hashin's criterion, may also be considered.

The Tsai-Wu failure criterion is a well known first-ply failure criterion and can be defined as (Daniel and Ishai, 1994):

$$F_{11}\sigma_1^2 + F_{22}\sigma_2^2 + F_{66}\tau_{12}^2 + F_1\sigma_1 + F_2\sigma_2 + 2F_{12}\sigma_1\sigma_2 = 1 \tag{4.1}$$

where F_i and F_{ij} are second and fourth order strength tensors, with $i, j = 1, 2 \ldots, 6$, and are given by:

$$\begin{array}{lll} F_{11} = \frac{1}{X_t X_c} & F_{22} = \frac{1}{Y_t Y_c} & F_{12} = \frac{-1}{2\sqrt{X_t X_c Y_t Y_c}} \\ F_1 = \frac{1}{X_t} - \frac{1}{X_c} & F_2 = \frac{1}{Y_t} - \frac{1}{Y_c} & F_{66} = \frac{1}{S^2} \end{array} \tag{4.2}$$

where X_t, X_c, Y_t and Y_c are the tensile and compressive failure stresses of the longitudinal and transverse direction, respectively and S is the shear failure stress.

Material stresses and material strains are related via the reduced stiffness matrix **Q**, see section 2.3.1. Hence, the Tsai-Wu failure criterion can be expressed in terms of material strain tensor components as:

$$G_{11}\epsilon_1^2 + G_{22}\epsilon_2^2 + G_{66}\epsilon_{12}^2 + G_1\epsilon_1 + G_2\epsilon_2 + 2G_{12}\epsilon_1\epsilon_2 = 1 \tag{4.3}$$

where the strain coefficients, G_{ij}, are found to be:

$$\begin{aligned}
G_{11} &= Q_{11}^2F_{11} + Q_{12}^2F_{22} + 2F_{12}Q_{11}Q_{12} \\
G_{22} &= Q_{12}^2F_{11} + Q_{22}^2F_{22} + 2F_{12}Q_{12}Q_{22} \\
G_{1} &= Q_{11}F_1 + Q_{12}F_2 \\
G_{2} &= Q_{12}F_1 + Q_{22}F_2 \\
G_{12} &= Q_{11}Q_{12}F_{11} + Q_{12}Q_{22}F_{22} + F_{12}Q_{12}^2 + F_{12}Q_{11}Q_{22} \\
G_{66} &= 4Q_{66}^2F_{66}
\end{aligned} \tag{4.4}$$

Material strains $(\epsilon_1, \epsilon_2, \epsilon_{12})$ can subsequently be related to laminate strains $(\epsilon_x, \epsilon_y, \epsilon_{xy})$ using the following transformation matrix:

$$\begin{bmatrix} \frac{1}{2}(1+c) & \frac{1}{2}(1-c) & s \\ \frac{1}{2}(1-c) & \frac{1}{2}(1+c) & -s \\ -\frac{1}{2}s & \frac{1}{2}s & c \end{bmatrix} \tag{4.5}$$

where $s = \sin(2\theta)$ and $c = \cos(2\theta)$. Substituting the transformed strains of equation (4.5) into the failure envelope equation (4.3), a failure envelope equation in terms of laminate strains and ply angle is obtained:

$$F(\epsilon_x, \epsilon_y, \epsilon_{xy}, s, c) = 0 \tag{4.6}$$

The objective is to construct a design envelope within which no failure occurs regardless of ply orientation. To this end, a geometric "envelope" was constructed, which is defined as the surface tangent to the family of failure surfaces, equation (4.6), parameterized using ply angle θ. The envelope equation is given by:

$$\frac{dF}{d\theta} = 0 \tag{4.7}$$

which can be expanded using the chain rule as:

$$\frac{dF}{d\theta} = c\frac{\partial F}{\partial s} - s\frac{\partial F}{\partial c} = 0 \tag{4.8}$$

where both F and F_θ are polynomial functions of s and c. Since both s and c are dependent upon the ply angle θ, they cannot be considered independently, but have to satisfy the following trigonometric relation:

$$s^2 + c^2 - 1 = 0 \tag{4.9}$$

The equation for the failure envelope is obtained by eliminating s and c between equations (4.6), (4.8), and (4.9). The elimination is achieved using Dixon's resultant

(Dixon, 1909) for the elimination of polynomial equations. The algebraic application details of Dixon's resultant are omitted for the sake of brevity, however commercially available mathematics software, such as Mathematica™, where Nakos and Williams (1997) provide packages which can be used to solve for Dixon's resultant. The result yields the following two equations, (4.10) and (4.11), each representing a surface traced out by the Tsai-Wu failure criterion in strain space for all ply orientations.

$$4u_6^2 I_2^2 - 4u_6 u_1 I_2^2 + 4(1 - u_2 I_1 - u_3 I_1^2)(u_1 - u_6) + (u_4 + u_5 I_1)^2 = 0 \quad (4.10)$$
$$u_1^2 I_2^4 - I_2^2(u_4 + u_5 I_1)^2 - 2u_1 I_2^2(1 - u_2 I_1 - u_3 I_1^2) + (1 - u_2 I_1 - u_3 I_1^2)^2 = 0 \quad (4.11)$$

where I_1 is the volumetric strain invariant and I_2 is the maximum shear strain (Gere, 2002), given by:

$$I_1 = \epsilon_x + \epsilon_y \qquad \text{and} \qquad I_2 = \sqrt{\left(\frac{\epsilon_x - \epsilon_y}{2}\right)^2 + \epsilon_{xy}^2} \quad (4.12)$$

The terms $u_i, i = (1 \ldots 6)$ are defined in terms of the strain coefficients of equation (4.3) and are given by:

$$\begin{aligned} u_1 &= G_{11} + G_{22} - 2G_{12} \\ u_2 &= (G_1 + G_2)/2 \\ u_3 &= (G_{11} + G_{22} + 2G_{12})/4 \\ u_4 &= G_1 - G_2 \\ u_5 &= G_{11} - G_{22} \\ u_6 &= G_{66} \end{aligned} \quad (4.13)$$

It should be clear that the feasible design space described by equations (4.10) and (4.11) are material dependent, since u_i is a function of the strain coefficients, G_{ij}, which are a function of the reduced stiffness matrix $\mathbf{Q}$ and material strength coefficients F_i, F_{ij}. It should also be noted that the failure envelopes prescribed by equations (4.10) and (4.11) represent a conservative approximation of the Tsai-Wu failure criterion in terms of strain invariants, and should not be confused with a strain invariant failure criterion such as that presented by Gosse and Christensen (2001) and hence should not be considered to be a new failure criterion.

On inspection, the first envelope (4.10) is a second order equation with respect to strain, and the second envelope (4.11) is a fourth order equation. These two envelope equations do not intersect one another, but may become tangent as shown in Figure 4.1. The safe region is the region common to the Tsai-Wu failure envelope for all ply orientation angles. As such, the envelope equation describing the inner envelope should always be used to evaluate laminate strength. Whether the inner envelope is represented by the second or fourth order equation depends on the properties of the material under consideration. When the fourth order equation is used to describe the inner envelope it is usually factorable into the product of two equations leading to a self intersecting non-smooth envelope.

The feasible design envelopes were plotted for three different materials to better understand their physical interpretation. As an example, consider three materials listed in Appendix A, Carbon-PEEK (AS4), Carbon-Epoxy (IM6) and Boron-Epoxy

(B5.6), having stiffness ratios, E_1/E_2, ranging from approximately 9 to 17. The actual strain envelope for various material orientation angles together with the two curves prescribed by the derived equations were plotted in Figure 4.1. In this case ϵ_{xy} has been set to zero, however, similar results can be generated for a range of ϵ_{xy} values. It is clear from the figure that in each case, one of the two equations accurately prescribes the inner strain envelope, which is in fact independent of the fiber orientation. A method of selecting the critical envelope equation is treated in the next section.

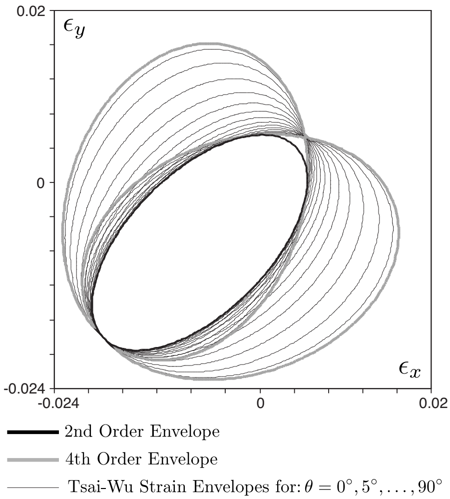

(a) Carbon-PEEK (AS4)

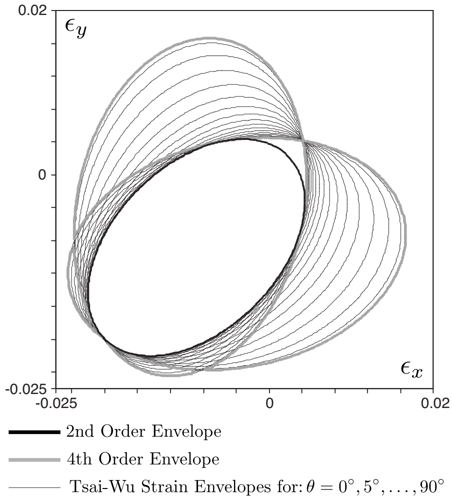

(b) Carbon-Epoxy (IM6)

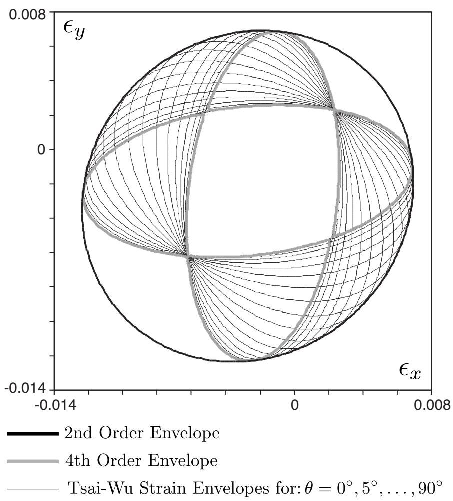

(c) Boron-Epoxy (B5.6)

Figure 4.1: *Strain envelopes for various fiber orientation angles, including the* 2^{nd} *and* 4^{th} *order solutions derived in equations* (4.10) *and* (4.11), *respectively,* ϵ_x *vs.* ϵ_y, *with* $\epsilon_{xy} = 0$

As can be seen from Figure 4.1, the conservative design envelopes prescribed by equations (4.10) and (4.11) are convex in the strain space, as they are the intersection of the infinite number of convex sets defined by the Tsai-Wu failure criterion. The Tsai-Wu failure criterion is only convex if the failure coefficients meet specific requirements, as presented by Bower and Koedam (1997). An expression for the laminate safety factor, based on the derived failure envelopes, is presented in the following section.

4.2 Formulation of a Strength Constraint

Equations (4.10) and (4.11) represent the laminate failure envelopes in strain space. In order to apply the envelopes as a constraint, or alternatively as an objective function for optimization, a simplified expression for laminate failure is proposed. The equations of the design envelopes can be reformulated in terms of a safety factor, λ_s, which can be defined as:

$$\lambda_s = \frac{b}{a} \tag{4.14}$$

where a is the distance between the origin and an arbitrary point P in the feasible design space, and b the length of a vector from the origin, through point P, to a point on the envelope boundary, P^*, as illustrated in Figure 4.2.

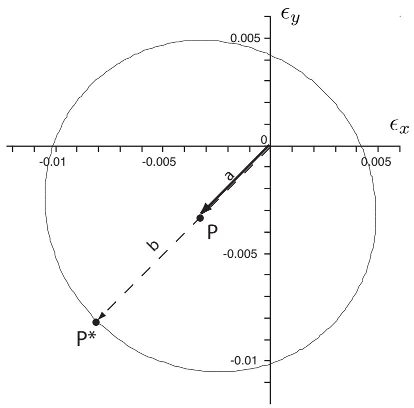

Figure 4.2: *Definition of λ_s with respect to an arbitrary point, P, within the design envelope and the corresponding point, P^*, on the boundary*

In essence, λ_s is a scaling factor, which when multiplying the values of applied strains, $\boldsymbol{\epsilon}$, at a generic point P, gives the values of $\boldsymbol{\epsilon^*}$ at the corresponding point on the boundary, P^*. Therefore, the strain invariants, I_1 and I_2, can be related to those at the boundary of the the failure envelopes by substituting $I_1^* = \lambda_s I_1$ and $I_2^* = \lambda_s I_2$ into the failure envelope equations, (4.10) and (4.11), yielding two polynomials in terms of λ_s:

$$\begin{aligned} f_1(\lambda_s) &= a_{12}\lambda_s^2 + a_{11}\lambda_s + a_{10} \\ f_2(\lambda_s) &= a_{24}\lambda_s^4 + a_{23}\lambda_s^3 + a_{22}\lambda_s^2 + a_{21}\lambda_s + a_{20} \end{aligned} \tag{4.15}$$

where the coefficients a_{ij} are functions of the strain invariants I_1 and I_2 and are found to be:

$$\begin{aligned}
a_{10} &= u_4^2 + 4u_1 - 4u_6 \\
a_{11} &= -4u_2I_1(u_1 - u_6) + 2u_4u_5I_1 \\
a_{12} &= 4u_6^2I_2^2 - 4u_3I_1^2(u_1 - u_6) - 4u_6u_1I_2^2 + u_5^2I_1^2 \\
a_{20} &= 1 \\
a_{21} &= -2u_2I_1 \\
a_{22} &= -2u_3I_1^2 + u_2^2I_1^2 - I_2^2(u_4^2 + 2u_1) \\
a_{23} &= 2u_2I_1^3u_3 - I_2^2(2u_4u_5I_1 - 2u_1u_2I_1) \\
a_{24} &= u_1^2I_2^4 - I_2^2(u_5^2I_1^2 - 2u_1u_3I_1^2) + u_3^2I_1^4
\end{aligned} \tag{4.16}$$

Solving for λ_s yields up to six roots, with the equation with the smallest positive real root representing the active envelope since the smallest safety factor is critical. The active envelope is not independent of the laminate strains. It is also noted that the fourth order envelope self-intersects and can therefore be thought of as two smooth curves, as can be seen in Figure 4.1(c). Corresponding to each of these two smooth curves is a positive root λ_s which is a continuous function of strains, as was demonstrated in later work (Khani et al., 2011).

Groenwold and Haftka (2006) first suggested using a factor of safety for strength optimization by directly maximizing λ_s. However, λ_s is not differentiable near the origin and hence may lead to numerical problems. To remedy this, the failure index, $r_s(\boldsymbol{\epsilon})$, is defined as the inverse of the factor of safety squared, which guarantees differentiability at all points within the failure envelope:

$$r_s(\boldsymbol{\epsilon}) = \frac{1}{\lambda_s^2} \tag{4.17}$$

where λ_s is the smallest positive real root obtained from (4.15). If the implemented failure criterion is quadratic, such as Tsai-Hill, the failure index, r_s, is identical to the failure criterion. Otherwise, the failure index is representative of the safety factor and is a function that has a value of 0 at the origin, when no strain is present, and a value 1 at the envelope boundary, which indicates laminate failure. Hence the strength constraint can be formulated as:

$$r_s(\boldsymbol{\epsilon}) - 1 \leq 0 \tag{4.18}$$

which is valid at any point within the laminate, and is only a function of the local strain. Based on Classical Lamination Theory the strain at any point in a laminate, (x, y, z), can be related to mid-plane strains, $\boldsymbol{\epsilon}^0$, and curvatures $\boldsymbol{\kappa}$, as follows:

$$\boldsymbol{\epsilon} = \boldsymbol{\epsilon}^0(x, y) + z\boldsymbol{\kappa}(x, y) \tag{4.19}$$

where $z \in [-\frac{h}{2}, \frac{h}{2}]$, is the thickness co-ordinate, and x and y are panel coordinates. For convenience of use in optimization for strength of thin plates and shells, it is advantageous to eliminate the dependency on thickness coordinate z in the formulation of the strength constraint. This can be achieved by stipulating that the worst case value is still safe. Thus, the strength constraint at any point (x, y) in the laminate becomes:

$$\max_{z}(r_s) - 1 \leq 0 \tag{4.20}$$

as the largest values of r_s on interval $z \in [-\frac{h}{2}, \frac{h}{2}]$ will be critical.

The function r_s is a convex function of laminate strains, $\boldsymbol{\epsilon}$, which is a linear function in z. Since all ply orientations are assumed to be present at any through-the-thickness point, it follows from the properties of convex functions that r_s is a unimodal function of z with a unique minimum. Hence the maximum will have to occur at one of the extreme fibers, i.e. $z = -\frac{h}{2}$ or $z = \frac{h}{2}$. This result may seem paradoxical at first since it is well-known that the most critical point through the thickness of a composite laminate need not be one of the extreme fibers. This counter-intuitive finding can be explained by noting that, in the derivation of the failure envelope, it is assumed that any ply orientation is possible at any given point. The conservative strain constraint, equation (4.18), does not take the actual order of layers in the laminate into account. Therefore, this approach may be excessively conservative for bending dominated problems, a fact that is confirmed by the numerical results presented in section 4.4.

For pure in-plane strains, e.g. in-plane loading of a symmetric laminate, the strains are constant through the thickness and the strength constraint, equation (4.18), can be directly applied. However, when bending curvatures are present the strength constraint may be replaced by two constraints:

$$r_s^+ - 1 \leq 0 \quad \text{and} \quad r_s^- - 1 \leq 0 \tag{4.21}$$

where $r_s^{\pm} = r(x, y, \pm h/2)$.

4.3 Optimization Formulation

The optimization problems for maximum stiffness and maximum strength of a panel under constant in-plane loads are formulated in this section. The availability of both formulations makes it straightforward to compare the results of strength-optimized and stiffness-optimized panels and provides a useful test for the intuitive notion that stiffness, which is far easier in mathematical treatment, is a good surrogate objective function for strength. Approximations for both laminate strength and laminate stiffness as objective functions are derived to improve optimization efficiency.

4.3.1 Strength Optimization

To maximize laminate strength, Groenwold and Haftka (2006) propose maximizing the factor of safety λ_s, which is equivalent to minimizing the failure index r. An expression for the failure index as a function of laminate strains, $\boldsymbol{\epsilon}$, was developed in section 4.2. The optimization design variables for the in-plane problem are the in-plane lamination parameters, $\mathbf{V_A}$. Laminate strains can be expressed as functions of the design variables using classical lamination theory:

$$\boldsymbol{\epsilon} = \mathbf{A}^{-1}(\mathbf{V_A}) \cdot \mathbf{N} \tag{4.22}$$

where $\mathbf{A}^{-1}$ is the compliance matrix, defined in terms of lamination parameters, $V_{i\mathbf{A}}$, as defined in equation (2.15). Note that, to maintain consistency with the stiffness optimization formulation derived in the next section, $\boldsymbol{\epsilon}$ refers to the engineering strain vector. Thus, the strength optimization problem can be formulated as:

$$\min_{V_{i\mathbf{A}}} r_s\big(\boldsymbol{\epsilon}(V_{i\mathbf{A}})\big) \tag{4.23}$$

subject to the constraints imposed by the lamination parameter design space, as defined in section 2.3.4.

To solve equation (4.23) efficiently, an approach is proposed in which the failure index, r_s, is approximated as a function of the lamination parameters, as this prevents excessive evaluations of the failure index. In most practical design optimization problems evaluation of the failure index require a computationally expensive finite element analysis. For this reason, it is customary to use an approximation in structural optimization (Haftka and Gürdal, 1992) to keep the number of function evaluations required to find the optimum to a minimum.

It can be shown that the failure index, r_s, is a homogeneous second order function with respect to the strains (Groenwold and Haftka, 2006). Therefore, it can be approximated using a second order Taylor series expansion in terms of strains:

$$r_s(\boldsymbol{\epsilon}) \approx r^{(k)} + \mathbf{g}^{(k)^T} \cdot \big(\boldsymbol{\epsilon} - \boldsymbol{\epsilon}^{(k)}\big) + \frac{1}{2!}\big(\boldsymbol{\epsilon} - \boldsymbol{\epsilon}^{(k)}\big)^T \cdot \mathbf{H}^{(k)} \cdot \big(\boldsymbol{\epsilon} - \boldsymbol{\epsilon}^{(k)}\big) \tag{4.24}$$

with

$$\mathbf{g}^{(k)} = \frac{\partial r_s}{\partial \boldsymbol{\epsilon}}\bigg|_{\epsilon=\epsilon^k} \qquad \text{and} \qquad \mathbf{H}^{(k)} = \frac{\partial^2 r_s}{\partial \boldsymbol{\epsilon} \partial \boldsymbol{\epsilon}}\bigg|_{\epsilon=\epsilon^k} \tag{4.25}$$

Using Euler's theorem (Kreyszig, 1999) of homogeneous functions, it can be shown that $\mathbf{g}^{(T)} \cdot \boldsymbol{\epsilon} = 2r_s$ and $\mathbf{H} \cdot \boldsymbol{\epsilon} = \mathbf{g}$, hence the approximation simplifies to:

$$r_s(\boldsymbol{\epsilon}) \approx \frac{1}{2}\boldsymbol{\epsilon}^T \cdot \mathbf{H}^{(k)} \cdot \boldsymbol{\epsilon} = \frac{1}{2}(\mathbf{S}\cdot\mathbf{N})^T \cdot \mathbf{H}^{(k)} \cdot (\mathbf{S}\cdot\mathbf{N}) \tag{4.26}$$

where $\mathbf{H}$ can be derived analytically in terms of the strain invariants using the chain rule:

$$\begin{aligned}\frac{\partial^2 r_s}{\partial \epsilon_k \partial \epsilon_l} = \sum_{p=1}^{2}\Bigg[\sum_{q=1}^{2}\Bigg[\bigg(\frac{\partial^2 r_s}{\partial \lambda_s^2}\cdot\frac{\partial \lambda_s}{\partial I_p}\cdot\frac{\partial \lambda_s}{\partial I_q} + \frac{\partial r_s}{\partial \lambda_s}\cdot\frac{\partial^2 \lambda_s}{\partial I_p \partial I_q}\bigg)\frac{\partial I_q}{\partial \epsilon_k}\Bigg]\frac{\partial I_p}{\partial \epsilon_l} \\ + \frac{\partial r_s}{\partial \lambda_s}\cdot\frac{\partial \lambda_s}{\partial I_p}\cdot\frac{\partial^2 I_p}{\partial \epsilon_k \partial \epsilon_l}\Bigg]\end{aligned} \tag{4.27}$$

where $k, l = 1 \ldots 3$.

Derivatives of the strain invariants with respect to the strains can be readily found by differentiation of equation (4.12). The derivative of λ_s with respect to the strain invariants is found by making use of the equations derived for the failure envelope (4.15), which can be rewritten as:

$$f_i(\lambda_s) = \sum_{n=0}^{N} a_n \lambda_s^n = 0 \tag{4.28}$$

where $N = 2$ or 4 and is related to the applicable failure envelope for $i = 1$ or 2 for which the corresponding coefficients a_n are defined in equation (4.16). To determine the derivative of λ_s, the equations listed above can be differentiated with respect to I_p which results in:

$$\sum_{n=0}^{N}\left(\frac{\partial a_n}{\partial I_p}\lambda_s^n + a_n\frac{\partial \lambda_s^n}{\partial I_p}\right) = 0$$

Therefore:

$$\frac{\partial \lambda_s}{\partial I_p} = -\frac{\sum_{n=1}^{N}\frac{\partial a_n}{\partial I_p}\lambda_s^n}{\sum_{n=1}^{N} n a_n \lambda_s^{n-1}} \tag{4.29}$$

The second order derivatives of λ_s can be found in a similar fashion by taking the derivative of equation (4.29) with respect to the strain invariant I_q.

The lamination parameters corresponding to the minimum value for the approximation of r_s can be found using any standard optimization algorithm. Solving the approximate problem successively, while updating the approximation after each new design step, will yield the optimum set of lamination parameters at convergence.

4.3.2 Stiffness Optimization

Maximum stiffness designs can also be formulated in terms of lamination parameters by minimizing the compliance (Setoodeh et al., 2006b). The minimization problem can therefore be formulated as:

$$\min_{V_{i\mathbf{A}}} \frac{1}{2}\mathbf{N}^T \cdot \mathbf{A}^{-1}(V_{i\mathbf{A}}) \cdot \mathbf{N} \tag{4.30}$$

subject to the constraints imposed by the lamination parameter design space as described in section 2.3.2. Compliance is the measure of the complementary work done by the external loads on the laminate and has been shown to be convex (Setoodeh et al., 2006b).

4.4 Numerical Results

The optimization formulations developed for strength and stiffness in the previous section were applied to several design problems. The purpose of the numerical tests is to, one, assess the behavior of the proposed strength formulation for different materials and two, to help us to discuss the relationship between strength-optimized and stiffness-optimized designs. Three different materials, AS6, IM6 and B5.6, were considered, as listed in Appendix A. All examples use the following combined axial and shear loading:

$$\begin{Bmatrix} N_x \\ N_y \\ N_{xy} \end{Bmatrix} = \begin{Bmatrix} 1-\omega \\ 0 \\ \omega \end{Bmatrix} \cdot N \tag{4.31}$$

with $w \in [0, 1]$, where $\omega = 0$ represents pure axial tension or compression, depending on the sign of N, and $\omega = 1$ represents pure shear loading. N was given a numerical value of $\pm 150 \cdot 10^6$ N/m. This is an arbitrary choice, but it provides a good range for r_s for the various materials when considering a laminate panel of unit dimensions.

The conservativeness of the strength formulation is quantified in the following subsection. The proposed optimization formulation is verified for the three materials under consideration in subsection 4.4.2. The optimization procedure is executed for balanced and unbalanced laminates for a range of tensile, compressive and shear loads in subsection 4.4.3.

4.4.1 Conservativeness of the Strength Envelope

The proposed failure index, r_s, assumes that all ply orientations are present in a laminate. In a real laminate layup this may not be the case. Hence, if the ply orientations that define the critical boundary of the failure envelope are not present, the formulation may lead to conservative designs. The origin of this conservativeness is readily understood when considering the maximum-strain criterion. This criterion is represented by a rectangular cuboid in strain space, where its faces are defined by the limit tensile, compressive and shear strains along the principle material axes. When assuming all ply angles to be present, the rectangular cuboid is limited by the smallest value of the limit tensile, compressive and shear strain of all possible plies. Therefore, assuming that all ply angles are present may yield overly conservative results, and was thus investigated further.

Two particular cases are likely to exhibit this conservative behavior; one, when all fibers are aligned in a single direction, such as under uniaxial loading; and two, when there is a strong variation of strain through the laminate thickness, such as when bending is dominant. The first case corresponds to pure tension, $\omega = 0$ in equation (4.31), $N_x = N$, and the second case to axial bending, M_x, which are most likely to be the worst case scenarios.

To assess the conservativeness of the failure envelope, the safety factor λ_s, defined using the envelope, is compared to the safety factor predicted by the Tsai-Wu failure criterion, λ_{TW}. The ratio of the safety factors, λ_{TW}/λ_s, for several laminates are presented in Table 4.1. The safety factor is significantly underestimated when considering the intuitively optimal 0° design for pure tension for all three materials investigated. When considering other laminates with different ply orientations present, the difference between the two safety factors is reduced. The safety factors only differ between 0 and 12% for the axially loaded laminate, $[\pm 45, 0_4, 90_2]_s$.

If the same laminate, $[\pm 45, 0_4, 90_2]_s$, is considered under bending loads, the difference between the lamination parameter based failure envelope predictions and the Tsai-Wu failure criterion can be as large as 33%. This is due to the fact that the relative through-the-thickness position of plies with different orientations influences the safety factor for the derived envelope and the Tsai-Wu failure criterion. For example, the plies can be rearranged to obtain a laminate with the same in-plane lamination parameters, but having different surface plies, $[0_4, \pm 45, 90_2]_s$, yielding different values for the conservativeness of the design. Hence, the failure envelope conservativeness is clearly influenced by the chosen stacking sequence. Since the envelope cannot explicitly take the order of the plies into account, the found designs for bending dominated problems are more conservative.

Keeping in mind that general engineering design practice often requires laminates to consist of several fiber orientations, and the need to account for multiple load cases, it can be concluded that for the purpose of practical design problems, the predicted

Table 4.1: *Ratio of the safety factor predicted by the design envelope and that obtained from the Tsai-Wu failure criterion (λ_{TW}/λ_s) for Carbon-PEEK (AS4), Carbon-Epoxy (IM6) and Boron-Epoxy (B5.6)*

Material	**Axial Tension** (N_x)				**Bending** (M_x)	
	$[0_8]_s$	$[90_8]_s$	$[\pm 45_4]_s$	$[\pm 45, 0_4, 90_2]_s$	$[\pm 45, 0_4, 90_2]_s$	$[0_4, \pm 45, 90_2]_s$
AS4	2.99	1.00	1.12	1.00	1.07	1.17
IM6	3.92	1.19	1.33	1.12	1.20	1.05
B5.6	2.62	1.00	2.26	1.00	1.33	1.17

factor of safety will only be slightly conservative with respect to the Tsai-Wu failure criterion. Hence, the proposed design envelope is well suited to in-plane strength optimization problems.

It can also be remarked that sandwich structures with composite face sheets are often used when bending loads are dominant. In such a case the face sheets are primarily loaded in their plane. Thus, the design of the face sheets would reduce to an in-plane design problem, for which the proposed failure envelope is well suited.

4.4.2 Verification of the Strength Formulation

The laminate strength was maximized for the three different materials for a combination of shear, $\omega = 0.50$, with either tensile or compressive loads in order to verify the proposed formulation. The results for an example set are plotted in Figure 4.3 in lamination parameter space, along with the contours of the function, r_s, which was minimized and the optimization path. The optimal values of the lamination parameters for each case are presented in Table 4.2. In each case the optimization is started from $V_{1\mathbf{A}} = V_{3\mathbf{A}} = 0$, which corresponds to a quasi-isotropic laminate.

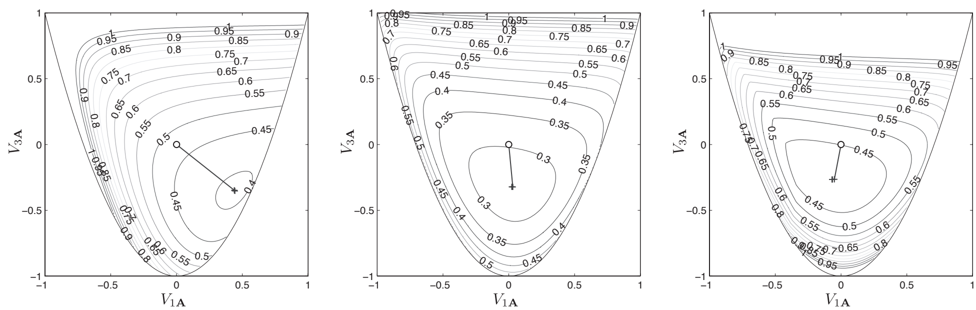

(a) AS4 - Tension (b) IM6 - Compression (c) B5.6 - Compression

Figure 4.3: *Sample optimization paths for the three investigated materials including function value contours, with* $\mathbf{N} = \pm N \cdot [0.5\ 0.0\ 0.5]^T$

The non-smooth failure index value contours in Figure 4.3(c) are caused by the non-smooth nature of the fourth order failure envelope, given by equation (4.11).

The bound formulation (Olhoff, 1989) may be implemented to deal with the lack of smoothness. The optimization procedure converged in a small number of iterations, typically less than 10, for a convergence tolerance of $1 \cdot 10^{-6}$ for the value of r_s. Often good convergence to near optimal solutions can be achieved in one iteration, as can be observed from Figure 4.3.

Table 4.2: *Optimum lamination parameters and $\sqrt{r}_s$ values for $\omega = 0.5$ for various materials and loading*

Material	Tension/Shear			Compression/Shear		
	$V_{1\mathbf{A}}$	$V_{3\mathbf{A}}$	$\sqrt{r}_s$	$V_{1\mathbf{A}}$	$V_{3\mathbf{A}}$	$\sqrt{r}_s$
Carbon-PEEK (AS4)	0.444	-0.353	0.394	0.155	-0.357	0.353
Carbon-Epoxy (IM6)	0.558	-0.293	0.339	0.023	-0.322	0.279
Boron-Epoxy (B5.6)	0.601	-0.248	0.510	-0.067	-0.266	0.412

The optimal lamination parameters for a range of ω values for the case of tension/shear loading are shown in Table 4.3. It is interesting to note that for Carbon-Epoxy (IM6) the optimal pure-tension design ($\omega = 0$) is an angle-ply laminate with fiber orientations of approximately $\pm 5°$. Brandmaier (1970) also found that, as a function of the material properties, maximum strength under unidirectional loading may not be achieved by aligning fibers in the primary stress direction.

Table 4.3: *Optimum lamination parameters and $\sqrt{r}_s$ values for a range of tension/shear load cases ($\omega = 0.1 \ldots 1.0$)*

ω	Carbon-PEEK (AS4)			Carbon-Epoxy (IM6)			Boron-Epoxy (B5.6)		
	$V_{1\mathbf{A}}$	$V_{3\mathbf{A}}$	$\sqrt{r_s}$	$V_{1\mathbf{A}}$	$V_{3\mathbf{A}}$	$\sqrt{r_s}$	$V_{1\mathbf{A}}$	$V_{3\mathbf{A}}$	$\sqrt{r_s}$
0.0	1.000	1.000	0.196	0.985	0.940	0.205	1.000	1.000	0.2847
0.2	0.692	0.305	0.307	0.796	0.324	0.272	0.794	0.261	0.4117
0.4	0.512	-0.163	0.372	0.626	-0.114	0.322	0.670	-0.092	0.4846
0.6	0.381	-0.531	0.411	0.494	-0.463	0.351	0.535	-0.397	0.5291
0.8	0.241	-0.884	0.426	0.307	-0.811	0.364	0.383	-0.707	0.5462
1.0	0.000	-1.000	0.455	0.000	-1.000	0.382	0.000	-1.000	0.5435

The optimization results presented in the following section are limited to in-plane loading of a laminate. The developed failure envelope, and subsequent optimization formulation, is applicable to design problems under in-plane and bending loads and combinations thereof. Pure bending loading does not differ in any essential way from the in-plane case. However, combined in-plane and bending loading requires in-plane and out-of-plane lamination parameters to be used as design variables simultaneously, which requires their combined design space to be defined. The feasible region in this case is available as an approximation, as discussed in section 2.3.4, and as such the basic approach is still applicable albeit with few changes in details. Therefore, all the following optimization results are restricted to in-plane loading of a laminate which, the author believes, is representative enough of the practical applications of the proposed approach.

4.4.3 Parametric Study of Strength versus Stiffness

Since a general optimization formulation for strength and stiffness was developed, it was interesting to investigate the difference between optimal solutions found for each of the optimization problems for a range of load cases. The results of the inverse of the safety factor, $1/\lambda_s = \sqrt{r_s}$, are plotted in Figure 4.4 for the three material systems as a function of the axial load to shear load ratio for different laminate constructions. The designs in Figures 4.4(a) and 4.4(b) are symmetric balanced composites and thus require only two lamination parameters. The remaining two figures are for unbalanced laminates, hence four in-plane lamination parameters were used during optimization.

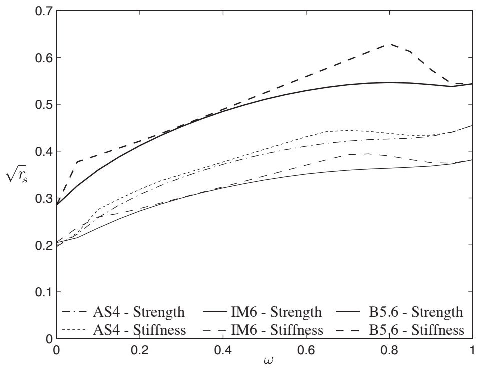

(a) Balanced, tension/shear

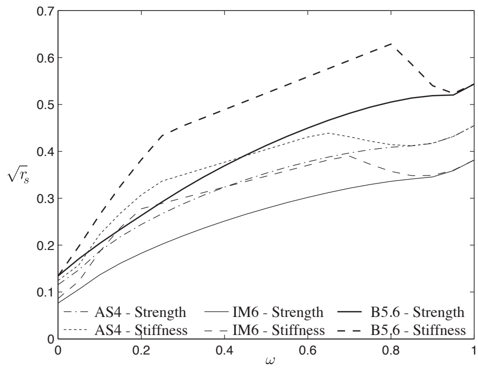

(b) Balanced, compression/shear

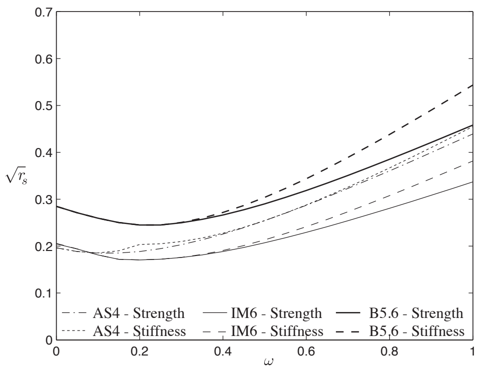

(c) Unbalanced, tension/shear

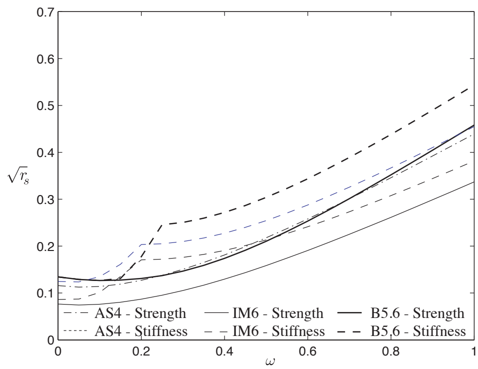

(d) Unbalanced, compression/shear

Figure 4.4: *Comparison of stiffness and strength driven optimal laminates for various materials under combined tension/shear or compression/shear loading*

One of the first noticeable trends was the closeness of the strength and stiffness optimized designs for pure tension/compression or shear loads (i.e. $\omega = 0$ or $\omega = 1$), they are extremely close, if not identical for balanced laminates. Only in the case of unbalanced laminates, particularly for Boron-Epoxy (B5.6), was there a significant difference between strength and stiffness optimized results observed.

As one might expect, the strength optimized designs will always have a factor of safety higher (lower $\sqrt{r_s}$) than or equal to the stiffness driven designs. The performance of combined tension and shear loaded laminates, Figures 4.4(a) and 4.4(c), was similar for both strength and stiffness based designs over the entire range of loading, with Boron-Epoxy (B5.6) deviating from this trend the most. The difference between stiffness and strength driven designs could be as much as 48% for the combined compression and shear loaded cases, Figures 4.4(b) and 4.4(d). Comparing balanced laminate, Figures 4.4(a) and 4.4(b)), with unbalanced laminate designs, Figures 4.4(c) and 4.4(d), for the same load cases, it can be seen that the unbalanced designs yield a higher factor of safety for $\omega > 0$, i.e. when shear loading is present.

Since the formulation for maximum stiffness is insensitive to the sign of the loading, one would expect the stiffness optimization to produce the same design for both tension and compression. This cannot be discerned from the figures (4.4), since the same set of lamination parameters will yield a different safety factor for tension and compression, however, the stiffness optimized designs were found to be identical, and they yielded the same lamination parameters for both load cases.

The difference between strength-optimal and stiffness-optimal laminate designs can be further highlighted by considering the Pareto front traced by both design objectives. The Pareto front for balanced Carbon-PEEK (AS4) and Boron-Epoxy (B5.6) laminates are presented in Figure 4.5, for a selected set of compressive-shear loading. Load cases were selected such that the largest difference between strength-optimal and stiffness-optimal designs were obtained and as such represent the "worst case" scenario. The Pareto fronts were traced by maximizing laminate strength, on the horizontal axis, while simultaneously imposing a lower bound on laminate stiffness, vertical axis. Laminate strength and stiffness values were normalized by the laminate strength and stiffness of the strength-optimal laminate design for each case.

The first noticeable trend was a much flatter Pareto front for Boron-Epoxy (B5.6) than for Carbon-PEEK (AS4). In the worst load case, $\omega = 0.2$, a 10% increase in stiffness resulted in almost a 50% reduction in laminate strength for Boron-Epoxy (B5.6). The same was true for Carbon-PEEK (AS4) to a lesser extent, where a 16% increase in laminate stiffness resulted in a 23% reduction in laminate strength. The differences between laminate stiffness and strength were found to be less severe for other ratios of compression-shear loads. However, it was clear that laminate strength is more sensitive to a change in layup than laminate stiffness.

Considering the balanced laminate designs, Figures 4.4(a) and 4.4(b), it was also interesting to investigate the path of optimum design variables in the lamination parameter design space for the load cases considered, as was done for Carbon-PEEK (AS4) and Boron-Epoxy (B5.6) in Figure 4.6. The designs in the top right-hand corner of the lamination parameter design space correspond to the pure tension or compression load cases ($\omega = 0$), following the lines to the bottom of the parabola where $\omega = 1$, corresponding to a pure shear. It should be kept in mind that $V_{1\mathbf{A}} = 1, V_{3\mathbf{A}} = 1$ corresponds to a laminate with only 0° fibers while $V_{1\mathbf{A}} = 0, V_{3\mathbf{A}} = -1$ to one with a ±45° layup. It is also clear from these figures that the designs for maximum compressive strength deviate more from the stiffness driven optima than those for maximum tensile strength.

Looking at a Carbon-PEEK (AS4) laminate, Figure 4.6(a), pure tension and pure shear result in identical laminate layups, 0° and ±45° respectively, for stiffness and strength driven optimization. However, in the case of pure compression, the strength

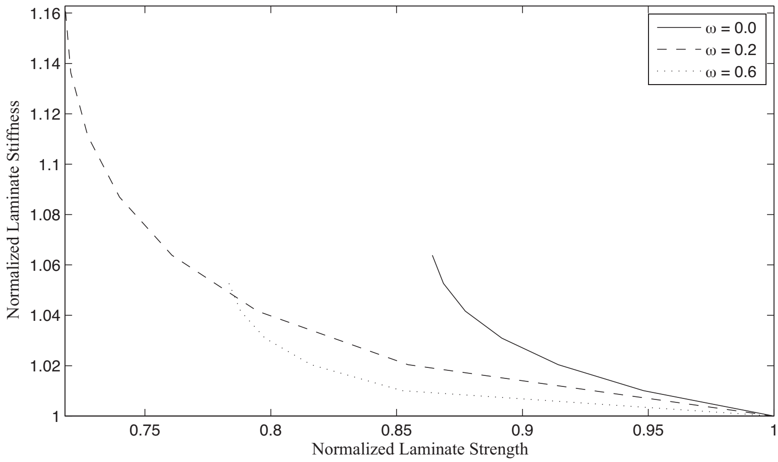

(a) Carbon-PEEK (AS4) $\omega = 0.0,\ 0.2,\ 0.6$

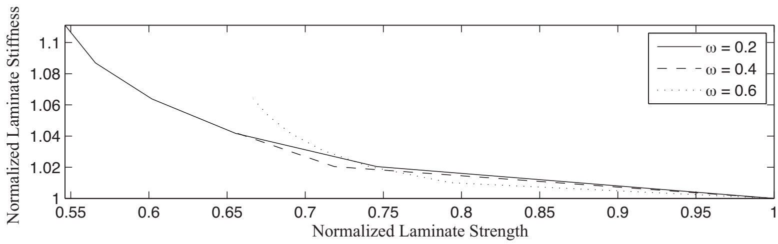

(b) Boron-Epoxy (B5.6), $\omega = 0.2,\ 0.4,\ 0.6$

Figure 4.5: *Pareto curves for maximum stiffness versus maximum strength for several compression-shear loaded panels* (Stiffness and strength values are normalized with respect to the the corresponding values for the corresponding strength-optimal design)

based design includes a small percentage ($< 5\%$) of 90° fibers. This improved the tensile strength in the direction perpendicular to the loading, reducing the laminates Poisson ratio and hence increased the laminates strength slightly.

The results for a Boron-Epoxy (B5.6) laminate shown in Figure 4.6(b) also indicate that a ±45° laminate layup yields the best design in the case of pure shear loading. It can also be seen that for the tension/shear designs optimal layups are all angle-ply laminates. The large difference between stiffness driven and strength driven optima for the compression/shear load case is also clearly visible.

The exact behavior of the optimal fiber orientation for maximum strength of a laminate is a complex function of material properties and failure allowables (Brandmaier, 1970). The clear dependency on the individual material properties was to be expected due to the strong material dependence of the Tsai-Wu failure criterion as is indicated by Groenwold and Haftka (2006). Identifying which material properties or ratios thereof and their influence on the degree of correlation between stiffness and strength optimized designs may be an interesting subject of future research.

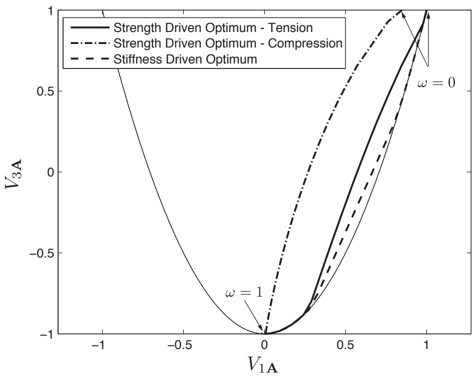

(a) Carbon-PEEK (AS4)

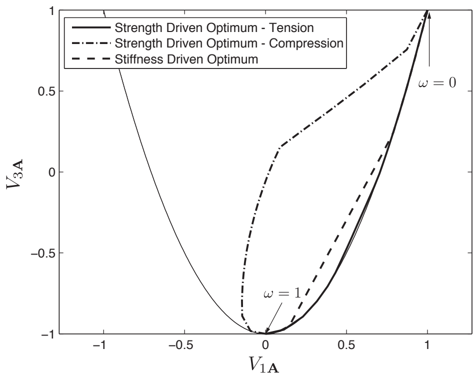

(b) Boron-Epoxy (B5.6)

Figure 4.6: *Optimization paths for strength and stiffness driven optima for balanced symmetric laminates*

4.5 Concluding Remarks

The implementation of the Tsai-Wu failure criterion in the lamination parameter design space was presented. Analytical expressions were found representing the conservative failure envelope in strain space. The equations for the envelope are functions of only two strain invariants and do not depend explicitly on the stacking sequence. The active envelope equation was used to formulate a failure index related to the factor of safety. The failure index was used to formulate an optimization problem to design panels for maximum strength for pure in-plane loading and combined in-plane and bending loads. The derived envelope was shown to accurately represent the factor of safety of practical laminates under in-plane loading, however, for bending dominated problems it was shown that it may be too conservative.

Panels under combined axial and shear loads were designed for maximum laminate strength and laminate stiffness. Results of strength-optimal and stiffness-optimal designs for various materials and load conditions were presented. Strength-optimal and stiffness-optimal designs were found to be similar for a large range of material properties and load cases. However, disparities between these two designs were also found, particularly for compression-shear load cases. It was found laminate strength was more sensitive to the layup than laminate stiffness for the considered materials, which implies that design for maximum strength will result in near-optimal laminate stiffness, however, the opposite is not necessarily true. It is thus concluded that while stiffness maximization might reasonably serve as an easier to evaluate surrogate for the preliminary design of composite structures, the derived conservative failure index offers a more attractive and easy to implement alternative. It should also be kept in mind that when moving to variable stiffness laminates, with significantly more complex stress states, properly capturing structural strength may result in large improvements with respect to equivalent maximum stiffness designs.

Two open problems remain to be investigated. The first is to investigate and understand how the shape of the conservative failure envelope depends on material stiffness properties and failure stresses. Such an analysis would also be quite useful for extending the present formulation to more complex failure criteria that differentiate between different failure modes such as Hashin's criterion. The second open problem is the convexity of the failure index function in lamination parameter space. Convexity would mean that strength-optimal designs are unique and that this unique optimum can be converged starting from arbitrary initial designs. Numerical experience seems to indicate that the failure index is indeed convex or nearly so. While the convexity of the failure index in strain space is straightforward to demonstrate based on the convexity of the underlying Tsai-Wu failure criterion, whether or not convexity carries over to the lamination parameter space is more challenging to assess.

CHAPTER 5
Design of Variable Stiffness Plates for Buckling

"If you do not change direction, you may end up where you are heading"

Lao Tzu

Design of laminated composite plates for improved buckling load has been well studied in the past. Rothwell (1969) study the influence of fiber angles on the compression and shear buckling loads of long rectangular plates with balanced, symmetric laminates. Schmit and Farshi (1976) present one of the first design routines incorporating buckling as a constraint. Designs are obtained from a fixed set of ply orientation angles while using ply thicknesses as continuous design variables, however, the applicability of the approach is limited since stacking sequence information is not considered. Grenestedt (1991) use lamination parameters to design simply-supported rectangular plates with a symmetric layup. The optimal solutions for balanced laminates are found to lie on the boundary of the lamination parameter feasible region and hence are easily converted to angle-ply laminates. The optimal unbalanced optimum is shown to be closely approximated with a single fiber orientation angle. In later work by Fukunaga et al. (1995) a similar approach is adopted to study the influence of bending-twisting coupling on buckling load. Optimal solutions are once again found to lie on the feasible region's boundary, facilitating the conversion to a laminate stack.

Biggers and Srinivasan (1993) conduct a parametric study of simply supported rectangular plates under uniaxial compression. In their study, laminate stiffness properties normal to the load direction are tailored by moving $0°$ plies from the center of the plate to the plate's edge. Buckling loads are shown to increase by up to 200%

This chapter is based on the paper, *Optimization of variable stiffness panels for maximum buckling load using lamination parameters* by S.T. IJsselmuiden, M.M. Abdalla, and Z.Gürdal, which appeared in the AIAA Journal, 48(1), pages 134 – 143, 2010. Note: symbols may have been changed to maintain consistency throughout this thesis.

compared to their baseline design. Kassapoglou (2008) present a Rayleigh-Ritz based analysis of plates under compression with two concentric layups. Several examples are treated which corroborate the advantage of multiple-patch designs in terms of improved buckling resistance. Both studies indicate that buckling loads can improve significantly when allowing designs with non-uniform panel stiffness in the transverse direction.

In all of the aforementioned studies, the designs are based on "traditional" laminates, meaning that the panel is defined by a single laminate or a small set of laminates. Hyer and Lee (1991) present one of the earliest works for which different fiber angles are defined within each element of the finite element model. A square plate with a hole consisting of 18 elements is designed for maximum buckling load using both a sensitivity analysis approach and a gradient-based search algorithm. A symmetric laminate, $[\pm 45/\theta_6]_s$ with θ as design variable, is designed independently for each element and the buckling load is shown to improve by up to 200% with respect to the baseline laminate, $[\pm 45/0_6]_s$. Banichuk et al. (1995) also demonstrate that significant improvements in buckling loads can be achieved by designing the local axis of orthotropy within each element. In later research, Setoodeh et al. (2009) optimize a rectangular plate using nodal based fiber angles as design variables and demonstrate similar performance improvements. However, the use of discrete orientations as design variables has several disadvantages as was discussed in section 1.3.1.

Gürdal and Olmedo (1993) present linear fiber angle variation as the first parameterization scheme for continuous fiber paths. The Ritz method is used to compute buckling loads of rectangular plates. Two example problems are treated, the first allows stiffness to vary along the load direction and the second allows it to vary perpendicular to the load. In the latter example, buckling loads are improved by 80% with respect to the constant stiffness optimum. The authors also highlight how, for a given buckling load, a wide range of average in-plane stiffnesses can be achieved. In later work by Tatting and Gürdal (2002) and Jegley et al. (2005), linear fiber angle variation is used to design, manufacture, and test several variable stiffness panels. Experimental results confirm the advantage of tailoring stiffness properties within the laminate. Alhajahmad (2008) presents a non-linear parameterization scheme for fiber paths based on Lobatto polynomials.

Past research clearly confirms the advantage of introducing stiffness tailoring to improve the compressive load carrying capacity of composite laminates with buckling constraints. Lamination parameters have been used successfully for variable stiffness designs in the past (see section 1.3.3). Until recently lamination parameters could not be implemented to maximize buckling loads of variable stiffness panels because the feasible region for combined in-plane and bending stiffness was unavailable. A conservative approximation scheme for the design of variable stiffness composite panels for maximum buckling load was derived such that it could be cast into the design approach presented in chapter 2. In the approximation the buckling load was expressed as a linear combination of the in-plane and bending stiffness tensors and the corresponding inverses. The presented research was built on work by Setoodeh et al. (2009), where a variable stiffness panel is designed using fiber angles to improve buckling performance. The approximation scheme by Setoodeh et al. (2009) was improved to guarantee homogeneity in stiffness space and convexity in lamination parameters space and is presented in this chapter. The developed approximation scheme retained the desirable properties of the earlier version including that of being separable. The adjoint method was used to compute the sensitivity of all the design variables, requiring only one back substitution using the already factored in-plane stiffness matrix.

A finite element formulation used for buckling analysis is presented in the next section. A new conservative approximation scheme for the laminate buckling load was developed and is presented in section 5.2. Since improved buckling performance typically leads to reduced laminate in-plane stiffness, it was also interesting to study the trade-off between laminates designed for maximum buckling load and laminates designed for maximum in-plane stiffness. Laminate in-plane stiffness was maximized by minimizing the overall compliance, for which an approximation is also presented. The design trade-off study was conducted using a combined objective function as presented in section 5.3. Several example problems were outlined and compared to results available from the literature in section 5.4, which is followed by conclusions in section 5.5.

5.1 Buckling Analysis

Analysis of variable stiffness laminates can be performed using constitutive relations that are based on classical lamination theory for thin laminates. The theory is valid for small strains and assumes that perfect bonding between layers exists. The classical Kirchhoff assumptions for a plate also apply. The only essential difference with traditional analysis is that stiffness properties now vary as a function of spacial location, and therefore each element will have a different stiffness matrix associated with it. The buckling load is determined using a finite element discretization of the buckling analysis through the following eigenvalue problem, see for example Cook (2002, chapter 18):

$$\left(\mathbf{K}_b - \lambda \mathbf{K}_g\right) \cdot \mathbf{a} = \mathbf{0} \tag{5.1}$$

where $\mathbf{K}_b$ is the global bending stiffness matrix, $\mathbf{K}_g$ is the global geometric stiffness matrix, $\mathbf{a}$ is the mode shape comprising deformation degrees of freedom, and λ is the load multiplier (or buckling factor). The mode shapes are normalized such that:

$$\mathbf{a}^T \cdot \mathbf{K}_b \cdot \mathbf{a} = 1 \tag{5.2}$$

The geometric stiffness matrix is constructed through an assembly of element geometric matrices. The stiffness matrix of each element takes the form:

$$\mathbf{K}_{g_e} = -n_x \mathbf{K}^x - n_y \mathbf{K}^y - n_{xy} \mathbf{K}^{xy} \tag{5.3}$$

where $\mathbf{n}_e = (n_x,\ n_y,\ n_{xy})^T$ is the vector of in-plane stress resultants averaged over the element based on nodal displacements as described next, and $\mathbf{K}^x$, $\mathbf{K}^y$ and $\mathbf{K}^{xy}$ are constant matrices that depend only on element geometry.

The averaged in-plane stress resultants can be expressed as:

$$\mathbf{n}_e = \mathbf{A}_e \cdot \mathbf{e}_e \tag{5.4}$$

where $\mathbf{A}$ is the in-plane stiffness matrix and $\mathbf{e}$ is the average strain vector given by:

$$\mathbf{e}_e = \overline{\mathbf{B}}_e \cdot \mathbf{u}_e \tag{5.5}$$

where $\mathbf{u}$ is the vector of in-plane displacements, $\mathbf{u}_e$ is the vector of the degrees of freedom associated with nodes connected to the e^{th} element, and $\overline{\mathbf{B}}$ is the average element strain displacement matrix, see Appendix B.1. The in-plane displacements can be found from the solution of the in-plane equilibrium equations:

$$\mathbf{K}_m \cdot \mathbf{u} = \mathbf{f} \tag{5.6}$$

where $\mathbf{K}_m$ is the membrane stiffness matrix and $\mathbf{f}$ is the vector of in-plane loads.

5.2 Conservative Approximation Formulation

A separable approximation for the buckling load multiplier of a plate is derived in the following section. A similar approximation is presented for structural compliance, which allows stiffness-optimal laminate designs to be found. A linear combination of the two aforementioned approximations is subsequently defined such that stiffness-optimal and buckling-optimal variable stiffness laminate designs can be compared.

5.2.1 Approximating Buckling

The buckling load factor is a function of both in-plane stiffness and bending stiffness, i.e. $\lambda(\mathbf{A}, \mathbf{D})$. In past research, a generalized reciprocal approximation, in which the response is approximated based on the inverse of the stiffness tensors, is used successfully for variable stiffness design (Abdalla et al., 2007; Setoodeh et al., 2006b). A similar approximation is treated by Setoodeh et al. (2009) in the context of buckling load minimization using fiber angles as design variables. Applying this approach to optimize variable stiffness panels for buckling has been difficult, since the approximation is found to be non-homogeneous and non-convex.

A convex approximation for the buckling load factor was formulated for the presented research with insight from the homogeneity properties of the buckling factor as a function of the in-plane and bending stiffness tensors. The generic convex, conservative approximation expression, equation (3.9), requires the nature of the response to be understood such that the parts contributing to the linear and reciprocal approximation terms can be identified.

When considering plates, the effect of in-plane and out-of-plane stiffness on buckling load can be treated as two individual parts. This is best clarified by inspecting the sensitivity of the a single eigenvalue with respect to an arbitrary design variable. The variable b is assumed to affect only the local stiffness properties of a single element, e. The expression of the sensitivity is obtained by differentiating equation (5.1) and can be written as:

$$\frac{\partial \lambda}{\partial b} = \lambda\, \mathbf{a}^T \cdot \left(\frac{\partial \mathbf{K}_b}{\partial b} - \lambda \frac{\partial \mathbf{K}_g}{\partial b} \right) \cdot \mathbf{a} \tag{5.7}$$

an equation that is composed of two terms. The first term is dependent on the derivative of bending stiffness and is local, which implies information from a single element is sufficient to evaluate its influence on the critical buckling factor. The second term, which is the derivative of the geometric stiffness, is not local. That is, the in-plane loads of all elements are influenced by changing the stiffness of a single element and therefore the geometric stiffness matrices of all elements will change. The second term essentially represents the effect of load redistribution within the plate. Note also that equation (5.7) assumes that the eigenvalue is unimodal. Difficulties may arise when evaluating derivatives if multiple eigenvalues are present, as is discussed in Seyranian et al. (1994).

Further insight into buckling factor dependency on in-plane and bending stiffness can be gained by inspecting equations (5.1) to (5.6). The buckling factor is a homogeneous function of order zero with respect to in-plane stiffness, as can be verified by noting the effect of scaling stiffness terms in equation (5.6) by a constant factor. If the applied load remains unchanged the resulting displacements (and strains) will be multiplied by the inverse of that factor and the in-plane stresses, equation (5.4), will remain unchanged. The physical meaning is that the buckling load factor depends on load redistribution which occurs due to a relative change in the in-plane stiffnesses over the domain. Additionally, the buckling load factor is homogeneous of order one with respect to the bending stiffness.

Instead of approximating the buckling load factor directly, we chose to express the approximation in terms of the inverse buckling factor $r_b = 1/\lambda$, which is a measure of structural compliance. The same homogeneity properties can be shown to hold for the inverse buckling factor, which is therefore homogenous of order zero with respect to the in-plane stiffness and of order one with respect to *inverse* bending stiffness. A homogenous approximation is obtained by expanding the inverse buckling factor linearly in terms of in-plane stiffnesses and the inverse bending stiffnesses, resulting in the following expression:

$$r_b \approx r_{b0} + \sum_{i=1}^{N} \left(\left. \frac{\partial r_b}{\partial \mathbf{A}_i} \right|_0 : (\mathbf{A}_i - \mathbf{A}_{0i}) + \left. \frac{\partial r_b}{\partial \mathbf{D}_i^{-1}} \right|_0 : \left(\mathbf{D}_i^{-1} - \mathbf{D}_{0i}^{-1}\right) \right) \tag{5.8}$$

where the $_0$ represents the design point about which the inverse buckling factor is expanded and $i = 1 \ldots N$ are the nodes, elements or design regions for which the design variables are defined. The : operator represents matrix inner product, which is simply the generalization of the dot-product to the matrix space.

Euler's theorem for homogeneous functions implies that, at any approximation point, the sum over all points for in-plane stiffness is always zero, i.e.:

$$\sum_{i=1}^{N} \left(\frac{\partial r_b}{\partial \mathbf{A}_i} : \mathbf{A}_i \right) = 0 \tag{5.9}$$

while the corresponding sum of bending terms gives the inverse buckling factor:

$$\sum_{i=1}^{N} \left(\frac{\partial r_b}{\partial \mathbf{D}_i^{-1}} : \mathbf{D}_i^{-1} \right) = r_b \tag{5.10}$$

Therefore, the final form of the approximation reduces to:

$$r_b \approx \sum_{i=1}^{N} \left(\mathbf{\Psi}_i^m : \mathbf{A}_i + \mathbf{\Phi}_i^b : \mathbf{D}_i^{-1} \right) \tag{5.11}$$

where $\mathbf{\Psi}^m$ and $\mathbf{\Phi}^b$ are the sensitivity tensors with respect to in-plane stiffness and the inverse bending stiffness, respectively, as defined in Appendix C.2. The inverse buckling factor approximation has therefore been cast into the generic form presented in section 3.2. Note that the approximation is characterized by linear terms that are dependent only on laminate in-plane stiffness, while the reciprocal terms are dependent only on laminate bending stiffness. Note also that the in-plane sensitivity tensors, $\mathbf{\Psi}^m$, satisfy equation (5.9):

$$\sum_{i=1}^{N} \mathbf{\Psi}_i^m : \mathbf{A}_i = 0 \tag{5.12}$$

Since the in-plane stiffness tensor is always positive definite, equation (5.12) implies that the sensitivity tensors $\mathbf{\Psi}^m$ are not necessarily definite. This lack of definiteness is not problematic since the $\mathbf{\Psi}^m$ appear only in linear terms, however, as shown in Appendix C.2, the sensitivity tensors $\mathbf{\Phi}^b$ are always positive definite and therefore the approximation as a whole is guaranteed to be convex. A detailed derivation of the sensitivity matrices is provided in Appendix C.2.

In work previously published by the author and Setoodeh et al. (2009) the variable stiffness buckling optimization problem is parametrized in terms of fiber angles, resulting in a non-convex design problem. As was suggested earlier, introducing lamination parameters as design variables results in a convex design space, however, two important observations have been made with respect to formulating an approximation scheme. In the aforementioned work the buckling factor is approximated directly using a reciprocal approximation. Firstly, the resulting approximation is non-homogenous. Secondly, the convexity of the terms dependent on in-plane stiffness cannot be guaranteed if the reciprocal is used as the sensitivities will not necessarily be positive definite. The approximation scheme presented here reproduces the homogeneity properties of the buckling factor and is convex. Thus, the proposed approximation is a suitable starting point for a successive approximation optimization methodology. Note also, that even though the presented approximation is guaranteed to be convex, the underlying design problem is not necessarily convex.

5.2.2 Approximating Compliance

When considering straight fiber composite designs, improving buckling performance often results in a deterioration of the overall in-plane stiffness. Olmedo and Gürdal (1993) also demonstrate that a range of critical buckling loads can be achieved for a fixed value of average in-plane stiffness and vice versa. It is therefore interesting to study the trade-off between in-plane stiffness design optimization and buckling performance optimization of variable stiffness laminates. The structural stiffness can be maximized by minimizing the compliance (Hammer et al., 1997; Setoodeh et al., 2006a). Using a similar approach as for buckling, an approximation for compliance, r_c, can be formulated as:

$$r_c \approx \sum_{i=1}^{N} \mathbf{\Phi}_i^m : \mathbf{A}_i^{-1} \tag{5.13}$$

where, in this case $\mathbf{\Phi}^m$, is the sensitivity of the in-plane stiffness with respect to the change in compliance of the point i. A derivation of the sensitivity matrix is provided in Appendix C.1.

5.3 Optimization formulation

Approximations for both the inverse buckling factor and compliance were presented in the previous section. Both approximations are cast such that they are readily solved using the developed optimization framework, presented in chapter 2. It was also interesting to explore solutions for laminate stiffness distributions that consider both in-plane stiffness and buckling. Two possibilities exist to explore the Pareto front covering these two designs. One option is to optimize for buckling while imposing a minimum bound on compliance, or vice versa. The second option is to create a combined objective function which includes the contribution of both responses. The latter, a combined buckling-stiffness optimization problem, was formulated as:

$$\min_{\mathbf{V}} \left(\alpha \cdot \frac{r_b}{\hat{r}_b} + (1-\alpha) \cdot \frac{r_c}{\hat{r}_c} \right) \tag{5.14}$$

where $\mathbf{V}$ is the vector of all design variables, $\hat{r}_b$ and $\hat{r}_c$ are arbitrary reference values used to normalize the critical buckling load, r_b, and the compliance, r_c. The relative importance of either the buckling load or stiffness is controlled via a predefined coefficient α which has a value between zero and one, and allows the trade-off between stiffness and buckling performance to be studied.

The approximations in equations (5.11) and (5.13) are separable, and thus can be solved locally at each node. The local optimization problem can therefore be formulated to fit the formulation presented in chapter 2 as:

$$\min_{\mathbf{V}_i} \left(\frac{\alpha}{\hat{r}_b} \cdot \left(\mathbf{\Psi}_i^m : \mathbf{A}_i + \mathbf{\Phi}_i^b : \mathbf{D}_i^{-1} \right) + \frac{(1-\alpha)}{\hat{r}_c} \cdot \mathbf{\Phi}_i^m : \mathbf{A}_i^{-1} \right) \tag{5.15}$$

where $\mathbf{V}_i$ is the vector of design variables associated with the i^{th} design region.

Three issues are worth mentioning at this point; one, it is worth noting that the Pareto front representing the trade-off between buckling and stiffness is not necessarily convex. Thus, in practice, points on the Pareto front are obtained by iteratively updating the design according to (5.15). While the iteration converges to a local minimum of the approximation, it is guaranteed only to be a stationary point of the objective function (5.14). This means that the iteration scheme can converge even for the non-convex portions of the Pareto front. Two, for α approaching unity, the buckling approximation (5.11) is not strictly convex which may lead to convergence problems. Convexity can be ensured using the methods explained in section 3.3. In the examples considered here, convexity is guaranteed using a proximal term in lamination parameter space. Three, buckling mode interaction can cause convergence problems if only a single buckling mode is taken into account during the optimization. This is remedied using the multi-modal design approach outlined in section 3.4.2.

5.4 Numerical Results

The purpose of this section is to illustrate the benefit of using variable stiffness design with lamination parameters and to study the mechanisms resulting in improved buckling loads. In the following section, two example problems, previously studied by Olmedo and Gürdal (1993), are investigated. In section 5.4.2 the trade-off between buckling and in-plane stiffness is studied and finally the post-buckling performance of several of the obtained laminates is evaluated.

5.4.1 Uniaxial Compression

Two example problems presented by Olmedo and Gürdal (1993) are outlined in Figure 5.1. Both consist of a simply supported rectangular panel subject to an axial compressive load per unit length, N_x. For case I, Figure 5.1(a), the edges of the panel straight and the panel is prevented from expanding in the lateral direction. The constraint on lateral expansion is removed for case II, Figure 5.1(b). A square configuration ($a/b = 1$) with side lengths of 15 inch (381 mm) and a total laminate thickness 0.06 inch (1.524 mm) was investigated. The material properties for unidirectional carbon-epoxy T300/5208 are listed in Appendix A.

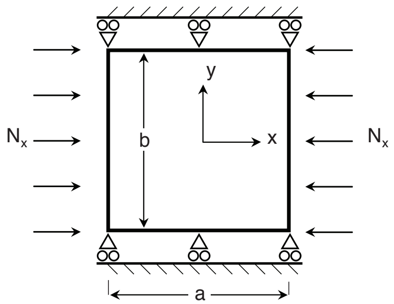

(a) **Case I:** Simply supported, enforced straight edges, no lateral expansion

(b) **Case II:** Simply supported, enforced straight edges

Figure 5.1: *Geometry, loading and boundary conditions for the considered panels*

Mesh Convergence

The panel was discretized into a selected number of equally sized elements and analyzed using a finite element routine programmed in Matlab$^{\text{TM}}$. A rectangular flat shell element, consisting of an eight degree of freedom bi-linear membrane element and a twelve degree of freedom Kirchhoff flexural element was implemented as described in Appendix B. To select an appropriate mesh density and verify the finite element routine, a mesh convergence study was conducted. The number of elements versus buckling load for the optimal constant stiffness and optimal variable stiffness designs by Olmedo and Gürdal (1993) are plotted in figure 5.2 for both example problems. The buckling load was normalized with respect to the results reported in Olmedo and Gürdal (1993). Two clear observations can be made, one, variable stiffness designs require a significantly larger number of elements to converge. This is attributed to the additional elements required to describe the stiffness distribution over the panel accurately. Two, in all cases the buckling load converges to a smaller value than that found by the aforementioned authors. Olmedo and Gürdal (1993) apply the Ritz method to solve the buckling problem which, for a finite set of coefficients, results in a slight overestimate of the actual buckling load.

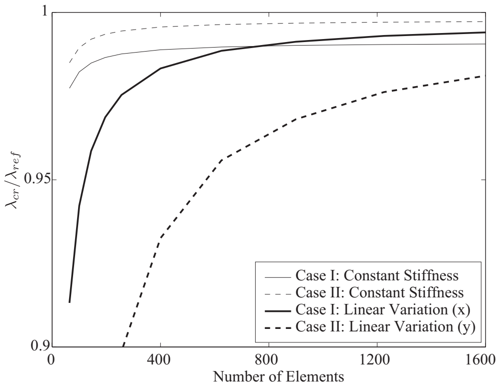

Figure 5.2: *Mesh convergence of the critical buckling load, normalized with respect to the reference results presented in Olmedo and Gürdal (1993)*

Comparison of Optimal Solutions

Design variables are defined at nodes, therefore, mesh density influences the accuracy of the solution and its resolution. For this reason the example problems were solved using two different mesh densities, 100 and 400 elements, respectively, to assess the influence of the increased number of elements on the represented optimal solution. With four design variables associated with each node, this resulted in a total of 484 and 1764 design variables, respectively, for the two aforementioned mesh densities. Due to the relatively high computational cost required to solve the optimization problems, higher mesh densities have currently not been considered, however, solution convergence was demonstrated and is presented towards the end of this section.

Buckling results were benchmarked against a quasi-isotropic panel, the optimum constant stiffness laminate design, $[\pm\theta_n]_s$, and the optimum linear variation results found by Olmedo and Gürdal (1993). Two different 'levels' of stiffness variation were implemented to evaluate the influence of variable stiffness design on the buckling performance of a panel. The first level only allowed stiffness to vary along one axis of the panel, in other words, the stiffness along the x-axis, the loading direction, remained constant while it varied along the y-axis or vice versa. The optimization was carried out using the formulation developed in section 5.2. The only required modification was that the sensitivities along the constant stiffness axis were summed, hence eliminating laminate stiffness variation along that axis. The second level allowed laminate stiffness to vary freely over the entire domain, and hence represented the 'absolute' variable stiffness optimum. In all cases the laminates were considered to be locally balanced and symmetric, hence only four lamination parameters were required to fully characterize the local laminate stiffness properties.

Normalized buckling loads and the associated improvements with respect to the quasi-isotropic design for the first and second cases are presented in Tables 5.1 and 5.2, respectively. Two general trends are clearly noticeable; one, the largest design improvements are achieved when stiffness is allowed to vary normal to the applied load, i.e. VS(y) and VS(x,y). This indicates that in-plane load redistribution has an important contribution to make to the improved buckling load, thus affirming the discussion in Olmedo and Gürdal (1993). Two, case II is more sensitive to mesh refinement, as the difference between the coarse and fine mesh are larger than for case I. Figure 5.2 also indicates that a finer mesh, of more than 1600 elements, is necessary to capture all the details for case II.

For case I, Table 5.1, performance improvements of up to 148% with respect to the quasi-isotropic panel and over 100% with respect to the optimum constant stiffness design were obtained. Increasing the number of elements yielded improved results due to the increased number of design variables and improved representation of the stiffness variations. Varying stiffness only along the y-axis yielded results within a few percent of full variable stiffness designs.

Table 5.1: *Optimal dimensionless buckling modes for several laminate configurations for case I. Improvement percentages are taken with respect to the equivalent quasi-isotropic design.* ($\tilde{N}_{cr} = N_{cr}a^2/E_1h^3$, QI: Quasi-isotropic $[\pm 45, 0, 90]_s$, CS: Constant Stiffness $[\pm 32]_s$, LV: Linear Variation $< 0, 50 >_s$, VS: Variable Stiffness)

	$\tilde{N}_{cr}$ **- 100 Elements**				$\tilde{N}_{cr}$ **- 400 Elements**			
	Mode 1	Mode 2	Mode 3	%	Mode 1	Mode 2	Mode 3	%
QI	1.0597	1.9865	3.6694	—	1.0681	2.0106	3.7151	—
CS	1.1885	2.6374	2.7023	12	1.1965	2.6669	2.7362	12
LV(x)	1.3568	2.4831	3.2501	28	1.4159	2.6835	3.3966	33
VS(x)	1.4890	2.1815	3.9966	41	1.5218	2.2016	4.0966	42
VS(y)	2.3802	2.3803	3.2894	125	2.5634	2.5642	3.4575	140
VS(x,y)	2.4692	2.4705	3.8688	133	2.6492	2.6493	4.0831	148

Results for case II, presented in Table 5.2, show that improvements of nearly 190% are possible. The difference between VS(y) and VS(x,y) was more pronounced for case II as lateral load redistribution played a more important role, as will be seen later. Note also that for most variable stiffness designs the first and second buckling mode coincide, reinforcing the necessity to include multiple modes in the design routine.

Table 5.2: *Optimal dimensionless buckling modes for several laminate configurations for case II. Improvement percentages are taken with respect to the equivalent quasi-isotropic design.* ($\tilde{N}_{cr} = N_{cr}a^2/E_1h^3$, QI: Quasi-isotropic $[\pm 45, 0, 90]_s$, CS: Constant Stiffness $[\pm 45]_s$, LV: Linear Variation $< 90, 15 >_s$, VS: Variable Stiffness)

	$\tilde{N}_{cr}$ **- 100 Elements**				$\tilde{N}_{cr}$ **- 400 Elements**			
	Mode 1	Mode 2	Mode 3	%	Mode 1	Mode 2	Mode 3	%
QI	1.3734	2.1334	3.7899	—	1.3842	2.1594	3.8373	—
CS	1.7316	2.2900	3.5099	26	1.7424	2.3161	3.5586	26
LV(y)	2.4250	2.4639	3.3500	77	2.9282	2.9499	4.0092	112
VS(x)	2.4278	2.4284	4.1722	77	2.5271	2.5271	4.2514	83
VS(y)	3.3121	3.6135	5.0002	141	3.5355	3.8054	5.1586	155
VS(x,y)	3.4773	3.4775	4.7799	153	3.9989	4.0473	5.2261	189

To gain more insight into the effects of stiffness variation on in-plane load redistribution, the pre-buckling stress resultants along several panel cross-sections are plotted in Figures 5.3 and 5.4 for cases I and II, respectively. The stresses are normalized by dividing by the magnitude of the pre-buckling stress value for a constant stiffness panel. Several different sections along the panel are considered; A-A' and B-B' are vertical sections normal to the loading direction, along the edge and center of the panel, whereas C-C' and D-D' are horizontal sections along the top and center of the panel. The stress resultant along the x-axis, $\hat{n}_x$, is plotted for the vertical sections and the stress resultant along the y-axis, $\hat{n}_y$, is plotted for the horizontal sections.

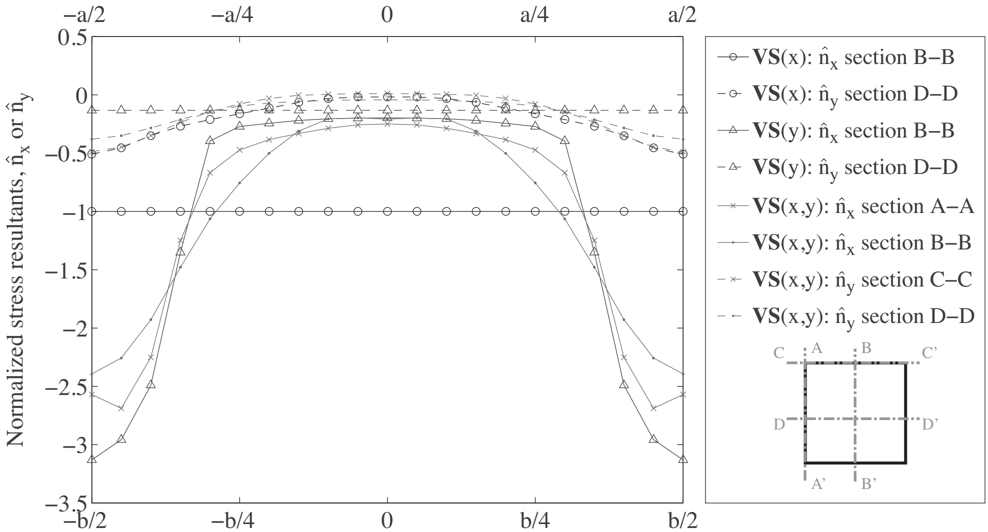

Figure 5.3: *Normalized in-plane stress resultants, $\hat{n}_x$ and $\hat{n}_y$, plotted along several sections of the plate for case I*

Similar trends for $\hat{n}_x$ are visible for both cases along the vertical sections. Stiffness variation along the x-axis, VS(x), results in constant stress along the panel width as the stiffness is uniform. The stress distributions are similar for both the case of variable stiffness along the y-axis, VS(y), and full variable stiffness, VS(x,y), for which highest gains in the buckling loads were achieved. The majority of the compressive stress is concentrated at the edge of the panel, whereas the center of the panel is barely loaded. This clearly demonstrates that the mechanism of load redistribution is primarily responsible for improved buckling load.

The distribution of $\hat{n}_y$ along the horizontal sections differs slightly between the two cases. The stress distribution for VS(y) is constant and has a small negative value for case I due to restricted expansion. When stiffness is allowed to vary along the x-axis, VS(x), a similar trend is visible for both cases; the center of the panel is subject to tensile stresses whereas the edges of the panel are compressed. The effect is more pronounced in case II as a straight edge condition is enforced while allowing lateral expansion. Even though lateral load redistribution is a secondary effect, it still has a large influence on the buckling load.

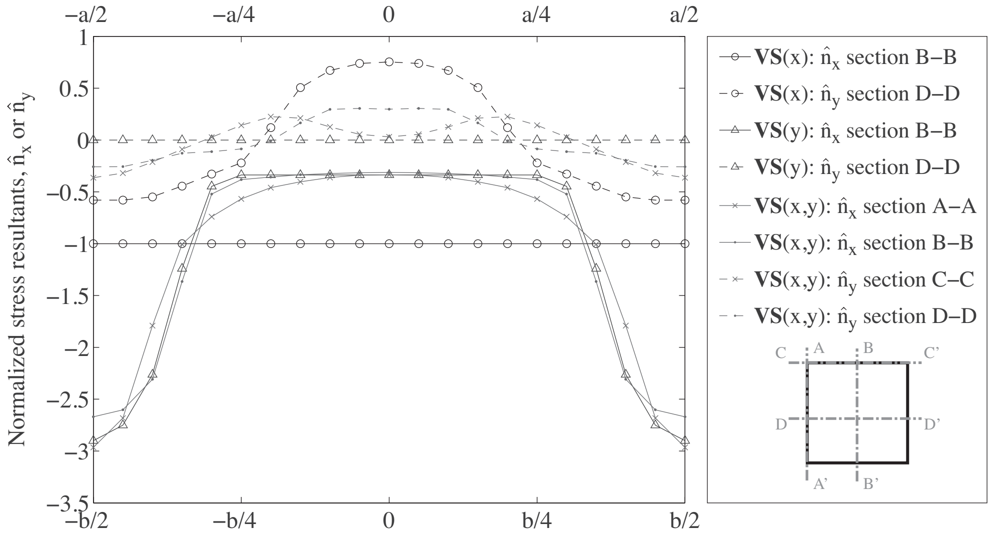

Figure 5.4: *Normalized in-plane stress resultants, $\hat{n}_x$ and $\hat{n}_y$, plotted along several sections of the plate for case II*

To reinforce the argument that buckling load improvements are primarily due to load redistribution the developed optimization routine can be run such that only out-of-plane lamination parameters are considered as design variables. The in-plane lamination parameters are fixed to zero, representing quasi-isotropic in-plane stiffness. For case II the optimum normalized buckling load is found to be only 20% higher than that of a quasi-isotropic laminate, which is equivalent to the buckling performance of the equivalent optimal constant stiffness design. However, the full variable stiffness optimum shows an improvement of almost 190%, thus the largest contribution is deemed to be associated with in-plane stiffness tailoring.

It is also interesting to discuss the lamination parameter distribution found for the maximum buckling load, as is shown in Figure 5.5. The Miki diagram (Gürdal et al., 1999) , shown in Figure 5.6, should be kept in mind to interpret the results in Figure 5.5. The in-plane stiffness contours, E_x, have been included in the Miki diagram for convenience. For both cases, the regions at the top and bottom edges of the panel for $V_{1\mathbf{A}}$ and $V_{3\mathbf{A}} \approx 1$ refer to values found in the upper-right corner of the Miki diagram, indicating that the panel is axially stiff in these regions. For case I, the center of the panel corresponds to values of in the upper-left corner of the Miki diagram, which are axially compliant, but stiff in the transverse direction, leading to the slight transverse tensile stresses at the center of the panel as seen in Figure 5.3. For case II, the regions at the center of the panel are values found towards the left boundary of the Miki diagram referring to regions with lower axial stiffness. The values for the out-of-plane lamination parameters are more difficult to associate with physical laminate properties, but are included for completeness.

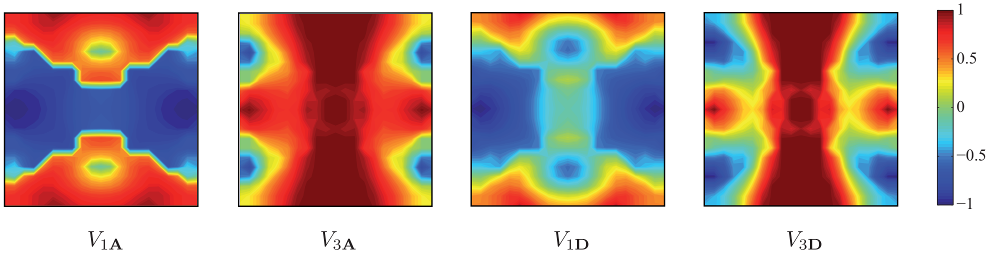

(a) Case I

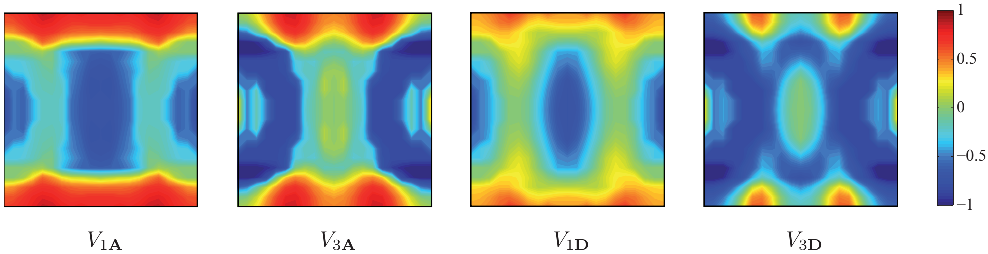

(b) Case II

Figure 5.5: *Optimal lamination parameter distribution for both load cases, for 400 elements*

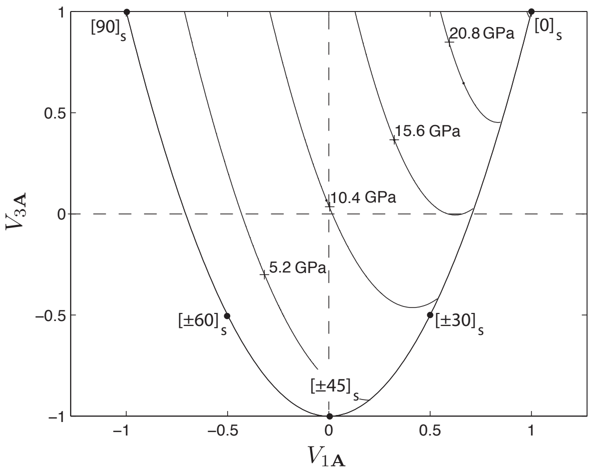

Figure 5.6: *Miki diagram for the in-plane lamination parameters with contours representing laminate axial stiffness, E_x*

Solution Convergence

Computational expense limited the number of elements which could be conveniently considered while conducting the presented design studies, however, it is important to demonstrate that the solution procedure converges as the mesh density, and therefore number of design variables, increases. The percentage difference between the optimal solution and the optimal solution found for a 100 element mesh, which corresponds to 484 design variables, for case II is presented in Figure 5.7. As can be seen in the figure there is only a 3% difference between the optimal buckling load found when using more than 26000 design variables compared to the 1764 design variables used for the 400 element mesh.

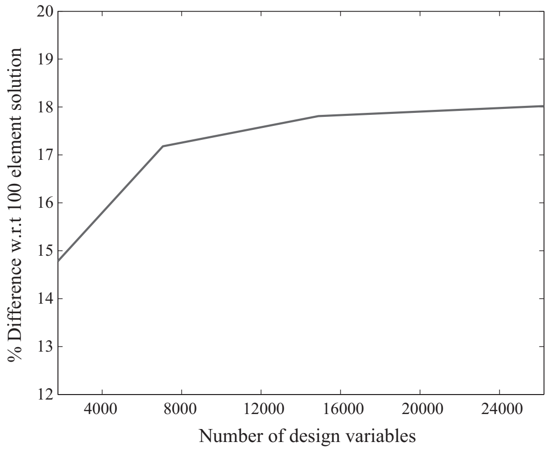

Figure 5.7: *Solution convergence of optimal buckling load for case II, shown as percent difference w.r.t the solution found for the 100 element mesh*

5.4.2 Stiffness versus Buckling Optimal Designs

An equation to study the trade-off between stiffness and buckling was presented in section 5.3, allowing the Pareto front to be computed by varying α over $(0, 1)$. The Pareto front for both constant stiffness and variable stiffness laminates are plotted in Figure 5.8. It is interesting to note that the Pareto front for variables stiffness laminates is not convex, hence uniqueness of the optimal solution is not guaranteed.

When considering designs with high axial stiffness, $\alpha \in (0, 0.3)$, the performance difference between variable and constant stiffness laminates is not large. These designs are dominated by fibers placed parallel to the applied load, leaving little room for stiffness tailoring. As was found in Table 5.2, the optimum buckling load ($\alpha = 1$) of a variable stiffness panel is twice that of the constant stiffness design and in excess of 2.5 times that of a quasi-isotropic laminate. Additionally, a variable stiffness panel with the same in-plane stiffness as a quasi-isotropic panel, i.e. $r_c/\hat{r}_c = 1$, can be designed to have a buckling load which is almost 150% higher than the quasi-isotropic panel, whereas for a constant stiffness panel the improvement is only around 22%.

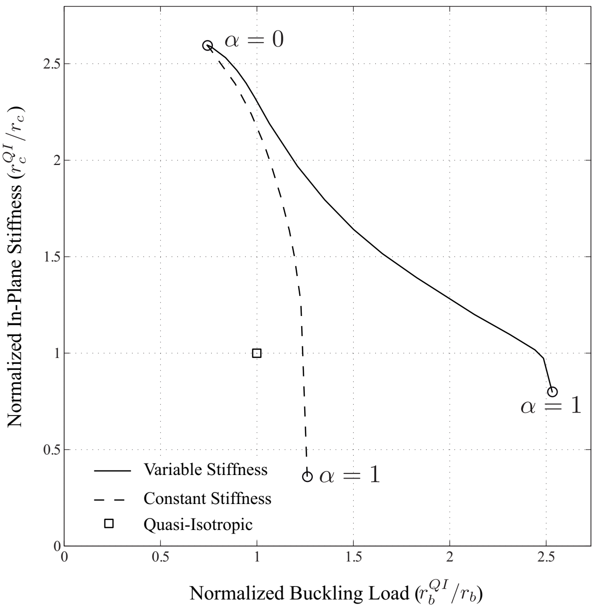

Figure 5.8: *Pareto front for stiffness ($\alpha = 0$) versus buckling ($\alpha = 1$) optimal designs for both variable and constant stiffness laminates. Values are generated using a 100 element finite element model and are normalized with respect to the stiffness and buckling load of a quasi-isotropic laminate*

5.4.3 Post-Buckling Behavior

In the previous subsection, the presented numerical results demonstrated that laminate stiffness tailoring can yield significant improvements in linear buckling loads. In aerospace applications, panel type structures are often permitted to enter the post-buckling regime during service. It is therefore interesting to study the post-buckling behavior of previously obtained designs to determine if linear buckling improvement are obtained at the expense of post-buckling performance. The last statement is largely motivated by the fact that the in-plane stress resultant distributions of the variable stiffness laminates resembles the stress resultant distribution of a buckled laminate.

Rahman et al. (2011) present a finite-element based perturbation method to study post-buckling behavior of variable stiffness panels. The primary goal was to develop an approach to allow for fast prediction of post-buckling behavior near the panel's bifurcation point, making it possible to include post-buckling as a response in future variable stiffness laminate optimization routines. Together with Rahman et al. (2011) the author also studied the post-buckling and failure behavior of several variable stiffness panels, the results of which are discussed briefly in this section.

To evaluate post-buckling behavior, the pre-buckling and post-buckling stiffness, denoted by K_{pr} and K_{po}, respectively, for several designs obtained for case II are compared in Table 5.3. The buckling loads were normalized with the critical buckling load of the quasi-isotropic design. Several designs along the previously obtained Pareto front are also included, where $\alpha = 0.0$ is a design with maximum axial stiffness, while $\alpha = 1.0$ represents a design with maximum buckling load. The design for $\alpha = 0.5$ was chosen as both stiffness and buckling are weighed equally for this design, while $\alpha = 0.85$ was selected as it has roughly the same pre-buckling stiffness as the quasi-isotropic design. Post-buckling stiffness should be computed for all critical buckling modes when the designs exhibited mode-clustering to determine the critical post-buckling stiffness. In several of the previously found designs, two closely spaced buckling modes were found, hence two post-buckling stiffness values were computed for these designs.

Table 5.3: *Buckling loads, pre-buckling and post-buckling stiffness for case II. Results are all normalized with respect to the quasi-isotropic design* (QI: Quasi-isotropic, CS: Constant Stiffness, VS: Variable Stiffness)

	N_{cr}	K_{pr}	K_{po}	K_{po}/K_{pr}
QI, $[\pm 45, 0, 90]_s$	1.0000	1.0000	0.5025	0.5025
VS(x,y), $\alpha = 0.0$	0.7391	2.5975	0.8833	0.3401
VS(x,y), $\alpha = 0.5$	1.6441	1.5102	0.7516	0.4977
VS(x,y), $\alpha = 0.85$	2.4173	1.0120	0.7180	0.7094
			0.4240	0.4190
VS(x,y), $\alpha = 1.0$	2.5319	0.7344	0.6372	0.8677
			0.4025	0.5481

All designs exhibit stable post-bucking behavior, typical of panels. In the post-buckling regime the stiffness of the quasi-isotropic panel is halved with respect to its pre-buckling stiffness. The design with $\alpha = 0.0$ has the highest pre-buckling and post-buckling stiffness, however, it exhibits the largest decrease in stiffness after buckling, reducing to 34% of the original stiffness. When $\alpha = 0.5$ the buckling load is 64% larger than the quasi-isotropic panel while both the pre-buckling and post-buckling stiffness are 50% higher than the quasi-isotropic design. For $\alpha = 0.85$ the pre-buckling stiffness is roughly the same as the quasi-isotropic panel, however, the buckling load is 140 % higher. In this case, two post-buckling stiffnesses were computed corresponding to the two critical buckling modes found at the optimum. The lower post-buckling stiffness will typically be critical if mode-spacing is small, and is approximately 15% lower than the quasi-isotropic panel for this design. When considering the optimum variable stiffness laminate design for buckling, $\alpha = 1.0$, both the pre-buckling and post-buckling stiffness are lower than the quasi-isotropic design, while the buckling load is 150% higher.

It is interesting to note that it is therefore possible to design a variable stiffness laminate such that the buckling load, pre-buckling stiffness and post-buckling stiffness are superior to those of a constant stiffness design. Additionally, if sufficient mode spacing is guaranteed, the optimal variable stiffness designs exhibit better post-buckling stiffness than the quasi-isotropic design. Thus, there seems to be a relationship between improving linear-buckling and post-buckling stiffness. Mode spacing can be achieved by introducing additional scaler multipliers in the bound-formulation as mentioned in section 3.4.2, but will result in a lower achievable maximum buckling load. It should also be kept in mind that loading into the post-buckling regime is typically permitted in aerospace applications, because the material failure limits are far from being reached, however, if the buckling load is doubled this may no longer be the case.

5.5 Concluding Remarks

An efficient design approach based on homogenous convex separable approximations for buckling of variable stiffness laminates subject to compressive loads was presented. The design problem was expressed using a separable conservative approximation scheme and the proximal point algorithm was used to ensure convergence of the in-plane parameters. Lamination parameters were used as design variables allowing stiffness and stress distributions to be determined without a priori knowledge of the laminate stacking sequence. Two example problems were studied, yielding buckling load improvements of up to 189 % with respect to the baseline quasi-isotropic laminates. Buckling load improvements of over 100% and 130% with respect to the optimal constant stiffness design were found for the two considered design problems, respectively. The stress distribution along several panel sections were presented, confirming that load redistribution is the primary mechanism responsible for improved buckling performance. A trade off between axial stiffness and buckling load was also presented. It was shown that a variable stiffness laminate with in-plane stiffness properties equivalent to a quasi-isotropic panel can be designed to withstand more than twice the compressive load before buckling.

The post-buckling behavior of several of the obtained optimal variable stiffness laminate designs was also evaluated and all designs were found to exhibit stable post-buckling behavior. The pre-buckling and post-buckling stiffnesses of each of the designs were also compared. The post-buckling stiffness of the optimal variable stiffness design for maximum buckling load was found to be 34% of its pre-buckling stiffness, while the post-buckling stiffness of a quasi-isotropic panel was found to decrease by only 50% when entering the post-buckling regime. However, several variable stiffness designs that were designed for a combination of maximum in-plane stiffness and maximum buckling were found to have superior pre-buckling and post-buckling stiffness when compared to the baseline quasi-isotropic design. Additionally, if mode-spacing were to be enforced during variable stiffness design optimization for maximum buckling, it is postulated that the initial post-buckling stiffness of the panel should improve significantly, however, it would come at the expense of a slightly lower maximum buckling load.

CHAPTER 6

Thermo-Mechanical Design of Variable Stiffness Plates

"If we all worked on the assumption that what is accepted as true is really true, there would be little hope of advance."

Orville Wright

During production, fiber-reinforced laminates are generally subject to elevated temperatures to ensure that resin curing can occur, after which they are allowed to cool to room temperature. Curing temperatures depend on the type of resin system being used and typically vary from 120°C to 180°C for thermoset resins to as high as 400°C for thermoplastic resins (Dave and Loos, 2000, Chapter 7). The longitudinal coefficient of thermal expansion (CTE) along the fiber direction, α_1, is often several orders of magnitude smaller than that of the transverse CTE, α_2. In multi-layered composites with layers oriented in different directions, this thermal mismatch may result in residual thermal stresses due to the nonuniform shrinkage of fiber and matrix materials during laminate cooling after the polymer cross-linking process.

Thermal stresses may significantly impact the buckling performance of laminated structures and has therefore been the subject of several studies in the past. Whitney and Ashton (1971) develop laminate plate equations, including the effect of expansional strains to account for hygrothermal effects. These equations are later generalized further by Flaggs and Vinson (1978). Thermal buckling and post-buckling of symmetrical laminates using a variational approach in conjunction with the Rayleigh-Ritz formulation is studied by Meyers and Hyer (1991). The authors study two different boundary conditions and the effect of altering principle material axis alignment with respect to plate boundaries. Finite element analysis including transverse shear

This chapter is based on the paper, *Thermomechanical Design Optimization of Variable Stiffness Composite Panels for Buckling* by S.T. IJsselmuiden, M.M. Abdalla, and Z.Gürdal, which appeared in the Journal of Thermal Stresses, 33(10), pages 1-16, 2010. Note: symbols may have been changed to maintain consistency throughout this thesis.

is used by Sai Ram and Sinha (1992) to investigate the effect of moisture and temperature on static instability of composite plates.

All of the aforementioned reference works focus primarily on modeling thermal effects on a single laminate. Subsequent parametric studies have been conducted for a fixed set of laminates to determine the effect of thermal loads, material properties and boundary conditions on elastic stability, however, in multi-segment and variable stiffness laminates the effect of in-plane residual stresses on buckling response are particularly relevant. An optimization strategy based on fiber angles in a multi-patch laminate to maximize buckling performance including thermal effects is presented by de Faria and Hansen (1999). Optimal designs are shown to have buckling loads twice that of designs for which residual stresses are neglected. The importance of including thermal loads when designing multi-segment composite plates and cylinders for buckling is demonstrated by Foldager et al. (2001). The authors design thermally tailored structures in a two-stage optimization process, in which the laminate is initially designed neglecting thermal effects and subsequently optimized including the residual stresses. Autio (2001) demonstrates how lamination parameters can be incorporated to design thermo-mechanically loaded plates with holes for buckling, fundamental frequency and in-plane stiffness.

Compressive load carrying capacity can be increased significantly when stiffness is allowed to vary spatially, as was shown in chapter 5, however, the importance of including thermal effects when designing variable stiffness structures should not be underestimated. Olmedo and Gürdal (1993) demonstrate that the buckling load can be increased by over 80% using linear fiber angle variation. Later Tatting and Gürdal (2002), Wu and Gürdal (2001) and Wu et al. (2002) use linear variation to design, manufacture and test variable stiffness panels. The test results yield buckling loads well in excess of those predicted by simple models and theory. Upon further investigation some of the discrepancy in predicted and experimental load carrying capacity is shown to be attributable to residual stresses present due to curing.

A simplified thermo-mechanical framework is presented by Abdalla et al. (2009b) to predict residual stress state of variable stiffness laminates. In this chapter a thermo-mechanical optimization formulation based on the aforementioned analysis framework is presented. The objective was to investigate the influence of the variation of thermal properties over the structural domain on the optimal designs and to determine how the thermal properties could be tailored to improve the buckling performance even further. The used thermo-mechanical buckling analysis formulation is presented in the following section. A conservative approximation of the buckling load, to fit the framework developed in chapter 2, was derived and is presented in section 6.2, followed by numerical results for an example problem and concluding remarks.

6.1 Thermo-Mechanical Buckling Analysis

In order to perform design optimization, a buckling analysis framework including thermal effects must be developed. This was achieved by extending the mechanical buckling analysis presented in section 5.1. The mechanical and thermal effects were assumed to be separable and thermal load variation was assumed to be constant along the panel thickness. The buckling load was determined using a finite element discretization of the linear buckling analysis through the following eigenvalue problem:

$$\left(\mathbf{K}_b - \Delta T \mathbf{K}_g^{Th} - \lambda \mathbf{K}_g^{M}\right) \cdot \mathbf{a} = \mathbf{0} \tag{6.1}$$

where $\mathbf{K}_b$ is the global bending stiffness matrix, $\mathbf{K}_g^{Th}$ and $\mathbf{K}_g^{M}$ are the global geometric stiffness matrices due to an applied unit thermal and mechanical load respectively, $\mathbf{a}$ is the mode shape comprising deformation degrees of freedom, and λ is the load multiplier or buckling factor.

Assuming that the cross-linking of the polymeric matrix takes place at cure temperature, T_c, there will be spatially distributed residual stresses in the laminate at room temperature. In addition, application of a thermal load at operating temperature, T_o, will induce thermal stresses that will reduce the effect of the cure induced stresses. Hence the total temperature change, ΔT, in equation (6.1) can be expressed as the difference between operating temperature and curing temperature:

$$\Delta T = T_o - T_c \tag{6.2}$$

The mode shapes are normalized such that:

$$\mathbf{a}^T \cdot \left(\mathbf{K}_b - \Delta T \mathbf{K}_g^{Th}\right) \cdot \mathbf{a} = 1 \tag{6.3}$$

The geometric stiffness matrix is constructed through an assembly of element geometric matrices. The geometric stiffness matrix of each element takes the form:

$$\mathbf{K}_{g_e} = -n_x \mathbf{K}^x - n_y \mathbf{K}^y - n_{xy} \mathbf{K}^{xy} \tag{6.4}$$

where $\mathbf{n}_e = (n_x,\ n_y,\ n_{xy})^T$ is the vector of in-plane stress resultants averaged over the element due to either thermal or mechanical loads, and $\mathbf{K}^x$, $\mathbf{K}^y$ and $\mathbf{K}^{xy}$ are constant matrices that depend only on element geometry.

The averaged in-plane stress resultants are no longer only a function of in-plane strains as in equation (5.4) in chapter 5, but also a function of the thermal load vector, $\mathbf{N}^{Th}$, and are expressed as:

$$\mathbf{n}_e = \mathbf{A}_e \cdot \mathbf{e}_e - \mathbf{N}_e^{Th} \tag{6.5}$$

where $\mathbf{A}$ is the in-plane stiffness matrix and $\mathbf{e}$ is the average strain vector of element e as given in equation (5.5) and is a function of the in-plane nodal displacements, which can be found from the solution of the in-plane equilibrium equations:

$$\mathbf{K}_m \cdot \mathbf{u} = \mathbf{f} + \mathbf{f}^{Th} \tag{6.6}$$

where $\mathbf{K}_m$ is the membrane stiffness matrix, $\mathbf{f}$ is the vector of in-plane loads, $\mathbf{f}^{Th}$ the total thermal load vector and $\mathbf{u}$ is the vector of in-plane displacements.

6.2 Conservative Approximation Formulation

A separable approximation of the thermo-mechanical buckling load, similar to that of the buckling load presented in chapter 5, is presented below. It was shown that, to ensure convexity of the approximation, the inverse buckling load factor, $r_b = 1/\lambda$, must be expanded linearly in terms of laminate in-plane stiffness and reciprocally with respect to laminate bending stiffness. This is because the terms in the buckling eigenvalue problem related to the geometric stiffness matrix, which depend on in-plane stiffness terms in the case of a plate, and cannot be guaranteed to be convex if they are expanded reciprocally. The reciprocal terms, related to the material stiffness matrix, are convex and expanding the geometric terms linearly guarantees the approximation as a whole to be convex.

Applying the same methodology to the buckling expression developed in section 6.1, the inverse buckling load factor can be expressed as:

$$r_b^{Th} \approx \sum_{i=1}^{N} \left(\boldsymbol{\Psi}_i^m : \mathbf{A}_i + \boldsymbol{\Phi}_i^b : \mathbf{D}_i^{-1} + \boldsymbol{\Omega}_i \cdot \mathbf{N}_i^{Th} \right) \tag{6.7}$$

where $\boldsymbol{\Psi}^m$ and $\boldsymbol{\Phi}^b$ are the sensitivity tensors with respect to the in-plane laminate stiffness, $\mathbf{A}_i$, and the inverse laminate bending stiffness, $\mathbf{D}_i^{-1}$, respectively, and $\boldsymbol{\Omega}_i$ is the sensitivity with respect to the thermal stress resultants, $\mathbf{N}^{Th}$, which are a function of the in-plane lamination parameters as shown in subsection 2.3.3. The approximation above differs with respect to the approximation developed for plate buckling, equation (5.11), in two respects; one, the in-plane sensitivity matrix, $\boldsymbol{\Psi}^m$, contains an additional contribution from the geometric stiffness associated with the thermal stresses. Two, an additional linear term, $\boldsymbol{\Omega} \cdot \mathbf{N}^{Th}$, is required to account for the total thermal load vector present in equation (6.6). A detailed derivation of the sensitivities is included in Appendix C.3.

Equation (6.7) is also separable and hence the global optimization problem can again be posed as N individual minimization problems:

$$\min_{\mathbf{V}_i} \left(\boldsymbol{\Psi}_i^m : \mathbf{A}_i + \boldsymbol{\Phi}_i^b : \mathbf{D}_i^{-1} + \boldsymbol{\Omega}_i \cdot \mathbf{N}_i^{Th} \right) \tag{6.8}$$

where $\mathbf{V}_i$ is a vector of lamination parameters associated with the i^{th} design region subject to the the feasible region constraints for the lamination parameters, and where $i = 1 \ldots N$, are the number of regions in which the structure is discretized. For the most general case, different stiffness properties are assigned to each node.

The multi-modal nature of the buckling problem necessitates the use of a dual method with bound formulation, as presented in section 3.4.2. Additionally, the proximal point algorithm, following Rockafellar (1976), was implemented to ensure convergence while retaining a separable approximation, as presented in section 3.3.1.

6.3 Numerical Results

In order to demonstrate the influence of pre-buckling stresses due to thermal loads on the buckling performance and on the stiffness distribution of an optimum variable stiffness laminate, a previously treated example problem was revisited, see section 5.4.1. The design objective was to obtain the maximum buckling load for a simply supported panel under uniaxial compression, shown in Figure 6.1. Straight edge conditions in the plane of the plate were imposed both when applying thermal and mechanical loads. No restraining forces were applied when computing the thermal stresses, i.e. the edges were free to expand or contract while maintaining straight edge condition. A square configuration ($a/b = 1$) was investigated with side lengths

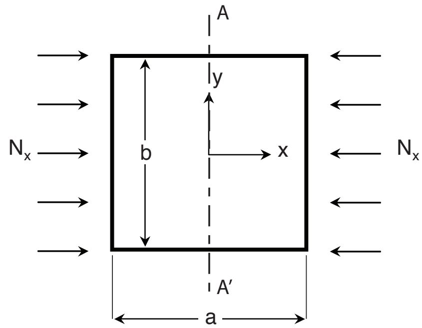

Figure 6.1: *Geometry and loading of a simply supported plate, with enforced straight edges*

of 15 inch (381 mm) and a 0.06 inch (1.524 mm) thick laminate based on a carbon-epoxy T300/5208, as listed in Appendix A.

A finite element model was created using four noded rectangular plate elements with bilinear in-plane displacements and Kirchhoff bending elements. The plate was discretized using a mesh of 20 by 20 equally spaced elements for which the individual element stiffness properties were computed from the four nodal values of the in-plane and out-of-plane lamination parameters, resulting in a total of 1764 design variables.

In order to investigate the influence of a temperature difference on the optimum stiffness distribution and buckling performance, the approximation developed in section 6.2 was incorporated into the optimization framework outlined in chapter 2. This was subsequently used to compute the optimal stiffness distributions for three cases of a plate with the following design temperature differences, ΔT_d:

- Case I: $\Delta T_d = T_d - T_c = 0°\text{C}$
- Case II: $\Delta T_d = T_d - T_c = -100°\text{C}$
- Case III: $\Delta T_d = T_d - T_c = -200°\text{C}$

where ΔT_d represents a chosen design value of ΔT in equation (6.2) and T_d is the nominal design operating temperature. Case I can be interpreted as an optimal design for which stresses due to thermal loads are neglected during optimization or as an optimal design for a laminate with identical operating and curing temperatures. Cases II and III can be thought of as optimal designs that account for thermal stresses due to a temperature difference of 100°C and 200°C, respectively, or as the optimal designs for laminates with nominal operating temperatures that are 100°C and 200°C below the curing temperature, respectively. The obtained results were also compared to a baseline quasi-isotropic plate, the optimum constant stiffness plate, $[\pm 45_n]_s$, and the optimum solution found using linear variation given in Olmedo and Gürdal (1993), all of which did not account for thermal stresses during design optimization.

In the following subsection the buckling performance of the three previously obtained optimal designs are compared for a range of operating temperatures, which differ from their nominal design operating temperature. Subsequently the mechanical and thermal stress distributions of the optimal laminate designs are studied followed by a discussion of the several buckling mode shapes.

6.3.1 Buckling Loads

The developed design optimization framework was used to determine the optimal stiffness distributions for each of the three presented design cases. To assess the influence of including thermal stresses in the design optimization process on panel buckling performance, the mechanical buckling load, λ, of the obtained optimal designs were compared for a range of applied thermal loads, ΔT_s. Assuming that the curing temperature, T_c, for all laminates is identical, it is possible to compare the buckling performance of the optimal designs relative to their nominal design temperature, i.e. comparing $\lambda(\Delta T_d + \Delta T_s)$ for each design. Similarly, it interesting to compare the buckling performance of the different designs relative to a thermal stress-free state, i.e. comparing $\lambda(\Delta T_s)$ for each design.

For explanation purposes it is useful to present the results using both aforementioned temperature scales. The first, $\lambda(\Delta T_d + \Delta T_s)$, represents the buckling load of the laminate if it were to be perturbed by a temperature difference, ΔT_s, relative to its design operating temperature. The corresponding results are presented in Figure 6.2(a), and highlight the improvement in buckling load due to both an improved laminate stiffness distribution and the residual thermal stresses present due to the difference between curing and operating temperature. The second temperature scale, ΔT_s, allows the influence of the design temperature difference, ΔT_d, on the optimal stiffness distribution, $\mathbf{V}^*$, to be isolated as the thermal stresses present due to the design temperature difference, which are different for the three cases, are neglected. The corresponding results are presented in Figure 6.2(b), and highlight the improvement in buckling loads solely due to a change in laminate stiffness distribution. Essentially the two figures differ only by a temperature shift corresponding to the design temperature difference ΔT_d of a given case.

Several interesting trends are immediately clear from Figure 6.2(a). One, laminates for which the value of the design temperature difference, ΔT_d, was more negative have higher maximum buckling loads. Two, the temperature range over which a design exhibits good buckling behavior increases when the design temperature difference value decreases. For example, the range of temperatures for which case III has a normalized buckling load above 4 is $\Delta T_d + \Delta T_s \in [-380, 180]$°C. This is considerably larger than the equivalent temperature ranges for case II and case I, which are $[-270, 100]$°C and $[-180, 0]$°C respectively. Three, the maximum buckling load for a given design occurs at a temperature below the predefined design temperature, hence residual stresses introduced by the temperature difference still have a beneficial effect for a certain range below the design temperature. This effect is also present in the experimental results presented by Tatting and Gürdal (2002) for the design using linear fiber angle variation (LV), where buckling loads are found to be higher than those determined numerically, as is later confirmed by Abdalla et al. (2009b). This can also be deduced from Figure 6.2(a), during design the presence of thermal stresses were neglected, hence, the design temperature for linear variation was $\Delta T_d = 0$°C or $T_d = T_c$, resulting in a normalized buckling load of 2.93 being predicted. Testing was subsequently conducted at room temperature, which is approximately 100°C below curing temperature, corresponding to $\Delta T_s = -100$°C, resulting in a buckling load of 4.39. It is also interesting to note that the overall buckling performance of the linear variation design and case I, both of which neglected thermal stresses during design, are similar.

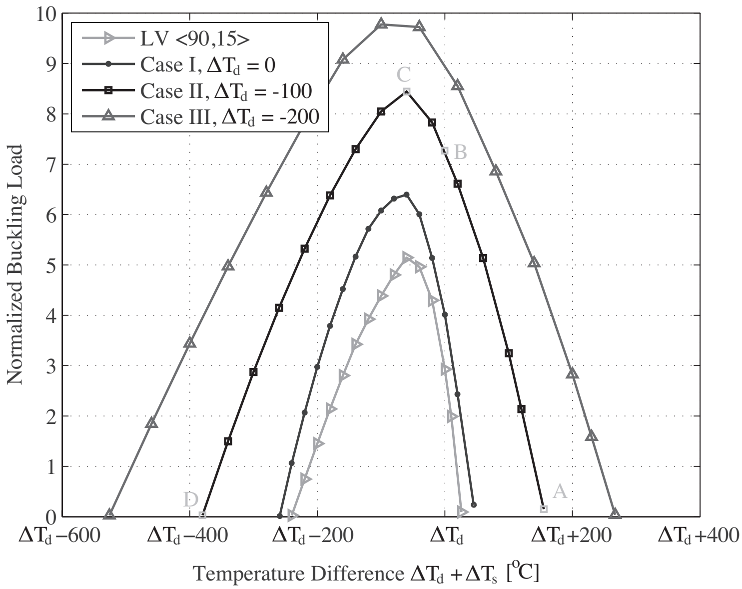

(a) Laminate buckling performance relative to their respective design temperature difference

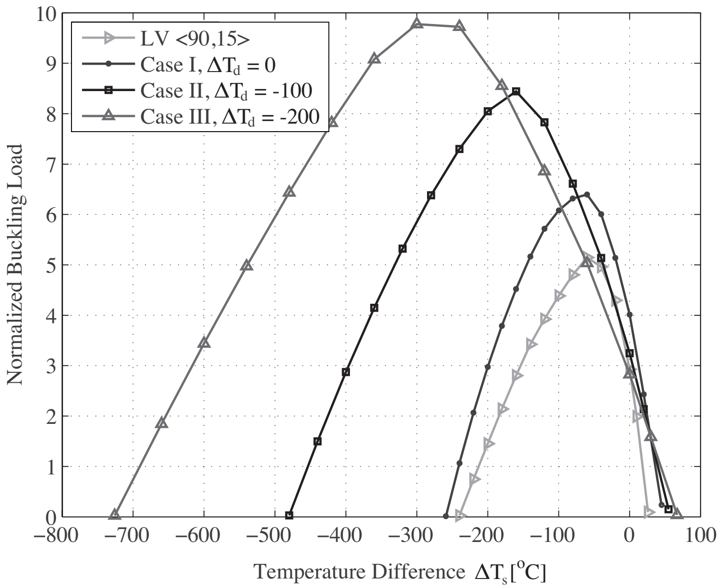

(b) Laminate buckling performance relative to a thermal stress-free state

Figure 6.2: *Comparison of normalized buckling load versus temperature difference for several design cases, buckling loads were normalized such that* $\tilde{\lambda}_{cr} = \lambda_{cr} a^2 / E_1 h^3$ *and LV* $< 90, 15 >$ *is the optimum solution found by Olmedo and Gürdal (1993) using linear fiber angle variation*

To quantify the improvement in buckling performance solely due to a change in laminate stiffness distribution, it is useful to consider Figure 6.2(b), where designs are compared relative to a thermal stress-free configuration. At $\Delta T_s = 0$, case I has the highest buckling load, since this corresponds to its design temperature, $\Delta T_s = \Delta T_d$. The same is true for case II at $\Delta T_s = -100$ and for case III at $\Delta T_s = -200$. The corresponding values of the buckling load are listed in Table 6.1. Results for cases I, II and III were compared to a quasi-isotropic laminate, the constant stiffness optimum, $[\pm 45]_s$, and the best solution found by Olmedo and Gürdal (1993) using linear variation, $< 90, 15 >$[1]. The constant stiffness designs remained unaffected by the temperature change for this problem, as the edges remained free to expand and contract. At $\Delta T_s = 0$, case I had a buckling load 20% higher than case II and 35% higher than case III, however, at $\Delta T_s = -200$, case III had a buckling load three times higher than case I and in excess of six and a half times higher than that of the quasi-isotropic plate.

Table 6.1: *Comparison of normalized buckling load versus temperature difference relative to a thermal stress-free state for several design cases and correspond to Figure 6.2(b), buckling loads were normalized such that* $\tilde{\lambda}_{cr} = \lambda_{cr} a^2 / E_1 h^3$

Design	**Temperature Change**[†] ΔT_s		
	0°C	−100°C	−200°C
Quasi-Isotropic, $\mathbf{V} = \mathbf{0}$	1.3842	1.3842	1.3842
$[\pm 45_n]_s$	1.7424	1.7424	1.7424
Linear Variation, $< 90, 15 >$	2.9282	4.3855	1.4518
Case I, $\Delta T_d = 0$°C	4.0157	6.0802	2.9758
Case II, $\Delta T_d = -100$°C	3.2468	7.2615	8.0472
Case III, $\Delta T_d = -200$°C	2.5481	6.2637	9.0829

† Relative to a thermal stress-free configuration

6.3.2 In-Plane Stress Distribution

To understand the mechanism(s) behind improved buckling loads it is useful to study the stress distributions present in the different designs due to mechanical or thermal loads. The axial stress resultant, n_x, due to a unit negative temperature change and a unit compressive load, respectively, is plotted in Figure 6.3(a) and 6.3(b) along section A-A' in Figure 6.1. Section A-A' divides the plate along its center perpendicular to the load direction. Inspecting Figure 6.3(a), it can be seen that a negative thermal load results in compressive stresses at the edge and tensile stresses at the center of the plate even though no mechanical loads are applied. Additionally Figure 6.3(b) shows that, for all the designs, the edges are responsible for carrying the majority of the compressive loads. Load redistribution was shown to be the primary mechanism behind improved buckling performance of variable stiffness laminates in chapter 5. The onset of global buckling for all designs is therefore delayed due to the loads being

[1] This notation follows the convention presented by Olmedo and Gürdal (1993), and corresponds to a laminate with fiber angles varying linearly from 90° at the center to 15° at the edges

directed to the panel's edges and due to the favorable stress distribution caused by thermal loading even if thermal effects were not considered during optimization. For cases II and III, where thermal effects were considered during design, the central section is stiffer and carries more compressive load. This seems to contradict the aforementioned notion of distributing the compressive loads to the edges, however, due to the compressive stresses present at the edges, global panel buckling is no longer the only buckling mode to be considered, as local edge buckling can also start to occur, as will be seen by inspecting the mode shapes in the following section. Hence, for cases II and III the compressive loads at the edges are relieved slightly, which must be compensated for by the central section. Therefore, a more intricate axial stress distribution profile is present when thermal stresses are taken into account.

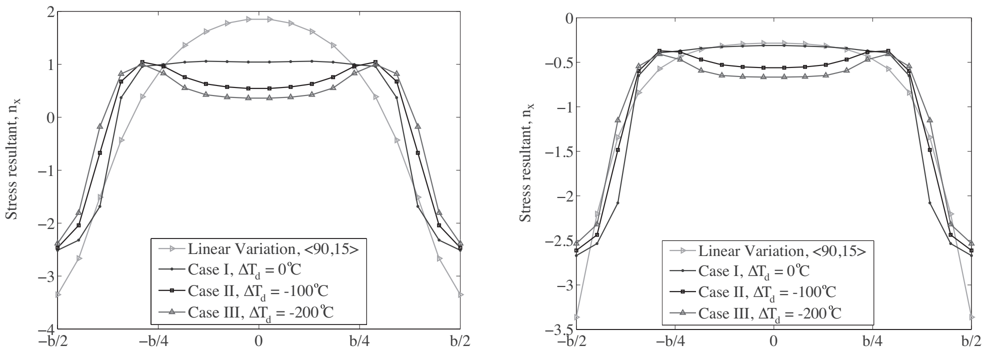

(a) Unit negative thermal load (b) Unit compressive load

Figure 6.3: *In-plane stress resultant in the x-direction, n_x, for an applied unit thermal or compressive load, plotted along section A-A', see Figure 6.1 for section definition*

6.3.3 Buckling Modes

It is also interesting to investigate the influence of thermal stresses on the critical buckling mode shapes. The mode shapes at four points along the curve presented in Figure 6.2(a) are plotted for case II in Figure 6.4. All the designs in Figure 6.2 have two points at which the normalized buckling load becomes zero, for case II these are points A and D and correspond to the temperature differences at which thermal buckling occurs, in other words, the panel buckles without the application of mechanical load. The buckling mode shapes are also plotted at the design operating temperature, point B, and at the maximum buckling load, point C, for case II.

Point A is the thermal buckling mode due a positive temperature differential with respect to the design operating temperature, $\Delta T_d + \Delta T_s = 158°\text{C}$. The mode shape, a single half-wave, can be understood by referring to Figure 6.3(a). If a negative thermal load is applied, tensile stresses occur at the center and compressive stresses occur at the edge of the panel. The opposite occurs when a positive thermal load is applied, causing compressive stresses at the panel center resulting in the presented mode shape. Point D, shown in Figure 6.4(d), represents the thermal buckling load due to a negative temperature difference with respect to the design operating temperature, $\Delta T_d + \Delta T_s = -381°\mathrm{C}$. The compressive loads which occur at the edges due to the negative thermal load result in edge buckling, with two half-waves along top and bottom panel edges. The mode shape shown in Figure 6.4(b) corresponds to design temperature for case II, $\Delta T_d + \Delta T_s = 0°\mathrm{C}$ and consists of two half-waves spanning the entire length of the panel. The maximum buckling load for this panel is found at point C. The corresponding mode shape is presented in Figure 6.4(c) and seems to be a combination of two global half-waves and two half-waves along the edge, which is a combination of the mode shapes found for point B and D.

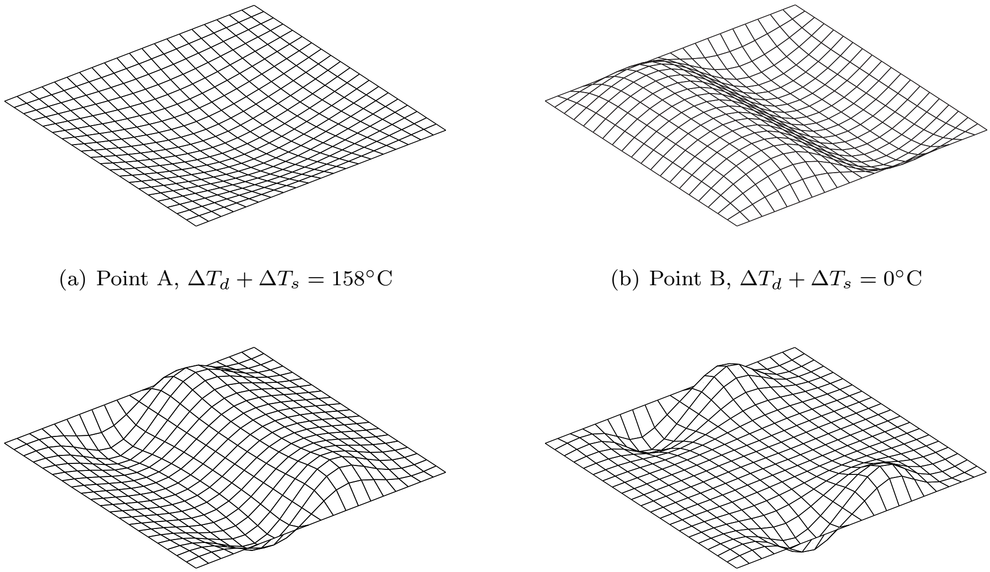

(a) Point A, $\Delta T_d + \Delta T_s = 158°\mathrm{C}$

(b) Point B, $\Delta T_d + \Delta T_s = 0°\mathrm{C}$

(c) Point C, $\Delta T_d + \Delta T_s = -60°\mathrm{C}$

(d) Point D, $\Delta T_d + \Delta T_s = -381°\mathrm{C}$

Figure 6.4: *Critical buckling mode shapes plotted for several different applied temperature differences for case II, corresponding to points presented in Figure 6.2(a)*

Both the numerical results presented here, and experimental results presented by Tatting and Gürdal (2002), have shown that residual stresses due to curing beneficially influence the buckling performance of variable stiffness plates. The general mechanism believed to be responsible for this trend can best be deduced from Figure 6.3. From a mechanical point of view, buckling performance improves primarily due to load redistribution. This results in stiffer sections which carry the compressive loads and compliant sections that carry a small fraction of the load. In general, composite materials have small or negative coefficients of thermal expansion in the axial direction and large coefficients of thermal expansion in the transverse direction. Therefore, when laminates are cured above their operating temperature, i.e. $\Delta T < 0$, will result in compliant regions shrinking more than the stiffer regions. Hence, the net residual stresses in compliant regions will be tensile while stiffer regions will contain compressive stresses, resulting in improved buckling performance.

It is clear from the aforementioned discussions that correctly tailoring laminate stiffness and thermal properties in the laminate allows for significant improvements in buckling performance, however, it is also clear that designing for the correct temperature regime is crucial for variable stiffness laminates.

6.4 Concluding Remarks

A method of including thermal loads into an optimization framework for variable stiffness panels was presented. Expressing designs in terms of lamination parameters made it possible to find the most generalized solution without a priori knowledge of laminate stacking sequences. The numerical results confirmed the importance of including thermal effects in the design of variable stiffness panels for buckling, since the pre-buckling stress state significantly influenced a panel's buckling behavior. Improvements in ultimate panel buckling loads in the order of four to six times that of the corresponding quasi-isotropic panel were demonstrated. Three different temperature differences, $\Delta T_d = 0°\text{C}$, $-100°\text{C}$ and $-200°\text{C}$, respectively, were studied. The temperature difference essentially represents the difference between curing temperature and operating temperature of the laminate. The buckling load of the optimal variable stiffness laminate including residual thermal stresses for $\Delta T_d = -200°\text{C}$ was found to be 550 % higher than a quasi-isotropic laminate, 420% higher than the optimum constant stiffness laminate and 205% higher than the optimum variable stiffness laminate neglecting residual thermal stresses. The range of operating temperatures over which a panel exhibited good buckling behavior was shown to increase significantly when including thermal effects in the design process.

It is important to remember that thermal effects are strongly dependent on laminate thickness, hence the results presented in this chapter hold for panels with similar thickness to side-length ratios. Both the behavior and the sensitivity of variable stiffness designs may change significantly for different laminate configurations. In the future a more exhaustive study of thermal effects for various structural configurations should be conducted. It would also be interesting to study the influence of material thermal and stiffness properties, and their interdependence, on the optimum solution.

CHAPTER 7

Design of Variable Stiffness Plates with Thickness Variation

"*There is no top. There are always further heights to reach.*"

Jascha Heifetz

Advanced fiber placement machines allow courses to be steered while individual tows are cut and restart on-the-fly, hence both the local fiber angle orientation and laminate thickness can be controlled and considered to vary continuously within a laminate. The buckling load of a plate is a function of both the laminate in-plane stiffness distribution and the bending stiffness distribution, which are linear and cubic functions of the local laminate thickness respectively. It is therefore interesting to investigate the influence of laminate thickness distribution, in addition to stiffness distribution, on the buckling load and to identify the structural mechanisms resulting in improved load carrying capacity.

In a parametric study, Biggers and Srinivasan (1993) demonstrate that the buckling load of a uniaxially loaded quasi-isotropic composite panel can be increased by removing stiff 0°, fibers from the center of the plate and placing them near the plate boundaries. In another publication Biggers and Pageau (1993) demonstrate how a similar approach can be used to improve shear-buckling of a panel by distributing the ±45° to form multiple reinforcing laminate sections. In a later work, Joshi and Biggers (1996) use the method of feasible directions to determine optimal continuous thickness distributions for isotropic and anisotropic plates to maximize panel buckling loads. Kassapoglou (2008) develop a Rayleigh-Ritz based analysis approach to compute the buckling load of laminated panels with two concentric layups. Presented

This chapter is based on the paper, *Thickness tailoring of variable stiffness panels for maximum buckling load* by S.T. IJsselmuiden, M.M. Abdalla, and Z.Gürdal, which was presented at the 17th International Conference on Composite Materials, 2009. Note: symbols may have been changed to maintain consistency throughout this thesis.

results show that panel buckling loads can be improved by including a central patch, locally improving the bending stiffness. Buckling load improvements in the aforementioned publications result from two fundamentally different mechanisms influencing panel buckling. Improvements demonstrated by Biggers and Srinivasan (1993) and Joshi and Biggers (1996) are attributed primarily to in-plane load redistribution while improvements presented by Kassapoglou (2008) are attributed to local improvements in panel bending stiffness, effectively suppressing the dominant buckling mode.

An approximation to design variable stiffness panels for maximum buckling load was presented in chapter 5. Significant improvements in panel buckling loads were demonstrated, which were shown to result primarily from in-plane load distribution. To study the influence of continuously varying laminate thickness on the buckling load, the previously derived approximation scheme was extended to include laminate thickness as a design variable, as shown in section 7.1. The approximation is subsequently used to optimize a previously studied example problem in section 7.2, both to demonstrate the method and to identify the mechanisms resulting in improved buckling load. Several concluding remarks are presented in section 7.3.

7.1 Conservative Approximation Formulation

A conservative separable approximation of the inverse buckling factor was derived in chapter 5. A generic method of including thickness as a design variable in the developed design optimization framework was presented in section 3.2.4. In this section a similar approximation and optimization formulation is presented, developed specifically for variable stiffness laminate buckling with thickness variation. Laminate buckling analysis was conducted as in section 5.1, by solving the eigenvalue problem:

$$\left(\mathbf{K}_b - \lambda \mathbf{K}_g\right) \cdot \mathbf{a} = \mathbf{0}$$

where $\mathbf{K}_b$ is the global bending stiffness matrix and is a function of the element bending stiffness matrices, $\mathbf{D}_e$, the global geometric stiffness matrix, $\mathbf{K}_g$, is an implicit function of the in-plane stiffness matrices, $\mathbf{A}_e$, $\mathbf{a}$ is the mode shape comprising deformation degrees of freedom, and λ is the buckling factor.

The goal is to design the thickness and lamination parameter distribution such that the buckling load is maximized, which can be achieved by minimizing the inverse buckling factor, $r_b = 1/\lambda$, as was done in chapter 5. The optimization problem becomes unbounded when laminate thickness is included as a design variable if the total laminate weight is not constrained. The total laminate weight can be constrained by placing an upper bound on the total volume, $\mathcal{V}_0$. The optimization problem can therefore be formulated as:

$$\min_{\mathbf{V}} r_b \qquad \text{s.t} \qquad \mathcal{V} \leq \mathcal{V}_0 \tag{7.1}$$

where $\mathbf{V}$ is a vector of all design variables including both extensional and flexural lamination parameters and laminate thickness. The lamination parameters are also bound by their feasible region, see section 2.3.4, and thickness is typically constrained with a suitable lower bound, also known as the minimum gauge thickness, h^L:

$$h^L \leq h \tag{7.2}$$

In the problem formulation in equation (7.1) it is assumed that only one eigenvalue is present during optimization, however, for multimodal problems all critical buckling modes must be incorporated during design. To address problems with multiple eigenvalues the bound formulation presented by Olhoff (1989) can be used as discussed in section 3.4.2. An independent parameter, β, is introduced such that the minimization problem becomes:

$$\min \beta \quad \text{s.t.} \quad \begin{aligned} \beta &\geq r_{bj} \\ \mathcal{V} &\leq \mathcal{V}_0 \end{aligned} \tag{7.3}$$

where r_{bj}, for $j = 1, 2, \ldots M$, are the inverse buckling factors corresponding to the first M critical buckling modes. The problem subsequently can be solved using the dual-method, see section 3.4.2, resulting in the following nested optimization problem:

$$\max_{\boldsymbol{\mu},\nu} \left(\min_{\mathbf{V}} \sum_{j=1}^{M} \mu_j r_{bj} + \nu \left(\frac{\mathcal{V}}{\mathcal{V}_0} - 1 \right) \right) \tag{7.4}$$

where $\boldsymbol{\mu}$ and ν are the Lagrange multipliers for the multiple eigenvalues and volume constraint, respectively, and are by definition positive. Additionally, the bound formulation forces the Lagrange multipliers associated with the inverse buckling factor to sum to unity.

To solve equation (7.4) using the framework developed in chapter 2 a suitable expression for both the inverse buckling factor and volume must be derived. The total volume, $\mathcal{V}$, is simply the sum of the product of thickness, h, and area, $\mathcal{A}$, of each design region, i:

$$\mathcal{V} = \sum_{i=1}^{N} \mathcal{A}_i h_i$$

The design regions can be defined at node level, element level, or span over multiple elements. In the present work, design variables were defined at nodes and element properties were computed via reciprocal interpolation, as defined in section 2.3.6. Laminate volume is therefore already a separable linear function in terms of thickness and hence requires no further approximation to be incorporated into the design framework.

It was shown in section 5.2 that, to ensure convexity of the approximation, the inverse buckling load factor, $r_b = 1/\lambda$, had to be expanded linearly in terms of laminate in-plane stiffness and reciprocally with respect to laminate bending stiffness. This is because the terms in the buckling eigenvalue problem related to the geometric stiffness matrix, which depend on in-plane stiffness terms in the case of a plate, cannot be guaranteed to be convex if they are expanded reciprocally. The reciprocal terms, related to the global bending stiffness matrix, are convex and expanding the geometric terms linearly guarantees the approximation as a whole is convex. The inverse buckling factor was therefore approximated in section 5.2 as:

$$r_b \approx r_{b0} + \sum_{i=1}^{N} \left(\left. \frac{\partial r_b}{\partial \mathbf{A}_i} \right|_0 : (\mathbf{A}_i - \mathbf{A}_{0i}) + \left. \frac{\partial r_b}{\partial \mathbf{D}_i^{-1}} \right|_0 : \left(\mathbf{D}_i^{-1} - \mathbf{D}_{0i}^{-1} \right) \right)$$

The equation above is linear in terms of in-plane stiffness, however, the optimization problem given in equation (7.4) is expressed in terms of lamination parameters and laminate thickness of each design point. The in-plane stiffness matrix is a linear function of in-plane lamination parameters and therefore, the above approximation can be used directly when laminate thickness is constant, as was done in chapter 5. If laminate thickness is introduced as a design variable, the linear in-plane stiffness terms lose their linearity in terms of the design variables and were therefore linearized as follows:

$$\left.\frac{\partial r_b}{\partial \mathbf{A}_i}\right|_0 : \mathbf{A}_i \approx \left.\frac{\partial r_b}{\partial \mathbf{A}_i}\right|_0 : \left(\hat{\mathbf{A}}_{0i} h_i + \hat{\mathbf{A}}_i h_{0i}\right) \tag{7.5}$$

where $\hat{\mathbf{A}}$ is the material dependent part of the stiffness matrix and is only a function of lamination parameters and h_i is the laminate thickness, as can be seen by referring to equation (2.16).

The buckling factor is homogenous of order one in terms of the bending stiffness and homogenous of order zero in terms of in-plane stiffness, as discussed in section 5.2. Therefore, the approximation can be expressed in the standard form as:

$$r_b = \sum_{i=1}^{N} \left(\left.\mathbf{\Psi}_i^m\right|_0 : \hat{\mathbf{A}}_i + \left.\mathbf{\Phi}_i^b\right|_0 : \mathbf{D}_i^{-1} + \left.\alpha_i\right|_0 h_i \right) + \mathcal{C}_0 \tag{7.6}$$

where the linear thickness terms are collected in α_i:

$$\alpha_i = \left.\mathbf{\Psi}_i^m\right|_0 : \hat{\mathbf{A}}_{0i} \tag{7.7}$$

The objective function and volume constraint have now been approximated in a form consistent with the framework developed in chapter 2, and can therefore be solved as before.

7.2 Numerical Results

To demonstrate the design process developed and the benefit of including laminate thickness tailoring in the design process the example problem, previously treated in chapter 5, was reevaluated for both uniaxial and biaxial compression. The two load cases are outlined in Figure 7.1 and both consist of a simply supported rectangular panel subject to a compressive edge load per unit length, N_x and/or N_y. The edges are constrained to deform uniformly and hence remain straight. A square configuration, $a/b = 1$, with edge length of 15 inch (381 mm) and a uniform initial thickness, h_0, of 0.06 inch (1.524 mm) was studied. The initial volume of the plate was used as an upper bound for the volume constraint. The used material properties for unidirectional carbon-epoxy T300/5208 are listed in Appendix A.

The plate was discretized into a selected number of equally sized four-noded rectangular elements with bilinear in-plane displacements and Kirchhoff bending elements, as discussed in Appendix B. A finite element routine programmed in Matlab$^{\mathrm{TM}}$ was used to compute the required panel buckling loads and sensitivities. The presented results were generated using a mesh consisting of 21 uniformly distributed nodes along each edge, resulting in a total of 2205 design variables, 5 for each node.

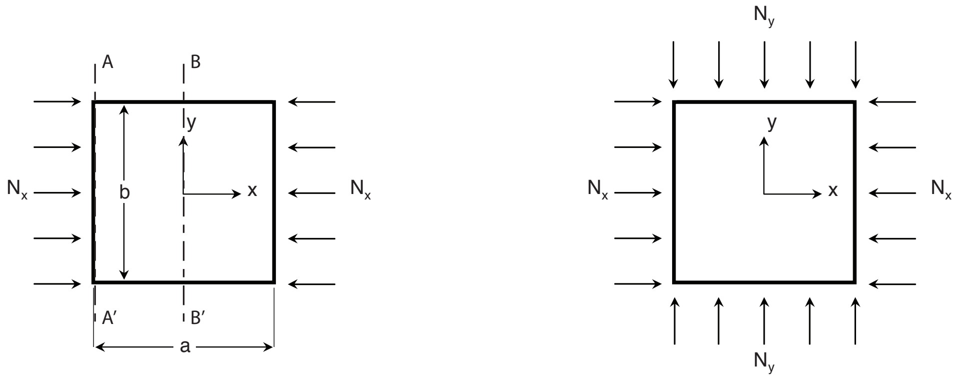

(a) Uniaxial compressive loading (b) Biaxial compressive loading

Figure 7.1: *Geometry, loading and boundary conditions for the considered panels*

The developed optimization routine was used to compute the optimal thickness and stiffness distributions using the damping strategy formulated in stiffness space, presented in section 3.3.2, to control solution convergence. The optimization problem for both load cases was solved for a range of different lower bounds on laminate thickness, $\hat{h}^L = 1.0, 0.9, \ldots 0.4$, to assess the influence of minimum gauge thickness on the optimal solution and to avoid excessive differences between maximum and minimum laminate thickness.

7.2.1 Uniaxial Compression

The first four buckling loads, minimum laminate thickness and maximum laminate thickness for the obtained optimal designs are presented Table 7.1. Buckling loads were all normalized with the critical buckling load of an equivalent quasi-isotropic laminate with uniform thickness. The buckling loads for the optimal constant stiffness laminate with uniform thickness, $[\pm 45_n]_s$, is also presented for comparison.

The optimal variable stiffness design with uniform thickness, $\hat{h}^L = 1.0$, is identical to the solution found in chapter 5, and resulted in a buckling load improvement in the order of 190% with respect to the quasi-isotropic design. The remaining results demonstrate that tailoring both stiffness and thickness dramatically improves the buckling performance of a plate. Improvements in the order of 270 to 500% were achieved when tailoring both laminate stiffness and thickness, compared to 190% when only laminate stiffness properties were tailored.

Several interesting trends can be identified from the tabulated results. The mode spacing tends to decrease as the bound on minimum thickness decreases, λ_4 is approximately twice as large as λ_1 for the optimal variable stiffness design with uniform laminate thickness whereas these two modes differ by only 13% when the lower bound on thickness is 0.4. Therefore, higher buckling loads are achievable by increasing the design freedom, however, as a consequence more modes tend to become active during the optimization process. The remaining trends are best identified when visualized.

Table 7.1: *Normalized buckling loads for a range of laminate designs for the uniaxial load case, with $\hat{\lambda} = \lambda/\lambda_{cr}^{QI}$, $\hat{h} = h/h_0$ and h^L the lower bound on thickness*

Design	$\hat{h}_{min}$	$\hat{h}_{max}$	$\hat{\lambda}_1$	$\hat{\lambda}_2$	$\hat{\lambda}_3$	$\hat{\lambda}_4$
Quasi Isotropic	1.000	1.000	1.000	1.560	2.772	3.969
Constant Stiffness $[\pm 45_n]_s$	1.000	1.000	1.259	1.673	2.571	3.855
Variable Stiffness, $\hat{h}^L = 1.0$	1.000	1.000	2.888	2.891	3.778	5.293
Variable Stiffness, $\hat{h}^L = 0.9$	0.900	1.826	3.711	3.723	4.641	6.348
Variable Stiffness, $\hat{h}^L = 0.8$	0.800	2.063	4.184	4.196	4.990	6.550
Variable Stiffness, $\hat{h}^L = 0.7$	0.700	2.197	4.559	4.572	5.305	6.632
Variable Stiffness, $\hat{h}^L = 0.6$	0.600	2.303	5.231	5.377	5.873	6.801
Variable Stiffness, $\hat{h}^L = 0.5$	0.500	2.356	5.655	5.668	6.160	6.859
Variable Stiffness, $\hat{h}^L = 0.4$	0.400	2.411	6.060	6.063	6.301	6.860

The critical buckling load multiplier, $\hat{\lambda}_1$, and the minimum and maximum thickness ratios, $\hat{h}_{min}$ and $\hat{h}_{max}$, respectively, are plotted against the applied lower bound on thickness, $\hat{h}^L$, for both the uniaxial and biaxial load cases in Figure 7.2. As the lower bound on thickness decreases for the uniaxial load case the critical buckling load increases almost linearly for the considered range, as can be seen in Figure 7.2(a). For the uniaxial load case the minimum thickness always reaches the set lower bound whereas the maximum thickness ratio tends towards an asymptote, see Figure 7.2(b).

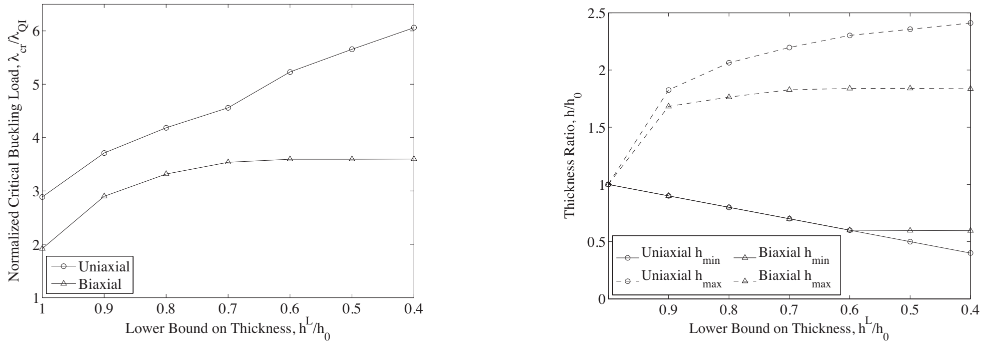

(a) Normalized buckling loads

(b) Normalized thicknesses

Figure 7.2: *Comparison of the trends in critical buckling load, minimum and maximum thickness for different bounds on minimum thickness for the uniaxial and biaxial load cases*

The optimal lamination parameter and thickness distribution for designs with $\hat{h}^L = 0.9$ and $\hat{h}^L = 0.4$ are presented in Figure 7.4 and Figure 7.5, respectively. The general trends in lamination parameter distributions for both designs are similar and also correspond to the optimal lamination parameter distribution of the uniform thickness laminate found in chapter 5, see Figure 5.5, page 101. As discussed in chapter 5, the optimal stiffness distribution results in the compressive loads being transferred primarily to the edge of the panel, while the complaint region in the center only carries a small portion of the compressive load. The thickness distribution, see Figure 7.4(e) and 7.5(e), also results in the majority of the compressive loads being transferred to the panel's edge, since the thickness reduces primarily in the central section of the panel and builds-up towards the edges. This trend also supports the effectiveness of the design strategy demonstrated by Biggers and Srinivasan (1993), where the axially stiff 0° layers are distributed to the panels edge, effectively increasing both the panels edge stiffness and thickness, while reducing the central panel stiffness and thickness. Investigating the laminate thickness distribution in more detail, the largest thickness buildup is found towards the corners and the central edge sections. The thickness distribution for the design with $\hat{h}^L = 0.9$ is less intricate than when $\hat{h}^L = 0.4$. The minimum thickness for both panels is found at the center of the panel, however, for the former the thickness buildup only occurs at the edges whereas for the later there are also sections of slight thickness buildup at $\frac{1}{4}$ and $\frac{3}{4}$ length of the panel, locally increasing bending stiffness aiding to suppress the two half-waves present in mode 1, as will be discussed later with reference to Figure 7.7(d).

To highlight the effect of the obtained laminate thickness distribution on the in-plane loads within the panel, the in-plane stress resultants in the x-direction, n_x, along section A-A' and B-B' are plotted in Figure 7.3. The stress resultants for the variable stiffness designs with uniform thickness, $\hat{h}^L = 1.0$, and variable thickness designs with $\hat{h}^L = 0.9$ and $\hat{h}^L = 0.4$ are presented in the figure. The values were normalized such that the average compressive load per unit length was equal to unity, hence regions for which $\hat{n}_x > -1$ carry less load than an equivalent constant stiffness panel while regions for which $\hat{n}_x < -1$ carry more compressive load than an equivalent constant stiffness panel. The in-plane stiffness variation results in the majority of the compressive load being carried by the panel edges while the central section remains relatively unloaded, as was discussed in chapter 5. The introduction of thickness variation further strengthens the load redistribution effect, resulting in a fourfold increase in the compressive loads present along the edges while the central section transmits less than 20% of the nominal compressive load.

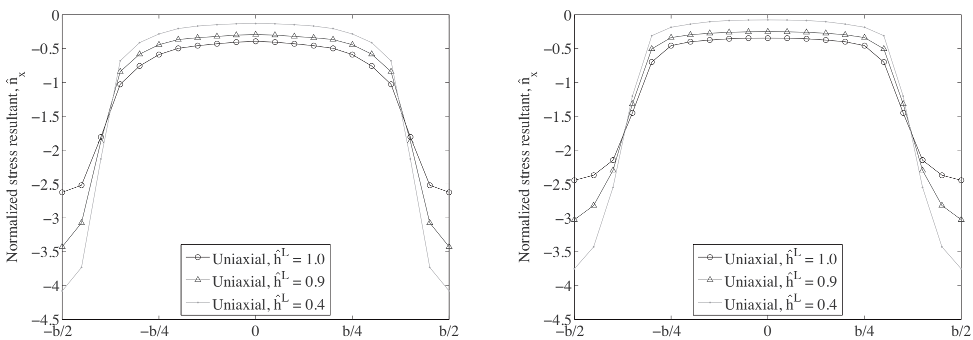

(a) $\hat{n}_x$ along section A-A'   (b) $\hat{n}_x$ along section B-B'

Figure 7.3: *Normalized in-plane stress resultant in the x-direction, $\hat{n}_x$, plotted along the panel width for the uniaxial load case, see Figure 7.1 for section definition*

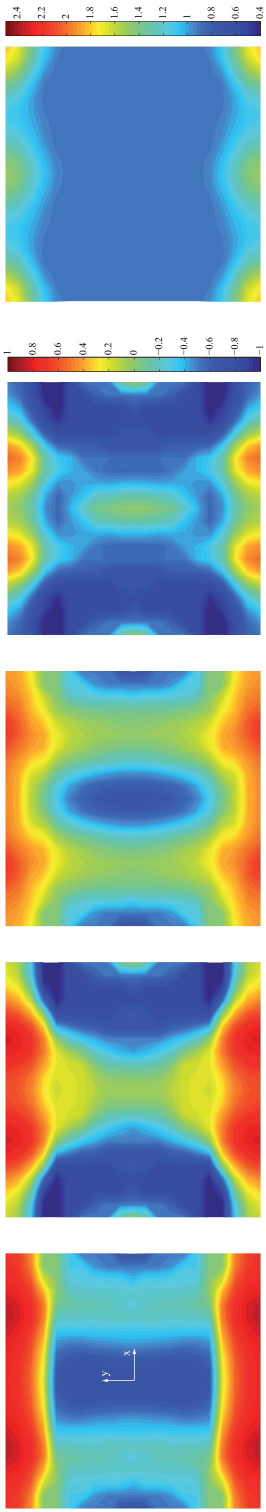

(a) V_{1A} (b) V_{3A} (c) V_{1D} (d) V_{3D} (e) $\hat{h}$

Figure 7.4: *Optimal lamination parameter and thickness distribution for the uniaxially loaded variable stiffness laminate with* $\hat{h}^L = 0.9$

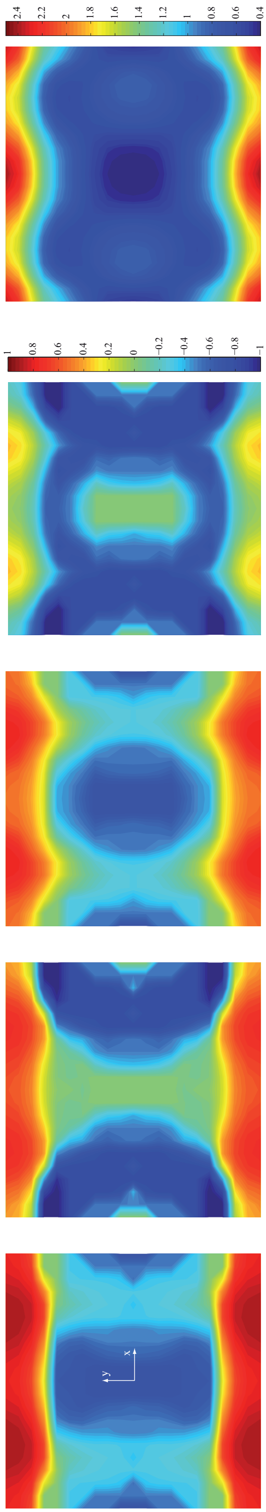

(a) V_{1A} (b) V_{3A} (c) V_{1D} (d) V_{3D} (e) $\hat{h}$

Figure 7.5: *Optimal lamination parameter and thickness distribution for the uniaxially loaded variable stiffness laminate with* $\hat{h}^L = 0.4$

It was also interesting to investigate the effect of thickness and stiffness tailoring on the panel buckling modes. The first four buckling modes for the optimal designs with $\hat{h}^L = 0.9$ and $\hat{h}^L = 0.4$ are presented in Figures 7.6 and 7.7, respectively. The first noticeable difference is that the half-waves present in Figure 7.6 span the entire panel width whereas the buckling waves tend to be more central in Figure 7.7, hence, the optimal thickness distribution tends to force modes to localize towards the center of the panel. The first two mode shapes for both designs are asymmetric while modes three and four are both symmetric. The first and second modes for the design with $\hat{h}^L = 0.9$ consist of two asymmetric half-waves and a single asymmetric half-wave, respectively, as can be seen in Figures 7.6(a) and 7.6(a). The first and second modes for the design with $\hat{h}^L = 0.4$ consist of two asymmetric half-waves and a three asymmetric half-waves respectively, as can be seen in Figure 7.7(a) and 7.7(a). Modes three and four are similar for both designs and consist of two and four symmetric half-waves, respectively.

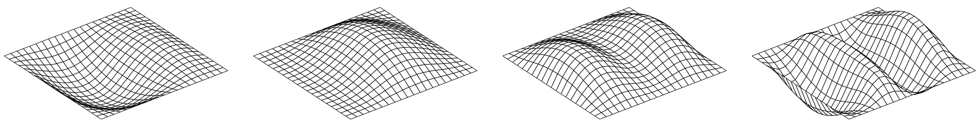

(a) Mode 1 (b) Mode 2 (c) Mode 3 (d) Mode 4

Figure 7.6: *First four buckling modes for* $\hat{h}^L = 0.9$

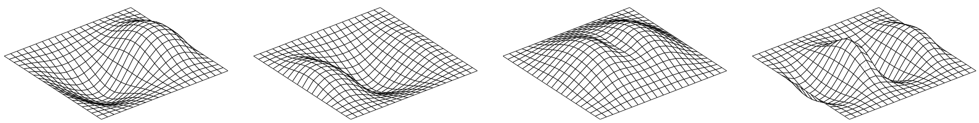

(a) Mode 1 (b) Mode 2 (c) Mode 3 (d) Mode 4

Figure 7.7: *First four buckling modes for* $\hat{h}^L = 0.4$

7.2.2 Biaxial Compression

A similar set of optimal designs was generated for a biaxially loaded panel, with $N_x = N_y$, allowing both laminate thickness and stiffness variation. Once again the buckling loads were normalized with the critical buckling load of an equivalent quasi-isotropic laminate with uniform thickness and are presented in Table 7.2. The optimal constant stiffness laminate with uniform thickness, $[\pm 45_n]_s$, is also presented for comparison.

The buckling load of the optimal variable stiffness laminate with uniform thickness is 90% higher than the quasi-isotropic base line. The buckling load improves to 260% of the quasi-isotropic value when thickness tailoring is also included, which once again is a significant improvement with respect to only allowing laminate stiffness tailoring. Similar trends to those of the uniaxial example are seen with respect to decreasing mode spacing as the minimum gauge thickness is decreased. The fourth mode, λ_4, is

Table 7.2: *Normalized buckling loads for a range of laminate designs for the biaxial load case, with* $\hat{\lambda} = \lambda/\lambda_{cr}^{QI}$*,* $\hat{h} = h/h_0$ *and* h^L *the lower bound on thickness*

Design	$\hat{h}_{min}$	$\hat{h}_{max}$	$\hat{\lambda}_1$	$\hat{\lambda}_2$	$\hat{\lambda}_3$	$\hat{\lambda}_4$
Quasi Isotropic	1.000	1.000	1.000	2.496	2.496	3.969
Constant Stiffness $[\pm 45_n]_s$	1.000	1.000	1.259	2.677	2.677	4.628
Variable Stiffness, $\hat{h}$=1.0	1.000	1.000	1.919	2.962	2.962	3.874
Variable Stiffness, $\hat{h}$=0.9	0.900	1.682	2.899	3.316	3.316	4.283
Variable Stiffness, $\hat{h}$=0.8	0.800	1.763	3.317	3.524	3.524	4.233
Variable Stiffness, $\hat{h}$=0.7	0.700	1.827	3.537	3.564	3.595	4.166
Variable Stiffness, $\hat{h}$=0.6	0.600	1.839	3.594	3.619	3.625	4.145
Variable Stiffness, $\hat{h}$=0.5	0.597	1.840	3.595	3.618	3.621	4.134
Variable Stiffness, $\hat{h}$=0.4	0.596	1.836	3.599	3.616	3.618	4.132

twice as large as λ_1 for the uniform thickness design whereas these two modes differ by only 15% when the lower bound on thickness is 0.4. Due to symmetry of the biaxial loading problem λ_2 and λ_3 are practically identical in all cases.

The trends relating both to laminate thickness and maximum buckling load were found to differ with respect to the uniaxial load case, as can be seen in Figure 7.2 presented earlier on page 124. The maximum buckling load reaches an asymptote, and only improves marginally as the lower bound on thickness is decreased below 0.7. As opposed to the uniaxial load case, the normalized minimum thickness, $\hat{h}_{min}$, does not reduce far beyond 0.6, even when the lower bound on thickness is decreased further while the maximum thickness, $\hat{h}_{max}$, also reaches an asymptote.

The optimal lamination parameter and thickness distributions for designs with $\hat{h}^L = 0.9$ and $\hat{h}^L = 0.4$ are presented in Figures 7.8 and 7.9, respectively. The lamination parameter distributions for both designs are essentially identical other than a slight difference between the $V_{3\mathbf{D}}$ distributions. The effect of stiffness and thickness tailoring were almost independent for this load case. The lamination parameter distribution is quarter-symmetric corresponding to the problem symmetry, however, it remains quite intricate and difficult to interpret. The in-plane lamination parameters in Figure 7.8(a) and 7.8(b) indicate that the fibers tend to be perpendicular to the load towards the middle of each edge, i.e. 90° at the left and right edges while they tend to 0° at the top and bottom edges. In all of the corners the fiber angles tend towards ±45°. The mechanical effect of the obtained stiffness distribution is best interpreted by inspecting the in-plane stress resultants, as will be discussed later.

The thickness distribution for both designs with $\hat{h}^L = 0.9$ and $\hat{h}^L = 0.4$ is presented in Figures 7.8(e) and 7.9(e), respectively. The maximum thickness buildup was found to occur in the corners for both cases while the thickness in the central sections tended towards the lower bound. Unlike the uniaxial load case, the thickness buildup in the corners for the biaxial case are attributed primarily to improved bending stiffness, which is aimed at suppressing the buckling modes as will be seen later, and not to load redistribution as found for the uniaxial case. Similarly, the slight thickness buildup found around the central section of the panel in Figure 7.9(e) results in locally improved bending stiffness, suppressing the relevant buckling modes.

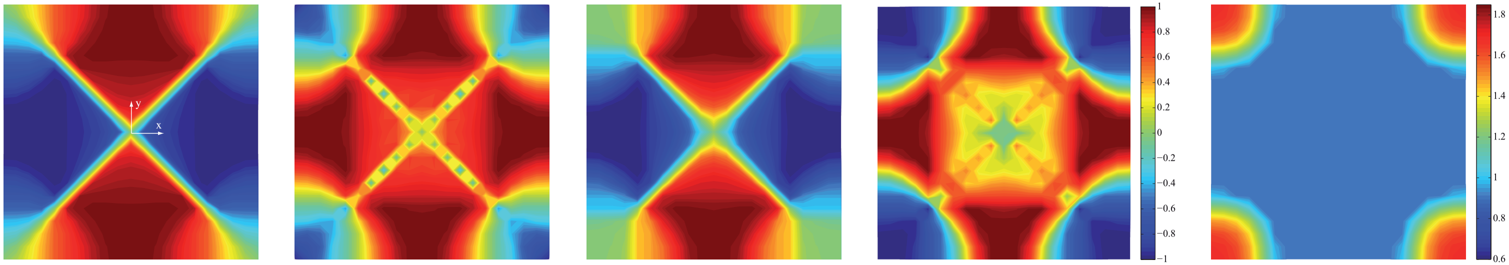

(a) $V_{1\mathbf{A}}$ (b) $V_{3\mathbf{A}}$ (c) $V_{1\mathbf{D}}$ (d) $V_{3\mathbf{D}}$ (e) $\hat{h}$

Figure 7.8: *Optimal lamination parameter and thickness distribution for the biaxially loaded variable stiffness laminate with* $\hat{h}^L = 0.9$

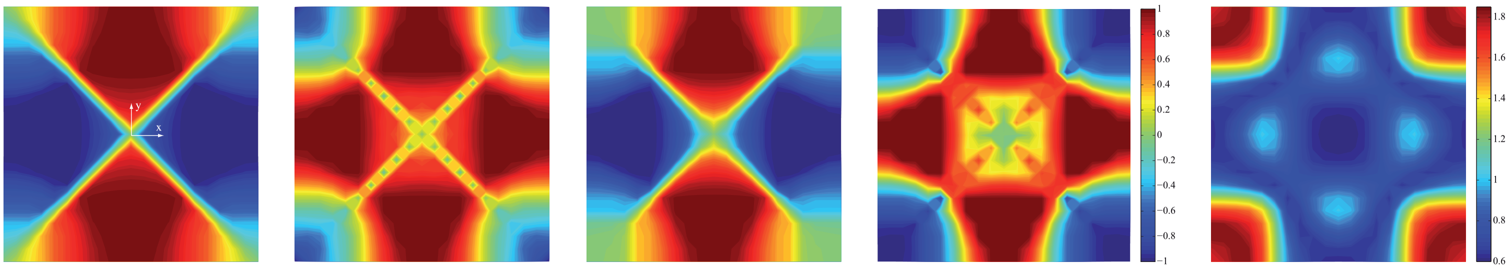

(a) $V_{1\mathbf{A}}$ (b) $V_{3\mathbf{A}}$ (c) $V_{1\mathbf{D}}$ (d) $V_{3\mathbf{D}}$ (e) $\hat{h}$

Figure 7.9: *Optimal lamination parameter and thickness distribution for the biaxially loaded variable stiffness laminate with* $\hat{h}^L = 0.4$

Once again, the in-plane stress resultants were plotted, see Figure 7.10, in order to interpret the effect of the optimal laminate stiffness and thickness distribution on the in-plane loads within the panel, and were normalized as for the unidirectional load case. The stress resultants of the uniform thickness design and two cases including thickness variation, $\hat{h}^L = 0.9$ and $\hat{h}^L = 0.4$, are presented. The stress resultants of the uniform thickness uniaxially loaded panel are also presented for comparison purposes. Once again the compressive load is carried primarily by the panel edges for all the presented designs while the central sections carry little load. At section A-A', Figure 7.10(a), the load distribution for both the uniaxial and biaxial load cases are similar, with approximately a quarter of the panel, $-\frac{b}{2}$ to $-\frac{3b}{8}$ and $\frac{3b}{8}$ to $\frac{b}{2}$, carrying the majority of the compressive loads. Towards the panel center, section B-B' in Figure 7.10(b), the effect is less pronounced for the biaxial load case where approximately half of the panel, $-\frac{b}{2}$ to $-\frac{b}{4}$ and $\frac{b}{4}$ to $\frac{b}{2}$, carries the majority of the compressive loads.

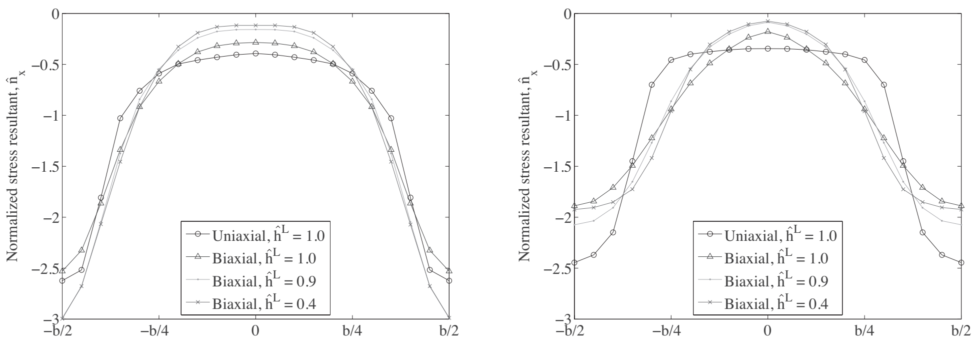

(a) $\hat{n}_x$ along section A-A'

(b) $\hat{n}_x$ along section B-B'

Figure 7.10: *Normalized in-plane stress resultant in the x-direction, $\hat{n}_x$, plotted along the panel width for the biaxial load case see Figure 7.1 for section definition*

The first four buckling modes for the laminate designs with $\hat{h}^L = 0.9$ and $\hat{h}^L = 0.4$ are presented in Figures 7.11 and 7.12, respectively. The mode shapes are similar for both cases with mode one consisting of a single half-wave. Modes two and three for the first design, see Figures 7.11(b) and 7.11(c), consist of two half-waves along a single axis and are identical other than being rotated by 90° with respect to each other, which is related to the problem symmetry. Mode four, Figure 7.11(d), consists of two half-waves along both loaded axes. For the second design, $\hat{h}^L = 0.4$, modes two, three and four are similar to the first design, $\hat{h}^L = 0.9$, however, the waves are oriented along the plate diagonals instead of the main loading axes. Once again, including laminate thickness tailoring in the design process tends to localizes the buckling modes towards the center of the plate, in this case by increased bending stiffness in the corners. For the second design, additional thickness buildup was found near the central areas along each edge, see Figure 7.9(e), hence, the half-waves align along the diagonals due to the locally increased bending stiffness.

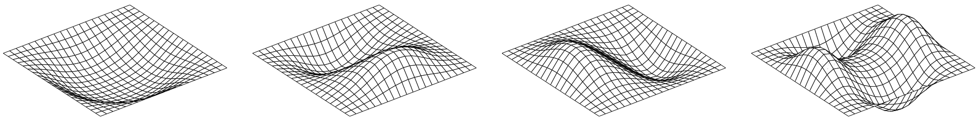

(a) Mode 1 (b) Mode 2 (c) Mode 3 (d) Mode 4

Figure 7.11: *First four buckling modes for* $\hat{h}^L = 0.9$ *with biaxial loading*

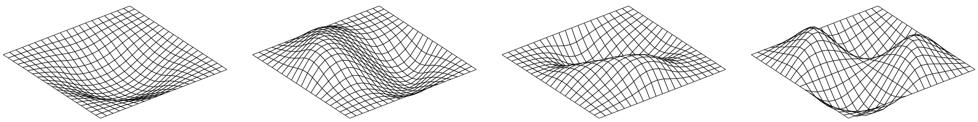

(a) Mode 1 (b) Mode 2 (c) Mode 3 (d) Mode 4

Figure 7.12: *First four buckling modes for* $\hat{h}^L = 0.4$ *with biaxial loading*

7.3 Concluding Remarks

A separable, conservative approximation scheme to maximize buckling loads of variable thickness and variable stiffness laminates was developed based on the approximation scheme presented in chapter 5. It was shown that to retain overall approximation convexity the in-plane stiffness terms had to be expanded linearly in terms of both lamination parameters and thickness. To ensure that the problem remained bounded, a constraint on maximum laminate volume was imposed.

Laminate buckling loads are a function of both laminate in-plane stiffness and bending stiffness distribution, which are linear and cubic functions of laminate thickness respectively. For uniform thickness laminates, see chapter 5, in-plane load redistribution was found to be the primary mechanism responsible for improved laminate buckling load. In order to investigate the primary buckling load improvement mechanisms for variable thickness laminates, the developed approximations were used to solve the previously studied example problem for both uniaxial and biaxial compressive loads.

Significant improvements in maximum buckling load were obtained for both load cases when allowing laminate thickness to vary spatially. Uniaxial buckling loads were shown to improve up to 500% with respect to a baseline quasi-isotropic laminate when tailoring both laminate stiffness and thickness, while improvements were limited to 190% when laminate thickness was constant. Buckling load improvements of 130-380% were found with respect to the optimal constant stiffness design. Compared to the optimal variable stiffness design with constant thickness, improvements in the order of 30-100% were obtained depending on the minimum allowable thickness. The optimal thickness distributions for the uniaxial load case were shown to reinforce the load redistribution effect, resulting in a majority of the compressive loads being transferred to the stiff panel edges. The thickness distribution also tended to force buckling modes to localize towards the central section of the laminate. As more thickness variation was permitted, thickness buildup also occurred in central sections of the panel, locally increasing the laminate bending stiffness.

The distinction between load redistribution and improved bending stiffness as a primary mechanism for increased buckling load was less pronounced for the biaxial load case. The optimal laminate stiffness distribution was found to be practically independent of the optimal thickness distribution. The in-plane stiffness distribution, as for the uniaxial load case, results primarily in load redistribution to the edges while the central section of the panel remains relatively unloaded, however, the thickness distribution tended to reinforce bending stiffness at specific sections within the panel.

The studied example problems demonstrated that when thickness variation is included in the variable stiffness design routine for maximum laminate buckling load, both load redistribution and improved laminate bending stiffness play a role. In-plane stiffness tailoring was found to distribute compressive loads effectively to sections of the laminate that were well suited to transmitting these loads. The thickness distribution was found to support the load redistribution mechanism partially, while also locally improving bending stiffness to either suppress buckling modes or by localizing the modes such that they had a shorter wave-length.

CHAPTER 8
Design of Variable Stiffness Shells for Buckling

> "*There is little doubt that the considerable benefits offered by composites have yet to be fully exploited ...*"
>
> Adam Quilter

An approximation to maximize the buckling load of a plate was developed in Chapter 5. A homogenous convex approximation of the buckling equation was obtained by expanding the geometric stiffness terms linearly with respect to the in-plane stiffness matrix terms, $\mathbf{A}_i$, while expanding the material stiffness matrix reciprocally in terms of the flexural stiffness matrix terms, $\mathbf{D}_i$. Using the approximation within the developed design optimization framework demonstrated the significant performance improvements possible when tailoring laminate stiffness properties of panels loaded under compression.

A generalization of the buckling load approximation of a plate was developed for arbitrary shell structures and is presented in this chapter. In order to extend this approach to general shell structures the finite element analysis equations are revisited in section 8.1, to highlight the influence of the material stiffness matrices, $\mathbf{A}_i$ and $\mathbf{D}_i$, on the buckling load. An approximation of the buckling load, which is consistent with the previously developed approximation form, was derived and is discussed in section 8.2. Subsequently, the approximation was used to solve an example problem highlighting the coupling between in-plane and out-of-plane laminate stiffness properties in section 8.3.

This chapter is based on the paper, *Maximizing buckling loads of variable stiffness shells using lamination parameters* by S.T. IJsselmuiden, M.M. Abdalla, and Z.Gürdal, which was presented at the 50th AIAA/ASME/ASCE/AHS/ASC Structures, Structural Dynamics, and Materials Conference, 2009. Note: symbols may have been changed to maintain consistency throughout this thesis.

8.1 Buckling Analysis for Shells

The linear buckling load for generic shell structures can be obtained in a similar manner to that presented for flat plates in chapter 5 by solving the following eigenvalue problem:

$$\left(\mathbf{K}_m - \lambda \mathbf{K}_g\right) \cdot \mathbf{a} = \mathbf{0} \tag{8.1}$$

where $\mathbf{K}_m$ is the global material stiffness matrix, $\mathbf{K}_g$ is the global geometric stiffness matrix, $\mathbf{a}$ is the mode shape comprising of deformation degrees of freedom, and λ is load multiplier or buckling factor. The mode shapes are normalized such that:

$$\mathbf{a}^T \cdot \mathbf{K}_m \cdot \mathbf{a} = 1 \tag{8.2}$$

The geometric stiffness matrix is constructed through an assembly of element geometric matrices. The stiffness matrix of each element takes the form:

$$\mathbf{K}_e^g = -n_x \mathbf{K}^x - n_y \mathbf{K}^y - n_{xy} \mathbf{K}^{xy} \tag{8.3}$$

where $\mathbf{n}_e = (n_x,\ n_y,\ n_{xy})^T$ is the vector of in-plane stress resultants averaged over the element, and $\mathbf{K}^x$, $\mathbf{K}^y$ and $\mathbf{K}^{xy}$ are constant matrices that depend only on element geometry.

The averaged in-plane stress resultants can be expressed as:

$$\mathbf{n}_e = \mathbf{A}_e \cdot \mathbf{e}_e \tag{8.4}$$

where $\mathbf{A}$ is the in-plane stiffness matrix and $\mathbf{e}$ is the average strain vector given by:

$$\mathbf{e}_e = \overline{\mathbf{B}}_e \cdot \mathbf{u}_e \tag{8.5}$$

where $\mathbf{u}$ is the vector of displacements, $\overline{\mathbf{B}}$ is the average element strain displacement matrix, and $\mathbf{u}_e$ is the vector of the degrees of freedom associated with nodes connected to the e^{th} element. The displacements can be found from the solution of the equilibrium equations:

$$\mathbf{K}_m \cdot \mathbf{u} = \mathbf{f} \tag{8.6}$$

where $\mathbf{f}$ is the vector of applied loads.

The primary difference between the analysis for arbitrary shell structures and flat plates is that the material stiffness matrix, $\mathbf{K}_m$, and the global geometric stiffness matrix, $\mathbf{K}_g$, are now a function of *both* the laminate in-plane and bending stiffness matrices. The material stiffness matrix is simply an assembly of all the element material stiffness matrices, which are a explicit functions of the element in-plane and bending stiffness matrices, $\mathbf{A}_e$ and $\mathbf{D}_e$, respectively. The geometric stiffness matrix, $\mathbf{K}_g$, is an explicit function of the element in-plane stress resultants, $\mathbf{n}_e$, which are an implicit function of the in-plane and bending stiffness matrices through the displacements calculated from the equilibrium equation (8.6).

8.2 Conservative Approximation Formulation

A homogenous conservative approximation was developed for the inverse buckling load factor of a flat plate in chapter 5. The approximation was developed based on insight that highlighted the difference in contribution of the material stiffness and geometric stiffness matrix to the approximate function. The approximation was readily implemented since the material stiffness matrix is only a function of the laminate bending stiffness matrix, while the geometric stiffness matrix is only a function of laminate in-plane stiffness. However, for shell structures this is no longer the case as the material and geometric stiffness matrices are a function of both in-plane and bending stiffness, i.e. $\mathbf{K}_m(\mathbf{A}, \mathbf{D})$ and $\mathbf{K}_g(\mathbf{A}, \mathbf{D})$.

A similar homogenous, conservative approximation can be derived for the inverse buckling factor, $r_b = 1/\lambda$, of a shell. The chosen form for the approximation can best be understood by investigating the Rayleigh quotient (Canfield, 1993) for the eigenvalue problem (8.1), which is given by,

$$r_b \approx \frac{\mathbf{a}^T \cdot \mathbf{K}_g \cdot \mathbf{a}}{\mathbf{a}^T \cdot \mathbf{K}_m \cdot \mathbf{a}} \tag{8.7}$$

where the material stiffness matrix, $\mathbf{K}_m$, is linear in terms of stiffness, whereas the geometric stiffness matrix, $\mathbf{K}_g$, is linear in terms of internal forces, and therefore, non-linear in terms of stiffness.

To create an approximation that is consistent with the Rayleigh quotient the terms in the numerator, the geometric stiffness terms, are expanded with respect to stiffness, whereas the terms in the denominator, the material stiffness terms, are expanded with respect to the inverse stiffness (compliance). Therefore, the Taylor series expansion of the inverse buckling factor can be written as:

$$\begin{aligned} r_b \approx r_{b0} + \sum_{i=1}^{N} \Bigg(& \underbrace{\left.\frac{\partial \hat{r}_b}{\partial \mathbf{A}_i}\right|_0 : (\mathbf{A}_i - \mathbf{A}_{0i}) + \left.\frac{\partial \hat{r}_b}{\partial \mathbf{D}_i}\right|_0 : (\mathbf{D}_i - \mathbf{D}_{0i})}_{\text{geometric stiffness terms}} \\ & + \underbrace{\left.\frac{\partial \check{r}_b}{\partial \mathbf{A}_i^{-1}}\right|_0 : \left(\mathbf{A}_i^{-1} - \mathbf{A}_{0i}^{-1}\right) + \left.\frac{\partial \check{r}_b}{\partial \mathbf{D}_i^{-1}}\right|_0 : \left(\mathbf{D}_i^{-1} - \mathbf{D}_{0i}^{-1}\right)}_{\text{material stiffness terms}} \Bigg) \end{aligned} \tag{8.8}$$

where the $_0$ represents the design point about which the inverse buckling factor is expanded and $i = 1 \ldots N$ are the nodes, elements or regions for which the design variables are defined. The in-plane and bending stiffness matrices are $\mathbf{A}_i$ and $\mathbf{D}_i$, respectively, and the : operator represents matrix inner product. The portion of the inverse buckling factor related explicitly to the material stiffness terms is denoted by $\check{r}_b$ while $\hat{r}_b$ represents the portion related to the geometric stiffness terms. Note that the sum over the geometric stiffness terms is always zero for a dead load, as these terms account for stress redistribution within the structure, in other words:

$$\sum_{i=1}^{N} \left(\frac{\partial \hat{r}_b}{\partial \mathbf{A}_i} : \mathbf{A}_i + \frac{\partial \hat{r}_b}{\partial \mathbf{D}_i} : \mathbf{D}_i \right) = 0 \tag{8.9}$$

Since the stiffness matrix is always positive definite, equation (8.9) implies that the sensitivity matrix is not necessarily positive definite. For this reason, the geometric stiffness terms are expanded linearly as convexity cannot be guaranteed in the case where the reciprocal is used, however, for a linear expansion the approximation is guaranteed to be convex. The material stiffness terms expanded with respect to compliance are always convex, and therefore the approximation as a whole is guaranteed to be convex.

The buckling factor is homogenous of order zero with respect to the geometric stiffness and of order one with respect to the material stiffness, as was also demonstrated for planar structures in chapter 5. The approximation of the inverse buckling factor can therefore be simplified to:

$$r_b \approx \sum_{i=1}^{N} \left(\boldsymbol{\Psi}_i^m : \mathbf{A}_i + \boldsymbol{\Psi}_i^b : \mathbf{D}_i + \boldsymbol{\Phi}_i^m : \mathbf{A}_i^{-1} + \boldsymbol{\Phi}_i^b : \mathbf{D}_i^{-1} \right) \tag{8.10}$$

where $\boldsymbol{\Psi}_i^m, \boldsymbol{\Psi}_i^b, \boldsymbol{\Phi}_i^m$, and $\boldsymbol{\Phi}_i^b$ are the sensitivity matrices associated with each design point in the structure. A detailed derivation of the sensitivities can be found in Appendix C. The approximation form presented in equation (8.10) is readily integrated into the optimization framework presented in chapter 3. In the following section an example problem is used to demonstrate the effectiveness of the developed approximation when determining the optimal laminate stiffness distribution.

8.3 Numerical Results

An example problem was selected to demonstrate the design process of a variable stiffness shell. The aim was to ensure that the material stiffness and geometric stiffness terms in the buckling equation (8.1) were functions of both the in-plane and bending design variables. A curved panel, shown in Figure 8.1, was subject to a uniform external pressure load. The curved edges were clamped while the straight edges were hinged, hence only allowing a rotation about the z-axis. The chosen configuration ensured that the geometric stiffness term in equation (8.1) is also a function of the bending stiffness, thus, ensuring that all terms in equation (8.10) were present during optimization.

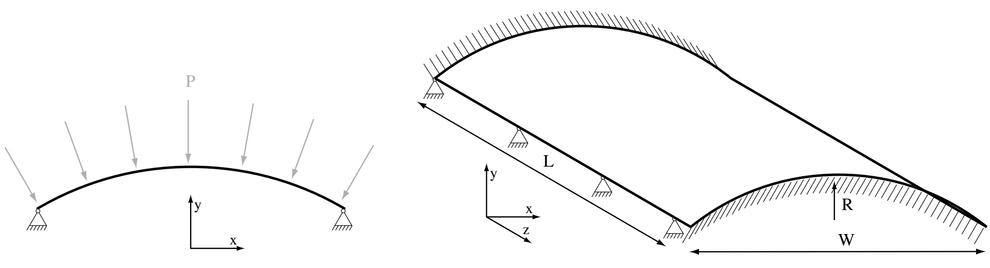

Figure 8.1: *Example problem geometry with uniform external pressure. Curved edges are clamped and straight edges are hinged, only rotation about z-axis is permitted*

A finite element routine based on element templates prescribed in Felippa (2000) and Felippa (2003) was implemented in Matlab^{TM}. The plate was discretized into 960 triangular elements with 521 nodes, resulting in 2084 design variables, 4 design variables per node, for designs with constant laminate thickness, and 2605 design variables, 5 design variables per node, when allowing local laminate thickness to vary. The length, L, and width, W, of the panel were both 2 m and the radius, R, was set to 2.924 m. The material properties for carbon-epoxy IM6/SC1081, listed in Appendix A, were used to evaluate material stiffness matrices.

The approximation developed in section 8.2 was implemented in the optimization framework presented in chapter 3 to maximize the buckling load of the presented example problem. The design problem was first solved for stiffness variation while maintaining constant laminate thickness. Extensional stiffness is a linear function of laminate thickness whereas the bending stiffness is a cubic function of thickness. Therefore, three different total laminate thicknesses, 4.57 mm, 9.91 mm, and 19.8 mm, respectively, were prescribed to study the effect of laminate thickness on the optimal stiffness distribution and the possible improvements. The studied laminate thicknesses resulted in the side length to thickness ratio, W/h, varying from approximately 400 to 100. For a second design problem, both the stiffness and thickness were allowed to vary throughout the structure, allowing the effect of in-plane load redistribution and increased bending stiffness on the buckling load to be highlighted. The nominal laminate thickness, h_0, in this case was taken to be 9.91 mm.

8.3.1 Variable Stiffness Design with Constant Laminate Thickness

The optimal stiffness distribution was obtained for each of the three different laminate thicknesses. The optimal constant stiffness design, obtained by defining a single set of design variables for the entire panel, were also computed for comparison purposes. The first four eigenvalues, which are normalized with respect to the critical buckling load factor of a quasi-isotropic laminate with the same thickness, are presented in Table 8.1. All three designs show an improvement in the order of 70-80% with respect to a quasi-isotropic laminate while improving between 15-20% with respect to the best constant stiffness design. The importance of including multiple critical modes during the design optimization routine is clear from the close modes spacing at the optimum, particularly for the first two designs with a laminate thickness of 4.57 mm and 9.91 mm, respectively.

Table 8.1: *Normalized buckling loads for a range of laminate designs, where h_0 is the nominal laminate thickness, W the panel width, CS a constant stiffness laminate, VS a variable stiffness laminate and $\hat{\lambda} = \lambda/\lambda_{cr}^{QI}$*

Design #	$h_0[mm]$	W/h_0	$\hat{\lambda}_1$	$\hat{\lambda}_2$	$\hat{\lambda}_3$	$\hat{\lambda}_4$
1 (CS)	4.95	404	1.471	1.724	2.277	2.499
2 (VS)	4.95	101	1.711	1.723	2.110	2.396
3 (CS)	9.91	202	1.582	1.583	2.252	2.413
4 (VS)	9.91	202	1.813	1.817	2.297	2.500
5 (CS)	19.8	101	1.497	2.068	2.206	2.505
6 (VS)	19.8	404	1.737	1.784	2.233	2.444

It was useful to study the pre-buckling deformation and buckling modes of the obtained designs to understand the influence of the optimal stiffness distribution on the structural response in general. The pre-buckling deformations due to the applied uniform pressure of both the quasi-isotropic design and optimal design found for laminate thicknesses of $h_0 = 4.57$ mm and $h_0 = 19.1$ mm are presented in Figure 8.2. For the first design, the largest deformation of the quasi-isotropic laminate, Figure 8.2(a), occurred along the hinged vertical edges due to their rotational freedom. Significantly smaller rotations about the hinges were present in the variable stiffness panel, Figure 8.2(b), suggesting a local increase in bending stiffness. Additionally, the largest deformations no longer occurred along the hinged edges, but were located close to the clamped edges, indicating a reinforcement of the central section. For the third design, $h_0 = 19.1$ mm, the additional thickness resulted in significantly improved bending stiffness and hence the deformation of the quasi-isotropic laminate was more uniform. The largest deformations were found towards the center of the curved panel, as can be seen in Figure 8.2(c). Similar deformation trends can be seen in Figure 8.2(d) for the optimal variable stiffness solution as seen for the first optimal design, where the largest deformations tended towards the clamped edges indicating reinforcement of the central section.

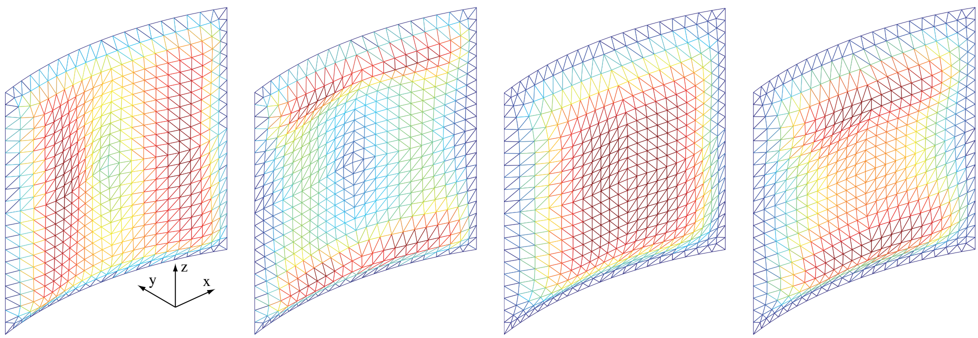

(a) QI, $h_0 = 4.57$ mm (b) VS, $h_0 = 4.57$ mm (c) QI, $h_0 = 19.1$ mm (d) VS, $h_0 = 19.1$ mm

Figure 8.2: *Pre-buckling deformation due to the applied pressure load of a baseline quasi-isotropic (QI) laminate and the optimal variable stiffness design (VS) for laminates with a nominal thickness of $h_0 = 4.57$ mm and $h_0 = 19.1$ mm, respectively*

The first two buckling modes of the previously discussed optimal designs are presented in Figure 8.3. The first buckling mode of the first design, Figure 8.3(a), is asymmetric and consists of four half-waves along the width and a single half-wave along the length of the curved panel. The second mode, Figure 8.3(b), is symmetric and consists of three half-waves along the width. The first buckling mode of the thicker laminate, Figure 8.3(c), is symmetric with a single half-wave along the length and three half-waves along the width. The waves are wider and slightly shorter when compared to those found for the thinner laminate in Figure 8.3(b). The second buckling mode, Figure 8.3(d), is asymmetric and consists of two half-waves along the width and a single half-wave along the height and are concentrated towards the center of the panel.

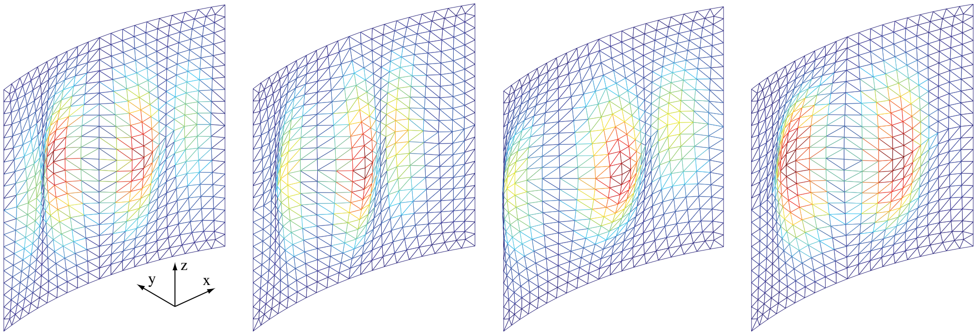

(a) λ_1, $h_0 = 4.57$ mm (b) λ_2, $h_0 = 4.57$ mm (c) λ_1, $h_0 = 19.1$ mm (d) λ_2, $h_0 = 19.1$ mm

Figure 8.3: *First two buckling modes of the optimal variable stiffness design (VS) for laminates with a nominal thickness of $h_0 = 4.57$ mm and $h_0 = 19.1$ mm, respectively*

The optimal lamination parameter distribution for the design with $h_0 = 4.57$ mm and $h_0 = 19.1$ mm are presented in Figures 8.4 and 8.5, respectively, where the horizontal edges are clamped while the vertical edges are hinged. The distributions are relatively intricate, particularly for the in-plane lamination parameters, however, they can be interpreted globally by making use of the Miki-diagram, see Figure 5.6 on page 101. The central section in all of the lamination parameter distribution figures consists roughly of a horizontal red band stretching from one hinged edge to the opposite edge. This region corresponds to a laminate with a large percentage of the fibers aligned with the x-axis as $V_{1,3\mathbf{A}}, V_{1,3\mathbf{D}} \rightarrow 1$, and hence will have high axial and bending stiffness along this direction. This region therefore acts as a stiffener between the two hinged edges, suppressing the out-of-plane deformation in this region due to the applied pressure, as can be seen in Figures 8.2(b) and 8.2(d).

Studying the flexural lamination parameters in more detail, Figures 8.4(c), 8.4(d), 8.5(c), and 8.5(d), the location and number of red "cells" coincide with the location and number of half-waves found for the critical buckling modes of the optimal designs, given in Figures 8.3(a) and 8.3(c), respectively. Along the horizontal clamped edges there are several regions for both designs where $V_{1\mathbf{D}} \rightarrow -1$ and $V_{3\mathbf{D}} \rightarrow 1$. These regions correspond to laminates with a large percentage of plies aligned along the z-axis and hence the laminate locally has a larger bending stiffness along this axis. These regions also coincide with the location of the buckling half-waves, and therefore, act to suppress these buckling modes.

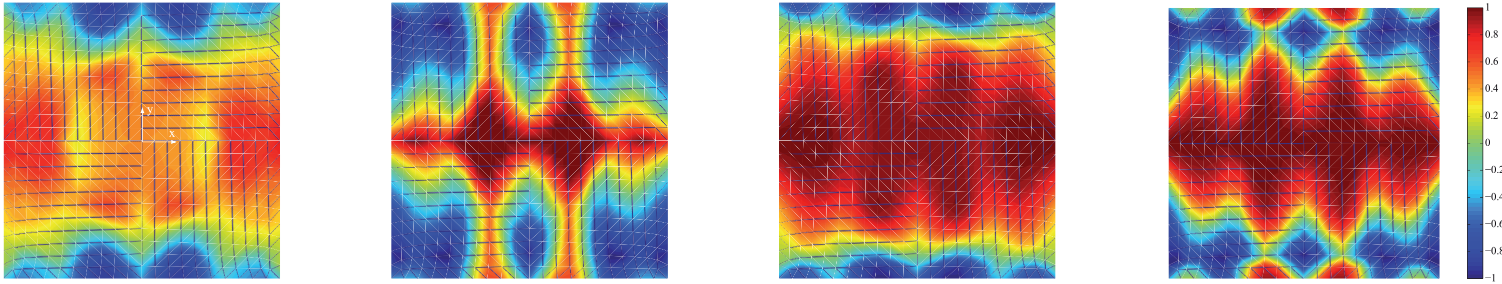

(a) $V_{1\mathbf{A}}$ (b) $V_{3\mathbf{A}}$ (c) $V_{1\mathbf{D}}$ (d) $V_{3\mathbf{D}}$

Figure 8.4: *Optimal lamination parameter for maximum buckling load for a laminate with a nominal thickness of* $h_0 = 4.57$ *mm*

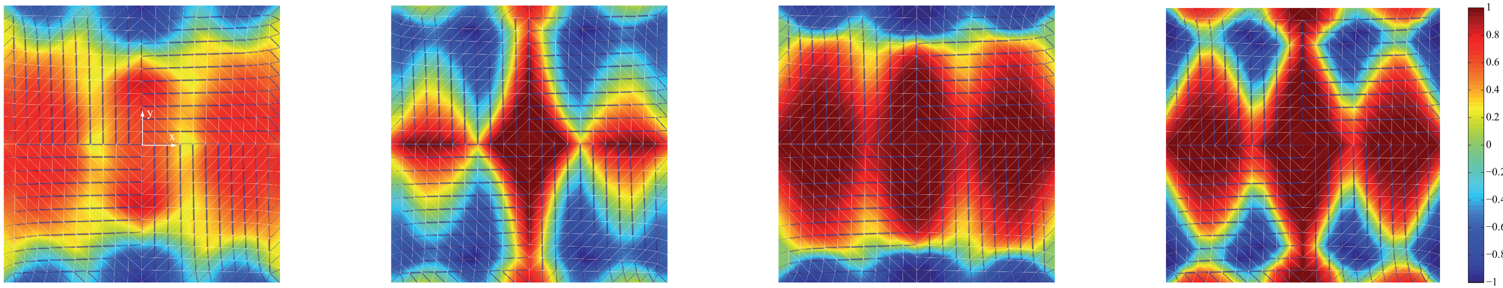

(a) $V_{1\mathbf{A}}$ (b) $V_{3\mathbf{A}}$ (c) $V_{1\mathbf{D}}$ (d) $V_{3\mathbf{D}}$

Figure 8.5: *Optimal lamination parameter for maximum buckling load for a laminate with a nominal thickness of* $h_0 = 19.1$ *mm*

The obtained results seemed to indicate that the design problem was predominantly governed by the laminate's bending performance, which was not unexpected considering the geometry and loading. The relatively uniform nature of the flexural lamination parameter distributions, particularly in the central section of the panel, supported the relatively small difference in critical buckling load found between the optimal constant stiffness and variable stiffness designs.

8.3.2 Variable Stiffness Design with Variable Laminate Thickness

The buckling load approximation presented in section 8.2 is readily extended to include thickness as a design variable, as explained in section 3.2.4. Hence, the developed optimization routine was also used to compute the optimal thickness and stiffness distributions simultaneously. Including thickness as a design variable required the total structural volume to be bound. The initial structural volume, $\mathcal{V}_0$, was based on the initial thickness, $h_0 = 9.81$ mm. The optimization problem therefore consisted of maximizing the buckling load, subject the aforementioned volume constraint, and was solved for a range of different lower bounds on laminate thickness, $\hat{h}^L = h/h_0 = 1.0, 0.9, \ldots 0.4$. This was to assess the influence of minimum gauge thickness on the optimal solution.

The first four eigenvalues of the obtained optimal designs are presented in Table 8.2. All values are normalized with respect to the critical buckling load of a quasi-isotropic laminate with uniform thickness, h_0. The optimum constant stiffness solution obtained previously is also provided for comparison purposes. Two trends were noticed from the tabulated data, one, the minimum and maximum laminate thickness both converged to an asymptote, after which they did not change, even if the lower bound, $\hat{h}^L$, was further reduced. Two, as the lower bound on thickness was decreased, the spacing between the first four critical eigenvalues also decreased. As was the case for the planar structures studied and presented in chapter 7, significant improvements in the critical buckling load are achieved when allowing thickness to vary over the structure. The maximum buckling load, found when $\hat{h}^L < 0.6$, was 150% higher than the quasi-isotropic laminate and approximately 60% higher than the best constant stiffness solution.

Table 8.2: *Normalized buckling loads for a range of laminate designs, with $\hat{\lambda} = \lambda/\lambda_{cr}^{QI}$, $\hat{h} = h/h_0$ and h^L the lower bound on thickness*

Design	$\hat{h}_{min}$	$\hat{h}_{max}$	$\hat{\lambda}_1$	$\hat{\lambda}_2$	$\hat{\lambda}_3$	$\hat{\lambda}_4$
Quasi Isotropic	1.000	1.000	1.000	1.163	1.503	1.789
Constant Stiffness	1.000	1.000	1.582	1.583	2.252	2.413
Variable Stiffness, $\hat{h}^L = 1.0$	1.000	1.000	1.813	1.817	2.297	2.500
Variable Stiffness, $\hat{h}^L = 0.9$	0.900	1.313	2.182	2.183	2.336	2.456
Variable Stiffness, $\hat{h}^L = 0.8$	0.800	1.397	2.358	2.360	2.439	2.499
Variable Stiffness, $\hat{h}^L = 0.7$	0.700	1.470	2.453	2.456	2.520	2.540
Variable Stiffness, $\hat{h}^L = 0.6$	0.600	1.481	2.460	2.488	2.497	2.592
Variable Stiffness, $\hat{h}^L = 0.5$	0.580	1.496	2.499	2.502	2.541	2.570
Variable Stiffness, $\hat{h}^L = 0.4$	0.575	1.494	2.499	2.507	2.559	2.560

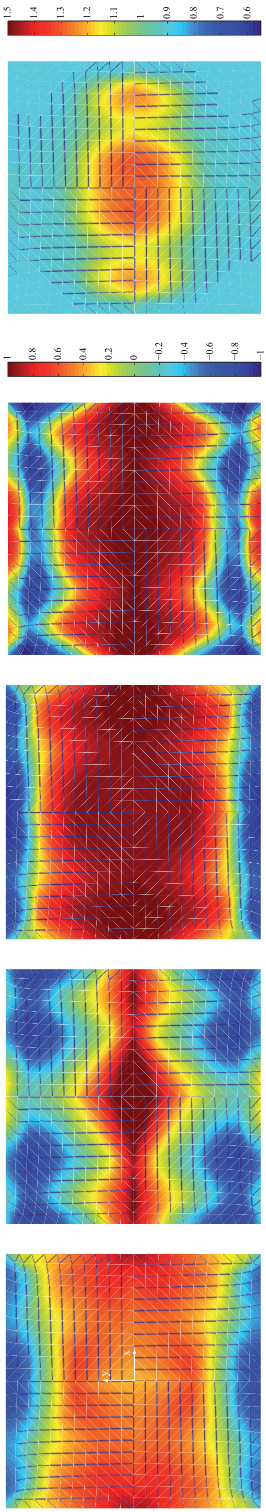

(a) $V_{1\mathbf{A}}$ (b) $V_{3\mathbf{A}}$ (c) $V_{1\mathbf{D}}$ (d) $V_{3\mathbf{D}}$ (e) $\hat{h}$

Figure 8.6: *Optimal lamination parameter and thickness distribution for the optimal variable stiffness solution with* $\hat{h}^L = 0.9$

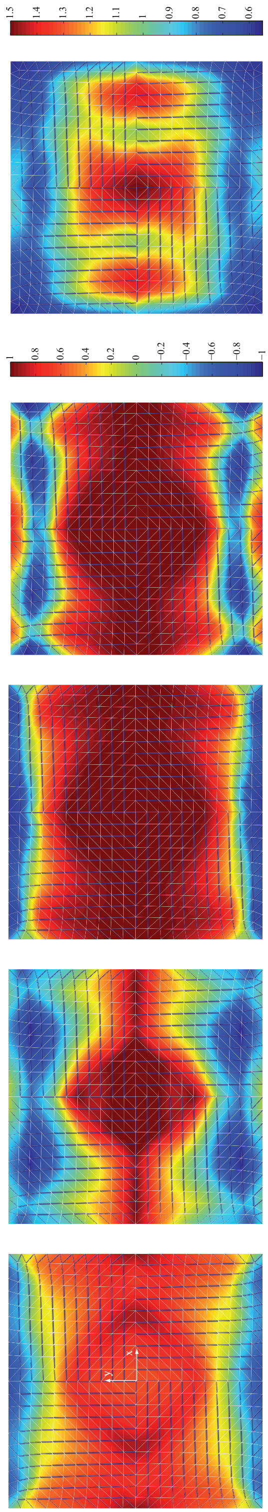

(a) $V_{1\mathbf{A}}$ (b) $V_{3\mathbf{A}}$ (c) $V_{1\mathbf{D}}$ (d) $V_{3\mathbf{D}}$ (e) $\hat{h}$

Figure 8.7: *Optimal lamination parameter and thickness distribution for the optimal variable stiffness solution with* $\hat{h}^L = 0.4$

The optimal lamination parameter and thickness distributions for the designs with $\hat{h}^L = 0.9$ and $\hat{h}^L = 0.4$ are presented in Figures 8.6 and 8.7, respectively. The in-plane and flexural lamination parameter distributions, $V_{1,3\mathbf{A}}$ and $V_{1,3\mathbf{D}}$, respectively, were found to have similar features to those found previously for the constant thickness designs, which were discussed in subsection 8.3.1. The extensional and bending stiffnesses of the panel's central region, connecting the two hinged edges, were found to be largest along the x-axis. Only small differences in lamination parameter distributions were found between the design for $\hat{h}^L = 0.9$ and $\hat{h}^L = 0.4$, where the most noticeable was the slightly larger central red region seen in 8.7(b) when compared to Figure 8.6(b).

Thickness buildup for both designs was found to occur primarily in the central regions of the panel with a bias along the x-axis, as can be seen Figures 8.6(e) and 8.7(e). The local thickness increase resulted in improved bending stiffness and hence higher buckling loads. Additional thickness buildup was found towards the clamped edges for the design with $\hat{h}^L = 0.4$, see Figure 8.7(e), which also suggested locally improved bending stiffness. The pre-buckling deformations and buckling modes were found not to differ significantly compared to those presented for the previous design problem in subsection 8.3.1 and were therefore not reproduced.

8.4 Concluding Remarks

A conservative convex separable approximation, matching the approximation form discussed in chapter 3, for the buckling load of shell structures was presented. To retain convexity of the approximation it was necessary to expand the geometric stiffness terms linearly with respect to the element stiffness matrices while the material stiffness matrix was expanded reciprocally. Similarly, it was necessary to linearize the geometric stiffness terms in terms of thickness when laminate thickness was included as a design variable. The optimization framework developed in chapter 3 was subsequently used to solve an example problem for several different nominal laminate thicknesses. Improvements of 15-20% with respect to the best constant stiffness design were obtained for panels with a range of side-length to thickness ratios. Including thickness as a design variable resulted in laminate designs improving over 60% with respect to the best constant stiffness design, and 150% with respect to a baseline quasi-isotropic laminate.

The obtained lamination parameter and thickness distributions indicated that increased buckling loads were obtained primarily due to improved laminate bending stiffness. This is in contrast to the results obtained for flat panels in chapters 5 and 6 , where the primary mechanisms were found to be related to in-plane load redistribution. The importance of both the laminate's extensional and bending stiffness in improving the buckling performance of a structure was also seen in chapter 7. As the structures, and the laminates of which they comprise, become more complex it will inevitably become difficult to identify the primary mechanisms resulting in improved buckling performance. The developed convex conservative separable approximation of the buckling load implemented within the developed design optimization framework has, thus far, proven to be an effective tool in for optimizing variable stiffness composite structures.

CHAPTER 9

Design Application: Fuselage Window Belt Section

"As far as the laws of mathematics refer to reality, they are not certain, and as far as they are certain, they do not refer to reality"

Albert Einstein

A substantial portion of the presented research was conducted within the scope of the AUTOW-Project, part of the European Union sixth framework program, which focused on using fiber placement technology to design and manufacture structures using dry tow placement technology. Thus far, the presented research has focused primarily on the development of an efficient variable stiffness design routine in terms of lamination parameters and the derivation of structural response approximations that were cast into the form required by the developed design framework.

To demonstrate the capabilities of the variable stiffness design approach for more realistic problems, two design studies were conducted within the AUTOW-Project, the first of which is presented in this chapter. The chosen design problem replicated a portion of a window-belt section of a light business jet. The design study objective was twofold, one, to demonstrate the improvements possible in terms of strength using the variable stiffness concept, and two, to deliver a set of fiber paths manufacturable with the available fiber placement machine for experimental validation.

The majority of modern aircraft are built using the stressed-skin concept, where fuselage and wing skins are required to carry a substantial portion of the structural loads. Often holes must be introduced in these skins, be it for practical purposes or passenger comfort, resulting in undesired stress concentrations. Cabin pressurization leads to the presence of large tensile forces in the fuselage skin. Stress concentrations,

The work presented in this chapter was conducted as part of the AUTOW-Project, see http://www.autowproject.eu for more details. Several results and figures published in project deliverable D30 have been used and are not original work done by the author. The author would like to thank Dassault Aviation (DAv) for their contribution to the research presented here.

which occur due to the presence of windows, must be accounted for by reinforcing these regions, something which is even more prevalent in small business jets due to the relatively small window pitch compared to commercial airliners.

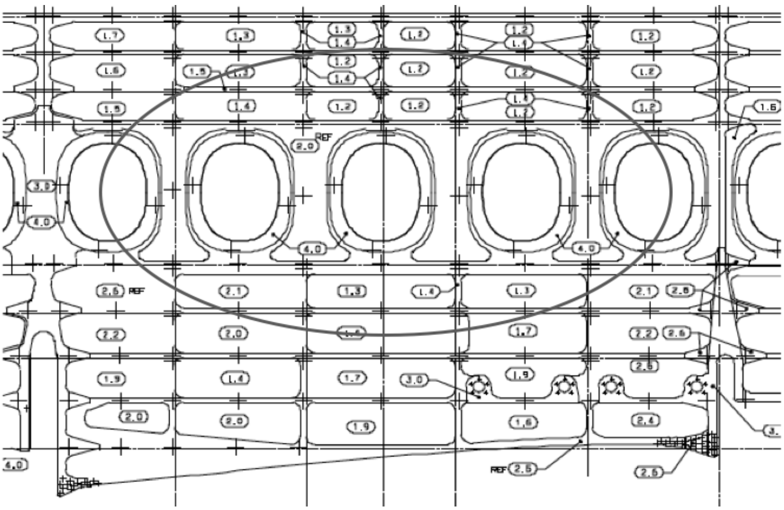

Figure 9.1: *Example of a window belt section of an average size business jet (Source DAv)*

An example of a window belt section of a small business jet is presented in Figure 9.1. Working together with Dassault Aviation this was used to define an example problem to study how stiffness tailoring might be introduced to reduce the presence of stress concentrations and increase the ultimate failure load. A simplified problem description is presented in section 9.1. Subsequently, three different laminate design studies were conducted. The initial design studies were conducted to obtain straight fiber designs to serve as a baseline, and are presented in section 9.2. In a second design study, section 9.3, the developed variable stiffness optimization routine was used to maximize laminate strength and retrieve possible fiber paths. Due to limitations both in time and manufacturing capabilities, a third set of designs was obtained using linear variation such that they could be manufactured and tested using the available resources, these are discussed in section 9.4. An overview and comparison of the different designs is presented in section 9.5. Unfortunately experimental results were unavailable at the time of writing of this thesis and could therefore not be included in this chapter.

9.1 Problem Description

The goal of the developed example problem was to capture essential aspects of the window-belt design, while simplifying it enough such that it could be designed, manufactured and tested within the limited time and resource budgets available. The maximum panel dimensions were limited by the working-envelope of the fiber placement machine and the dimensions of the one mega-newton tensile test-bench, however, the chosen design dimensions were realistic. To simplify experimental testing further, the panel was considered to be loaded only under tension and to be flat, and therefore panel curvature and pressure loads were not considered. Two cut-outs were integrated on each side of the panel to replicate the stress state typically found around a window. A description of the test specimen geometry and loading is provided below followed by the used design criteria and finite element model specifications. Material properties for carbon-epoxy IM7/8552 used during the design studies are listed in Appendix A.

9.1.1 Geometry and Loading

Several design configurations were studied to capture the essential failure mechanisms of the window-belt section along the central hole in a simplified test-specimen. The final geometry and loading, as defined by Dassault Aviation, are presented in Figure 9.2. The test specimen consisted of a 1m by 1.4m panel with a large central hole having a diameter of 310mm. The edges included a waist-section with a radius of approximately 1.24m to simulate the stress field caused by adjacent windows. Two load introduction points were included, which were aligned with the bands along the window as indicated in Figure 9.2(b). The specimen was padded up to a thickness of approximately 10mm towards the fixtures to ensure proper load introduction. Initial load and laminate thickness were selected such that failure of an isotropic laminate would occur at a reasonable load level, ensuring sufficient safety margin such that all test specimens could be tested to failure using the available test-bench. Therefore, a sixteen-ply quasi-isotropic laminate was set as a baseline, having a predicted failure load of P = 633 kN.

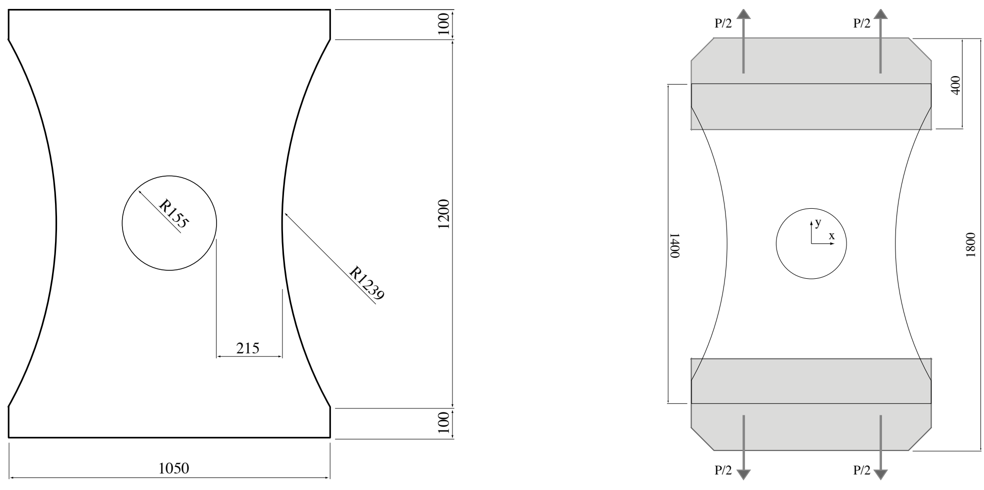

(a) Geometry and dimension (b) Two load introduction points

Figure 9.2: *Simplified window belt geometry, dimensions and loading with padded up section for load introduction*

9.1.2 Design Criteria

The design study objective was to investigate configurations for a 16-ply balanced symmetric laminate to improve its ultimate load carrying capacity. Laminate failure is notoriously difficult to predict, which is reflected by the large number of laminate failure criteria available both in the literature and within the different aerospace corporations, see for example Hinton et al. (2004). Two different laminate failure criteria were implemented to optimize and compare the different designs in this chapter. The first criteria was defined by Dassault Aviation, referred to as the “Hole Edge Strain Criteria”, and the second was based on the conservative Tsai-Wu failure envelope derived earlier in chapter 4.

Hole Edge Strain Criteria

Dassault makes use of hole edge strains to define laminate failure when designing components with large holes, such as a window-belt section. Hole edge strain is defined as the strain in the direction tangent to the hole’s edge. In a finite element model strains along a hole’s edge are typically computed by inserting rod-elements with weak axial stiffness between all nodes located along the hole’s edge. A mesh edge length of 5mm is specified along the hole’s edge and the principal strains along this edge are not permitted to exceed a predefined critical value. Laminate failure can therefore be expressed as the point at which the normalized critical strain, ϵ_{cr}, exceeds unity:

$$\epsilon_{cr} = \max\left(\frac{\epsilon_{max}}{\epsilon_t}, \frac{\epsilon_{min}}{\epsilon_c}\right) > 1 \tag{9.1}$$

where ϵ_{max} and ϵ_{min} are the maximum and minimum principle strains found along the circumference of the hole, normalized by the tensile and compressive failure strains, ϵ_t and ϵ_c, respectively. An optimization problem to maximize laminate strength can subsequently be formulated as:

$$\min \epsilon_{cr} \tag{9.2}$$

where different sets of design variables were used to solve for the above equation, which will be discussed when the individual design studies are presented in section 9.2, 9.3 and 9.4.

Failure Index: Tsai-Wu

In addition to the failure criterion given in equation (9.1), the Tsai-Wu based failure criterion originally developed in chapter 4 was used. This failure criteria was integrated into the developed variable stiffness laminate design framework together with Khani et al. (2011). For this case laminate strength is maximized through the following optimization problem:

$$\min\left(\max r_i\right) \tag{9.3}$$

where $\max r_i$ is the critical failure index value within the structure. The failure index values were calibrated such that ultimate failure of the baseline quasi-isotropic design occurred at the same load as that predicted by equation (9.1).

For practical applications additional design rules are often implemented to ensure laminate robustness, such as the ten percent rule, which specifies that at least ten percent of the plies should be in the $0°, 90°, 45°$ and $-45°$ direction. Doing so ensures robustness of the stack to secondary loading which is difficult to account for when modeling. An equivalent laminate robustness constraint, presented by Abdalla et al. (2009a), was implemented in the lamination parameter design space by restricting the ratio of minimum to maximum in-plane laminate stiffness. Therefore, to ensure laminate robustness an equivalent five percent rule was implemented as a constraint for several of the conducted design studies. A five percent rule was implemented instead of the traditional ten percent rule to allow for more design freedom.

9.1.3 Finite Element Model Description

The test specimen was quarter-symmetric and therefore only a quarter of the structure was modeled to reduce the computational burden during the design studies. Two different mesh densities were considered, initial design studies were conducted with mesh (1), with an hole-edge length of 10mm, while later the designs selected for manufacturing were validated with a finer model having the 5mm hole-edge length specified by Dassault aviation. Mesh (1) has a total of 455 nodes 822 elements while mesh (2) consists of 1843 nodes and 3514 elements.

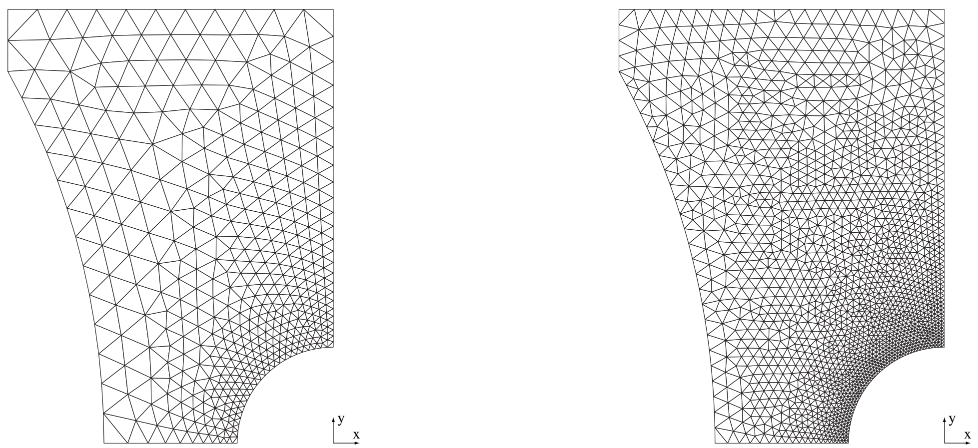

(a) Mesh (1), 10mm hole-edge length   (b) Mesh (2), 5mm hole-edge length

Figure 9.3: *Two different mesh densities were used for the design studies and validation of the manufactured designs respectively*

The following boundary conditions were applied, where U and R represent the displacement and rotation, respectively, about axis 1 (x), 2 (y) or 3 (z):

- U1 = U3 = R1 = R2 = R3 = 0, along the top edge (clamped)
- U2 = R1 = R3 = 0, along the bottom edge (symmetry)
- U1 = R2 = R3 = 0, along the right edge (symmetry)
- U2 equal for all nodes along the top edge (straight edge)

Modeling was conducted using an finite element code implemented in Matlab™ based on templates defined by Felippa (2003), presented in Appendix B, and validated with Abaqus™ version 6.8. Hole edge strains were computed in Abaqus using rod-elements connected to adjacent nodes along the holes edge with weak axial stiffness, essentially representing a virtual strain-gauge. Hole edge strains were computed directly from nodal displacements when using the in-house finite element code. Verification of the in-house code was conducted for several different laminate configurations and critical failure strains along the hole's edge were not found to deviate more that 4% with respect to the results obtained with Abaqus. Additionally, critical failure strains predicted by mesh (1) were within 0.8% of those predicted by mesh (2), indicating that mesh (1) was suitable enough for the design studies.

9.2 Constant Stiffness Laminate Design Study

Constant stiffness laminates refer to laminates that consist of a single stacking sequence over the entire structure. Four alternate design problems are presented in this section using the two failure criteria defined in section 9.1. All results were compared to the baseline sixteen-ply quasi-isotropic laminate, $[0_2, 90_2, \pm 45_2]_s$. The following design problems were solved:

CSD1: Parametric study of designs based on 0, ±45, 90 degree plies
CSD2: $\min_{\boldsymbol{\theta}} (\epsilon_{cr})$ with $\theta \in [0, 5, 10 \ldots 90]$
CSD3: $\min_{\mathbf{V}} (\max r_i)$
CSD4: $\min_{\mathbf{V}} (\max r_i)$ with equivalent 5% rule

where all laminates were restricted to be balanced and symmetric, thus a maximum of four plies were designed for a total laminate thickness of 16-plies.

The first design study, CSD1, was simply a parametric study of the critical failure strains for different percentages of the constituent plies. The second study, CSD2, the critical strain was minimized using a generic genetic algorithm with 5° ply-encoding, where all angles are measured from the horizontal x-axis of the panel, see for example Gürdal et al. (1999). The designs for CSD3 and CSD4 were obtained in lamination parameters space using the design framework presented in chapter 3, by defining a single set of lamination parameters for the entire structure. The obtained lamination parameters were subsequently converted to a stacking sequences using either a heuristic search method or solving analytically for $[\pm\theta_1, \pm\theta_2]_{2s}$ when possible (Gürdal et al., 1999). Since the presented problem was governed only by laminate in-plane stiffness, the conversion from lamination parameters to stacking sequences was relatively straight forward. The obtained results are summarized in Table 9.1.

The quasi-isotropic laminate, design #1, was used as a baseline. As expected, results from the parametric design study, CSD1, demonstrated that aligning fibers with the primary load direction, the y-axis, was beneficial. For practical purposes it was necessary to include a minimum of plies in all directions, however, aligning a majority of plies in the load-direction, design #2, caused ultimate load carrying capacity of the laminate to be increased by 28%. Using a genetic algorithm to determine the laminate with the lowest critical strain, CSD2, yielded several results with similar critical strain values. The best design, #3, had an ultimate load approximately 64%

Table 9.1: *Overview of designs obtained for the different constant stiffness design problems. All designs are manufacturable and designs satisfying the equivalent five percent rule are marked (*ϵ_{cr}*:* critical hole edge strain, r_i: failure index)

#	Method	Laminate Info	ϵ_{cr}	$\max r_i$	5%	Man
1	–	$[0_2, 90_2, \pm 45_2]_s$, baseline	0.9919	0.9953	✓	✓
2	CSD1	$[0_2, 90_4, \pm 45]_s$	0.7809	0.8609	✓	✓
3	CSD2	$[\pm 80_2, \pm 75, 90_2]_s$	0.6099	0.6307		✓
4	CSD3	$[\pm 67.5]_{4s}$	0.7206	0.4751		✓
5	CSD4	$[\pm 49, \pm 86]_{2s}$	0.7169	0.5175	✓	✓

higher than the baseline quasi-isotropic laminate. The equivalent five percent rule was not applied as a constraint for this design case and therefore it did not satisfy the laminate robustness requirements.

The gradient-based optimization problems, CSD3 and CSD4, yielded a single design point in lamination parameter space, which could subsequently be converted to multiple equivalent laminates. The results presented here were obtained using a direct-solution method (Gürdal et al., 1999), which only allows for a maximum of two different ply orientation angles to be found. If a larger set of laminates is required, to obtain a more robust laminate, a genetic algorithm can be used to retrieve suitable laminates. Design #5 satisfied the equivalent five percent rule and had a failure index that was approximately 60% higher than the quasi-isotropic case and was 45% improvement in terms of critical strains.

9.3 Variable Stiffness Laminate Design Study

A method of approximating the strength of variable stiffness laminates, based on the conservative formulation of the Tsai-Wu failure criterion presented in chapter 4, is presented by Khani et al. (2011). This approximation, which follows the approximation form presented in chapter 3, was used with the developed optimization framework to maximize the strength of the considered window-belt section, the results of which are presented in this section. The following design problems were considered:

VSD1: $\min_{\mathbf{V_i}} (\max r_i)$
VSD2: $\min_{\mathbf{V_i}} (\max r_i)$ with equivalent 5% rule
VSD3: Direct solution for $[\pm\theta_{1i}, \pm\theta_{2i}]_{2s}$
VSD4: Solution for $[\pm\theta_{1i}, \pm\theta_{2i}]_{2s}$ with curvature constraints

Note that subscript i indicates that the lamination parameters, $\mathbf{V}$, failure indices, r, and fiber angles, $[\pm\theta_1, \pm\theta_2]$, are defined independently for each of the i nodes within the structure.

In the first design problem, VSD1, the lamination parameter distribution maximizing laminate strength was obtained. In the second problem, VSD2, laminate strength was maximized while the stiffness was constrained to satisfy the equivalent five percent rule. This allowed the penalty of ensuring laminate robustness on maximum laminate strength to be evaluated. Two different methods were used to obtain the fiber angle distribution corresponding to the optimum found for VSD1. The first, VSD3, the local stacking sequence was solved analytically (Gürdal et al., 1999), while in the second case, VSD4, a fiber angle retrieval strategy developed by van Campen (2011) was used including constraints on in-plane curvature for which the retrieval algorithm was seeded with the results obtained from VSD3. The in-plane curvature constraints were based on the minimum achievable turning radius of two materials considered during the AUTOW-Project. The minimum turning radius, R_{min}, for these materials was 80mm and 200mm.

The critical strain and failure index of each optimal design are presented in Table 9.2, where unity indicates failure. It is immediately clear that substantial gains in strength are possible with proper stiffness tailoring. The designs indicate that strength improvements in the order of 100-350% are possible, both in terms of critical strain and in terms of failure index. The obtained lamination parameter distribution for designs #6 represented the theoretical optimum stiffness distribution for maximum strength in terms of the failure index. The critical hole edge strain of the optimum variable stiffness design, #6, was also substantially improved with respect to the baseline laminate. Enforcing laminate robustness through the equivalent five percent rule, resulted in the maximum failure index increasing with respect to design #6. Additional performance reduction occurred when converting stiffness distributions to fiber angle distributions, even if design constraints were neglected as in design #8. Incorporating constraints on minimum turning radius lead to a further decrease in maximum achievable strength, as can be seen for designs #9 and #10.

Table 9.2: *Summary of designs obtained for the different variable stiffness optimization problems. Manufacturable designs satisfying the equivalent five percent rule are marked* (ϵ_{cr}: critical hole edge strain, r_i: failure index)

#	Method	Laminate Info	ϵ_{cr}	$\max r_i$	5%	Man
6	VSD1	Lamination Parameters	0.2859	0.2157		
7	VSD2	Lamination Parameters, 5% Rule	0.3316	0.2692	✓	
8	VSD3	$[\pm\theta_{1i}, \pm\theta_{2i}]_{2s}$ for #6	0.3037	0.2884		
9	VSD4	R_{min} = 80mm for #6	0.4279	0.3424		✓*
10	VSD4	R_{min} = 200mm for #6	0.5828	0.3966		✓*

* Designs would require individual tow control for manufacturing, not available on the current machine

The optimal lamination parameter distribution corresponding to design #6 is presented in Figure 9.4. The lamination parameter distribution is difficult to interpret in detail, however, what is clear from the presented results is that a stiff band exists along the vertical axis alongside the hole, corresponding to the blue and red region in the $V_{1\mathbf{A}}$ and $V_{3\mathbf{A}}$ plots, respectively. The complex stress state around the hole however, makes it difficult to interpret the results here visually. Similar lamination parameter distributions were found for VSD2, where the five percent rule was enforced for laminate robustness, with the variation in lamination parameter distribution being slightly less pronounced due to the smaller available design space.

To interpret the optimal solution obtained in the lamination parameter space better, it was useful to solve for the corresponding fiber angle distribution, VSD3.

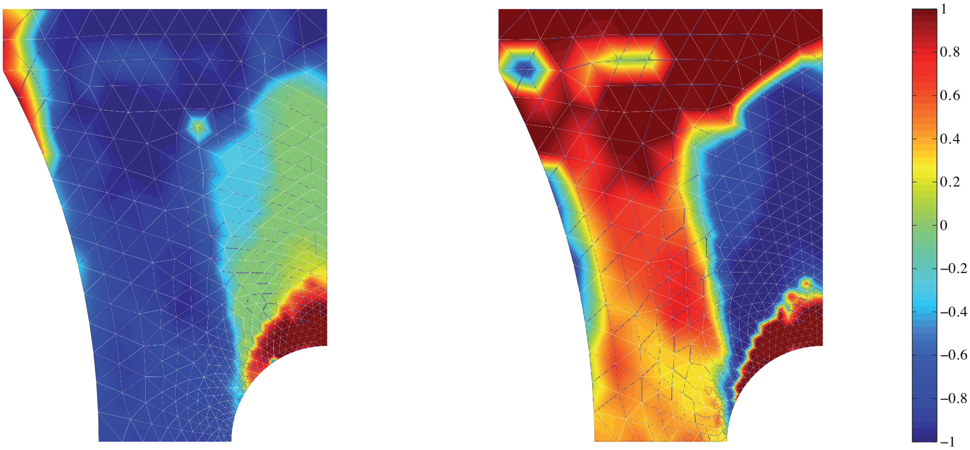

(a) $V_{1\mathbf{A}}$ (b) $V_{3\mathbf{A}}$

Figure 9.4: *Optimal lamination parameter distribution for maximum laminate strength*

Laminate strength for this design problem was only a function of laminate in-plane stiffness, therefore, a direct analytical solution method was used (Gürdal et al., 1999), which assumed that two design plies, $[\pm\theta_1, \pm\theta_2]_s$, of equal thickness were present. The method cannot always guarantee a real solution, nor can manufacturing constraints be taken into account, however, it does provide insight into possible fiber orientations. The obtained fiber angle distribution of one of the plies is presented in Figure 9.5(a), which highlights the following general trends; one, there is a stiffer vertical band containing 90° fibers alongside the hole spanning the entire length of the panel and two, there is a more compliant region with 0° fibers directly above the hole and the laminate becomes gradually stiffer, 20° to 50° fibers, towards the top edge of the panel. Including realistic manufacturing constraints resulted in less severe fiber angle variation and a less pronounced vertical band adjacent to the hole, as can be seen in Figure 9.5(b).

To understand how the stiffness distribution improves the strength of the panel, it was interesting to investigate the failure index distribution, plotted in Figure 9.6, for both the baseline laminate, design #1, and the optimal laminate stiffness distribution, design #6. The stress concentration, which is the red region found at the holes edge, causes initial failure, as can be seen in Figure 9.6(a). The effect of the stress concentration around the hole was reduced significantly by tailoring the stiffness distribution and the design tends to a "fully-stressed" design, as seen from Figure 9.6(b).

9.4 Manufacturable Designs using Linear Variation

In the previous section the developed strength optimization framework was used to demonstrate the potential improvements in strength that can be achieved using fiber steering. The results also provided insight into the effect of curvature constraints,

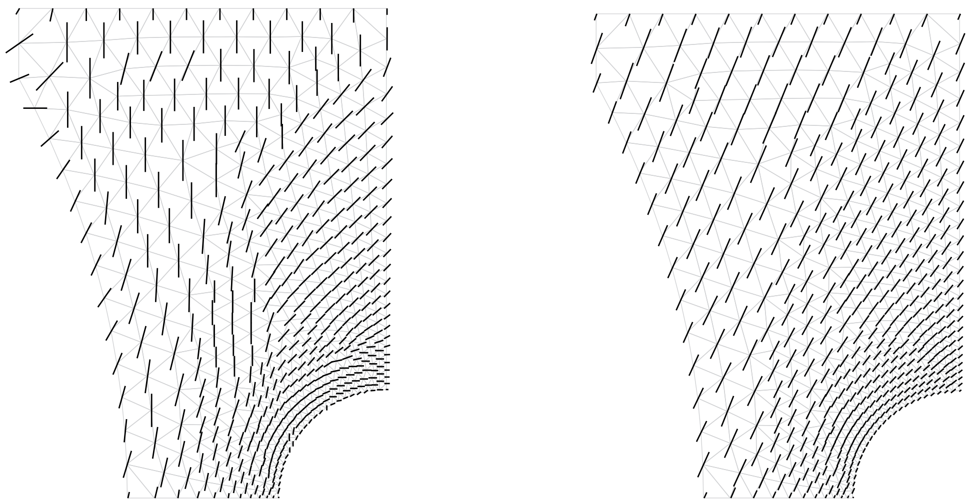

(a) $+\theta_2$ ply for design #8, without manufacturing constraints

(b) $+\theta_2$ ply for design #10, with a minimum steering radius of 200mm

Figure 9.5: *Fiber angle distributions of a single ply obtained for a* $[\pm\theta_1, \pm\theta_2]_s$ *laminate corresponding to the optimum lamination parameter distribution of design #6*

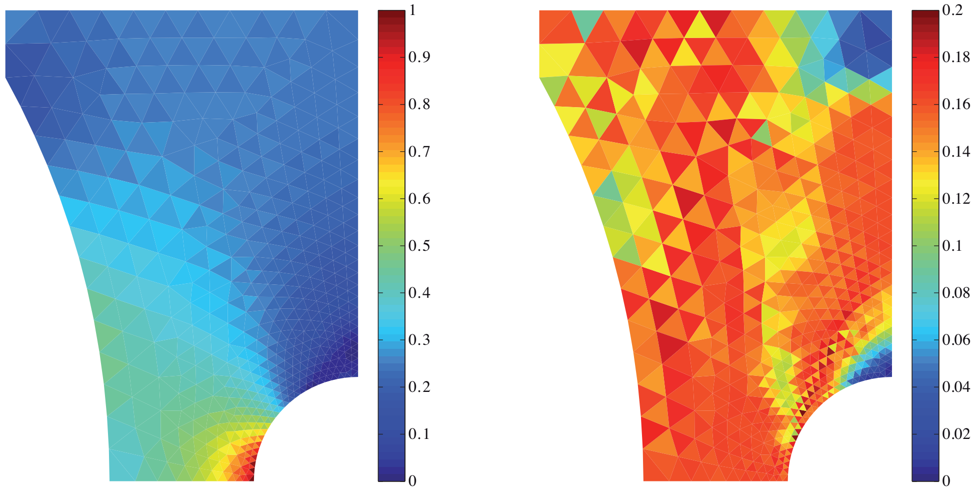

(a) Baseline design #1

(b) Variable stiffness design #6

Figure 9.6: *Failure index distribution for the baseline quasi-isotropic laminate, design #1, and the optimal variable stiffness laminate, design #6*

which are necessary to ensure manufacturability, on fiber path variations. Due to the limitations of the available fiber placement software and machine, additional manufacturing constraints had to be considered. Therefore, it was necessary to explore solutions that capture as much of the theoretical improvements as possible, however, these needed to be solutions that consisted of fiber paths that were readily manufacturable with the available hardware and software.

Linear variation, a fiber path parameterization scheme briefly discussed in section 1.3.1, was used to conduct two separate design studies. The parameters describing linear variation are schematized in Figure 9.7, where the fiber angle varies linearly from angle T_0 to angle T_1 over the characteristic distance d. The axis of variation, x', is rotated by angle ϕ with respect to the global x-axis. With this convention a layer can be represented in a compact notation by $\phi < T_0, T_1 >$. Linear fiber angle variation was used as it allowed manufacturable paths to be generated for the given hardware and software within the available time.

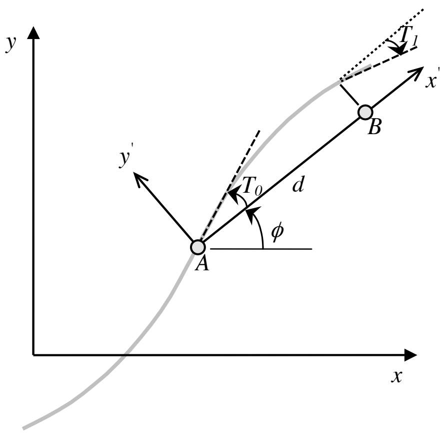

Figure 9.7: *Schematic representation of a fiber path defined using linear variation, which can be compactly denoted as $\phi < T_0, T_1 >$ and where d represents a predefined length over which the variation occurs (Reproduced from Gürdal et al. (2008))*

To convert a single fiber path into a ply, the fiber path should be repeated several times to cover the entire structure's surface. Two different fiber-path replication strategies were used, the parallel path method and the shifted path method, as shown in Figure 1.11. Designs obtained with the two aforementioned path replication strategies are presented in the following subsections.

9.4.1 Parallel Path Designs

Parallel paths are generated by placing each subsequent course adjacent to the previously placed course. The parallel path method has several advantages; one, no thickness variation occurs due to overlaps or gaps within a single ply, which simplifies manufacturing and comparison of steered and traditional laminate configurations. Two, the parallel path method exists as a standard replication strategy within existing fiber-placement software and therefore, entire plies can be generated automatically from a single course path. The primary disadvantage associated with parallel path designs is that the maximum curvature increases with each successively placed path, which may result in local fiber buckling or kinking. In practice this results in a decreased set of manufacturable fiber paths that can be considered. Additionally, the stiffness variation dictated by the parallel paths may not be suitable for the considered problem.

Since it was difficult to find intuitive parallel paths that suitably matched the trends in stiffness distribution found in section 9.3 a genetic algorithm was used to search for fiber paths. Critical hole edge strain was used as an objective function, equation (9.2). Due to the quarter-symmetry of the problem, the origin of the reference path coordinate frame (x,y) was centered at the center of the central hole (0,0). The characteristic distance, d, was set to 262.5 mm or 350 mm for variation along the x-direction or y-direction, respectively. This allowed the fiber angle, θ, to vary from T_0 to T_1 and back to T_0 along half of the plates length or width, which was believed best to capture the desired stiffness variation. The course width was taken to be 50 mm, equivalent to the width of eight, quarter-inch tows.

A genetic algorithm was used to search the design space for optimal solutions. Initial solutions were found to consist of four identical design plies, therefore, to make the designs more robust, such that they satisfied the equivalent five percent rule, the outer plies were replaced with a $\pm 40°$ ply. This in turn facilitates manufacturing as the steered plies can be placed on an already placed straight fiber ply. Two of the designs found using a genetic algorithm are presented Table 9.3. Both designs contain only mild-steering and tend to represent plies with fibers aligned primarily along the vertical axis. Both designs result in an increased load carrying capacity with respect to the baseline of between 50-55% in terms of critical strains or between 75-88% in terms of failure index.

Table 9.3: *Overview of two obtained parallel path designs, both designs are manufacturable and satisfy the equivalent five percent rule* (ϵ_{cr}: critical hole edge strain, r_i: failure index)

#	Method	Laminate Info	ϵ_{cr}	$\max r_i$	5%	Man
11	LVD1	$[\pm 40, 90 < \pm 10, 0 >_3]_s$	0.6454	0.5705	✓	✓
12	LVD1	$[\pm 40, 90 < \pm 15, 0 >_3]_s$	0.6643	0.5339	✓	✓

A sample ply and its balanced counterpart corresponding to the steered ply in design #12 are presented in Figure 9.8. As can been seen, the solution relies predominantly on aligning fibers along the load direction, however, it is not able to capture the desired softening above the hole, as was seen in the variable stiffness designs presented in section 9.3.

9.4.2 Shifted Path Designs

Using a parallel path strategy did not yield results with significantly large differences with respect to constant stiffness alternatives. Therefore, it was decided to explore the shifted-path replication strategy in order to find a steered solution that captures the desired stiffness distribution more accurately. Using shifted paths has the advan-

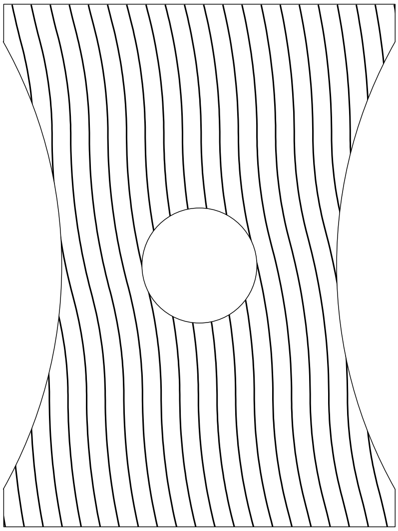

(a) Design #12: $90 < 15, 0 >$

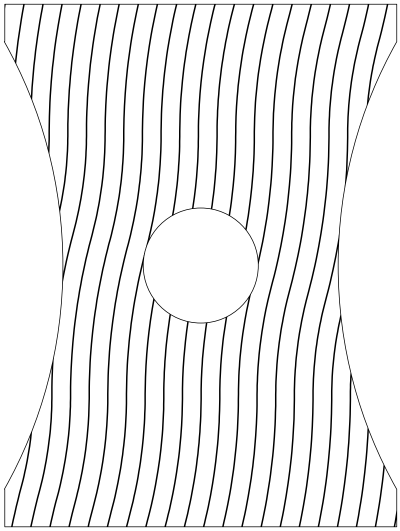

(b) Design #12: $90 < -15, 0 >$ (balanced ply)

Figure 9.8: *Plot of course centerlines of the parallel path design #12 and the corresponding balanced ply*

tage that the maximum curvature is identical for each path, while it can be easily implement in fiber-placement software by programming multiple fixed offsets of reference path. The primary disadvantage is that thickness variation will occur within the laminate due to gaps and overlaps, however, the location of the gaps or overlaps may be designed such that structural performance benefits from those features. As was the case for the parallel path method, stiffness variation is defined by a single path, which may not be suitable for the considered problem.

A parametric study, using the same reference path parameters as used in the parallel path study, was conducted to search for suitable fiber paths. The parametric study was conducted intuitively by defining paths resulting in stiffer vertical bands beside the central hole while softening towards the center of the panel. Using the shifted path strategy will inevitably result in a non-uniform thickness distribution within the laminate due to gaps or overlaps. In all of the considered designs the reference-path was shifted such that no gaps occurred, hence, only overlaps were present in all designs. This mitigated any issues associated with resin-rich areas, however, since the laminate thickness was not uniform, designs had to be selected such that they were comparable to those obtained in previous sections. Two options for comparison were available; one, the design could be chosen such that the failure load was identical to a reference design and subsequently compare panel weights, or two, the shifted path panels could be designed such that they had the same weight as the baseline. Predicting failure loads precisely using numerical methods is difficult and may vary with respect to those determined experimentally. Therefore, it was more suitable to select the second option as it was relatively straightforward to ensure equal weight designs. Thereafter, each design could be tested to failure and performance subsequently compared directly.

Table 9.4: *Overview of two obtained shifted path designs, both designs are manufacturable and satisfy the equivalent five percent rule* (ϵ_{cr}: critical hole edge strain, r_i: failure index)

#	Method	Laminate Info	ϵ_{cr}	$\max r_i$	5%	Man
13	LVD2	$[0 < \pm 68, \pm 80 >_2, \pm 35]_s$	0.5445	0.5049	✓	✓
14	LVD2	$[0 < \pm 40, \pm 80 >, \pm 40 \pm 90_2]_s$	0.5260	0.4111	✓	✓

Two of the best designs found during the parametric study are presented in Table 9.4. Note: due to the thickness buildup only 12 plies are required for both designs to have the same weight as the 16-ply baseline laminate. Both designs were found largely to satisfy the five percent rule, with design #14 having a small region within the laminate that slightly violated this constraint. The nature of the stiffness variation for both designs was similar with only the degree of stiffness variation changing. Design #14 was superior both in terms of critical strain and failure index, even though only 4 of the 12 plies were steered. Design #14 also had the largest degree of fiber angle variation and therefore the largest thickness buildup. Design #13 had slightly higher critical strain values, however, performance was worse in terms of failure index.

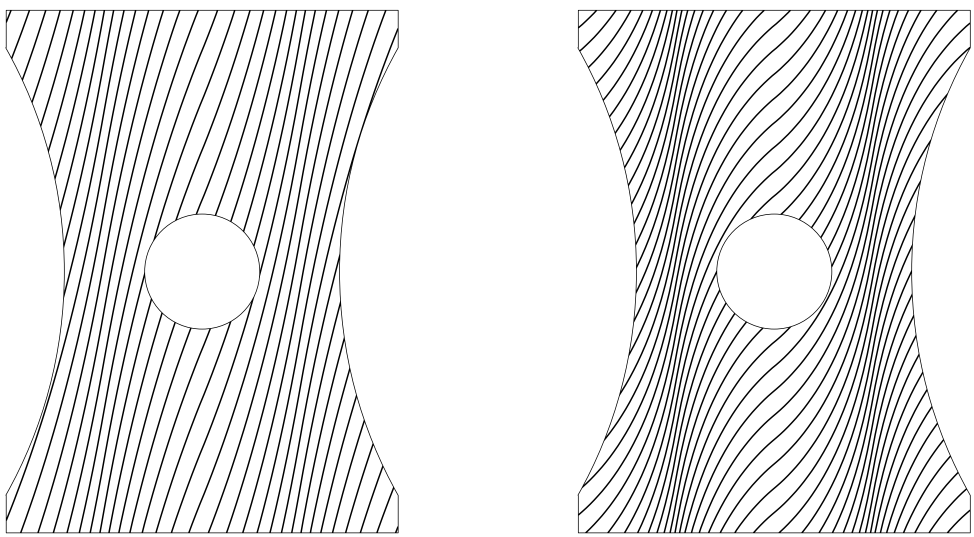

(a) Design #13 $< 68, 80 >$

(b) Design #14 $< 40, 80 >$

Figure 9.9: *: Plot of course centerlines of the shifted path designs #13 and #14, where closer course spacing corresponds to larger percentage of overlaps*

In order to visualize the obtained designs, the course centerline for designs #13 and #14 are presented in Figure 9.9. Both plies contain a comparatively soft section above the hole and become stiffer in the band alongside the hole. The designs result in overlaps occurring in the stiffer band, further reinforcing the load-redistribution to this band. The closer centerlines are to each other, the more thickness buildup occurs locally. The more severe fiber angle variation of design #14 resulted in larger thickness buildups.

The normalized thickness distribution of both laminates is presented in Figure 9.10. The thickness distribution was computed using the finer mesh, Mesh (2), to capture the overlaps that occur due to path shifting better. The maximum thickness for both laminates was similar, however, design #14 had a well defined thicker vertical band adjacent to the hole, essentially acting as a built-in stiffener transferring the majority of the loads around the hole.

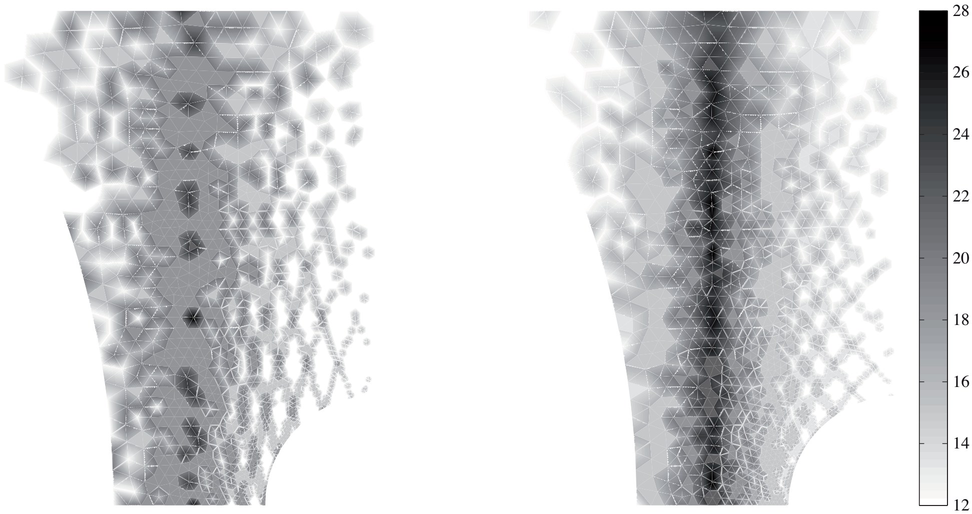

(a) Design #13 $< 68, 80 >$ (b) Design #14 $< 40, 80 >$

Figure 9.10: *: Plot of the thickness distribution of shifted path designs #13 and #14, where the colorbar indicates the total number of plies in the laminate at any given location. Due to steering, thicker vertical bands occur beside the hole that are almost twice as thick as the nominal laminate thickness of 16 plies.*

9.5 Design Comparison

The performance of the designs obtained using the different design methods are summarized in Table 9.5 and were computed using Mesh (1). Percent difference in critical hole edge strain and failure index with respect to design #1 are tabulated for each design. Note that the critical failure index was calibrated such that both failure criteria predict failure of the quasi-isotropic laminate for the same applied load, see section 9.1. Designs that were manufacturable using the available fiber placement machine and those satisfying the equivalent five percent rule are marked.

Table 9.5: *Overview of designs obtained for the different design problems. Manufacturable designs satisfying the equivalent five percent rule are marked* ($\%\epsilon_{cr}$ and $\%r_i$ = percent improvement in terms of critical hole edge strain and failure index, respectively, compared to the baseline)

#	Method	Laminate Info	$\%\epsilon_{cr}$	$\%r_i$	5%	Man
1	–	$[0_2, 90_2, \pm 45_2]_s$, baseline	0	0	✓	✓
2	CSD1	$[0_2, 90_4, \pm 45]_s$	27	16	✓	✓
3	CSD2	$[\pm 80_2, \pm 75, 90_2]_s$	63	58		✓
4	CSD3	$[\pm 67.5]_{4s}$	38	109		✓
5	CSD4	$[\pm 49, \pm 86]_{2s}$	38	92	✓	✓
6	VSD1	Lamination Parameters	247	361		
7	VSD2	Lamination Parameters, 5% Rule	199	270	✓	
8	VSD3	$[\pm\theta_{1i}, \pm\theta_{2i}]_{2s}$ for #6	227	245		
9	VSD4	$R_{min} = 80$mm for #6	132	191		✓*
10	VSD4	$R_{min} = 200$mm for #6	70	151		✓*
11	LVD1	$[\pm 40, 90 < \pm 10, 0 >_3]_s$	54	74	✓	✓
12	LVD1	$[\pm 40, 90 < \pm 15, 0 >_3]_s$	49	86	✓	✓
13	LVD2	$[0 < \pm 68, \pm 80 >_2, \pm 35]_s$	82	97	✓	✓
14	LVD2	$[0 < \pm 40, \pm 80 >, \pm 40 \pm 90_2]_s$	89	142	✓	✓

* Designs would require individual tow control for manufacturing, not available on the current machine

The best constant stiffness design satisfying the five percent rule was design #5 and this was 38% stronger than the baseline design in terms of critical hole edge strain. Design #5 was optimized in terms of the failure index, which was improved by 92% with respect to the baseline laminate.

The theoretically optimal solution, design #6, was found in terms of lamination parameters and by far supersedes all other designs both in terms of critical strain and failure index. Even when constraining laminate robustness, design #7, theoretical stiffness distributions resulted in strength improvements of 199% and 270% in terms of critical strain and failure index, respectively. Converting design #6 into a stacking sequence while enforcing realistic turning radii, designs #9 and #10, resulted in improvements in the failure index in the order of 150-190%.

The two designs found using parallel path fiber path shifting, which had uniform thickness, showed improvements of roughly 50% with respect to the baseline design in terms of strains and 75-85% in terms of failure index. Both designs were readily manufacturable and contained only mild-steering. The designs did not fully capitalize on the benefits that could be achieved with steering, as the steered plies only deviate slightly from a straight fiber configuration containing 90° plies. In fact, the straight fiber design #4 is comparable in terms of strength. The shifted path designs #13 and #14 showed strength improvements between 80-90% in terms of strain and more than 95% in terms of failure index with respect to the baseline. These designs were believed best to capture the desired stiffness distribution found in the theoretical studies conducted with lamination parameters. These designs yielded a particularly elegant solution in which the optimal fiber angle distribution also resulted in a beneficial thickness distribution, taking full advantage of the fiber steering capabilities.

A trade-off meeting took place together with Dassault Aviation to select a design for manufacturing and testing. The parallel path and shifted path designs were compared in terms of their relative performance, ease of manufacturing and to see if the capabilities of steering were adequately demonstrated, however, the primary design selection driver was the total time required to manufacture the selected design due to the tight project timeline. The fiber placement software available at Dassault only allowed a single spline to be shifted in parallel and hence, designs #10 and #11 were most suited from a manufacturing point of view, however, in terms of demonstrating the benefit of fiber placement the shifted path designs #13 and #14 were most suitable. Due to time restrictions it was decided to manufacture the parallel path design with most steering, hence design #11 was selected to be manufactured.

9.6 Concluding Remarks

Several design studies were conducted to maximize the strength of a simplified window-belt section of a light business aircraft and the results presented in this chapter. Designs were presented for traditional straight fiber laminates and for variable stiffness laminates. Two strength criteria were used; one, based on hole edge strain values defined by Dassault Aviation, and two, a failure index based on the Tsai-Wu criterion as presented in chapter 4. An approximation of the failure index, satisfying the approximation form presented chapter 3, is developed by Khani et al. (2011). The variable stiffness optimization framework developed in chapter 2 was subsequently used to maximize laminate strength in terms of lamination parameters successfully. Constraints on laminate robustness, via an equivalent five percent rule presented by Abdalla et al. (2009a), and manufacturing, by limiting fiber path curvature, were also applied. Tailoring laminate stiffness properties yielded a 350% increase in theoretical laminate strength with respect to a quasi-isotropic baseline laminate. Imposing constraints on laminate robustness and minimum steering radius to ensure manufacturability limited the achievable strength increase to 150% with respect to the baseline design.

Due to time limitations and constraints imposed by the available fiber placement software and hardware, alternative designs based on linear fiber angle variation were also obtained. Designs using parallel path and shifted path replication strategies were studied. The shifted path strategies were found to match the stiffness distributions obtained in the theoretical studies best and also yielded the largest improvements in strength. Due to software limitations it was, however, only possible to manufacture parallel path designs. The parallel path design selected to be manufactured had an ultimate load 49% higher than the baseline design in terms of hole edge strain and 86% higher in terms of failure index.

It is interesting to note that the trends in improved laminate strength were not always consistent in terms of critical edge hole strain and failure index. It would therefore also be interesting to study the origin of the difference in results obtained when using the two different failure criteria as objective function.

CHAPTER 10

Design Application: Aircraft Wing Rib

"*Experience is a hard teacher because she gives the test first, the lesson afterwards*"

Vernon Law

The design and manufacture of a full-scale demonstrator using dry-fiber placement was one of the main hardware related deliverables of the AUTOW-Project. A sine-wave rib, located close to the wing-root of a large business aircraft, was selected as the most suitable demonstrator component for the developed technologies. Israel Aerospace Industry (IAI) was responsible for providing the design requirements, finite element modeling and laminate design for the demonstrator, which was manufactured and tested during the project. A competitive variable stiffness design was also developed to demonstrate the capabilities of the design optimization approach presented in this thesis. Initially the objective was to design the same full-scale test article designed and manufactured by the industrial partners. Due to the geometric complexity of the sine-wave rib, it was decided to investigate an alternative design, which was geometrically less complex, yet made use of fiber steering to improve structural performance. For this example problem the optimization routine was coupled with NASTRAN™ to conduct all analysis and sensitivity computations, thereby also demonstrating how to integrate the developed framework with a commercial finite element code.

The geometric description, finite element model and design requirements of both the original sine-wave rib and a geometrically less complex alternative are presented in section 10.1. In order to couple the developed optimization framework to the

The work presented in this chapter was conducted as part of the AUTOW-Project, see http://www.autowproject.eu for more details. Several results and figures published in project deliverables D15, D16, D23 and D25 have been used and are not original work done by the author. The author would like to thank Israel Aerospace Industries (IAI) and Institut für Flugzeugbau (IFB) for their contributions to the presented research.

chosen commercial finite element environment the desired sensitivity data had to be obtained, several post-processing computations were required and are described in section 10.2. The obtained numerical results are presented and discussed in section 10.3, followed by conclusions in section 10.4.

10.1 Problem Description

Israel Aerospace Industries provided the design requirements, initial geometry and loading for the studied full-scale component based on typical load cases used internally when designing light business jets. The sine-wave rib used is located towards the central wing-box and therefore, is subject to high-crushing loads due to global wing bending and local aerodynamic forces. The sine-wave rib is shown schematically in Figure 10.1 within a test-rig designed to replicate the considered load case. The test-rig consisted of a front and rear lug to simulate the connection of the rib to the front and rear spar and the top and bottom wing skins, which were stiffened to prevent them from buckling during testing. The test-rig load case was derived from aircraft-level finite element analysis to ensure that loads present in reality were replicated during the test.

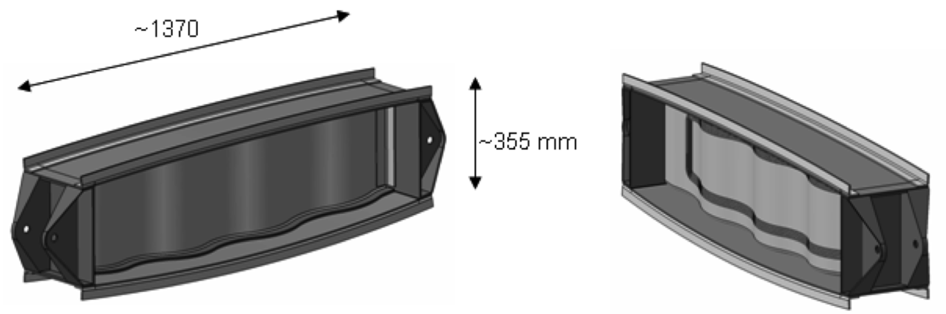

Figure 10.1: *Schematic representation of a sine-wave rib within the used test-fixture with a rough indication of the overall dimensions (Source IAI)*

10.1.1 Design Requirements

The design requirements were provided by Israel Aerospace Industries in a technical report by Aharon et al. (2009). The design objective was to minimize overall structural weight while meeting the design requirements discussed below.

Load requirements:

- Ultimate load 1.5 times limit load
- No buckling up to ultimate load is allowed
- Strength criteria: maximum strain and stress damage tolerance values
- Considered loads: aerodynamic loads, crushing load, wing fuel tank pressure

Four individual load cases were defined. Two were based on SBT-envelope diagrams (Shear, Bending and Torsion) for a typical business jet wing. Additionally, wing-crushing load and fuel pressure load cases were defined. These load cases were subsequently used to define the load distribution on the test-rig used for the experimental program to replicate the loads experience by the rib in reality. A schematic overview of the applied loads and boundary conditions is presented in Figure 10.2. The loads, P1 to P7, are distributed forces applied on a predefined area and are all of different magnitude. The front lug is restricted from translation in all directions while the rear lug is on a sliding support.

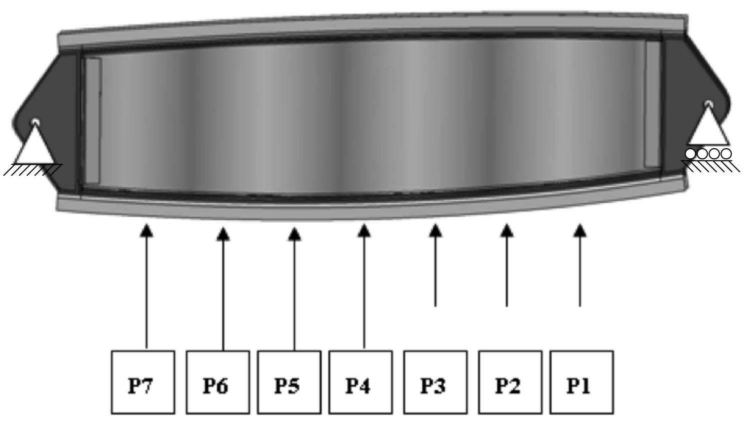

Figure 10.2: *Schematic representation test-fixture loads (Source IAI)*

Material specifications and environmental conditions:

- A-basis material allowables, at extreme environmental conditions, were used
- Nominal fiber volume of 60% was assumed with cured ply thickness of 0.13 mm
- Service temperatures ranging from $-55°C$ to $+70°C$
- Lightning strike protection - glass ply insulation used at fastener locations
- Prevention of galvanic corrosion of the wing skin
- Fuel resistance - the used resin system was assumed to be fuel resistant

The material properties of the dry-fiber material developed during the AUTOW-Project were unavailable during the design process. Therefore, material properties for carbon-epoxy IM7/8552, listed in Appendix A, were used as was done by Israel Aerospace Industries. The A-basis values were used to account implicitly for the imposed environmental conditions, because the ribs are considered as single load path structural members within the wing-box. Aluminum with an elastic modulus of 73 GPa and a Poisson's ration of 0.3 was used for the wing skins, stiffeners are front and rear lug.

Manufacturing specifications:

- Fabrication tool is IML based
- Interfaces and tolerances were specified
- Account for AUTOW fiber placement machine limitations

The rib was manufactured at the Dutch National Aerospace Laboratory (NLR) using the available automated fiber placement machine. The following design requirements, related specifically to the used manufacturing technology, were considered:

- Tows require approximately 50 mm of preceding length to be laid up
- No individual tow-cutting available, hence results in a "saw-tooth" pattern
- Minimum steering radius 200mm
- The maximum gap between tows is about 2 mm
- Minimum radius between flange and web is 10 mm

Fastener specifications:

The rib is connected at the top and bottom wing skin by a double row of fasteners along the flange with a pitch of seven times the fastener diameter of $3/16^{\mathrm{th}}$ of an inch. The two rows of fasteners are separated by 20 mm while the outer trace is located 12.91 mm from the flange edge. A similar double row of fasteners is applied to connect the rib to the front and rear lug with a pitch of 4 times the fastener diameter. Fasteners were modeled using CBUSH elements in NASTRAN or spot-welding connections in Catia V5$^{\mathrm{TM}}$.

10.1.2 Sine-Wave Rib Geometry

The sine-wave rib geometry is presented schematically in Figure 10.3 and roughly has a length of 1370 mm and a hight of 350 mm with a flange width of 51mm. The rib consists of two zones; Zone A, which contains the flange and the outer sections of the web. Laminate sizing in this region is driven primarily by the bearing stresses due to the fasteners. The second region, Zone B, consists of the inner web and is thinner than the outer web and flange regions.

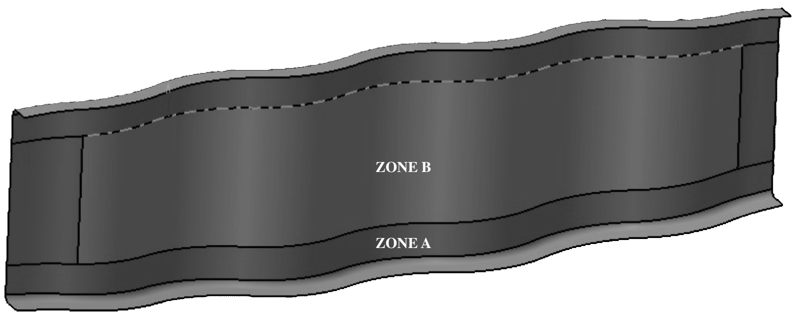

Figure 10.3: *Sine-wave rib geometry and design zones (Source IFB)*

10.1.3 Flat Rib Geometry

The objective was to replace the geometrically complex sine-wave rib with an equivalent flat rib. The less complex geometry simplifies both the required tooling and manufacturing process and hence, should also result in reduced part cost. The flat rib geometry, presented in Figure 10.4, was derived from the sine-wave geometry and simply follows the centerline of the sine-wave rib, essentially connecting the already flat front and rear sections of the sine-wave rib. As for the sine-wave rib, the flat rib was divided into an outer region, Zone A, containing the flange and outer sections of the web and an inner region, Zone B, containing a thinner inner web section. The fastener specifications for the flat rib remain as before, however, overall test-rig loading was modified slightly to ensure that the applied distributed loads were aligned with the rib centerline.

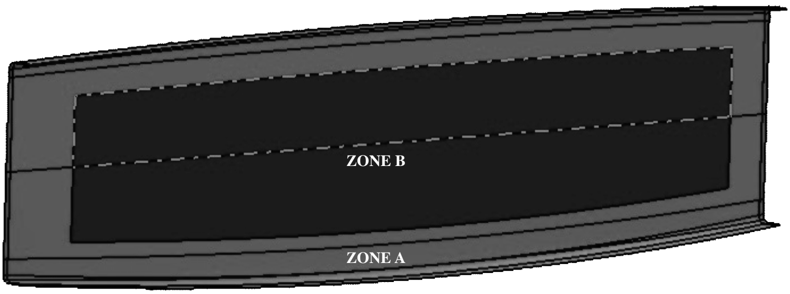

Figure 10.4: *Flat rib geometry and design zones (Source IFB)*

10.1.4 Problem Formulation

The primary reason for introducing an out-of-plane sine-wave in the rib geometry is to help the structure resist the large crushing loads present due to both aerodynamic and wing bending forces. Compressive loads typically result in structural instability or buckling. The out-of-plane dimension of the sine wave increases the second moment of area, which is directly related to the stability characteristics of the part, however, the increased geometric complexity results in additional manufacturing difficulties and cost.

The goal of the presented design study was to investigate the possibility of using a geometrically less complex part, a flat rib, to replace the sine-wave rib meeting the same design requirements presented in section 10.1.1. Since buckling is the critical load case for this structure, it was selected as the primary design driver and this allowed the design optimization approach presented in chapter 8 to be used. Weight was not minimized directly as it is a discrete function of the number of plies, however, a fixed laminate thickness was defined such that the final design contained the minimum number of plies necessary to meet the imposed design requirements. The optimization problem was therefore formulated simply as obtaining the stiffness distribution, $\mathbf{V}$, such that the critical buckling load is maximized:

$$\max_{\mathbf{V}}(\lambda_{cr}) \tag{10.1}$$

For several practical reasons only the stiffness distribution of the inner web region, Zone B, was designed. The laminate layup defined in Zone A was defined by Israel Aerospace Industries and was not modified for the variable stiffness design process. The layup was driven primarily by the bearing stresses presented due to the fasteners, which was difficult to include in the variable stiffness design process developed thus far. Additionally, due to the workaround required to compute buckling sensitivity data, the finite element analysis would become unmanageable for models requiring sensitivities for more than a thousand elements.

10.2 Response and Sensitivity Analysis

In order to apply the developed optimization framework together with a commercial finite element code it is necessary to ensure that the correct response and sensitivity data is obtained from the analysis. In this case NASTRAN was used to conduct the finite element analysis using the SOL-200 solution sequence to compute the required sensitivities. In NASTRAN design variables are defined using the DESVAR card and can subsequently be related to material stiffness properties in the MAT2 card via the DVMREL card. The MAT2 cards allow the thickness independent part of the ABD stiffness matrices to be defined. The actual laminate thickness is subsequently included via the PSHELL card. Details are not included here for brevity, however, they are well documented in NASTRAN's Design Sensitivity and Optimization user's guide by MSC-Software (2005).

The developed approximation form for the inverse buckling factor, presented in chapter 8, requires terms related to the geometric stiffness matrix to be expanded linearly in terms of nodal stiffness properties, whereas the terms related to the global stiffness matrix are expanded reciprocally. Therefore, to obtain sensitivity data from NASTRAN in the correct form, several issues must be considered:

1. the response and sensitivity values must be inverted
2. sensitivity data with respect to the geometric stiffness and material stiffness matrices must be separated
3. stiffness and sensitivity data must be interpolated from elements to nodes and vice-versa

A script was created to extract and post-process the sensitivity and response data from the NASTRAN output files using the steps described below. Once formatted correctly, the data could be integrated directly into the previously developed design optimization framework. The stiffness distribution obtained after a single iteration of the optimizer was subsequently used to write an updated NASTRAN input deck to be used for the next design iteration. This process was repeated until the predefined convergence criteria was met.

Inverting response and sensitivities

As mentioned previously, to maximize the buckling load the inverse of the buckling load factor is considered as the objective function. Since NASTRAN computes the buckling load factor, it must be inverted externally:

$$r_b = \frac{1}{\lambda} \tag{10.2}$$

This also implies that the sensitivities are computed with respect to the buckling load multiplier and not its inverse. Therefore, the required sensitivities, $\partial r_b / \partial \mathbf{A}_e$, must be computed via the chain rule,

$$\frac{\partial r_b}{\partial \mathbf{A}_e} = -\frac{1}{\lambda^2}\frac{\partial \lambda}{\partial \mathbf{A}_e} \tag{10.3}$$

where $\partial\lambda/\partial\mathbf{A}_e$ is the sensitivity of the buckling load multiplier, λ, with respect to the in-plane stiffness of an arbitrary element. The same relation holds for the bending stiffness related sensitivities.

The stiffness properties of a single element in NASTRAN are constructed using four MAT2 cards via a PSHELL card. The design variables are related to the MAT2 card entries, and are per definition independent of laminate thickness. The sensitivities output by NASTRAN only contain the material dependent terms, and hence should be post-process to account for the laminate thickness such that:

$$\frac{\partial \lambda}{\partial \mathbf{A}_e} = \frac{1}{h}\frac{\partial \lambda}{\partial \hat{\mathbf{A}}_e} \tag{10.4}$$

where $\partial\lambda/\partial\hat{\mathbf{A}}_e$ is the sensitivity of the buckling load with respect to element stiffness $\hat{\mathbf{A}}_e$ related only to the material dependent MAT2 terms. The same approach should be used to account for thickness for the bending stiffness sensitivity terms.

Separating geometric stiffness and material stiffness sensitivities

The developed optimization framework requires the construction of a convex approximation of the objective function to ensure solution convergence. In chapter 8 it was shown that the sensitivities related to the material stiffness matrix in the buckling eigenvalue approximation, see section (8.10), are strictly convex. However, this is not the case for the geometric stiffness matrix terms, therefore, to construct an appropriate approximation, the contribution of these two terms to the buckling sensitivities must be separated.

In NASTRAN the contribution of the geometric stiffness matrix to the overall buckling sensitivities is neglected by default, hence, the sensitivities only contain the derivatives with respect to the material stiffness matrix. The contribution of the geometric stiffness matrix can be included by setting a parameter, PARAM DSKON = 1.0, in the bulk data file. Therefore, the individual contribution of the geometric stiffness matrix to the total sensitivity can be isolated by subtracting the material stiffness dependent sensitivity from the total sensitivity. In other words, in order to construct the desired hybrid approximation using NASTRAN, the sensitivity analysis must be conducted twice, once including the geometric stiffness and once neglecting it. Additionally, the sensitivities related to the material stiffness matrix are expanded reciprocally with respect to the in-plane and bending laminate stiffness, therefore, $\partial\check{r}_b/\partial\mathbf{A}_e^{-1}$ is required, which can be shown to be:

$$\frac{\partial \check{r}_b}{\partial \mathbf{A}_e^{-1}} = -\mathbf{A}_e \cdot \frac{\partial \check{r}_b}{\partial \mathbf{A}_e} \cdot \mathbf{A}_e \tag{10.5}$$

where $\partial\check{r}_b/\partial\mathbf{A}_e^{-1}$ is the derivative of the material dependent part of the inverse buckling load with respect to the compliance.

Interpolating data between nodes and elements

A process of linear interpolation of compliance between nodes and elements was described in section 2.3.6 in an effort to ensure smoothness of the obtained stiffness distribution. The design variables are defined at nodes, however, for finite element analysis the stiffness matrices are required for each element. Therefore, the stiffness of each element is defined as:

$$\bar{\mathbf{A}}_e^{-1} = \sum_{i \in \mathcal{I}_e} w_{e,i} \mathbf{A}_i^{-1}$$

where i denotes the node numbers and $\mathcal{I}_e$ is the set of nodes connected to element e. The sum is weighed by integration weighing coefficients w_e as discussed in section 2.3.6. When using triangular elements, as was the case here, the weighing factors simplify to 1/3. Therefore, the element compliance matrix is constructed by adding a third of the compliance matrix of each attached node. Since the sensitivities are computed at element level in NASTRAN, the inverse interpolation process must be applied to obtain the sensitivities at nodes. The same process must be applied to the flexural stiffness terms.

Workaround Buckling Sensitivities

The sample problem studied in chapter 5 was used to verify the correct integration of the optimization framework and NASTRAN. During initial testing, errors were identified in the sensitivity data being computed by NASTRAN (version 2010, first release). A workaround was provided by MSC Software, however, it caused significant increase in required analysis time. Therefore, design studies were limited to models with fewer than a thousand elements for which sensitivities were to be computed. With the workaround implemented, the design optimization results using NASTRAN for the aforementioned sample problem were found to correlate well with previously obtained results.

10.3 Numerical Results

The numerical results for both the sine-wave rib and flat rib are presented in this section. First the initial finite element model, laminate design and numerical results provided by Israel Aerospace Industries for the manufactured sine-wave rib are presented as a baseline. Subsequently, the stiffness distribution of the inner web section of the sine-wave rib was optimized for maximum buckling load. Even thought designing the stiffness distribution of the sine-wave rib was not in the current project scope, it was optimized for two reasons; one, to demonstrate that the optimization framework also works for more complex structural geometries, and two, to have an additional benchmark for result comparison. Finally, the optimal stiffness distribution and total laminate thickness for the inner web section of the flat rib, meeting the design requirements imposed in section 10.1, is presented in section 10.3.3.

10.3.1 Baseline Sine-Wave Rib

The initial sine-wave rib design and finite element model was provided by Israel Aerospace Industries. The laminate stacking sequences for both the thicker flange section and thinner inner web section are presented in Table 10.1. The flange, with a total thickness of 3.77 mm, consists of 29 plies. The 0° plies in the flange are not straight but following the sine-wave geometry. The inner web, with a total thickness of 1.95 mm, consists of 15 plies that run continuously from the flange into the inner web section, hence 14 plies are dropped from the flange to the inner web section. In the manufactured product, plies were dropped off progressively to avoid a sudden change in laminate thickness, however, these details were not accounted for in the finite element model.

Table 10.1: *Laminate stacking sequence for Zone A, the flange, and Zone B, the web, as defined by Israel Aerospace Industry for the manufactured sine-wave rib. A total of 14 plies were dropped from the flange to the web area.*

Ply #	1	2	3	4	5	6	7	8	9	10	11	12	13	14	15
Zone A	0	90	45	90	-45	0	45	90	-45	0	45	90	0	-45	0
Zone B	0	90					45	90	-45	0		90			0

Ply #	16	17	18	19	20	21	22	23	24	25	26	27	28	29
Zone A	-45	0	90	45	0	-45	90	45	0	-45	90	45	90	0
Zone B			90		0	-45	90	45					90	0

Israel Aerospace Industries reported a buckling load factor, λ_{cr}, of 2.61 for the aforementioned sine-wave rib design. The corresponding critical buckling mode is presented in Figure 10.5 and is characterized by local buckling of the web section with four diagonal half-waves. The reported maximum and minimum principle strains were 4700 μs and -5490 μs respectively while the principle shear strain was reported to be 5760 μs.

10.3.2 Optimized Sine-Wave Rib

The initial finite element model provided by IAI contained in excess of 28000 quadrilateral elements. As mentioned in section 10.2, a workaround was required to compute the required sensitivity data, which limited the amount of elements used for design to approximately a thousand. The laminate stiffness distribution was optimized for the inner web section only, hence, the number of elements in this region were limited. A mesh refinement study was conducted by IFB to determine the minimum number of elements which could be used in this region while still capturing the correct buckling modes. A final model was selected, shown in Figure 10.6, and contained approximately 1300 elements and 761 nodes in the inner web region. The buckling load predicted by this model was approximately 9% higher than the original model. Triangular elements were used for the inner web to simplify the interpolation of sensitivity and stiffness values between nodes and element centroids.

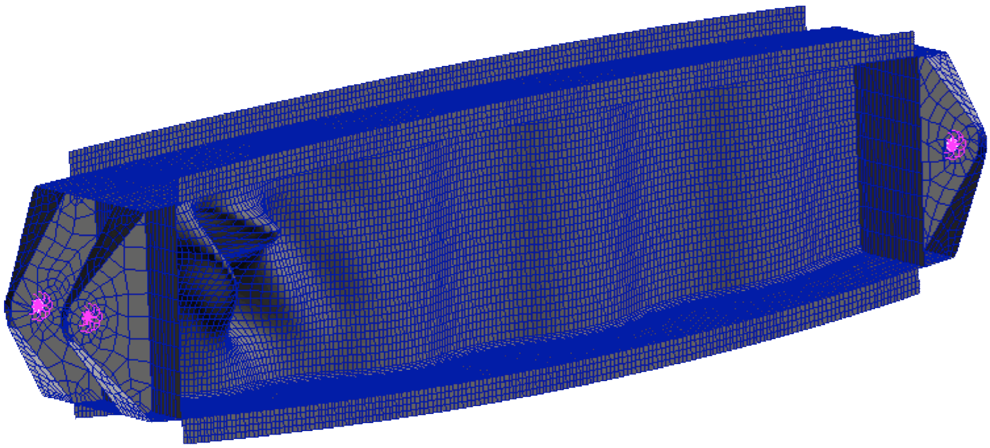

Figure 10.5: *Critical buckling mode and original finite element model for the original design. A critical buckling load factor, λ_{cr}, of* 2.61 *was reported (Source IAI)*

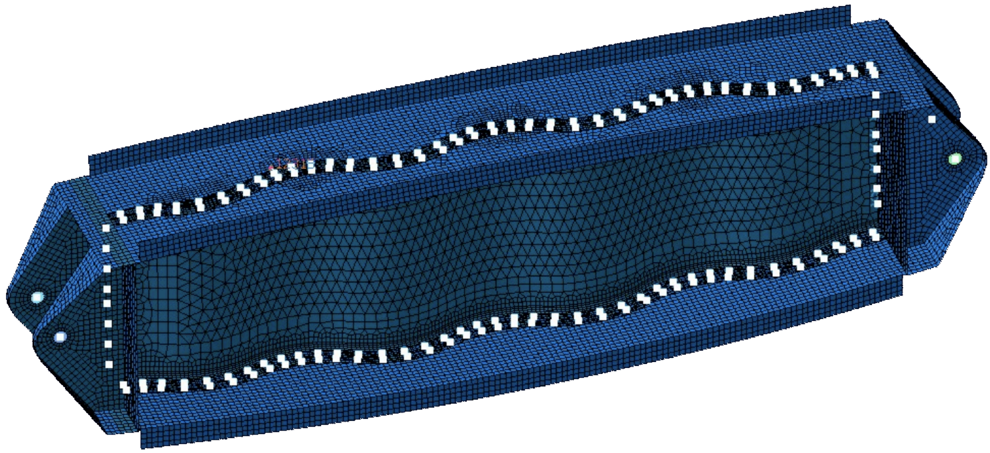

Figure 10.6: *Final sine-wave rib finite element model with the inner web mesh containing* 1373 *triangular elements for which the individual laminate stiffness properties were optimized (Source IFB)*

A total of ten eigenvalues were included during the optimization. The design problem was solved using four processors for both analysis and optimization and required a total of 63 hours, or 2.65 days, to complete. A total of nine analysis iterations were required till convergence, of which five were accepted as a feasible descent step. Four iterations were rejected and only used to update the optimizer damping values. The optimum lamination parameter distributions are presented in Figure 10.7 and were found to be very intricate, which made it difficult to interpret the results intuitively and are therefore provided for completeness.

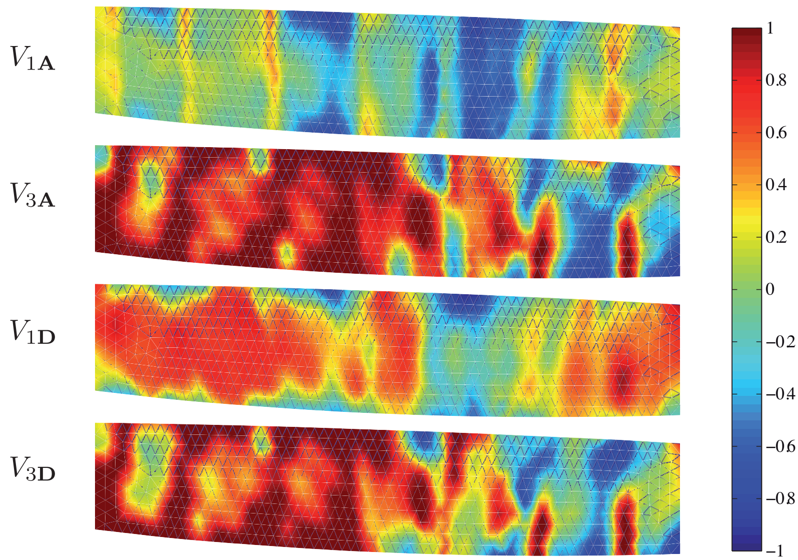

Figure 10.7: *Optimum lamination parameter distributions for maximum buckling load of the sine-wave rib model*

The first two critical buckling loads for the obtained designs are presented in Table 10.2. The optimum variable stiffness design based on lamination parameters was found to have a critical buckling load approximately 30% higher than the baseline design provided by Israel Aerospace Industries and 20% higher than an equivalent quasi-isotropic design.

Table 10.2: *Summary of buckling loads for the different laminate designs of the sine-wave rib inner web. The percent difference in weight, Δw, is computed with respect to the total weight of the baseline sine-wave rib. The layup in the flange and outer web remained identical to that of the baseline design provided by Israel Aerospace Industries (IAI)*

Layup	**# of Plies**	$\boldsymbol{\lambda}_1$	$\boldsymbol{\lambda}_2$	$\%\boldsymbol{\Delta}w$
Baseline Layup by IAI	15	2.8947	3.0752	0.0
Quasi-Isotropic ($\mathbf{V} = 0$)	15	3.0564	3.2508	0.0
VS Optimum - Lamination Parameters	15	3.7192	3.7997	0.0

The critical buckling modes of the quasi-isotropic and variable stiffness designs are presented in Figure 10.8. The buckling modes consist primarily of several local buckles towards the end of the rib, which corresponds to the region of the largest crushing load. The increased load carrying capacity of the sine-wave rib compared to the flat rib is due to the geometry, which isolates the buckles to a smaller region.

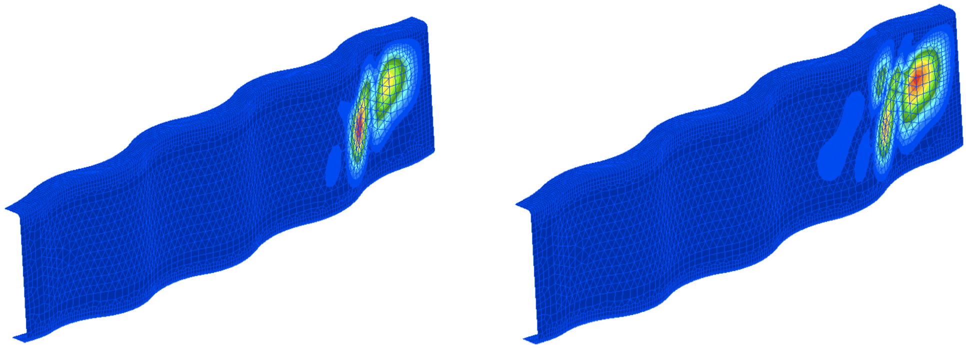

(a) Quasi-isotropic laminate (b) Optimal variable stiffness laminate

Figure 10.8: *Critical buckling modes of the sine-wave rib for the quasi-isotropic and optimum variable stiffness laminates*

10.3.3 Optimized Flat Rib

A geometrically less complex flat rib design is presented in this section as an alternative to the original sine-wave rib design present by Israel Aerospace Industries. The objective was to obtain the lightest possible design while allowing fiber steering in the inner web section. The laminate layup of the outer web and flange, Zone A, was left unchanged. The rib is buckling critical, therefore, the stiffness distribution and final fiber angle distribution were designed to maximize the buckling load. The laminate thickness in the central section was selected empirically such that a feasible, balanced symmetric design could be obtained.

As for the sine-wave rib, a finite element model with a suitable amount of elements in the inner web section was required to ensure a tractable optimization problem. After conducting mesh sensitivity studies, a final model, shown in Figure 10.9, was selected with a total of 748 elements and 431 nodes in the inner web section. The flat rib was less sensitive to mesh refinement than the sine-wave rib and the buckling loads for the course model used differed by approximately 2% with respected to further refined models.

Initially several finite element analysis runs were conducted to determine the initial performance of the flat rib configuration. Using the same 15-ply laminate configuration as the sine-wave rib resulted in a critical buckling load multiplier, λ_{cr}, of 0.477, whereas a minimum of 1.5 was required to meet the design requirements. Adding an additional 90° ply, which results in the flat rib having the same total weight as the sine-wave rib, yielded a buckling load multiplier of 0.603, which is still substantially

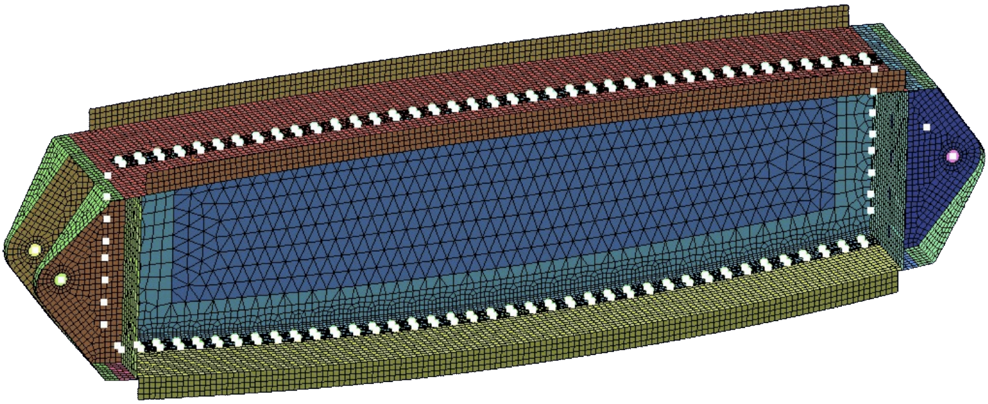

Figure 10.9: *Flat rib finite element model with the inner web mesh containing* 748 *triangular elements for which the individual laminate stiffness properties were optimized (Source IFB)*

below the required value. Therefore, it was decided to conduct the optimization using a 24-ply laminate, with a total thickness of 3.12 mm, in the inner web sections such that a feasible final solution was found.

A total of 1724 design variables, four per node, and the ten most critical eigenvalues were included in the optimization process. Four parallel processors where used to conduct the finite element analysis runs while a single processor was used for the optimization process. A total time of 89 hours, or 3.7 days, was required, where the largest computational cost was attributed to the finite element and sensitivity analysis required to obtain the appropriate information for the optimizer. A total of 21 iterations, of which 15 were accepted as feasible decent steps, was required to find the optimum. Six iterations were rejected, however, the rejected solutions were used to calibrate the damping values in the developed adaptive damping scheme as explained in section 3.3.3.

The convergence behavior of the buckling solution is presented in Figure 10.10. The required design value of the inverse buckling factor, $1/\lambda_d = 1/1.5 = 0.66$, is also plotted. Several interesting observations can be made from this figure; one, the approximate function value is initially not conservative, however, the adaptive damping scheme developed in chapter 2, ensures that it becomes conservative as the optimization progresses. Two, even though the problem is relatively complex both in terms of geometry and response, both the actual and approximate function value exhibit good convergence behavior. Three, we note that at the optimum the inverse buckling load multiplier satisfies the requirement of being less that 0.66, and therefore a feasible solution in terms of buckling is found.

The lamination parameter distributions for the optimum solution are presented in Figure 10.11. However, as was the case in earlier examples, it is difficult to physically interpret the solution from these distributions. Therefore, the results were included for completeness.

The optimal lamination parameter distribution was subsequently used to obtain a suitable fiber angle distribution best matching the optimal laminate stiffness distribution while satisfying the imposed manufacturing constraints. The obtained variable

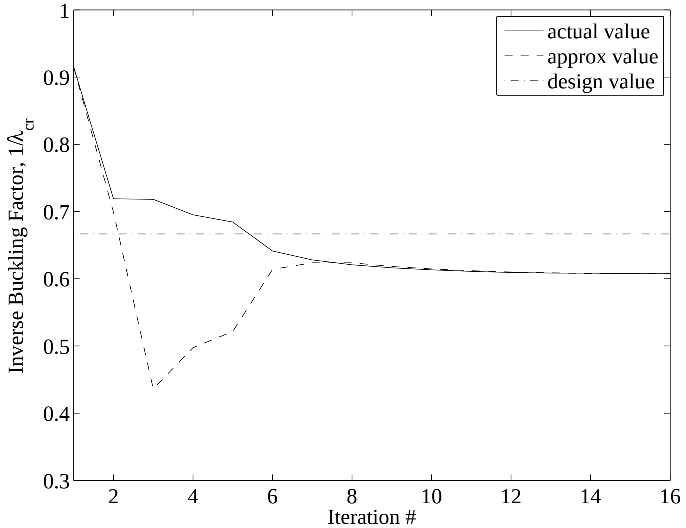

Figure 10.10: *Solution convergence of the inverse buckling factor, $1/\lambda_{cr}$ and approximate inverse buckling factor, $1/\tilde{\lambda}$. The design value, $1/\lambda_d$, is plotted for reference*

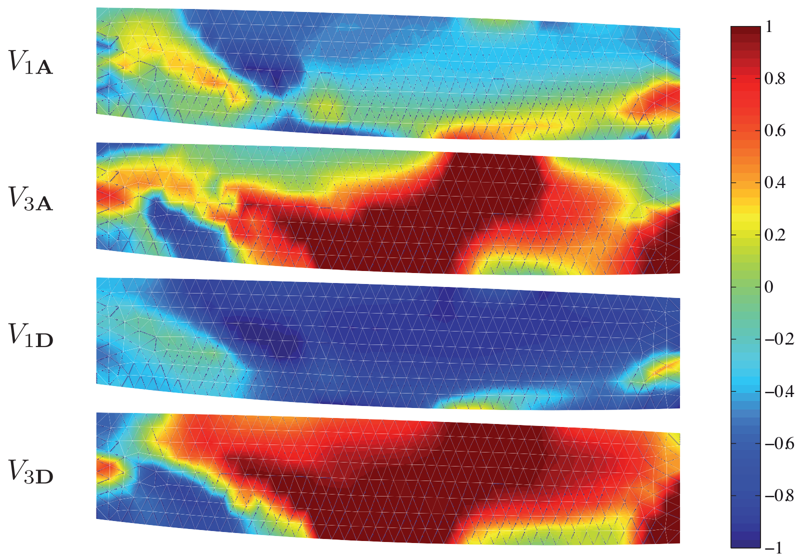

Figure 10.11: *Optimum lamination parameter distributions for maximum buckling load of the flat rib model*

stiffness laminate consisted of 24 steered plies and was constrained to be locally balanced and symmetric. Therefore, six independent fiber angles were defined per design region resulting in a $[\pm\theta_1, \pm\theta_2, \ldots \pm\theta_6]_s$ laminate being defined at each node. A minimum turning radius of 200mm was imposed as a manufacturing constraint. A detailed description the fiber angle retrieval process is provided by van Campen (2011).

The obtained fiber angle distribution is presented in Figure 10.12. The rib was loaded eccentrically due to the c-shaped cross-section, which resulted in bending moments in the web section of the rib. In the outer layers, ply 1-3, the fibers were aligned primarily along the vertical direction and contain little steering. These plies increased bending stiffness along vertical axis of the rib and therefore, suppressed the induced bending moments. The inner layers, ply 4-6, contained a significant amount of steering and contributed primarily to in-plane load redistribution to improve the buckling load and to transferring shear loads. The 4^{th} ply contained a vertically stiff region towards the center of the web while the sides tended towards $\pm 45°$ fiber angles. In the inner two plies fibers tended to be aligned primarily along the horizontal axis.

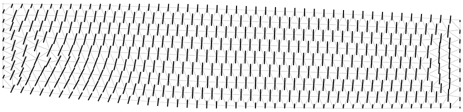

(a) Ply 1

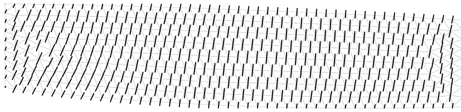

(b) Ply 2

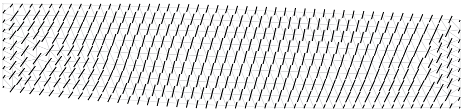

(c) Ply 3

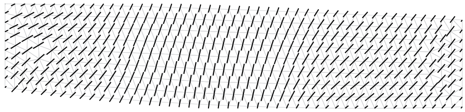

(d) Ply 4

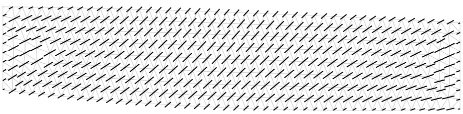

(e) Ply 5

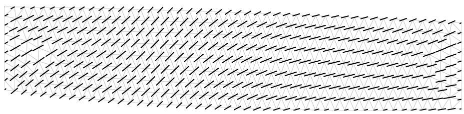

(f) Ply 6

Figure 10.12: *Fiber angle distribution best matching the optimum stiffness distribution while satisfying the imposed manufacturing constraints. Only the balanced plies are shown for the total laminate layup of* $[\pm\theta_1, \pm\theta_2, \ldots \pm \theta_6]_s$ *(Source van Campen (2011))*

The buckling load multipliers of several flat rib designs are presented in Table 10.3, together with the number of plies and the percent difference in weight with respect to the original sine-wave rib. Adding an additional ply caused the inner-web section of the flat rib design to have the same weight as the original sine-wave rib, however, the buckling load was almost 4.5 times lower. To ensure that a feasible solution was found, eight additional plies were incorporated in the design of the inner web section, resulting in a flat-rib that was 15% heavier than the original sine-wave rib. Even with eight additional plies a quasi-isotropic layup did not satisfy the buckling load requirement of 1.5 time ultimate load. However, once variable stiffness solutions were permitted in the inner-web section, the buckling load factor was improved by more than 50%, hence, satisfying the buckling requirements. At present only the inner web of the rib was designed using the variable stiffness approach, however, the stiffness distribution over the entire rib should be allowed to vary to assess the true potential of steering.

Table 10.3: *Summary of buckling loads for the different laminate designs of the flat rib inner web. The percent difference in weight, Δw, is computed with respect to the total weight of the baseline sine-wave rib. To meet the design requirements $\lambda_1 > 1.5$. The layup in the flange and outer web remained identical to that of the baseline design provided by IAI*

Layup	# of Plies	$\boldsymbol{\lambda}_1$	$\boldsymbol{\lambda}_2$	$\%\boldsymbol{\Delta}w$
Baseline Layup by IAI	15	0.4766	0.5654	-3.0
Layup by IFB $[90_5, 0_3, \pm 45_4]$	15	0.5254	0.6516	-3.0
Modified Layup by IFB + 90 $[90_6, 0_3, \pm 45_4]$	16	0.6034	0.7074	0.0
Quasi-Isotropic ($\mathbf{V} = 0$)	24	1.0933	1.4838	15.2
VS Optimum - Lamination Parameters	24	1.6460	1.7070	15.2
VS Optimum - Converted to Fiber Angles	24	1.5223	1.7661	15.4

The critical buckling modes of the 24-ply quasi-isotropic and optimum variable stiffness design are plotted in Figure 10.13. The buckling modes for both designs were similar and consisted roughly of a single half-wave along the length of the rib. The first buckling mode of the steered design extended over a larger section of the web. Comparing the bucking modes of the flat rib and sine-wave rib also clearly demonstrated the advantage the sine-wave geometry provides. The critical buckling mode of the sine-wave was found to be local while that of the flat rib was global. The sine-wave geometry effectively act as stringers, constraining the buckling to occur locally, hence improving the critical buckling load of the sine-wave rib.

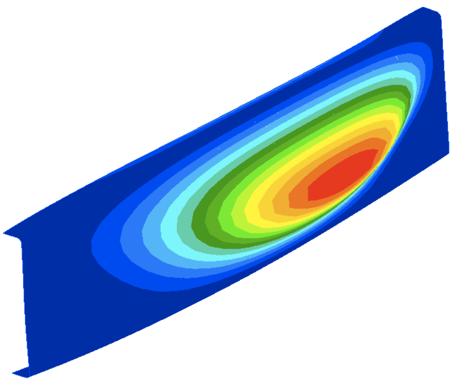

(a) Quasi-isotropic laminate

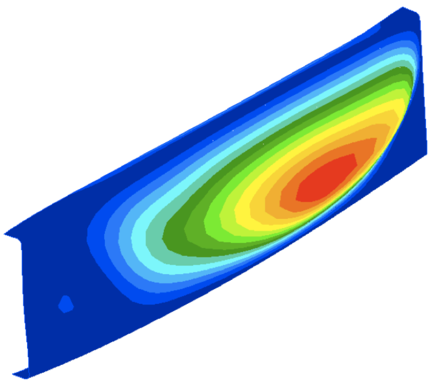

(b) Optimal variable stiffness laminate

Figure 10.13: *Critical buckling modes of the flat rib for the quasi-isotropic and optimum variable stiffness laminates*

The stiffness distribution in the inner web of the flat rib was optimized to maximize the buckling load, however, several other design requirements were also imposed in section 10.1, including constraints on maximum principle strains and environmental conditions and machine limitations during manufacturing. Environmental conditions were accounted for by using the material properties corrected for these conditions, while the manufacturing constraints are taken into account during the fiber angle retrieval step developed by van Campen (2011).

Constraints on maximum principle strains were not imposed during the optimization process for primarily two reasons; one, the computational cost in the current problem setup would become unmanageable and two, in the initial designs the critical strains were found at the fastener locations in the flange, which was not explicitly part of the inner web design region. To ensure that a feasible design was obtained, it was therefore necessary to compute the maximum and minimum principle strains and maximum shear strain for the optimum flat rib. The principle strains were computed at laminate level and were found to be well within the imposed design limits, hence, the optimum flat rib solution satisfied all the design requirements for the applied load case.

10.4 Concluding Remarks

The conclusions regarding the optimizer and the final sine-wave rib and flat rib designs are discussed separately below.

Optimizer Performance

A successful integration of the developed design optimization framework and a commercial finite element code was presented in this chapter. The laminate stiffness distributions of two relatively complex structural parts, a sine-wave and flat rib, were designed for maximum buckling load. The presented example problems and results allowed several important aspects of the design routine to be confirmed, one, it was possible to construct the buckling approximation in the form presented in chapter 8 using sensitivities computed by NASTRAN. Therefore, a convex approximation was guaranteed and good convergence behavior was demonstrated. Two, even for relatively complex structural problems, approximately twenty finite element analyses were sufficient to obtain a converged solution of the optimal laminate stiffness distribution. Three, the stiffness properties of only the inner web sections were designed, hence, it was demonstrated that the framework is also suitable for designing the stiffness properties of a selected part of a structure.

Two issues arose while using NASTAN to compute the laminate buckling sensitivities; one, due to a bug in the current NASTRAN version, a workaround had to be implemented to obtain correct sensitivity data, however, this came at a large computational cost. The number of element stiffness properties that could be designed in a tractable optimization problem was therefore limited to approximately a thousand. Therefore, a coarse mesh was used and only the inner web section of the rib could be designed. For more realistic results, a finer mesh should be used while considering the entire rib during optimization. Two, tracking modes between iterations is difficult to implement when using an external finite element code and negatively effects the optimization damping scheme. This can be remedied partly by applying a single averaged damping value for all the buckling modes, however, this may reduce the convergence efficiency.

Final Wing Rib Designs

The overall objective of the conducted design study was to investigate the possibility of replacing a geometrically complex sine-wave aircraft wing rib with a simpler flat rib to reduce part costs, while using fiber steering to compensate for the loss in buckling performance. Initially, the optimal laminate stiffness distribution for maximum buckling load of the inner web section of the sine-wave was obtained as an additional benchmark. The variable stiffness sine-wave rib design was shown to have a 30% higher buckling load than the baseline design provided by Israel Aerospace Industries and 20% higher than an equivalent quasi-isotropic design.

The buckling load of the flat rib, with a laminate identical to the baseline sine-wave rib, was found to be roughly six times lower than the baseline sine-wave rib, clearly demonstrating the efficiency of the sine-wave geometry in improving buckling performance. It was not possible to compensate for the reduced buckling performance solely through fiber steering. Therefore, additional plies were included in the inner web section resulting in 15% weight increase of the flat rib meeting the same design requirements. Optimizing the laminate stiffness distribution of the flat-rib web section mitigated larger weight penalties. The variable stiffness flat-rib design was found to have a 50% higher buckling load than an equivalent quasi-isotropic design.

The optimal sine-wave rib and flat rib designs showed improvements in buckling load of 30% and 50% with respect to their baseline designs, respectively. These improvements were less than initially expected and are thought to be attributed primarily to two aspects. One, due to computational limitations the laminate stiffness properties of only the inner web sections were designed. The layup in the flange and outer web sections remained unchanged, hence the load-paths were largely fixed in the outer sections and hence limiting the room for improvement. Larger, improvements in buckling performance and, therefore, a reduced weight penalty are expected when the stiffness properties of the entire rib are designed. Two, due to the c-shape of the wing ribs the web was loaded eccentrically, the resulting bending moments were not redistributed as efficiently as is seen for structures dominated by in-plane loads, as only the outer plies make a meaningful contribution to the laminate bending stiffness.

CHAPTER 11

Conclusions and Recommendations

> *"After climbing a great hill, one only finds that there are many more hills to climb."*
>
> Nelson Mandela

The design flexibility offered by modern automated fiber placement machines enables a new class of composite structures to be manufactured, which allow the directional properties of composite materials to be fully exploited. Steering fiber paths such that the fiber angle orientation varies spatially allows significant improvements in structural performance to be achieved. Despite the apparent potential, the design tools currently available to engineers do not exploit the steering capabilities of automated fiber placement machines. The goal of the research conducted and presented in this thesis was outlined in section 1.4 and ultimately summarized as:

to demonstrate that developing an efficiently design tool for variable stiffness composite structures is both productive and worthwhile,

a conclusion that remains to be drawn. To this end, an overview of the research and results presented within this thesis and the conclusions to which they lead are presented in this chapter. The discussion is separated into two parts, section 11.1, in which the generic implementation of the novel design optimization framework for variable stiffness composite structures and the developed approximation scheme is discussed, and section 11.2, in which the results of the considered design optimization problems are discussed. Several interesting and perhaps essential topics to consider in the future of variable stiffness composite design are discussed in section 11.3. For conclusions related specifically to each of the topics presented within this thesis the reader should refer to the relevant section provided at the end of each chapter.

11.1 Design Optimization Framework

A multi-step variable stiffness composite design optimization framework, which is shown schematically in Figure 11.1, was presented to tailor the laminate stiffness properties of composite structures to maximize their structural performance. The design procedure consisted of three steps, one, the optimal conceptual laminate stiffness and thickness distribution was designed to maximize a predefined performance metric. Two, the optimal fiber angle distribution was obtained to satisfy the imposed manufacturing constraints while retaining the achieved structural performance gains. Three, the fiber angle distribution was converted to continuous fiber paths to be used for manufacturing purposes. Postponing the design of detailed ply, course and tow level detail to the second and third steps allows laminate stiffness properties to be designed to maximize structural performance using efficient gradient based optimization routines, hence, minimizing the required number of finite element analyses.

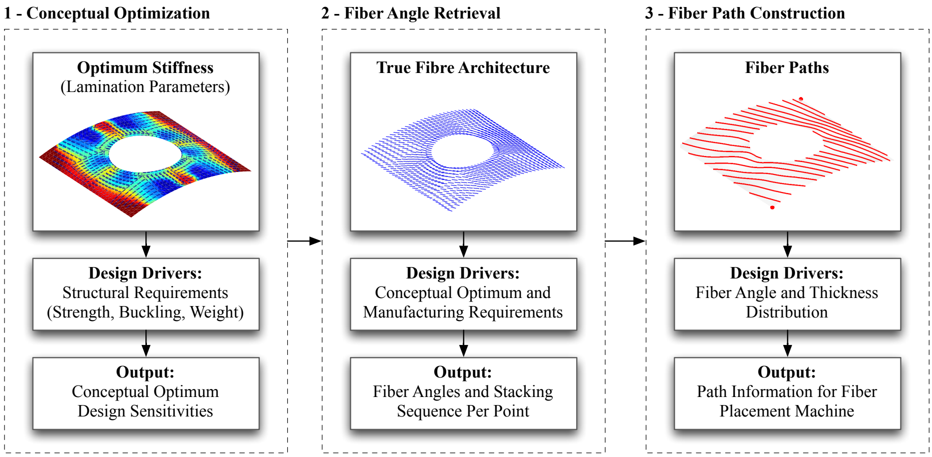

Figure 11.1: *Schematic overview of the developed multi-step optimization approach*

The primary focus of the presented work was the development of a conservative convex separable approximation of a generic response directly in terms of the laminate stiffness matrices. The approximation was developed specifically for composite laminate design, and has been used in both the first and second step of the developed design optimization framework. The developed approximation consisted of two terms, the first term approximated the considered structural response and its derivatives, while the second was used to guarantee convexity and conservativeness of the approximation as a whole. The presented generalized approximation methodology was implemented to maximize structural stiffness and to solve several buckling related design problems. Approximations to maximize structural strength or natural frequency using the presented design framework have also been developed and are presented in Khani et al. (2011) and Nagy (2011), respectively. Even though the aforementioned structural responses cover a large range of possible design problems, approximations for a larger set of structural responses, for example the thermal response, should be developed in the future.

Using lamination parameters to parametrize the laminate stiffness matrices in the response approximations allowed the convex nature of the approximation to be retained. This allowed an efficient design optimization routine, based on successive response approximations, to be developed and enabled the solution of variable stiffness design optimization problems with several thousand design variables. The separable nature of the response approximations allows the local optimization problems to be solved in parallel, further reducing computation time on multi-processor computer systems. An adaptive damping scheme was implemented to control solution convergence and approximation conservativeness while design updates were based on feasible descent steps, which guarantees global convergence. Typically, less than thirty finite element analyses were required to converge to the optimal solution, while roughly 80-90% of the performance gains were already achieved within the first 3-5 design iterations. The effectiveness of the developed design optimization framework was demonstrated by solving several example problems, reviewed in section 11.2, however, additional effort may be exerted to study and improve the adaptive damping scheme further.

The developed response approximations can also be parameterized in terms of ply angle orientations and stacking sequence, which permits their use in subsequent steps of the developed design optimization framework. In this case, the response approximations are no longer convex in terms of the design variables. The local nature of the response approximation implies that its accuracy tends to deteriorate away from the approximation point. Therefore, if manufacturing constraints restrict the attainable laminate stiffness distribution excessively, intermediate updates of the approximation may be required to retain sufficient accuracy. An example of how fiber angles are retrieved using the developed response approximation is presented in van Campen (2011). Alternatively, a globally accurate response approximation may be generated, as presented in Irisarri et al. (2011), and subsequently used to solve for the optimal fiber angle distribution.

11.2 Design of Variable Stiffness Laminates

Homogenous convex separable approximations were derived and presented for several buckling related design optimization problems. Initial design studies were restricted to flat plates subject to compressive uniaxial and biaxial loading. Numerical results reiterated the benefits of adopting variable stiffness laminates as a structural design concept. It was demonstrated that the critical buckling load of a simply supported plate could be increased almost twofold with respect to the best constant stiffness design. A trade off between axial stiffness and buckling load was presented in chapter 5. It was shown that a variable stiffness laminate with in-plane stiffness properties equivalent to a quasi-isotropic panel can be designed to withstand more than twice the compressive load before buckling. In-plane load redistribution was found to be the primary mechanism resulting in improved buckling loads when varying the stiffness properties while laminate thickness remained constant. Post-buckling analysis was conducted in Rahman et al. (2011), and demonstrated that variable stiffness laminate designs had similar or superior post-buckling stiffness when compared to the equivalent constant stiffness solutions.

A method of including thermals stresses during the buckling design optimization process was presented in chapter 6. Numerical results confirmed the importance of including thermal effects in the design of variable stiffness panels for buckling, since the pre-buckling stress state significantly influences a panels buckling behavior. The residual thermal stresses were also shown to have a beneficial influence on the compressive load carrying capacity of the plate if the temperature difference between curing temperature and operating temperature was not excessive. The range of operating temperatures over which the panel exhibits good buckling behavior was also shown to increase significantly when including thermal effects in the design process.

Including laminate thickness as a design variable, presented in chapter 7, allowed the achievable performance gains to increase even further, with buckling load increasing fivefold with respect to the baseline quasi-isotropic design. Compared to the optimal variable stiffness design with constant thickness improvements in the order of 30-100% were obtained depending on the minimum allowable thickness. The optimal thickness distributions for the uniaxial load case were shown to reinforce the load redistribution effect, however, for the biaxial load case the improved buckling performance was both due to in-plane load redistribution and increased local bending stiffness. Therefore, when thickness variation is included in the variable stiffness design routine for maximum laminate buckling load, both load redistribution and improved laminate bending stiffness played a role.

The buckling approximation was extended to be applicable to general shell structures in section 8. An example problem, a curved panel subject to a uniform pressure load, was presented to demonstrated the applicability of the derived approximation. The buckling load of the optimal variable stiffness laminate design was shown to improve 15-20% with respect to the best constant stiffness design when enforcing uniform thickness. The buckling load increased 60% with respect to the best constant stiffness solution when allowing thickness to vary spatially. The optimum laminate stiffness distribution indicated that the improved buckling load was primarily due to improved laminated bending stiffness.

Two practical design applications were also studied to demonstrate the effectiveness of the developed design optimization approach. The first problem considered the design of a simplified window belt section for maximum tensile strength, presented in chapter 9. Optimal variable stiffness solutions, meeting the imposed in-plane curvature constraints, were shown to be 50% stronger than the best constant stiffness solution. Due to time limitations and constraints imposed by the available fiber placement software and hardware, alternative designs based on linear fiber angle variation were also obtained. Designs using parallel path and shifted path replication strategies were studied. The shifted path strategies were found to match the stiffness distributions obtained in the theoretical studies best and also yielded the largest improvements in strength, roughly 25% higher than the optimal constant stiffness solution.

The second practical design application, presented in chapter 10, was the design of an aircraft wing rib to meet a range of imposed design requirements, however, buckling was considered as the primary design driver. Other than demonstrating the benefit of using stiffness variation for more practical structures, the analysis for this design problem was conducted entirely using an external commercial finite element solver. Since a specific approximation form has been developed, it is important that the external solver can be used to construct the desired approximation. A method of obtaining the derivatives required to construct the generalized buckling approximation of a shell structure was presented in chapter 10. Due to a potential bug in the current version of the external commercial software used in the present research, a computationally expensive workaround was implemented and therefore, the size of the optimization problems that could be considered was limited. Nevertheless, for this more practical design problem the optimizer was found to perform satisfactorily.

As the loading, boundary conditions, structures and the laminates of which they comprise become more complex it will inevitably become difficult to identify the primary mechanisms resulting in improved buckling performance. The developed convex conservative separable approximation of the buckling load implemented within the developed design optimization framework has, thus far, proven to be an effective tool for optimizing variable stiffness composite structures.

The presented research focused primarily on demonstrating the applicability of the developed variable stiffness design optimization framework, however, to assess the true benefit of fiber steering it would be beneficial to conduct a range parametric studies for structures with different dimensions, load cases and materials to qualitatively evaluate in which situations laminate stiffness variation will provide the most benefit. The considered design problems were all limited to a single design load case. In the future, it would therefore be interesting to investigate more complex combinations of load cases and its effect on the optimal laminate stiffness distribution.

11.3 Future Developments

Design studies conducted thus far, both theoretical and experimental, along with numerical results presented in this thesis reaffirm the benefit of adopting variable stiffness laminates for aerospace structural applications. The developed optimization framework, including response approximation methodology, has proven to be an efficient design tool for this new class of composite structures. However, several challenges remain to be addressed in order to design and apply variable stiffness laminates.

11.3.1 Design Optimization Framework

Several extensions to the developed design framework can be envisaged to further improve the structural performance of variable stiffness laminates. Typically, composite laminates are restricted to be symmetric and balanced, which eliminates extension-shear coupling and extension-bending coupling while also minimizing bending-twisting coupling. The same restrictions were imposed on the variable stiffness laminates in the design studies presented in this thesis. Removing these design restrictions will result in further improvements in structural performance, as was seen when designing plates for maximum strength in chapter 4. Additionally the developed design framework currently assumes that the part geometry is predefined. Further gains in structural performance may still be achieved through including shape and/or topology optimization in the design process. The advantages of simultaneous design of part geometry and laminate stiffness, using an isogeometric design optimization routine, is currently under investigation and will be presented in Nagy (2011).

Detailed tow-level information is required to manufacture composite laminates with automated fiber placement technology. In the current multi-step design approach only the course paths are generated and hence, detailed tow-level information remains to be determined. Additionally, software currently used to control fiber placement machines often run computationally expensive simulations to ensure that a given design is manufacturable. In the industrial setting it would therefore be highly beneficial if the design optimization framework could already guarantee design manufacturability.

11.3.2 Application of Variable Stiffness Laminates

Numerical results have demonstrated that structural performance improves significantly when tailoring laminate stiffness properties to meet the imposed design requirements, however, this may come at the expense of design robustness. In a first step, Abdalla et al. (2009a) presented a method of including robustness constraints, similar to the traditionally used ten percent rule, when considering in-plane laminate design problems. However, it is essential that further effort be made to investigate the performance of variable stiffness laminates when subject to off-design operating conditions before they are adopted for practical design applications. Additionally, robustness with respect to manufacturing defects, which still occur occasionally with the current generation of fiber placement machines, remains to be investigated.

In the aerospace industry the certification process is an important hurdle that must be overcome before variable stiffness laminates can be adopted. Traditionally, specific laminate stacks are tested and certified for use in aerospace components, an approach which would not be feasible when using variable stiffness laminates. Therefore, it is essential that trustworthy predictive modeling capabilities be developed and incorporated in the certification process. A finite element procedure, developed to capture the local stress fields that are present when manufacturing composite structures using automated fiber placement, is presented in Fagiano (2010). This is an essential step in developing suitable damage models, however, a significant amount of research remains to be conducted to develop suitable predictive analysis capabilities. The amount of experimental data available for variable stiffness composite structures is limited, primarily due to the novel nature of these structural components. Generating, collecting and disseminating experimental data would be an invaluable contribution to the research community and greatly support further development of design and analysis capabilities.

APPENDIX A

Material Properties

Several different materials were used to conduct the design studies presented in this thesis, and are tabulated below.

Table A.1: *Tabulated material properties for the materials used to conduct the design studies presented in this thesis* (AS4/APC2: carbon-PEEK, IM6/SC1081: carbon-epoxy, IM7/8552: carbon-epoxy, B5.6/5505: boron-epoxy, T300/5208: carbon-epoxy)

	AS4*	**IM6***	**IM7†**	**B5.6***	**T300‡**
Longitudinal Modulus (E_1, GPa)	142	177	156	201	181
Transverse Modulus (E_2, GPa)	10.3	10.8	10.5	21.7	10.3
Shear Modulus (G_{12}, GPa)	7.2	7.6	6.0	5.4	7.17
Poisson's Ratio (ν_{12})	0.27	0.27	0.30	0.17	0.28
Longitudinal Tensile Strength (X_t, MPa)	2280	2860		1380	
Longitudinal Compressive Strength (X_c, MPa)	1440	1875		1600	
Transverse Tensile Strength (Y_t, MPa)	57	49		56.6	
Transverse Compressive Strength (Y_c, MPa)	228	246		125	
Shear Strength (S, MPa)	71	83		62.6	
Longitudinal CTE (α_1, $10^{-6}/°C$)					0.02
Transverse CTE (α_2, $10^{-6}/°C$)					22.5

† source: material data sheets used within the AUTOW project

* source: Daniel and Ishai (1994)

‡ source: Tsai (1988)

In addition to the material properties listed in the above table for IM7/8552, the following failure allowables were used for the design studies conducted within the AUTOW project. The allowable principle strains used during the rib design, see chapter 10, were defined as $\epsilon_t^{11} = 5200\mu$s, $\epsilon_c^{11} = 4500\mu$s and $\gamma_t^{12} = 9000\mu$s. While designing the simplified window belt section, see chapter 9, critical hole edge strains were taken to be $\epsilon_t = 22800$ μstrain and $\epsilon_c = -13800$ μstrain.

APPENDIX B

Finite Element Analysis

Two different finite element implementations were used to conduct the studies presented in this thesis. Initial research was focused on panels for which the extensional and flexural solutions could be computed separately. A flat rectangular bilinear shell element was implemented, consisting of an 8 degree of freedom membrane element and a 12 degree of freedom Kirchhoff-plate element for bending. A few key components of the used finite element formulation are outlined in this appendix. In order to study structures with more intricate geometry, an 18 degree of freedom flat triangular shell element was implemented and used for the studies presented in chapter 8. The element was built up by combining a triangular membrane and bending element. The 12 degree of freedom membrane triangular element, with drilling degrees of freedom, was implement based on a template by Felippa (2003), while a 9 degree of freedom Kirchhoff-plate Bending Triangular element (KBT) was implemented based on a template provided in Felippa (2000). Both elements are well documented in the aforementioned literature and are therefore not repeated here.

B.1 Flat Rectangular Shell Element

In the following sections the membrane and bending stiffness matrices used to evaluate the buckling loads of the rectangular plates considered in chapter 5 to 7 are presented.

B.1.1 Membrane Element

The in-plane stiffness matrix can be written in the following form:

$$\mathbf{K}_{me} = \begin{bmatrix} \mathbf{k}^{11} & \mathbf{k}^{12} \\ sym. & \mathbf{k}^{22} \end{bmatrix} \tag{B.1}$$

The above 4×4 sub-matrices are given in terms of the laminate extensional stiffness, $\mathbf{A}$, as follows (Reddy, 2004):

$$
\begin{aligned}
\mathbf{k}^{11} &= A_{11}\mathbf{S}^{xx} + A_{16}(\mathbf{S}^{xy} + \mathbf{S}^{yx}) + A_{66}\mathbf{S}^{yy} \\
\mathbf{k}^{12} &= A_{12}\mathbf{S}^{xy} + A_{16}\mathbf{S}^{xx} + A_{26}\mathbf{S}^{yy} + A_{66}\mathbf{S}^{yx} \\
\mathbf{k}^{22} &= A_{66}\mathbf{S}^{xx} + A_{26}(\mathbf{S}^{xy} + \mathbf{S}^{yx}) + A_{22}\mathbf{S}^{yy}
\end{aligned} \tag{B.2}
$$

where the elements of the $\mathbf{S}^{xx}$, $\mathbf{S}^{xy}$, and $\mathbf{S}^{yy}$ matrices depend on the in-plane shape functions ψ_i and are defined as:

$$
S_{ij}^{\xi\eta} = \int_{\Omega_e} \frac{\partial\psi_i}{\partial\xi}\frac{\partial\psi_j}{\partial\eta}dxdy \ (i,j = 1,\ldots,4) \tag{B.3}
$$

Note that in the presented work, only square bilinear elements were used with fixed side length s. Therefore, matrices $\mathbf{S}^{xx}$, $\mathbf{S}^{xy}$, etc. were the same for all elements and could be computed and stored. Note also that the derivative terms, $\partial\mathbf{K}_{me}/\partial A_{\rho\sigma}$, required to evaluate the sensitivity matrices in the equation (C.21), are readily obtained on inspection of equation (B.2).

Finally, to evaluate the geometric stiffness matrix, equation (5.3), the in-plane stress resultants were required. These can be obtained via the in-plane strains, which can be related to the in-plane deformations via the average strain displacement matrix, $\mathbf{B}$. For a square element with side s this matrix is given by:

$$
\overline{\mathbf{B}}_e = \frac{1}{2s}\begin{bmatrix} -1 & 1 & 1 & -1 & 0 & 0 & 0 & 0 \\ 0 & 0 & 0 & 0 & -1 & -1 & 1 & 1 \\ -1 & -1 & 1 & 1 & -1 & 1 & 1 & -1 \end{bmatrix} \tag{B.4}
$$

B.1.2 Bending Element

The bending stiffness matrix according to classical laminate theory is computed as follows (Reddy, 2004):

$$
\begin{aligned}
\mathbf{K}_{be} =& D_{11}\mathbf{T}^{xxxx} + D_{12}(\mathbf{T}^{xxyy} + \mathbf{T}^{yyxx}) + 2D_{16}(\mathbf{T}^{xxxy} + \mathbf{T}^{xyxx}) \\
&+ 2D_{26}(\mathbf{T}^{xyyy} + \mathbf{T}^{yyxy}) + 4D_{66}\mathbf{T}^{xyxy} + D_{22}\mathbf{T}^{yyyy}
\end{aligned} \tag{B.5}
$$

where the elements of $\mathbf{T}^{xxxx}$, $\mathbf{T}^{xxyy}$, etc. depend on the element geometry and bending shape functions φ_i:

$$
T_{ij}^{\xi\eta\zeta\mu} = \int_{\Omega_e} \frac{\partial^2\varphi_i}{\partial\xi\partial\eta}\frac{\partial^2\varphi_j}{\partial\zeta\partial\mu}dxdy \ (i,j = 1,2,\ldots,16) \tag{B.6}
$$

Notice that the derivative terms in equation (C.20) are easily obtained, for example:

$$
\frac{\partial\mathbf{K}_{be}}{\partial D_{11}} = \mathbf{T}^{xxxx} \qquad \text{or} \qquad \frac{\partial\mathbf{K}_{be}}{\partial D_{12}} = (\mathbf{T}^{xxyy} + \mathbf{T}^{yyxx})/2 \tag{B.7}
$$

APPENDIX C

Sensitivity Analysis

Detailed derivations of the sensitivity matrices required for the approximations developed for the objective functions treated in chapters 5 to 8 are presented in this appendix. The derivatives of the compliance, used to maximize structural stiffness, are presented in section C.1. The derivatives required to maximize the buckling load of plates are presented in section C.2 and are extended to include thermal effects in section C.3. Lastly, the derivatives required to maximize the buckling load of general shell structures are presented in section C.4. It should be noted that the sensitivities presented in the following sections represent the derivatives of the considered response with respect to the stiffness properties of an arbitrary *element*. To ensure that smooth solutions were found using the developed design framework, design variables were defined at *nodes* and the laminate stiffness properties were subsequently interpolated to the element, as explained in section 2.3.6. Similarly, the sensitivity matrices presented in this section should be interpolated to the nodes before being incorporated into the developed approximations.

C.1 Compliance

A variable stiffness laminate designed for maximum stiffness was studied in chapter 5. The optimization problem was posed as the minimization of the structural compliance, r_c, hence, the derivatives of the compliance with respect to the in-plane stiffness matrices were required. The compliance represents the energy stored within the structure and when using the finite element method it can be formulated as:

$$r_c = \frac{1}{2}\mathbf{u}^T \cdot \mathbf{K}_m \cdot \mathbf{u} = \frac{1}{2}\mathbf{f}^T \cdot \mathbf{u} \tag{C.1}$$

where $\mathbf{u}$ is the vector of nodal displacements and $\mathbf{f}$ the vector of applied forces as given in equation (5.6). When considering plates under in-plane loading, $\mathbf{K}_m$ represents the membrane stiffness matrix and is only a function of the laminate in-plane stiffness matrix, $\mathbf{A}$. Similarly when considering generalized shell structures, $\mathbf{K}_m$ represents the material stiffness matrix and contains both in-plane and bending stiffness related terms.

Taking the derivative of equation (5.6) with respect to an arbitrary stiffness related variable b and assuming that the applied force is a dead load, the derivative of the in-plane displacements can be expressed as:

$$\frac{\partial \mathbf{u}}{\partial b} = -\mathbf{K}_m^{-1} \cdot \frac{\partial \mathbf{K}_m}{\partial b} \cdot \mathbf{u} \tag{C.2}$$

The derivative of the compliance, r_c, with respect to an arbitrary stiffness related variable b can therefore be given by:

$$\frac{\partial r_c}{\partial b} = -\frac{1}{2}\mathbf{u}^T \cdot \frac{\partial \mathbf{K}_m}{\partial b} \cdot \mathbf{u} \tag{C.3}$$

Since b is associated to a specific element, the sensitivity is local and can be determined based on the information of a single element. The components of sensitivity matrix of element e with respect to the elements in-plane stiffness can therefore be given by:

$$\Phi^m_{\alpha\beta_e} = -\frac{\partial r_c}{\partial A^{-1}_{\alpha\beta}} = -\frac{1}{2}\sum_{\sigma,\rho} A_{\beta\sigma}A_{\rho\alpha}\left(\mathbf{u}_e^T \cdot \frac{\partial \mathbf{K}_{m_e}}{\partial A_{\rho\sigma}} \cdot \mathbf{u}_e\right) \tag{C.4}$$

Similarly, when general shell structures are studied, the derivatives with respect to the bending stiffness terms must also be considered, and are given by:

$$\Phi^b_{\alpha\beta_e} = -\frac{\partial r_c}{\partial D^{-1}_{\alpha\beta}} = -\frac{1}{2}\sum_{\sigma,\rho} D_{\beta\sigma}D_{\rho\alpha}\left(\mathbf{u}_e^T \cdot \frac{\partial \mathbf{K}_{m_e}}{\partial D_{\rho\sigma}} \cdot \mathbf{u}_e\right) \tag{C.5}$$

where $\alpha, \beta, \sigma, \rho = 1\ldots 3$ represent the components of the stiffness matrices of associated with element e.

C.2 Buckling of Plates

The finite element formulation to solve for the linear buckling load of a plate is given by equation (5.1). The derivative of a single buckling load with respect to an arbitrary stiffness related design variable b is given by:

$$\frac{\partial \lambda}{\partial b} = \lambda\, \mathbf{a}^T \cdot \left(\frac{\partial \mathbf{K}_b}{\partial b} - \lambda\frac{\partial \mathbf{K}_g}{\partial b}\right) \cdot \mathbf{a} \tag{C.6}$$

and is composed of two terms. The first term is local and can therefore be evaluated using information from a single element:

$$S_{b1} \equiv \mathbf{a}^T \cdot \frac{\partial \mathbf{K}_b}{\partial b} \cdot \mathbf{a} = \mathbf{a}_i^T \cdot \frac{\partial \mathbf{K}_{b_i}}{\partial b} \cdot \mathbf{a}_i \tag{C.7}$$

The second term in equation (C.6) is not necessarily local. This is due to the fact that even when the stiffness of a single element is altered, the distribution of the in-plane loads is altered for all elements and thus the geometric matrices of all elements would change. In the following, an efficient way for the evaluation of this term is described. Substituting from equation (5.3) into equation (C.6) and rearranging the terms S_{b2} can be defined as:

$$S_{b2} \equiv \mathbf{a}^T \cdot \frac{\partial \mathbf{K}_g}{\partial b} \cdot \mathbf{a} = -\sum_e \mathbf{s}_e^T \cdot \frac{\partial \mathbf{n}_e}{\partial b} \tag{C.8}$$

where the vector $\mathbf{s}_e$ can be calculated locally for element e as:

$$\mathbf{s}_e = \left(\mathbf{a}_e^T \cdot \mathbf{K}_x \cdot \mathbf{a}_e, \quad \mathbf{a}_e^T \cdot \mathbf{K}_y \cdot \mathbf{a}_e, \quad \mathbf{a}_e^T \cdot \mathbf{K}_{xy} \cdot \mathbf{a}_e\right)^T \tag{C.9}$$

The derivative of the in-plane stress resultants is obtained by differentiating (5.4):

$$\frac{\partial \mathbf{n}_e}{\partial b} = \frac{\partial \mathbf{A}_e}{\partial b} \cdot \mathbf{e_e} + \mathbf{A}_e \cdot \frac{\partial \mathbf{e_e}}{\partial b} \tag{C.10}$$

Thus, the sum in equation (C.8) can be decomposed into two terms corresponding to the two terms in equation (C.10). The first term can be evaluated locally since only the in-plane stiffness matrix of the i^{th} element depends on b. The second term involves the derivative of the average strain of an arbitrary element with respect to the change of stiffness of the i^{th} element and is not local:

$$S_{b2} = -\mathbf{s}_i^T \cdot \frac{\partial \mathbf{A}_i}{\partial b} \cdot \mathbf{e}_i - \sum_e \mathbf{s}_e^T \cdot \mathbf{A}_e \cdot \frac{\partial \mathbf{e}_e}{\partial b} \tag{C.11}$$

To evaluate the second term in the above equation, which is denoted by S_{b22}, equation (5.5) is differentiated with respect to b to obtain:

$$\frac{\partial \mathbf{e_e}}{\partial b} = \overline{\mathbf{B}}_e \cdot \frac{\partial \mathbf{u}_e}{\partial b} \tag{C.12}$$

therefore, the strain term S_{b22} simplifies to:

$$S_{b22} = -\mathbf{g}_e^T \cdot \frac{\partial \mathbf{u}_e}{\partial b} \tag{C.13}$$

where the vector $\mathbf{g}$ is assembled from element contributions:

$$\mathbf{g}_e = \mathbf{B}_e^T \cdot \mathbf{A}_e \cdot \mathbf{s}_e \tag{C.14}$$

The derivative of the in-plane displacement vector is obtained by differentiation of equation (5.6) as:

$$\mathbf{K}_m \cdot \frac{\partial \mathbf{u}}{\partial b} = -\frac{\partial \mathbf{K}_m}{\partial b} \cdot \mathbf{u} \tag{C.15}$$

Defining the adjoint displacement vector $\mathbf{v}$ as the solution of the problem:

$$\mathbf{K}_m \cdot \mathbf{v} = -\mathbf{g} \tag{C.16}$$

hence, the strain term can be simplified to:

$$S_{b22} = -\mathbf{v}^T \cdot \frac{\partial \mathbf{K}_m}{\partial b} \cdot \mathbf{u_e} \tag{C.17}$$

which can be also evaluated locally.

Thus, all the calculations required to evaluate the sensitivity of the buckling load with respect to local change of stiffness of the i^{th} element can be calculated using information at the element level. The global redistribution of loads is accounted for totally through the evaluation of the adjoint displacement vector $\mathbf{v}$. Substituting the above sensitivity equations back into equation (C.6), it can be written as:

$$\frac{\partial\lambda}{\partial b} = \lambda\big(\mathbf{a}_i^T \cdot \frac{\partial \mathbf{K}_{bi}}{\partial b} \cdot \mathbf{a}_i\big) + \lambda^2\left(\mathbf{s}_i^T \cdot \frac{\partial \mathbf{A}_i}{\partial b} \cdot \mathbf{e}_i + \mathbf{v}_i^T \cdot \frac{\partial \mathbf{K}_i^m}{\partial b} \cdot \mathbf{u}_i\right) \tag{C.18}$$

Keeping in mind that:

$$\frac{\partial\,\lambda}{\partial \mathbf{D}_e^{-1}} = -\mathbf{D}_e \cdot \frac{\partial\,\lambda}{\partial \mathbf{D}_e} \cdot \mathbf{D}_e \tag{C.19}$$

and recalling that for the reciprocal approximation (5.11) the element sensitivities are decomposed into two separate bending and membrane parts as follows:

$$\Phi^b_{\alpha\beta_e} \equiv \frac{1}{\lambda^2}\frac{\partial\,\lambda}{\partial\, D^{-1}_{\alpha\beta}} = \frac{1}{\lambda}\sum_{\sigma,\rho} D_{\beta\sigma} D_{\rho\alpha}\big(\mathbf{a}_e^T \cdot \frac{\partial \mathbf{K}_{be}}{\partial D_{\rho\sigma}} \cdot \mathbf{a}_e\big) \tag{C.20}$$

and:

$$\Psi^m_{\alpha\beta_e} \equiv \frac{1}{\lambda^2}\frac{\partial\,\lambda}{\partial\, A_{\alpha\beta}} = \sum_{\sigma,\rho}\left(\mathbf{s}_e^T \cdot \frac{\partial \mathbf{A}_e}{\partial A_{\rho\sigma}} \cdot \mathbf{e}_e + \mathbf{v}_e^T \cdot \frac{\partial \mathbf{K}_{me}}{\partial A_{\rho\sigma}} \cdot \mathbf{u}_e\right) \tag{C.21}$$

where $\alpha, \beta, \sigma, \rho = 1 \ldots 3$ represent the components of the stiffness matrices of associated with element e.

C.3 Thermo-Mechanical Buckling of Plates

The sensitivity analysis is modified in this section to include the contribution of thermal loads. A simplified thermo-mechanical finite element analysis formulation was presented in chapter 6. The eigenvalue problem was presented in equation (6.1). The derivative of a single buckling mode with respect to an arbitrary stiffness variable b can therefore be given as:

$$\frac{\partial\lambda}{\partial b} = \lambda\,\mathbf{a}^T \cdot \left(\frac{\partial \mathbf{K}_b}{\partial b} - \Delta T\frac{\partial \mathbf{K}_g^{Th}}{\partial b} - \lambda\frac{\partial \mathbf{K}_g^{M}}{\partial b}\right) \cdot \mathbf{a} \tag{C.22}$$

The sensitivity consists of three terms, the first is local, and is identical to the first term in equation (C.6). Terms two and three are global, as a change in element in-plane stiffness results in a new stress distribution (be it due to mechanical or thermal loading), and hence influence all elements. Term two and three are essentially the same, however term two is most general, since it also includes the effects of thermal loads and hence will be treated here. As in equation (C.8), the derivative of the second term can be written as:

$$S_{b2} \equiv \mathbf{a}^T \cdot \frac{\partial \mathbf{K}_g^{Th}}{\partial b} \cdot \mathbf{a} = -\sum_e \mathbf{s}_e^T \cdot \frac{\partial \mathbf{n}_e}{\partial b} \tag{C.23}$$

where the vector $\mathbf{s}_e$ can be calculated locally as given in equation (C.9). The derivative of the in-plane stress resultants can be obtained by differentiation of equation (6.5) as:

$$\frac{\partial \mathbf{n}_e}{\partial b} = \frac{\partial \mathbf{A}_e}{\partial b} \cdot \mathbf{e_e} + \mathbf{A}_e \cdot \frac{\partial \mathbf{e_e}}{\partial b} - \frac{\partial \mathbf{N}^{Th}}{\partial b} \tag{C.24}$$

Thus, the sum in equation (C.23) can be decomposed into three terms corresponding to the terms in equation (C.24). The first and third term can be evaluated locally since only the in-plane stiffness matrix and thermal load vector of the i^{th} element depend on b. The second term involves the derivative of the average strain of an arbitrary element with respect to the change of stiffness of the i^{th} element and is not local. Equation (C.23) can therefore be written as:

$$S_{b2} = -\mathbf{s}_i^T \cdot \frac{\partial \mathbf{A}_i}{\partial b} \cdot \mathbf{e}_i - \sum_e \mathbf{s}_e^T \cdot \mathbf{A}_e \cdot \frac{\partial \mathbf{e}_e}{\partial b} + \mathbf{s}_i \cdot \frac{\partial \mathbf{N}^{Th}}{\partial b} \tag{C.25}$$

The second term in equation (C.25), which is denoted by S_{b22}, can be evaluated using the adjoint method presented in section C.2. In this case, the only difference is that the applied thermal load is still present when solving the equations of equilibrium (6.6). Therefore, the strain term can be simplified to:

$$S_{b22} = \mathbf{v}^T \cdot \frac{\partial \mathbf{f}^{Th}}{\partial b} - \mathbf{v}^T \cdot \frac{\partial \mathbf{K}_m}{\partial b} \cdot \mathbf{u_e} \tag{C.26}$$

where the first term is given by:

$$\frac{\partial \mathbf{f}^{Th}}{\partial b} = \mathcal{A} \cdot \overline{\mathbf{B}} \cdot \frac{\partial \mathbf{N}^{Th}}{\partial b} \tag{C.27}$$

and where $\mathcal{A}$ is the element area, hence:

$$S_{b22} = \mathcal{A}_e \cdot \overline{\mathbf{B}}_e \cdot \mathbf{v}_e \cdot \frac{\partial \mathbf{N}_e^{Th}}{\partial b} - \mathbf{v}^T \cdot \frac{\partial \mathbf{K}_m}{\partial b} \cdot \mathbf{u_e} \tag{C.28}$$

which can be also evaluated locally. Thus, all the calculations required to evaluate the sensitivity of the buckling load with respect to local change of stiffness of the i^{th} element can be calculated using information at the element level. The global redistribution of loads is accounted for totally through the evaluation of the adjoint displacement vector $\mathbf{v}$. Substituting the above sensitivity equations back into equation (C.22), and rearranging yields:

$$\frac{\partial \lambda}{\partial b} = \left(1 + \frac{\Delta T}{\lambda}\right) \Psi^m_{\alpha\beta_e} + \Phi^b_{\alpha\beta_e} + \Omega_e \tag{C.29}$$

where:

$$\Phi^b_{\alpha\beta_e} \equiv \frac{1}{\lambda^2} \frac{\partial\, \lambda}{\partial\, D^{-1}_{\alpha\beta}} = \frac{1}{\lambda} \sum_{\sigma,\rho} D_{\beta\sigma} D_{\rho\alpha} \big(\mathbf{a}_e^T \cdot \frac{\partial \mathbf{K}_{be}}{\partial D_{\rho\sigma}} \cdot \mathbf{a}_e\big)$$

$$\Psi^m_{\alpha\beta_e} \equiv \frac{1}{\lambda^2} \frac{\partial\, \lambda}{\partial\, A_{\alpha\beta}} = \sum_{\sigma,\rho} \left(\mathbf{s}_e^T \cdot \frac{\partial \mathbf{A}_e}{\partial A_{\rho\sigma}} \cdot \mathbf{e}_e + \mathbf{v}_e^T \cdot \frac{\partial \mathbf{K}_{me}}{\partial A_{\rho\sigma}} \cdot \mathbf{u}_e\right)$$

where $\alpha, \beta, \sigma, \rho = 1 \ldots 3$ represent the components of the stiffness matrices of element e, and the terms dependent explicitly on the thermal load are included in:

$$\Omega_e = -\mathcal{A}_e \cdot \overline{\mathbf{B}}_e \cdot \mathbf{v}_e \cdot \frac{\partial \mathbf{N}_e^{Th}}{\partial b}$$

C.4 Buckling of Shells

The components of the sensitivity matrices for shell structures can be derived similarly to those for plates, as presented in section C.2. The derivative of a single buckling load multiplier with respect to an arbitrary stiffness related design variable b is given by:

$$\frac{\partial \lambda}{\partial b} = \lambda\, \mathbf{a}^T \cdot \left(\frac{\partial \mathbf{K}_m}{\partial b} - \lambda \frac{\partial \mathbf{K}_g}{\partial b} \right) \cdot \mathbf{a} \tag{C.30}$$

where $\mathbf{K}_m$ and $\mathbf{K}_g$ are now functions of both the laminate in-plane and bending stiffness matrices. The first term is local, and can therefore be evaluated using the stiffness terms related to a single element. The second term is not local and can be solved for efficiently using the adjoint method, as presented in section C.2. Following the same procedure, it can be shown that the components of sensitivity matrices required to evaluate the buckling load approximation of a general shell are given by:

$$\Phi^m_{\alpha\beta_e} \equiv \frac{1}{\lambda^2} \frac{\partial\, \lambda}{\partial\, A^{-1}_{\alpha\beta}} = \frac{1}{\lambda} \sum_{\sigma,\rho} A_{\beta\sigma} A_{\rho\alpha} \big(\mathbf{a}_e^T \cdot \frac{\partial \mathbf{K}_{me}}{\partial A_{\rho\sigma}} \cdot \mathbf{a}_e \big) \tag{C.31}$$

$$\Phi^b_{\alpha\beta_e} \equiv \frac{1}{\lambda^2} \frac{\partial\, \lambda}{\partial\, D^{-1}_{\alpha\beta}} = \frac{1}{\lambda} \sum_{\sigma,\rho} D_{\beta\sigma} D_{\rho\alpha} \big(\mathbf{a}_e^T \cdot \frac{\partial \mathbf{K}_{me}}{\partial D_{\rho\sigma}} \cdot \mathbf{a}_e \big) \tag{C.32}$$

$$\Psi^m_{\alpha\beta_e} \equiv \frac{1}{\lambda^2} \frac{\partial\, \lambda}{\partial\, A_{\alpha\beta}} = \sum_{\sigma,\rho} \left(\mathbf{s}_e^T \cdot \frac{\partial \mathbf{A}_e}{\partial A_{\rho\sigma}} \cdot \mathbf{e}_e + \mathbf{v}_e^T \cdot \frac{\partial \mathbf{K}_{me}}{\partial A_{\rho\sigma}} \cdot \mathbf{u}_e \right) \tag{C.33}$$

$$\Psi^b_{\alpha\beta_e} \equiv \frac{1}{\lambda^2} \frac{\partial\, \lambda}{\partial\, D_{\alpha\beta}} = \sum_{\sigma,\rho} \left(\mathbf{v}_e^T \cdot \frac{\partial \mathbf{K}_{me}}{\partial D_{\rho\sigma}} \cdot \mathbf{u}_e \right) \tag{C.34}$$

where $\alpha, \beta, \sigma, \rho = 1 \ldots 3$ represent the components of the stiffness matrices of element e. Note that all the sensitivity matrices can be evaluated locally, as the global contribution of the geometric stiffness matrix is accounted for via the adjoint displacement vector $\mathbf{v}$.

Bibliography

M. Abdalla, C. Kassapoglou, and Z. Gürdal. Formulation of composite laminate robustness constraint in lamination parameters space. In *50th AIAA/ASME/ASCE/AHS/ASC Structures, Structural Dynamics, and Materials Conference*, number AIAA-2009-2478, Palm Springs, California,, May 4-7 2009a. AIAA.

M. M. Abdalla. *Applications of the Cellular Automata Paradigm in Structural Analysis and Design*. PhD thesis, Delft University of Technology, 2004.

M. M. Abdalla, S. Setoodeh, and Z. Gürdal. Design of variable stiffness composite panels for maximum fundamental frequency using lamination parameters. *Composite Structures*, 81(2):283–291, 2007. doi: 10.1016/j.compstruct.2006.08.018.

M. M. Abdalla, Z. Gürdal, and G. F. Abdelal. Thermomechanical response of variable stiffness composite panels. *Journal of Thermal Stresses*, 32(1):187 – 208, 2009b. doi: 10.1080/01495730802540916.

D. B. Adams, L. T. Watson, Z. Gürdal, and C. M. Anderson-Cook. Genetic algorithm optimization and blending of composite laminates by locally reducing laminate thickness. *Advanced in Engineering Software*, 35:35–43, 2004. doi: 10.1016/j.advengsoft.2003.09.001.

S. Aharon, Z. Karucharo, and H. Leibovich. Autow deliverable d16 - design of full scale component. Technical report, Israel Aerospace Industries, 2009.

A. Alhajahmad. *Design Tailoring of Panels for Pressure Pillowing Using Tow-Placed Steered Fibers*. PhD thesis, Delft University of Technology, 2008.

A. Alhajahmad. Optimal design of tow-placed fuselage panels for maximum strength with buckling considerations. *Journal of Aircraft*, 47(3):775–782, 2010. doi: 10.2514/1.40357.

A. Alhajahmad, M. M. Abdalla, and Z. Gürdal. Design tailoring for pressure pillowing using tow-placed steered fibers. *Journal of Aircraft*, 45(2):630–640, 2008. doi: 10.2514/1.32676.

M. Autio. Determining the real lay-up of a laminate corresponding to optimal lamination parameters by genetic search. *Structural and Multidisciplinary Optimization*, 20(4):301–310, 2000. doi: 10.1007/s001580050160.

M. Autio. Optimization of coupled thermal-structural problems of laminated plates with lamination parameters. *Structural and Multidisciplinary Optimization*, 21(1): 40–51, 2001. doi: 10.1007/s001580050166.

N. V. Banichuk, V. V. Saurin, and A. A. Barsuk. Optimal orientation of orthotropic materials for plates designed against buckling. *Structural and Multidisciplinary Optimization*, 10(3):191–196, 12 1995. doi: 10.1007/BF01742591.

J. F. M. Barthelemy and R. T. Haftka. Approximation concepts for optimum structural design - a review. *Structural and Multidisciplinary Optimization*, 5(3):129–144, 09 1993. doi: 10.1007/BF01743349.

S. B. Biggers and S. S. Pageau. Shear buckling response of tailored composite plates. *AIAA Journal*, 32(5):1100–1103, 1993. doi: 10.2514/3.12107.

S. B. Biggers and S. Srinivasan. Compression buckling response of tailored rectangular composite plates. *AIAA Journal*, 31(3):590–596, 1993.

A. Blom, B. Tatting, J. M. Hol, and Z. Gürdal. Fiber path definitions for elastically tailored conical shells. *Composites Part B*, 40(1):77–84, 2009a. doi: 10.1016/j.compositesb.2008.03.011.

A. W. Blom. *Structural Performance of Fiber-Placed, Variable-Stiffness Composite Conical and Cylindrical Shells*. PhD thesis, Delft University of Technology, 2010.

A. W. Blom, S. Setoodeh, J. M. A. M. Hol, and Z. Gürdal. Design of variable-stiffness conical shells for maximum fundamental eigenfrequency. *Computers and Structures*, 86(9):870–878, 2008.

A. W. Blom, M. M. Abdalla, and Z. Gürdal. Optimization of course locations in fiber-placed panels for general fiber angle distributions. *Composites Science and Technology*, In Press, 2009b. doi: 10.1016/j.compscitech.2009.12.003.

A. W. Blom, P. B. Stickler, M. Rassaian, and Z. Gürdal. Bending test of a fiber-reinforced composite cylinder. In *Proceedings of the 1st joint American-Canadian Technical Conference on Composites*, Newark, September 2009c.

M. Bloomfield, C. Diaconu, and P. Weaver. On feasible regions of lamination parameters for lay-up optimization of laminated composites. *Proceedings of the Royal Society A*, 465(1123–1143), 2009. doi: 10.1098/rspa.2008.0380.

M. V. Bower and D. H. Koedam. Tensor polynomial failure criterion: Coefficient limits based on convexity requirements. *Journal of Reinforced Plastics and Composites*, 16(5):435–477, 1997. doi: 10.1177/073168449701600504.

H. E. Brandmaier. Optimum filament orientation criteria. *Journal of Composite Materials*, 4(3):422–425, 1970. doi: 10.1177/002199837000400314.

M. Bruyneel, B. Colson, and A. Remouchamps. Discussion on some convergence problems in buckling optimisation. *Structural and Multidisciplinary Optimization*, 35(2):181–186, 2008. doi: 10.1007/s00158-007-0129-z.

D. Bushnell. Panda2-program for minimum weight design of stiffened, composite, locally buckled panels. *Computers & Structures*, 25(4):469–605, 1987. doi: 10.1016/0045-7949(87)90267-7.

R. A. Canfield. Design of frames against buckling using a rayleigh quotient approximation. *AIAA Journal*, 31(6):1143–1149, 1993. doi: 10.2514/3.11739.

G. Caprino and I. C. Visconti. A note on specially orthotropic laminates. *Journal of Composite Materials*, 16(5):395–399, 1982. doi: 10.1177/002199838201600504.

R. D. Cook. *Concepts and applications of finite element analysis, 4th Edition.* Number ISBN: 0-471-35605-0. Wiley, 2002.

R. Curran, S. Raghunathan, and M. Price. Review of aerospace engineering cost modelling: The genetic causal approach. *Progress in Aerospace Sciences*, 40(8): 487–534, 2004. doi: DOI:10.1016/j.paerosci.2004.10.001.

I. M. Daniel and O. Ishai. *Engineering Mechanics of Composite Material.* Oxford University Press In., Oxford, 1994.

R. S. Dave and A. C. Loos, editors. *Processing of Composites.* Hanser Publishers, 2000. ISBN 978-3-446-18044-4.

A. R. de Faria and J. S. Hansen. Optimal buckling loads of nonuniform composite plates with thermal residual stresses. *Journal of Applied Mechanics*, 66(2):388–395, 1999. doi: 10.1115/1.2791061.

C. G. Diaconu and H. Sekine. Feasible region in general design space of lamination parameters for laminated composites. *AIAA Journal*, 40(3):559–569, March 2002. doi: 10.2514/2.1683.

A. L. Dixon. The eliminant of three quantics in two independent variables. *Proceedings of the London Mathematics Society*, s2-7(1):49–69, 1909.

M. S. Eldred, V. B. Venkayya, and W. J. Anderson. Mode tracking issues in structural optimization. *AIAA Journal*, 33(10):1926–1933, 1995. doi: 10.2514/3.12747.

D. O. Evans. Fiber placement. In D. Miracle and S. Donaldson, editors, *ASM Handbook*, volume 21, pages 477–479. ASM International, 2001.

C. Fagiano. *Computational Modeling of Tow-Placed Composite Laminates with Fabrication Features.* PhD thesis, Delft University of Technology, 2010.

C. A. Felippa. Recent advances in finite element templates. Technical Report CU-CAS-00-14, College of Engineering, University of Colorado, 2000.

C. A. Felippa. A study of optimal membrane triangles with drilling freedoms. *Computer Methods in Applied Mechanics and Engineering*, 192(16-18):2125–2168, 2003.

D. L. Flaggs and J. R. Vinson. Hydrothermal effects on the buckling of laminated composite plates. *Fibre Science and Technology*, 11(5):353–365, 9 1978. doi: 10.1016/0015-0568(78)90031-3.

C. Fleury and L. A. Schmit Jr. Dual methods and approximation concepts in structural synthesis. *NASA Contractor Reports 3226*, 1980.

J. P. Foldager, J. S. Hansen, and N. Olhoff. Optimization of the buckling load for composite structures taking thermal effects into account. *Structural and Multidisciplinary Optimization*, 21(1):14–31, 2001. doi: 10.1007/s001580050164.

H. Fukunaga, H. Sekine, M. Sato, and A. Iino. Buckling design of symmetrically laminated plates using lamination theory. *Computers and Structures*, 57(4):643–649, 1995. doi: 10.1016/0045-7949(95)00050-Q.

J. M. Gere. *Mechanics of Materials.* Nelson Thornes, Cheltenham, United Kingdom, 2002.

H. Ghiasi, K. Fayazbakhsh, D. Pasini, and L. Lessard. Optimum stacking sequence design of composite materials part ii: Variable stiffness design. *Composite Structures*, In Press, Corrected Proof, 2010. doi: 10.1016/j.compstruct.2010.06.001.

J. H. Gosse and S. Christensen. Strain invariant failure criteria for polymers in composite materials. In *42nd AIAA/ASME/ASCE/AHS/ASC Structures, Structural Dynamics, and Materials Conference and Exhibit*, Seattle, WA, April 2001.

J. L. Grenestedt. Layup optimization against buckling of shear panels. *Structural Optimization*, 3(2):115–120, 1991. doi: 10.1007/BF01743281.

A. Groenwold, D. W. Wood, L. F. P. Etman, and S. Tosserams. Globally convergent optimization algorithm using conservative convex separable diagonal quadratic approximations. *AIAA Journal*, 47(11):2649–2657, 2009. doi: 10.2514/1.41975.

A. A. Groenwold and R. Haftka. Optimization with non-homogeneous failure criteria like tsai-wu for composite laminates. *Structural and Multidisciplinary Optimization*, 32(3):183–190, 2006.

Z. Gürdal and R. Olmedo. In-plane response of laminates with spatially varying fiber orientations - variable stiffness concept. *AIAA Journal*, 31(4):751–758, 1993. doi: 10.2514/3.11613.

Z. Gürdal, R. Haftka, and H. Prabhat. *Design and Optimization of Laminated Composite Structures.* Wiley, 1999.

Z. Gürdal, B. Tatting, and C. K. Wu. Tow-placement technology and fabrication issues for laminated composite structures. In *46th AIAA/ASME/ASCE/AHS/ASC Structures, Structural Dynamics and Materials Conference*, number AIAA 2005-2017, Austin, Texas, 18-21 April 2005.

Z. Gürdal, B. Tatting, and C. Wu. Variable stiffness composite panels: Effects of stiffness variation on the in-plane and buckling response. *Composites Part A: Applied Science and Manufacturing*, 39(5):911–922, 2008.

Z. Gürdal, S. T. IJsselmuiden, and J. M. van Campen. *Composite Laminate Optimization with Discrete Variables, Encyclopaedia of Aerospace Engineering*, volume 8, chapter 432. Wiley, 2010. doi: 10.1002/9780470686652.eae499.

R. Haftka and Z. Gürdal. *Elements of Structural Optimization.* Kluwer Academic Publishers, 1992.

R. Haftka and J. H. Starnes. Stiffness tailoring for improved compressive strength of composite plates with holes. *AIAA Journal*, 26(1):72–77, 1988. doi: 10.2514/3.9853.

V. B. Hammer. Optimal laminate design subject to single membrane loads. *Structural and Multidisciplinary Optimization*, 17(1):65–73, 1999. doi: 10.1007/BF01197714.

V. B. Hammer, M. P. Bendsøe, R. Lipton, and P. Pedersen. Parametrization in laminate design for optimal compliance. *International Journal of Solids and Structures*, 34(4):415–434, 1997. doi: 10.1016/S0020-7683(96)00023-6.

J. Herencia, R. Haftka, P. Weaver, and M. Friswell. Lay-up optimization of composite stiffened panels using linear approximations in lamination space. *AIAA Journal*, 49(9):2387–2391, 2008. doi: 10.2514/1.36189.

M. Hinton, P. D. Soden, and A.-S. Kaddour, editors. *Failure Criteria in Fibre-Reinforced-Polymer Composites.* Elsevier Science, 2004. ISBN 978-0-08-044475-8.

S. Honda and Y. Narita. Design for the maximum natural frequency of laminated composite plates by optimally distributed short fibers. *Journal of System Design and Dynamics*, 2(6):1195–1205, 2008.

S. Honda, Y. Oonishi, Y. Narita, and K. Sasaki. Vibration analysis of composite rectangular plates reinforced along curved lines. *Journal of System Design and Dynamics*, 2(1):76–86, 2008. doi: 10.1299/jsdd.2.76.

J. Huang and R. Haftka. Optimization of fiber orientations near a hole for increased load-carrying capacity of composite laminates. *Structural and Multidisciplinary Optimization*, 30:335–341, July 2005. doi: DOI10.1007/s00158-005-0519-z.

M. W. Hyer and R. F. Charette. Use of curvilinear fiber format in composite structure design. *AIAA Journal*, 29(6):1011–1015, 1991.

M. W. Hyer and H. H. Lee. The use of curvilinear-fiber format in to improve buckling resistance of composite plates with central holes. *Composite Structures*, 18(3):239–261, 1991.

S. T. IJsselmuiden, M. M. Abdalla, O. Seresta, and Z. Gürdal. Multi-step blended stacking sequence design of panel assemblies with buckling constraints. *Composites Part B: Engineering*, 2009. doi: 10.1016/j.compositesb.2008.12.002.

F.-X. Irisarri, M. M. Abdalla, and Z. Gürdal. An improved shepard's method for the optimization of composite structures. *AIAA Journal*, 2011. (accepted).

D. C. Jegley, B. Tatting, and Z. Gürdal. Tow-steered panels with holes subjected to compression or shear loads. *46th AIAA/ASME/ASCE/AHS/ASC Structures, Structural Dynamics and Materials Conference, Austin, Texas*, April 2005.

D. R. Jones, C. D. Perttunen, and B. E. Stuckman. Lipschitzian optimization without the lipschitz constant. *Journal of Optimization Theory and Applications*, 79(1): 157–181, 1993. doi: 10.1007/BF00941892.

M. G. Joshi and S. B. Biggers. Thickness optimization for maximum buckling loads in composite laminated plates. *Composites Part B: Engineering*, 27(2):105–114, 1996. doi: 10.1016/1359-8368(95)00027-5.

W. Karush. Minima of functions of several variables with inequalities as side constraints. Master's thesis, Dept. of Mathematics, Univ. of Chicago, Chicago, Illinois., 1939.

C. Kassapoglou. Composite plates with two concentric layups under compression. *Composites Part A: Applied Science and Manufacturing*, 39(1):104–112, 2008. doi: 10.1016/j.compositesa.2007.08.02.

C. Kassapoglou. Simultaneous cost and weight minimization of composite-stiffened panels under compression and shear. *Composites Part A*, 28:419–435, 1997.

Y. Katz, R. Haftka, and E. Altus. Optimization of fiber directions for increasing the failure load of a plate with a hole. In *ASC technical conference*, pages 62–71, 1989.

A. Khani, M. M. Abdalla, and Z. Gürdal. Maximum strength design of long composite non-circular cylinders. In *11th ECSSMMT Conference, Toulouse*, September 2009.

A. Khani, S. T. IJsselmuiden, M. M. Abdalla, and Z. Gürdal. Design of variable stiffness panels for maximum strength using lamination parameters. *Composites Part B: Engineering*, 42(3):546–552, 2011.

J. C. Klees, S. T. IJsselmuiden, M. M. Abdalla, D. H. Bassir, and Z. Gürdal. Fibre angle reconstruction for variable stiffness panels including curvature constraints. In *11th ECSSMMT Conference, Toulouse*, 2009.

N. Kogiso, S. Nakagawa, and Y. Murotsu. Lamination parameters applied to reliability-based in-plane strength design of composites. *AIAA Journal*, 41(11): 2200–2207, 2003.

E. Kreyszig. *Advanced Engineering Mathematics.* Wiley, New York, 8th edition, 1999.

H. W. Kuhn and A. W. Tucker. Nonlinear programming. In *Proceedings of 2nd Berkeley Symposium*, pages 481–492. Berkeley: University of California Press, 1951.

C. S. Lopes. *Damage and Failure of Non-Conventional Composite Laminates.* PhD thesis, Delft University of Technology, 2009.

Lucintel. Opportunities for composites in global aerospace market 2009-2028.

P. M. Manne and S. W. Tsai. Design optimization of composite plates: Part i—design criteria for strength, stiffness, and manufacturing complexity of composite laminates. *Journal of Composite Materials*, 32(6):544–571, 1998. doi: 10.1177/002199839803200603.

A. F. Martin and A. W. Leissa. Application of the ritz method to plane elasticity problems for composite sheets with variable fibre spacing. *International Journal for Numerical Methods in Engineering*, 28(8):1813–1825, 1989. doi: 10.1002/nme.1620280808.

C. A. Meyers and M. W. Hyer. Thermal buckling and postbuckling of symmetrically laminated composite plates. *Journal of Thermal Stresses*, 14(4):519–540, 1991. doi: 10.1080/01495739108927083.

M. Miki. Material design of composite laminates with required in-plane elastic properties. *Progress in Science and Engineering of Composites*, 2:1725–1731, 1982.

MSC-Software. *MSC.Nastran 2005 r3, Design Sensitivity and Optimization User's Guide*, 2005.

S. Nagendra, S. Kodiyalam, J. E. Davis, and V. Parthasarathy. Optimization of tow fiber paths for composite design. In *36th AIAA/ASME/ASCE/AHS/ASC Structures, Structural Dynamics, and Materials Conference*, volume 2, pages 1031–1041, New Orleans, Louisiana, April 1995. AIAA.

A. P. Nagy. *Isogeometric Design Optimization.* PhD thesis, Delft University of Technology, 2011.

A. P. Nagy, M. M. Abdalla, and Z. Gürdal. Fiberpath definition of regular surfaces (internal report). Technical report, Delft University of Technology, 2009.

H. Nakayasu and Z. Maekawa. A comparative study of failure criteria in probabilistic fields and stochastic failure envelopes of composite materials. *Reliability Engineering and System Safety*, 56(3):209–220, 1997. doi: 10.1016/S0951-8320(95)00085-2.

G. Nakos and R. Williams. Elimination with the dixon resultant. *Mathematica in Education and Research*, 6(3):11–21, 1997, http://library.wolfram.com/infocenter/Articles/2597/

N. Olhoff. Multicriterion structural optimization via bound formulation and mathematical programming. *Structural Optimization*, 1(1):11–17, 1989. doi: 10.1007/BF01743805.

R. Olmedo and Z. Gürdal. Buckling response of laminates with spatially varying fiber orientations. In *AIAA/ASME/ASCE/AHS/ASC Structures, Structural Dynamics, and Materials Conference, 34th and AIAA/ASME Adaptive Structures Forum*, pages 2261–2269, 1993.

L. Parnas, S. Oral, and U. Ceyhan. Optimum design of composite structures with curved fiber courses. *Composites Science and Technology*, 63:1071–1082, 2003. doi: 10.1016/S0266-3538(02)00312-3.

P. Pedersen. On optimal orientation of orthotropic materials. *Structural and Multidisciplinary Optimization*, 1(2):101–106, 06 1989. doi: 10.1007/BF01637666.

P. Pedersen. On thickness and orientational design with orthotropic materials. *Structural and Multidisciplinary Optimization*, 3(2):69–78, 06 1991. doi: 10.1007/BF01743275.

V. K. R. Pilaka. Design of realistic variable stiffness laminates a gradient-based optimizer for retrieving fiber orientation angles with average curvature constraints from lamination parameter distributions. Master's thesis, Delft University of Technology, 2010.

T. Rahman, S. T. IJsselmuiden, M. M. Abdalla, and E. L. Jansen. Postbuckling analysis of variable stiffness composite panels using a finite element based perturbation method. *International Journal of Structural Stability and Dynamics*, 11(3), 2011. doi: 10.1142/S0219455411004324.

J. N. Reddy. *Mechanics of Laminated Composite Plates and Shells.* CRC Press, second edition, 2004.

R. Rockafellar. Monotone operators and the proximal point algorithm. *SIAM Journal Control and Optimization*, 14(5):877–898, August 1976. doi: 10.1137/031405610.1137/031405610.1137/0314056.

A. Rothwell. Optimum fibre orientations for the buckling of thin plates of composite material. *Fibre Science and Technology*, 2(2):111–122, 1969. doi: 10.1016/0015-0568(69)90003-7.

K. S. Sai Ram and P. K. Sinha. Hygrothermal effects on the buckling of laminated composite plates. *Composite Structures*, 21(4):233–247, 1992. doi: 10.1016/0263-8223(92)90051-D.

L. A. Schmit and B. Farshi. Optimum design of laminated fibre composite plates. *International Journal for Numerical Methods in Engineering*, 11(4):623 – 640, 1976. doi: 10.1002/nme.1620110403.

K. Schueler, J. Miller, and R. Hale. Approximate geometric methods in application to the modeling of fiber placed composite structures. *Journal of Computing and Information Science in Engineering*, 4(3):251–256, September 2004. doi: 10.1115/1.1736685.

S. Setoodeh. *Optimal design of variable-stiffness fiber-reinforced composites using cellular automata.* PhD thesis, Delft University of Technology, 2005.

S. Setoodeh, M. M. Abdalla, and Z. Gürdal. Combined topology and fiber path design of composite layers using cellular automata. *Structural and Multidisciplinary Optimization*, 30(6):413–421, 2005. doi: 10.1007/s00158-005-0528-y.

S. Setoodeh, M. M. Abdalla, and Z. Gürdal. Approximate feasible regions for lamination parameters. In *11th AIAA/ISSMO Multidisciplinary Analysis and Optimization Conference*, Portsmouth, Virginia, 2006a.

S. Setoodeh, M. M. Abdalla, and Z. Gürdal. Design of variable stiffness laminates using lamination parameters. *Composites Part B: Engineering*, 37(4-5):301–309, 2006b. doi: 10.1016/j.compositesb.2005.12.001.

S. Setoodeh, M. M. Abdalla, S. T. IJsselmuiden, and Z. Gürdal. Design of variable-stiffness composite panels for maximum buckling load. *Composite Structures*, 87(1):109–117, 2009. doi: 10.1016/j.compstruct.2008.01.008.

A. P. Seyranian, E. Lund, and N. Olhoff. Multiple eigenvalues in structural optimization problems. *Structural Optimization*, 8(4):207–227, 1994. doi: 10.1007/BF01742705.

D. Shepard. A two-dimensional interpolation function for irregularly-spaced data. In *Proceedings of the 1968 23rd ACM national conference*, pages 517–524, 1968. doi: http://doi.acm.org/10.1145/800186.810616.

J. H. Starnes and R. Haftka. Preliminary design of composite wings for buckling, stress and displacement constraints. *Journal of Aircraft*, 16(8):564–570, 1979. doi: 10.2514/3.58565.

J. Stegmann and E. Lund. Discrete material optimization of general composite shell structures. *International Journal for Numerical Methods in Engineering*, 62(14): 2009–2027, 2005. doi: 10.1002/nme.1259.

W. Stroud and M. Anderson. Pasco: Structural panel analysis and sizing code, capability and analytical foundations. Technical Report TM-80181, NASA, 1981.

K. Svanberg. A class of globally convergent optimization methods based on conservative convex separable approximations. *SIAM Journal on Optimization*, 12(2): 555–573, 2002. doi: 10.1137/S1052623499362822.

B. Tatting and Z. Gürdal. Design and manufacture of elastically tailored tow placed plates. Technical Report CR-2002-211919, NASA, August 2002.

B. Tatting and Z. Gürdal. Automated finite element analysis of elastically-tailored plates. Technical Report CR-2003-212679, NASA, 2003.

M. W. Tosh and D. W. Kelly. On the design, manufacture and testing of trajectorial fibre steering for carbon fibre composite laminates. *Composites Part A: Applied Science and Manufacturing*, 31(10):1047–1060, October 2000. doi: 10.1016/S1359-835X(00)00063-4.

S. W. Tsai. *Composite Design (4th Edition)*. Think Composites, 1988.

S. W. Tsai and H. T. Hahn. *Introduction of Composite Materials*. Technomic Publishing Company, Lancaster, PA, 1980.

S. W. Tsai and N. J. Pagano. Invariant properties of composite materials. *Composite Material Workshop*, pages 233–252, 1968.

J. M. van Campen. *Optimum Lay-up Design of Variable Stiffness Composite Structures*. PhD thesis, Delft University of Technology, 2011.

P. Vannucci. Designing the elastic properties of laminates as an optimisation problem: a unified approach based on polar tensor invariants. *Structural and Multidisciplinary Optimization*, 31(5):378–387, 2006. doi: 10.1007/s00158-005-0566-5.

S. Venkataraman and R. T. Haftka. Structural optimization complexity: what has moore's law done for us? *Structural and Multidisciplinary Optimization*, 28(6): 375–387, 2004. doi: 10.1007/s00158-004-0415-y.

G. Verchery. Les invariants des tenseurs d'ordre quatre du type de l'élasticité. In *Proceedings of the Euromech Colloquium 115, Villard-de-Lans.*, pages 93–104. Published in Paris by Editions du CNRS in 1982 (in French), 1979.

J. Whitney and J. Ashton. Effect of environment on the elastic response of layered composite plates. *AIAA Journal*, 9(9):1708–1713, 1971. doi: 10.2514/3.49976.

F. Williams, D. Kennedy, R. Butler, and M. Anderson. Viconopt - program for exact vibration and buckling analysis or design of prismatic plate assemblies. *AIAA Journal*, 29(11):1927–1928, 1991. doi: 10.2514/3.10820.

C. Wu, Z. Gürdal, and J. Starnes. Structural response of compression-loaded, tow-placed, variable stiffness panels. In *43rd AIAA/ASME/ASCE/AHS/ASC Structures, Structural Dynamics, and Materials Conference*, number AIAA-2002-1512, Colorado, April 2002.

C. K. Wu and Z. Gürdal. Thermal testing of tow-placed, variable stiffness panels. In *42nd AIAA/ASME/ASCE/AHS/ASC Structures, Structural Dynamics, and Materials Conference and Exhibit*, number AIAA-2001-1190. AIAA, April 16-19 2001.

Curriculum Vitae

Samuel Tsunduka[1] *IJsselmuiden*[2] was born on September 17th 1982 in Soutpansberg, South Africa, where he spent his toddling years chasing the local wildlife with his partner-in-crime, Zoja. Already at an early age he started experimental work on the second law of thermodynamics, much to the dissatisfaction of his supervisors. Soon before starting his formal education, he moved to Johannesburg, where his wildlife chasing days prepared him well for the schools athletics activities and he quickly developed an affinity for the exact sciences. In 1990, he moved to Baltimore, USA, for a year to join the Wellwood Wildcats. During this time he started to develop his game playing skills on a top-of-the-line 386-SX22 computer. Moving from the african Bushveld to the more civilized neighborhoods of Baltimore resulted in him trading his bow and arrow for a bow and violin, which was undoubtedly an even more effective method of tormenting the neighbors. He completed primary school after returning to Johannesburg in 1991. Later, he attended Sandringham High School where he matriculated in 1999 with distinctions for Mathematics, Science, Afrikaans and Music. He also received two silver-scholar awards, one bronze-scholar award (yes that gold-scholar award did prove elusive) and the Neville-Holtz Science award.

In 2001, after spending a year traveling, he moved back to South Africa to start a degree in Mechanical Engineering at the University of Pretoria. After completing his first year with eleven distinctions and having dismounted his fare share of lawnmower engines, he decided to pursue a degree in Aerospace Engineering at Delft University of Technology in the Netherlands. This proved to be a good move and he quickly developed a passion for structural mechanics from the projects and subjects he followed during his undergraduate years. In his final year he joined a group of students to design, build, test and race a human powered submarine (WASUB) - an unforgettable experience - which ultimately led to the team bagging a majority of the prizes at the International Human Powered Submarine Races. Other than scoring a new

[1] A Shangaan name, meaning *to remember*

[2] A village in the Dutch province of Overijssel, however, the link to the family name is unknown, but Napoleon must have had something to do with it.

world record, the project also landed him a spot in the good-books with his future wife. As part of his masters program he spent three months in Caesarea, Israel, doing an internship at APCO Aviation where, he worked on the design and testing of a new entry-level paraglider. After surviving one too many crash-landings, he returned to Delft to start his final masters research project at the Aerospace Structures chair, for which he was awarded cum laude in March 2007. Soon hereafter he started his PhD at the same chair (but with a new desk), which was focused on developing an efficient design optimization routine for variable stiffness composite structures ... but by now you have already read all of that, right?

List of Publications

Books (Chapters):

Z. Gürdal, S.T. IJsselmuiden, and J.M. van Campen. *Composite Laminate Optimization with Discrete Variables.* Encyclopaedia of Aerospace Engineering, volume 8, chapter 432. Wiley, 2010.

Journal Papers:

Rahman, S.T. IJsselmuiden, M.M. Abdalla, and E.L. Jansen. *Postbuckling analysis of variable stiffness composite panels using a finite element based perturbation method.* International Journal of Structural Stability and Dynamics, 2011

A. Khani, S.T. IJsselmuiden, M.M. Abdalla and Z. Gürdal. *Design of Variable Stiffness Panels for Maximum Strength Using Lamination Parameters.* Composites Part B, 42(3), 2011

S.T. IJsselmuiden, M.M. Abdalla, and Z. Gürdal. *Thermomechanical design optimization of variable stiffness composite panels for buckling.* Journal of Thermal Stresses, 33(10), 2010.

S.T. IJsselmuiden, M.M. Abdalla, and Z.Gürdal. *Optimization of variable stiffness panels for maximum buckling load using lamination parameters.* AIAA Journal, 48(1), 2010.

S.T. IJsselmuiden, M.M. Abdalla, O.Seresta, and Z.Gürdal. *Multi-step blended stacking sequence design of panel assemblies with buckling constraints.* Composites Part B, 2009.

S.T. IJsselmuiden, M.M. Abdalla, and Z.Gürdal. *Implementation of strength based failure criteria in the lamination parameter design space.* AIAA Journal, 46(9), 2008.

S. Setoodeh, M.M. Abdalla, S.T. IJsselmuiden, and Z.Gürdal. *Design of variable-stiffness composite panels for maximum buckling load.* Composite Structures, 2008.

Conference Papers:

S.T. IJsselmuiden, M.M. Abdalla, A.P. Nagy and Z.Gürdal. *Design for Automated Fiber Placement: Steering For Improved Structural Performance*, ISCM 2010, Marknesse, The Netherlands

A. Khani, S.T. IJsselmuiden, M.M. Abdalla and Z. Gürdal. *Design Of Variable Stiffness Panels For Maximum Strength Using Lamination Parameters.* 14th European Conference on Composite Materials, Budapest, 7-10 June 2010.

S.T. IJsselmuiden, M.M. Abdalla, V. K. R. Pilaka and Z.Gürdal. *Design of Variables Stiffness Composite Structures for Advanced Fiber Placement Technology.* SAMPE 2010, Seattle.

S.T. IJsselmuiden, M.M. Abdalla, and Z.Gürdal. *Maximising buckling loads of variable stiffness shells using lamination parameters.* In 50th AIAA/ASME/ASCE/AHS/ ASC Structures, Structural Dynamics, and Materials Conference, 2009.

S.T. IJsselmuiden, M.M. Abdalla, and Z.Gürdal. *Thermo-mechanical design optimisation of variable stiffness composite panels for buckling.* In 11th ECSSMMT Conference, Toulouse, 2009.

S.T. IJsselmuiden, M.M. Abdalla, and Z.Gürdal. *Thickness tailoring of variable stiffness panels for maximum buckling load.* In 17th ICCM Conference, 2009.

J.C. Klees, S.T. IJsselmuiden, M.M. Abdalla, D.H. Bassir, and Z.Gürdal. *Fibre angle reconstruction for variable stiffness panels including curvature constraints.* In 11th ECSSMMT Conference, Toulouse, 2009.

T.Rahman, S.T. IJsselmuiden, M.M. Abdalla, and E.L. Jansen. *Postbuckling analysis of variable stiffness composite panels using a finite element based perturbation method.* In ASME 2009 International Mechanical Engineering Congress and Exposition, Lake Buena Vista, Florida, November 2009.

S.T. IJsselmuiden, M.M. Abdalla, S.Setoodeh, and Z.Gürdal. *Design of variable stiffness panels for maximum buckling load using lamination parameters.* In 49th AIAA/ASME/ASCE/ AHS/ASC Structures, Structural Dynamics, and Materials Conference, number AIAA-2008-2123, Schaumburg, IL, April 2008.

S.T. IJsselmuiden, M.M. Abdalla, and Z.Gürdal. *Design of composite structures for advanced fibre placement technology.* In 2nd South African International Aerospace Symposium, Stellenbosch, South Africa, 14-16 September 2008.

S.T. IJsselmuiden, M.M. Abdalla, and Z.Gürdal. *Implementation of strength based failure criteria in the lamination parameter design space.* In 48th AIAA/ASME/ ASCE/AHS/ASC Structures, Structural Dynamics, and Materials Conference, 2007.

S.T. IJsselmuiden, O.Seresta, M.M. Abdalla, and Z.Gürdal. *Multi-step stacking sequence design and blending of composite structures.* In 7th World Congress on Structural and Multidisciplinary Optimization, 2007.

Articles:

J.M.van Campen and S.T. IJsselmuiden. *Composites on the drawing board*, Leonardo Times, Aerospace Engineering TU Delft, 2008.

TU Delft
Delft University of Technology

ISBN 978-94-6113-032-7

9 789461 130327